A STUDY OF HYDRODYNAMICS AND MASS TRANSFER IN SMALL BORE DEEP SHAFT REACTORS

Nigel Norman Clark

Submitted in partial fulfilment of the requirements for the degree of Doctor of Philosophy in the Department of Chemical Engineering, University of Natal.

I declare that, except where otherwise indicated, this thesis represents my own original work.

ACKNOWLEDGEMENTS

The author would like to express his appreciation to his research supervisor, Dr. R.L.C. Flemmer, for encouragement and guidance in the preparation of this thesis.

Support for this work was provided by the Council for Mineral Technology (MINTEK), Randburg, South Africa. The author is grateful to Professor R.I. Edwards, and Mr. M.F. Dawson, of the MINTEK research group at the University of Natal, for their advice and assistance.

The author would also like to thank the academic staff of the Department of Chemical Engineering, in particular Mr. D.W. Wright, as well as Dr. D. Hamilton, of the Department of Chemistry, for guidance in this research. The author is also grateful to Mr. D. Penn, and the workshop and laboratory staff at the Department of Chemical Engineering, for the construction and erection of research apparatus.

TABLE OF CONTENTS

APPENDICES

LIST OF TABLES

LIST OF FIGURES

ABSTRACT

The phenomenology of vertical two phase flow was examined in respect of mass and momentum transfer as related to the design of deep shaft reactors. Experimental work on the bubble flow regime was performed in 50 mm and 100 mm diameter vertical pipes.

It was found that the limits of the regime of bubbly flow were strongly dependent on the method of gas introduction. In these terms it was possible to explain the strong divergences reported in the literature.

Following the development of a technique for assuring the synchronisation of quick-closing isolating valves, accurate holdup data were acquired to demonstrate the validity of extending the Zuber and Findlay drift-flux model to downflow.

An analytical technique was developed to enable the assessment of frictional losses from measurement of total head. It was established that existing models for the prediction of frictional losses were inadequate and Prandtl's mixing length paradigm was employed to generate a theory which provided an adequate description.

Mass transfer data were acquired and, although these exhibited a significant scatter, they suggest that the

small bore deep shaft reactor offers advantages as a gas-liquid contacting device.

CHAPTER 1

1. INTRODUCTION

Deep Shaft Reactors are formed from two vertical conduits either concentric or adjacent, joined at the base and communicating at the top via a header tank (see Fig 1.1). These conduits may be up to 3 m in diameter and 300 m long. Air is introduced near the top of the conduit carrying downward liquid flow, termed the downcomer, and a bubbly two phase flow is carried around the device into the header tank.

In such devices of narrow bore, frictional losses necessitate pumping to maintain flow, but for conduits of sufficiently large diameter, circulation may be maintained by the air lift effect in the riser [106,137]. Under these circumstances there is a danger that flow instabilities may lead to a reversal of circulation and the positioning of air introduction is critical [61].

The attraction of the D.S.R. is that the large hydrostatic pressures and high gas-liquid surface area result in good interphase mass transfer. The device may also be used in three phase reactor systems. Large bore D.S.R's have found increasing application in sewage treatment, especially in the United Kingdom [64] where they have

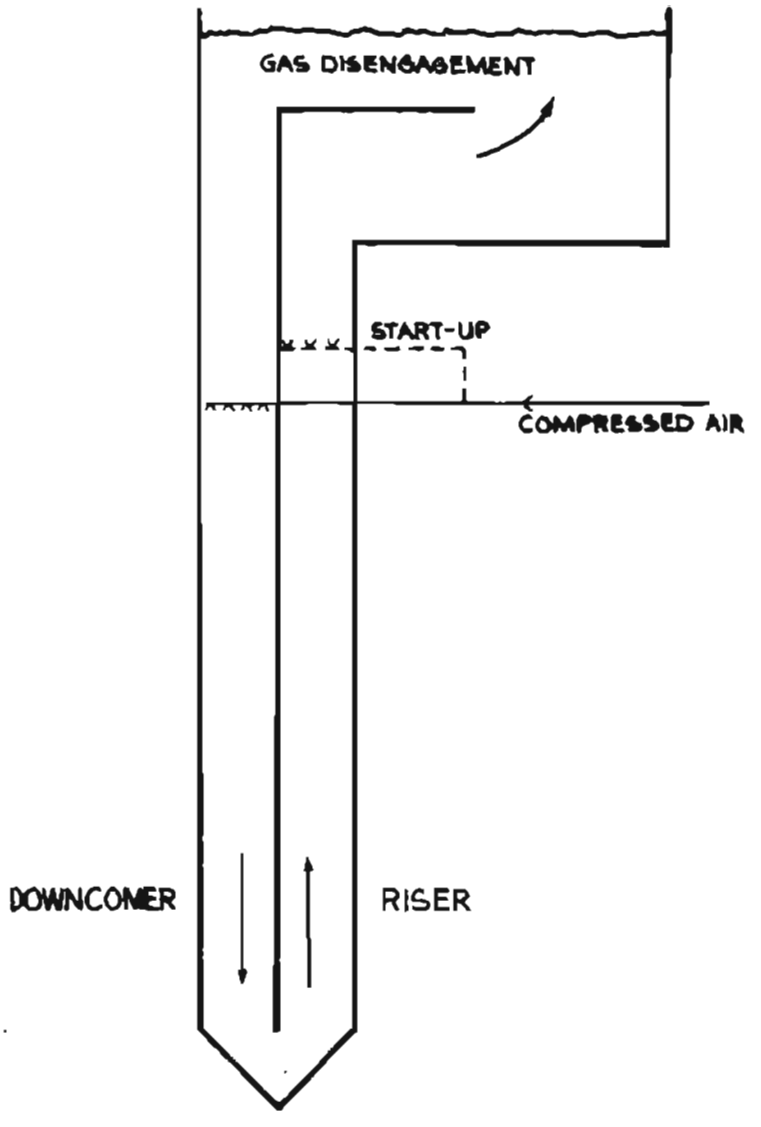

Fig 1·1 • Large bore deep shaft reactor with natural circulation (after Hines et al) •

replaced more conventional aeration equipment with the prospect of reducing operating costs.

In 1941 Nordell [169] filed a patent for a sewage treatment device incorporating some features of the D.S.R. The use of a small bore D.S.R. was suggested in 1955 by Robinson et al. [187] for treatment of uranium ore, and the concept has been revived recently by Clark and Flemmer [48], although no full scale plant has been constructed to date.

It is argued in this thesis that such narrow bore D.S.R.'s can provide significant advantages over traditional methods of gas/liquid mass transfer such as bubble columns, agitated vessels, and in some applications horizontal pipe reactors to which they are similar [3,4,129,197]. Although the phenomenology of large bore D.S.R.'s has been reported and subjected to some analysis [106,137], the literature does not offer the engineer a theoretical framework within which to design small bore reactors. For large bore D.S.R.'s wall effects are small, and the hydrodynamic theory is akin to that for bubble columns, which have been widely investigated [40,115,146,172,181,201].

Design of smaller bore devices requires a more precise knowledge of two phase flow, a field which has received increasing attention over the past two decades, yet which

is still not adequately described. Wallis [228] in a philosophical review of two phase flow literature, has termed current knowledge an "insecure science" and has commented on the lack of general theory available.

Thus it appears that an investigation of small bore D.S.R.'s is desirable on two counts. Firstly, to permit confident design of such reactors and secondly in order to permit pilot plant studies for scale up to large bore reactors. This investigation will also serve to increase current understanding of two phase flow, which has wide application in the fields of both chemical and nuclear engineering.

Such a study falls naturally into the following categories.

(i) Prediction and specification of the form in which the gas phase is dispersed in the liquid

(ii) establishment of theory to predict gas phase holdup

(iii) prediction and modelling of frictional losses

(iv) investigation of mass transfer properties

These categories are treated in the succeeding chapters.

CHAPTER 2

2. REGIMES OF TWO PHASE FLOW

2.1 INTRODUCTION

Two Phase Flow, unlike single phase flow, cannot be classified simply into Laminar, Transitional, or Turbulent Flow, since the manner in which the phases are interdispersed influences the overall fluid properties. Although an early classification due to Martinelli and co-workers [147,154] categorised flow by the turbulent or laminar nature of each phase, a more appropriate classification based on the type of interdispersion, or flow pattern, has been developed and attention has been given to defining the boundaries of the regions in which the various patterns occur. The pattern is dependent on gas and liquid superficial velocities and on the geometry of the apparatus. Comparison of horizontal and vertical two phase flows has shown that all patterns to be found in vertical flow exist in horizontal flow [208] whereas some horizontal patterns, typically stratified flows, are excluded in the vertical case [100].

Information is available on horizontal patterns [1,13,-31,112,218,232], but only the cases of vertical up and downflow, which are relevant to the D.S.R., are reviewed

here.

2.2 VERTICAL UPWARD COCURRENT FLOW

2.2.1 TERMINOLOGY FOR FLOW PATTERNS

Unless otherwise stated, the term "Two Phase" refers to air-water flow.

Govier et al. [86] have tabulated early nomenclature for the various flow patterns. More recent authors [31,85,-95,97,100,111,175,213,217] have agreed on the existence and description of four main flow patterns. These are, in order of ascending gas superficial velocity, the "bubble", "slug," "churn" or "froth" and "annular" or "annular-mist" regimes, and are illustrated in fig. 2.1.

Bubble flow consists of a dispersion of gas bubbles in a liquid continuum. Slug flow is a series of alternating gas and liquid slugs or plugs occupying almost the whole tube diameter. At higher velocities, slug flow tends to become churn of froth flow as the slugs lose their form due to violent mixing. As gas velocity is increased further, liquid flow is confined largely to an annulus at the tube wall and gas to a central core, which may contain some liquid in the form of wisps or droplets.

Full bore deep shaft reactors have been considered for

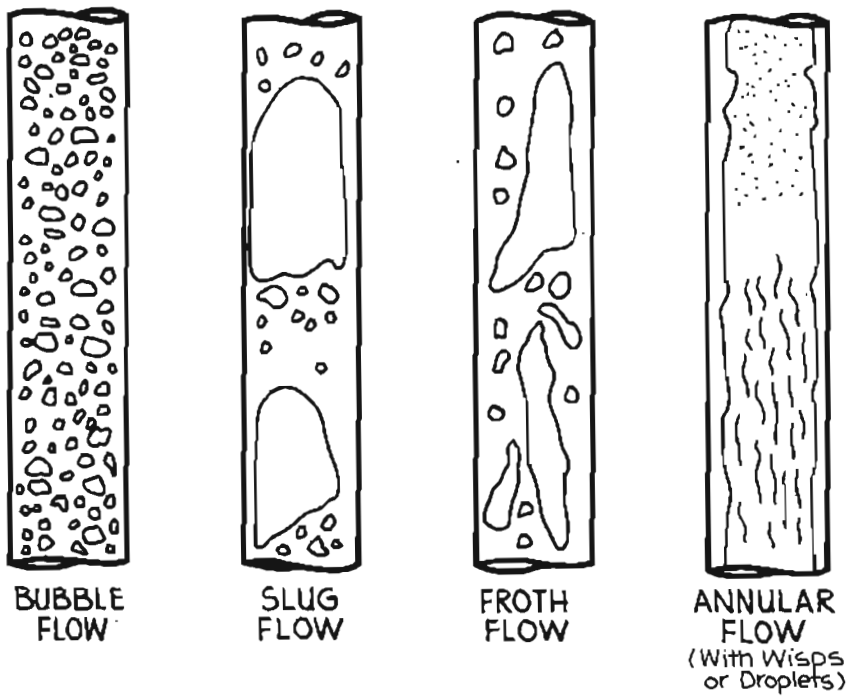

Fig 2·1 • Flow patterns in vertical upward gas-liquid flow •

operation only in the bubble flow regime [106,137] because this regime provides the high liquid holdup and hydrostatic head desirable for mass transfer. For regimes associated with greater gas phase holdup, the advantage of large hydrostatic head would be reduced. In considering similar devices of narrow bore, only this bubble flow regime and the transition from bubble to slug flow are relevant.

In bubble flow, the gas is distributed in discrete bubbles, small in comparison to the tube diameter. In slug flow the gas is present as large bubbles of nearly the tube diameter and up to several diameters in length separated by slugs of liquid [89]. Authors have differed in regarding either the liquid phase [85,86,89] or the gas phase [167,213] as the slug. The term "slug" is used below for the gas bubble.

The terms "Taylor bubble" and "Dumitrescu bubble" have also been associated with the gas bubble in slug flow [85,213]. Dome shaped bubbles encountered in incipient slug flow are referred to below as "caps" in agreement with Hills [103]

2.2.2 MECHANISM OF BUBBLE-SLUG TRANSITION

An understanding of the mechanism of the bubble-slug flow transition is of importance in this study. Although

archetypal bubble and slug flow may be described readily, the definition of the regime transition remains subjective. Hewitt [95] has defined this transition as the stage at which bubble diameter approaches that of the tube while Govier and Aziz [85] have defined it by the presence of slugs with length equal to diameter. Stuhmiller et al. [213] have viewed the transition statistically and have criticised the concept of a strict regime boundary.

The transition mechanism has received attention and is well understood. While very small bubbles rise in a straight line, bubbles of over 1,5 mm diameter follow a serpentine path [217]. This motion, together with velocity gradients and turbulence, promotes bubble contact and consequent coalescence [227]. The probability of coalescence on contact is governed by surface tension effects and is dependent on water purity [97,227]. In upflow bubble size will also increase with voidage due to the decrease in pressure with height.

Since bubbles of varying size have differing rise velocities [84], a bubbly flow with a variation in bubble size will promote greater incidence of bubble collision than a uniformly sized bubbly flow. This is discussed in greater detail with reference to "churn-turbulent" and "ideal" bubbly flows in chapter 3.

Bubble growth continues by the mechanism of collision until some cap bubbles of about 75% of the tube diameter are formed [85]. The time taken for this to occur has been regarded as the most important factor in the transition mechanism [111]. Although such caps have high terminal velocities in all but very small tubes, small bubbles trapped in the wake of the cap rise faster and are incorporated into the larger bubble. Hills [103] has reported that coalescence seldom occurs when a small bubble contacts the upper surface of a cap, but rather by absorbtion into the wake. Cap growth continues by this mechanism to form slugs of increasing length, until an equilibrium is reached between bubbles absorbed into the slug and those torn from its wake by turbulence [89]. In fully developed slug flow the liquid zone may still support a bubble population of up to 10% by volume [85].

Slug flow has been regarded as stable due to the uniform rise velocity of the slugs [89], while bubble flow has often been regarded as a transitory effect [100,189] with transition to slug flow inevitable. Nevertheless the bubble flow pattern may persist over a great pipe length, especially at low voidages [100,227] where bubble collision may be discouraged by hydrodynamic interactions between the bubbles [95]. Clearly in the extreme case where bubble population is too low to provide the gas volume for slug formation, bubble flow must be stable.

Particularly high turbulence in pipes may prohibit slug formation, leading to a stable "highly dispersed bubble flow" [217]. Hewitt [97] has provided a regime map which illustrates a similar flow pattern at high liquid flowrate termed "bubble flow with developing structure". The velocities associated with this pattern are a little high to warrant consideration in deep shaft reactors, but the fact that turbulence will have some retarding effect on slug formation should be noted.

2.2.3 MODELS DESCRIBING THE BUBBLE-SLUG TRANSITION BOUNDARY

Several models have been proposed in an attempt to predict the gas and liquid flowrates at which the transition from bubble to slug flow will occur. These are reviewed below.

(i) Model due to Govier and Aziz [85]

Govier and Aziz asserted that in typical incipient slug flow, gas slugs are spaced by seven pipe diameters and are of equal breadth and length. It was also asserted that at the point of transition the zone between the gas slugs still supported 25% by volume of gas as small bubbles. Combining these values with a knowledge of slug rise velocity relative to the fluid, it was possible to predict gas and liquid flowrates at the point of transition.

The model is unable to give a prediction of the time or pipe length required to complete transition, and due to the quantitive assumptions cannot be regarded as more than indicative. No direct account is taken of the retarding effect turbulence may have on slug formation.

(ii) Models Based on Bubble Proximity

Radovich and Moissis [180] considered a lattice of bubbles with a mean fluctuating velocity. A representation of collision frequency was found in terms of voidage and bubble diameter. This theory predicted a sharp increase in the number of collisions at voidages between 25 and 30%, with consequent slug formation, but very little coalescence would occur at voidages less than 10%. A quantitative answer cannot be obtained without a knowledge of the fluctuating velocity and probability of coalescence on contact. This information is not readily available.

Taitel et al. [217] concluded that coalescence would occur when bubbles were separated by less than half the bubble radius. This predicted a bubble to slug transition at voidages over 25%. This transition voidage could be given in terms of gas and liquid flowrates, with a knowledge of the bubble rise velocity. They have also suggested that for pipes of under 44 mm diameter, where bubble rise velocity exceeds slug rise velocity, no bubble flow may occur, since the faster moving bubbles are readily

absorbed into the wake of the slow moving slug. For larger diameter pipes, bubbles were considered to be swept over the faster moving slug with no coalescence. This may be criticised insofar as bubble flow may persist in small pipes if no caps are initially present, although it is acknowledged that slug flow may develop more readily in pipes of smaller diameter. Empirical data gathered by Taitel et al. [217] showed reasonable agreement with their theory.

It must be concluded that no model has been proposed which will predict the pipe length for which the bubble phase can endure, although proximity models may give some qualitative indication.

By far the most work on transition has appeared as empirical correlations or regime maps from observations of specific apparatus. Regime maps are described and compared below.

2.2.3 REGIME MAPS

The bubble-slug flow transition has been described mostly in terms of empirical or semi-empirical regime maps, which supply a clear boundary line between the two flow pattern regions. The axes of such maps are given as functions of the gas and liquid flowrates; typically as superficial velocities, or as the gas flow fraction vs. the two-phase

Froude number,

$$(\overline{W}_l + \overline{W}_g)/(gD)^{\emptyset.5},$$

where $\overline{W}_g$, $\overline{W}_l$ are the gas and liquid superficial velocities, g is the acceleration due to gravity, and D is the pipe diameter. { Many authors publishing in the field of two phase flow have preferred to use

$$(\overline{W}_g+\overline{W}_l)^2/gD$$

as the two phase Froude number. Either usage is accepted. The Froude number used here is preferred in the more current literature and is supported by Massey [155].} The use of the two phase Froude number has become entrenched in the regime literature due to an early theory of Griffith and Wallis [89] who demonstrated that the Froude number controlled a slug to annular pattern transition. Some authors of regime maps, together with their co-ordinate systems, are listed in Table 2.1.

The bubble to slug transition lines given in the regime maps of the authors listed in table 2.1 have been re-plotted for comparison in figure 2.2, using the axes of gas to liquid flow ratio, $\overline{W}_g/\overline{W}_l$, and the Froude number. In addition, the empirical equation of Weisman and Kang [233] for bubble to slug transition,

AUTHOR	PIPE SIZE	CO-ORDINATE SYSTEM
Griffith and Wallis [89]	25 mm	Flowing gas fraction vs. $(Fr)^2$
Oshinowo and Charles [175]	25 mm	Fr vs. sqr. root of gas to liquid flow ratio
Serizawa et al. [194]	60 mm	Superficial gas velocity vs. superficial liquid velocity
Vallascas [220]	35 mm	Flowing gas fraction vs. $(Fr)^2$ {results for $25^{\circ}C$}
Spedding and Nguyen [208]	45.5mm	Sqr. root of Fr vs. liquid to gas flow ratio
Taitel et al. [217]	50 mm	Superficial gas velocity vs. superficial liquid velocity

TABLE 2.1: AUTHORS OF REGIME MAPS FOR UPFLOW
[Fr is the two phase flow Froude number]

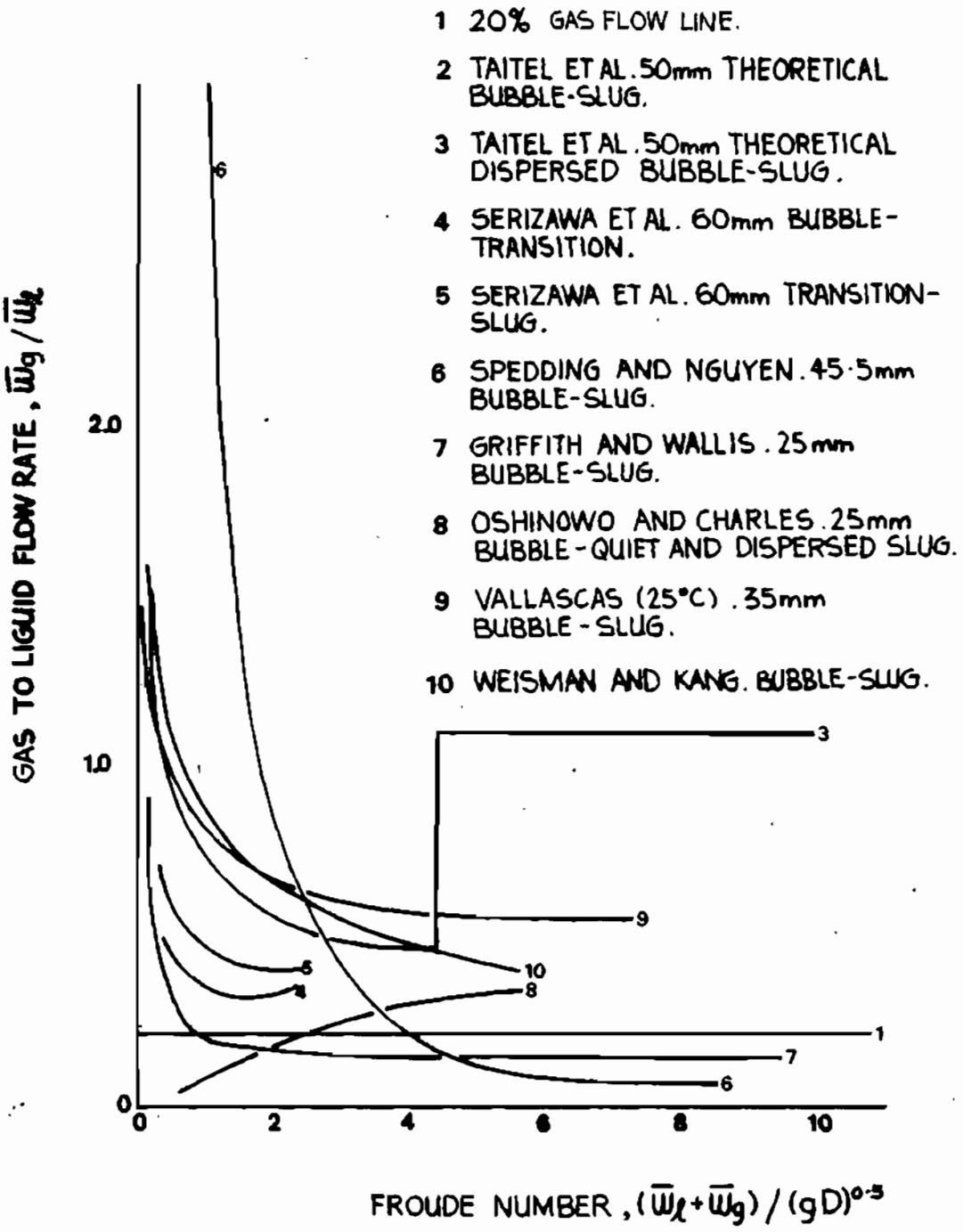

Fig 2·2 • Regime maps in upflow for authors given in table 2.1 •

$$\overline{W}_g/(gD)^{\emptyset.5} = 0.45(\overline{W}_g+\overline{W}_l)^{0.78}/(gD)^{\emptyset.39},$$

has been plotted for the case of a 50 mm pipe.

Little agreement was found among the authors in question, and some explanation of this fact was sought in the literature.

Subjectivity in definition of the transition, and the fact that such transitions may be an order broad [213] would account for some disagreement. Serizawa et al. [194] have defined a transition region to illustrate the broad change from bubble to slug flow patterns. It is also true that values would differ slightly by changing co-ordinate systems: for example, use of the Froude number incorporates an adjustment for pipe diameter, whereas a plot of gas superficial velocity vs. liquid superficial velocity does not. Differences in apparatus and fluid properties between investigators would appear to be a significant factor in the disagreement. Vallascas [220] has shown that fluid temperature affects the transition by altering surface tension. Wallis [227] has commented on the ability of water purity to influence bubble coalescence; such coalescence is certainly discouraged in strong electrolyte solutions [134]. Taitel et al. [217] have emphasized that regime boundaries vary with pipe diameter, so that a map determined on one set of apparatus may not be generalised by use of dimensional substitution.

The method of air introduction into the water stream has a profound effect on the ensuing flow pattern [100]. Herringe and Davis [91,92] have shown that varying cross-sectional void profiles are set up by different spargers, although similar profiles are approached after a large number of diameters. Iida [117] tested three different methods of air introduction to show a dependence of phase interdispersion on sparger design, and Griffith and Wallis [89] acknowledged that their apparatus encouraged the formation of slugs.

Oshinowo and Charles [176] mixed the gas and liquid simply in a copper "tee": this method of gas introduction might be considered to encourage slug formation, especially at low water flowrates, and would provide an explanation for the low transition line illustrated in figure 2.2. A similar method of gas introduction was used by Govier et al. [86] whose transition boundary also occurred at low gas to liquid flow ratios. Spedding and Nguyen [208], who have reported bubble flows at high gas flowrates, employed a more sophisticated mixing section which would have encouraged bubble dispersion. Some tests reported by Siemes [203], and by Zuber et al. [245] have shown the effect of distributor hole size on bubble behaviour in columns of static liquid. While a fine mesh provided a stable cloud of small bubbles up to fairly high voidages,

larger holes in the distributor lead to larger bubbles and subsequent coalescence. However, authors have differed considerably in describing the mechanism of bubble formation and discharge at an orifice [26,125]. The above indicates that the positioning of the regime boundary must be described not only in terms of gas and liquid flowrates, but in terms of fluid properties and arrangement of the apparatus as well. A firm definition of the transition must also be presented in each case.

2.3 VERTICAL DOWNWARD COCURRENT FLOW

2.3.1 FLOW PATTERNS

The study of downward two phase flow is of some interest as it has received far less attention in the literature than upward flow. Indeed, the term "vertical flow" frequently implies only the upward case.

As in upward flow various patterns have been observed [175,208,241]. These are the bubble, slug, froth and annular flows already described, together with a low gas velocity annular-type flow termed "falling film" by Oshinowo and Charles [175] and by Barnea et al. [15] and "wetted wall" by Yamazaki and Yamaguchi [241]. Spedding and Nguyen [208] have included this pattern in the term "annular flow". The term "falling film" is preferred here.

Hewitt and Hall-Taylor [100] have remarked that annular flow is easier to achieve in downflow than upflow, although this is most likely the falling film pattern. Hewitt and Wallis [101] have investigated countercurrent falling film flow.

Spedding and Nguyen [208] found bubbly downflow difficult to achieve, while Oshinowo and Charles [175] referred to the pattern as "bubble-coring" flow, since in downflow they observed that bubbles favoured the core of flow more than in upflow, with the outer liquid annulus almost gas free. It is of interest to note that such a flow appears to be a condition intermediate between a well dispersed bubbly flow and the falling film pattern.

Within the regime defined by gas and liquid flowrates suitable for the narrow bore deep shaft reactor, authors have reported bubble, slug and falling film flows, and transition between all these patterns must be considered.

2.3.2 BUBBLE FLOW BOUNDARY

Other than in recent work by Barnea et al. [14,15,16] no theory or mechanism has been supplied to define the limits of downward bubble flow. There is no reason why the Radovich and Moissis [180] proximity model for upflow may not be employed, since Barnea et al. [15] have extended

the work of Taitel et al. [217] in a similar fashion to the downflow case and have provided comprehensive theory to explain the bubble-slug transition in 25 mm and 50 mm pipes. In addition they have considered the mechanism involved in the falling film-slug transition and proposed a model based on the horizontal flow work of Taitel and Dukler [218].

Some regime maps exist to define the regime boundaries in downflow. Relevant authors and the map co-ordinate systems used are given in Table 2.2 and their boundaries for the regimes in question are given in figure 2.3 on the axes of gas to liquid flow ratio vs. Froude number. Yamazaki and Yamaguchi [241] show no bubble flow boundary as they did not achieve this pattern.

There is little agreement between the authors in the positioning of regime boundaries. As in upflow, fluid properties and configuration of the apparatus may be expected to influence results. Falling film flow may have been encouraged by the peripheral introduction of water in the mixing section used by Spedding and Nguyen [208]. The remaining authors [175,241] found falling film flow to commence only at higher gas rates.

Further investigation of downflow appears necessary for an adequate description of the limits of bubble flow.

AUTHOR	PIPE SIZE	CO-ORDINATE SYSTEM
Oshinowo and Charles [175]	25 mm	Fr vs. sqr. root of gas to liquid flow ratio
Yamazaki and Yamaguchi [240]	25 mm	Flowing gas fraction vs. total superficial velocity
Spedding and Nguyen [208]	45.5mm	Sqr. root of Fr vs. liquid to gas flow ratio
Barnea et al. [15]	51 mm	Superficial liquid and gas velocities

TABLE 2.2: AUTHORS OF REGIME MAPS FOR DOWNFLOW
[Fr denotes two phase Froude number]

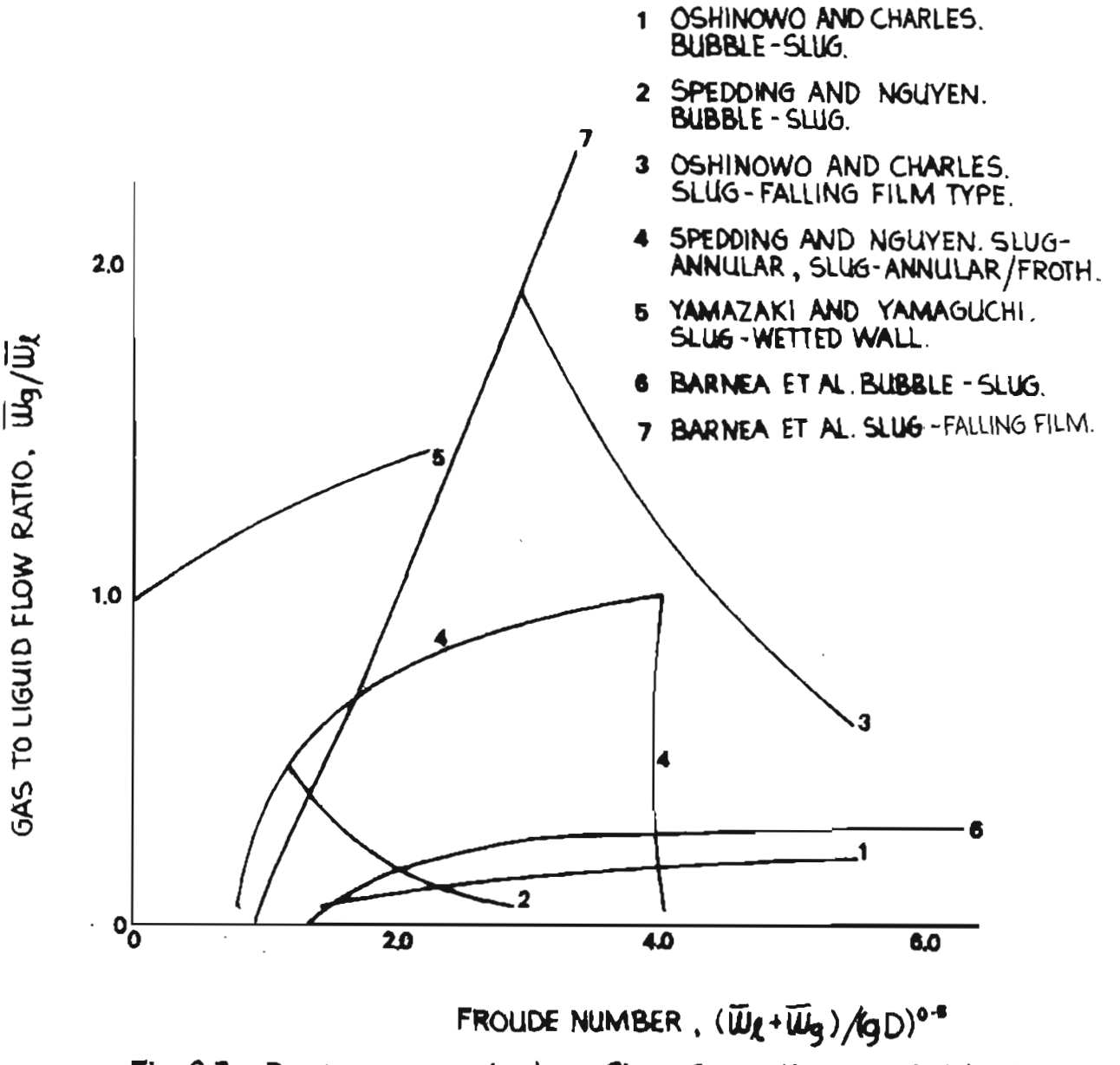

Fig 2.3 • Regime maps in downflow for authors in table 2.2 •

2.4 FLOW IN BENDS

Two phase flow in bends has been investigated by Oshinowo and Charles [175]. Bubble, bubble-slug, and slug flow patterns have been found to persist through a U-bend, which may be used to approximate the flow conditions at a D.S.R. base.

2.5 EXPERIMENTAL WORK

2.5.1 OBJECTIVES

Existing regime maps are inconsistent, with authors differing by up to an order of magnitude in the prediction of the bubble-slug transition in upflow. The method of gas introduction has been quoted as a source of disagreement [100] and it was considered necessary to establish the dependence of regime maps on sparger configuration. Such an investigation would also permit the selection of a sparger type suitable for further investigation into the bubbly flow regime. It is unfortunate that such an investigation must, in large part, be merely descriptive.

2.5.2 APPARATUS (50mm PIPE)

The apparatus illustrated in appendix A was constructed, all pipes and fittings being of a nominal 50 mm bore. A

500 litre tank supplied a Warman C32 centrifugal pump which circulated water through a 17 m downcomer and riser, linked at the base by a 1.5 m horizontal section. Air, metered with rotameters, was introduced via spargers placed in either leg of the apparatus. Glass sections of piping in the riser and downcomer permitted visual and photographic analysis of flow. Most photographs were produced using transmitted, rather than reflected, illumination, as recommended by Collier and Hewitt [60]. Fast flows were "frozen" using an electronic flashgun, although some static bubbling tests were photographed with studio lamps at a shutter speed of 1/1000 second.

Temperature was controlled in the rig by cooling coils in the header tank. The local climate was such as to provide adequately high temperatures.

Three sparger types were initially employed, termed types "A","B" and "C" as illustrated in figures 2.4, 2.5 and 2.6 respectively. In all three types of sparger, air was introduced through 33 holes of 1 mm diameter. In C, these were arranged to be evenly spaced along a circumference of the pipe, so that they were approximately 5 mm apart. In B they were arranged in three vertical banks of 11 holes 5 mm apart, each bank set 120^{o} from the other two in the pipe wall. Sparger A consisted of three similar banks, 120^{o} apart, in a 10mm copper tube set axially in the pipe. All three spargers were fitted together in the 50 mm pipe,

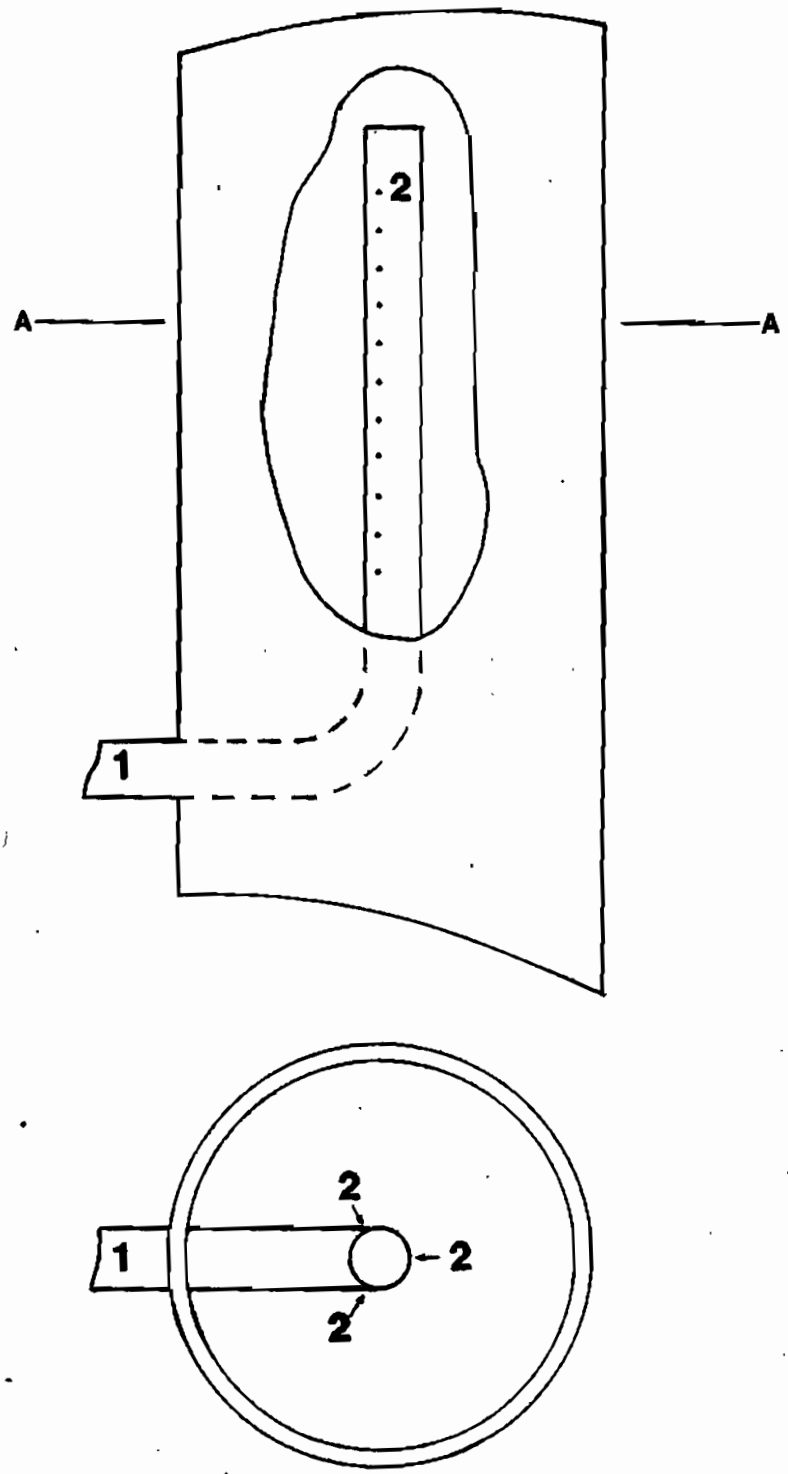

Section A-A

1 GAS INLET.
2 3 ROWS OF 11 HOLES, 1mm DIAM., 5mm SPACING.

Fig 2.4 • Sparger Type A •

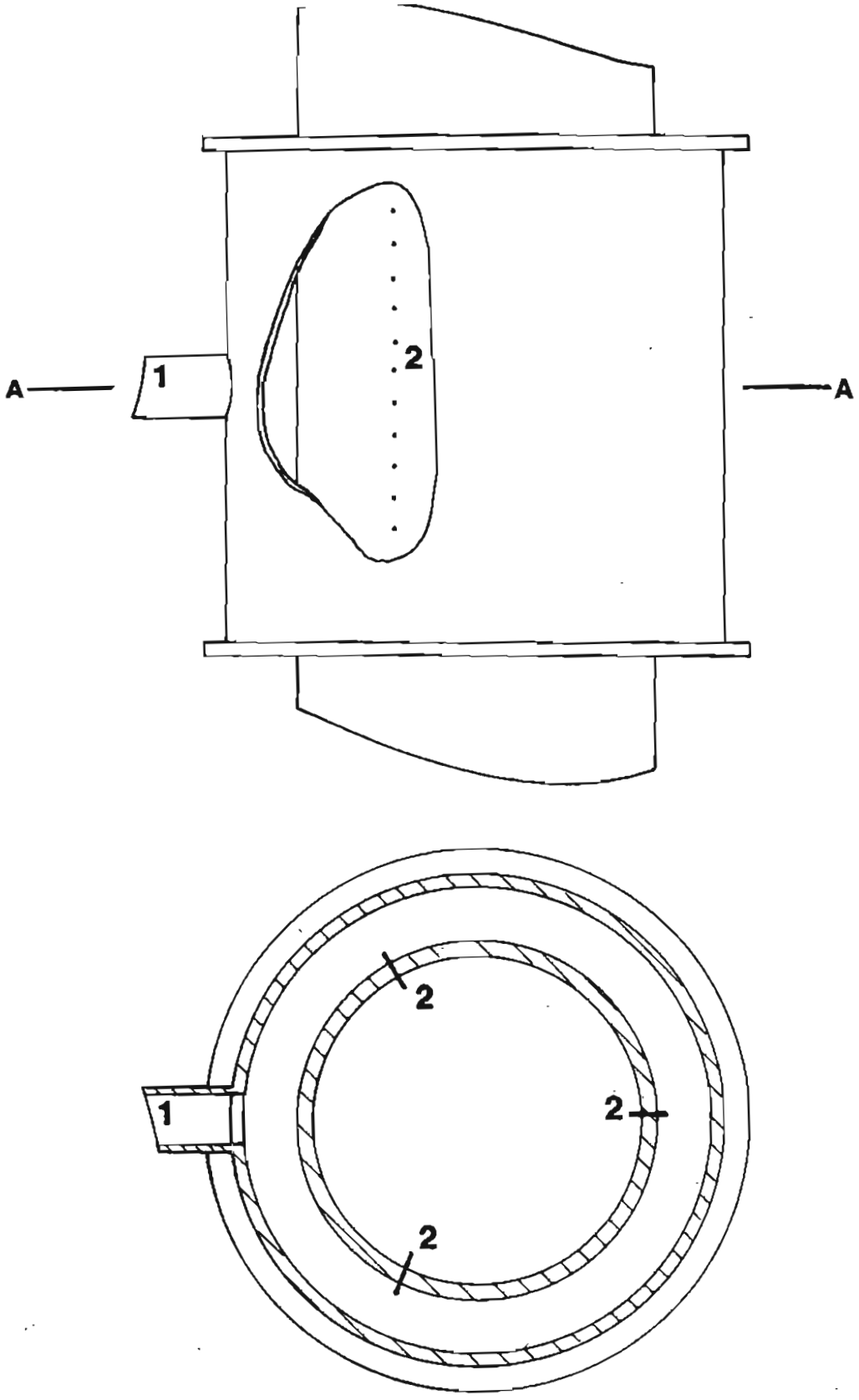

Section A-A

1 GAS INLET
2 3 ROWS OF 11 HOLES, 1mm DIAM., 5mm SPACING.

Fig 2·5 • Sparger Type B •

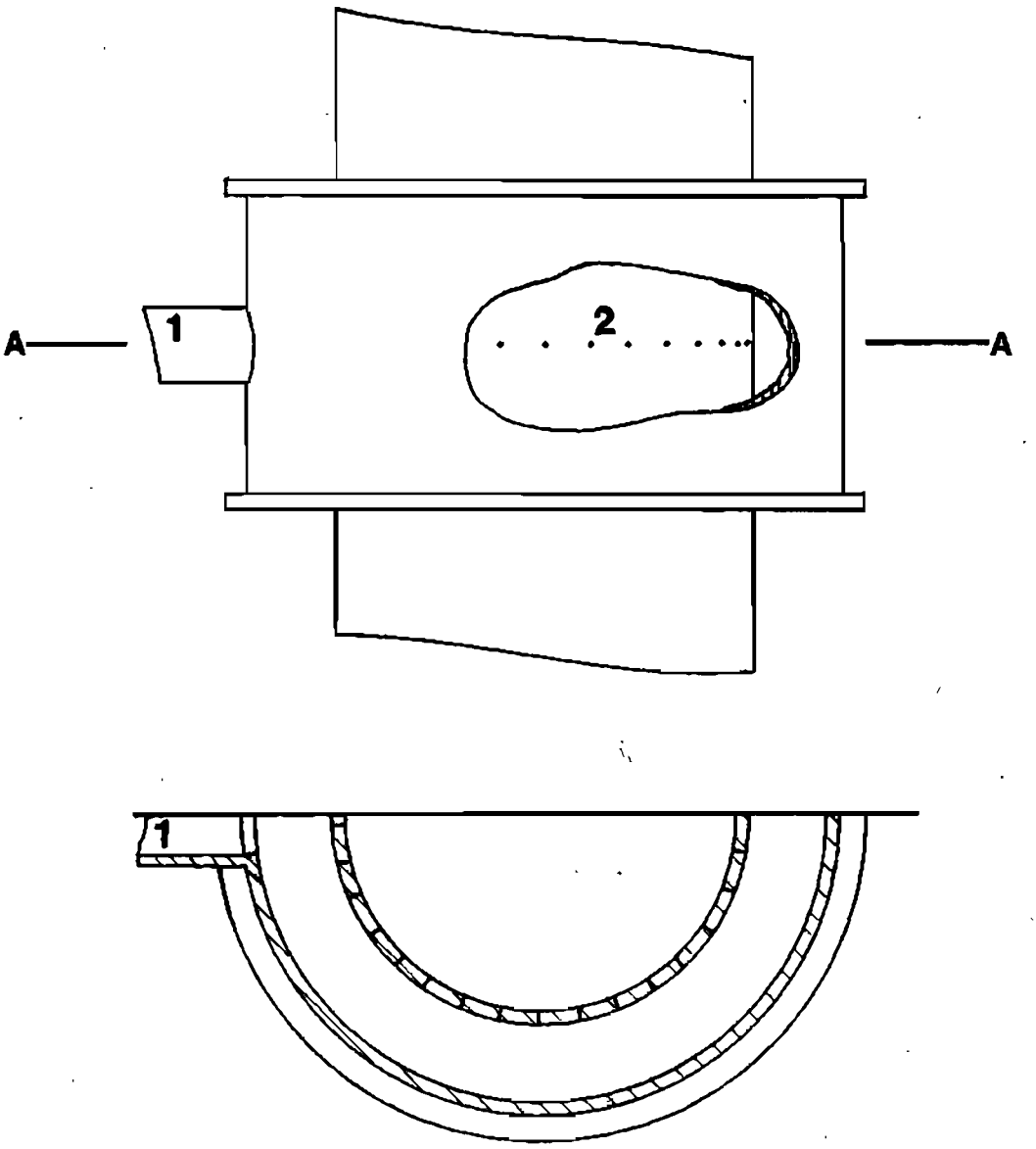

Section A-A

1 GAS INLET
2 1mm HOLES

Fig 2·6 • Sparger Type C •

one above the other.

In addition, some devices were constructed to obstruct the mixture flow at, or downstream of, the sparger, in order to evaluate the effect of increased local turbulence on bubble fragmentation. These were a wire mesh of 2 mm pitch, a plate drilled with 2 mm holes so that only 40% of the pipe cross sectional area remained for flow, and a stream-lined insert of 40 mm diameter which obstructed the flow core to raise fluid velocity. This last device is illustrated in figure 2.7

2.5.3 APPARATUS (100 mm PIPE)

A 100 mm bore, 4 m long, test section described in appendix B was constructed primarily to investigate holdup. However, observations on the bubble to slug flow transition are reported here. The spargers were of similar design to sparger A used in 50 mm flow, but consisted of four parallel 6 mm copper tubes, at constant radius from the pipes axis, and drilled with 1 mm holes. The tubes were 0,5 m long and situated at the base of the apparatus for upflow, and at the top for downflow investigation.

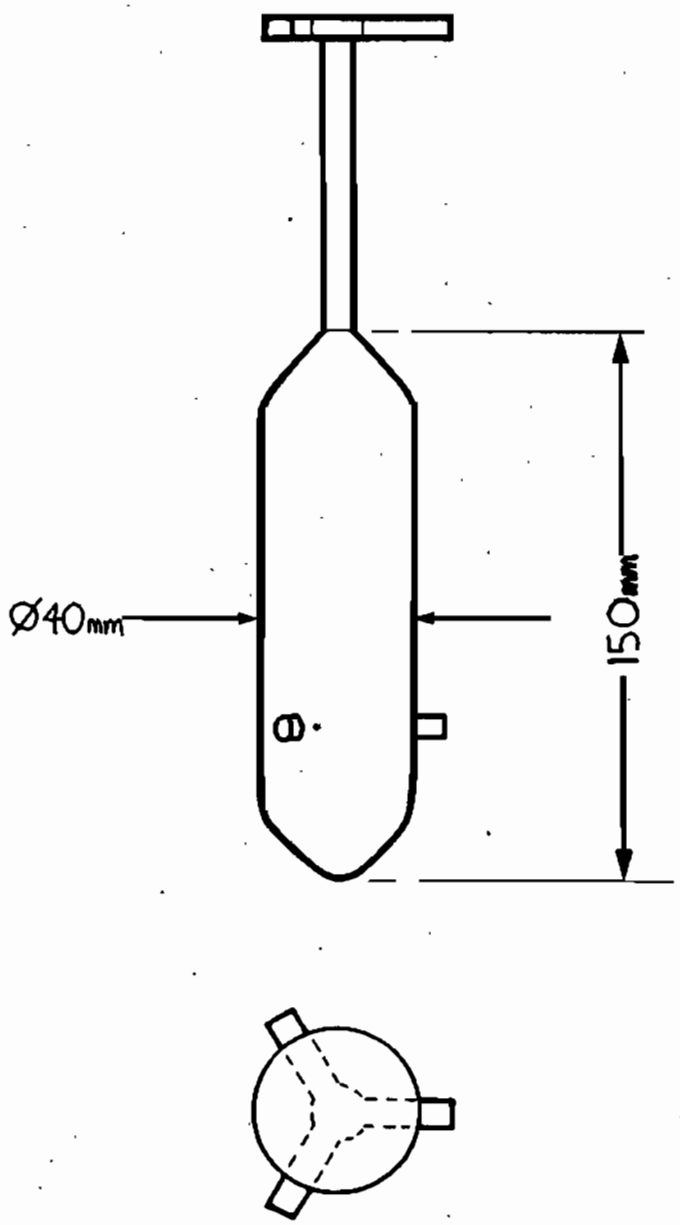

Fig 2·7 • Insert to diminish flow area •

2.6 RESULTS

2.6.1 BUBBLING THROUGH STAGNANT WATER (50 mm PIPE)

The spargers A, B, and C were installed in the 50mm bore rig immediately below a 2 m glass section. A valve in the rig was shut to prevent induced liquid circulation by the air-lift effect. Spargers A and B were observed to produce cap bubbles virtually from the onset of bubbling, while C was seen to maintain ideal bubbling up to a gas superficial velocity of 0.06 m/sec, whereafter an increasing number of slugs was formed. The bubble flows provided by A and B were indistinguishably similar, despite the fact that one represented gas introduction at the wall and the other at the centre. Photographs of the patterns produced by the three spargers are given in figures 2.8 - 2.10.

2.6.2 THE BUBBLE-SLUG TRANSITION IN UPFLOW (50mm pipe)

With water flow held constant, the following changes occurred with increase in gas flowrate. Initially, separate bubbles characteristic of ideal bubbly flow were observed. With increasing gas flow, preferential paths for the bubble rise developed, in a similar way to the channelling formed in fluidized beds. This occurred especially in the case of sparger 'C'. With further increase in gas flow, bubble clusters were observed.

Fig 2·8 • Typical bubble flow produced by sparger A •

Fig 2·9 • Typical bubble flow produced by sparger B •

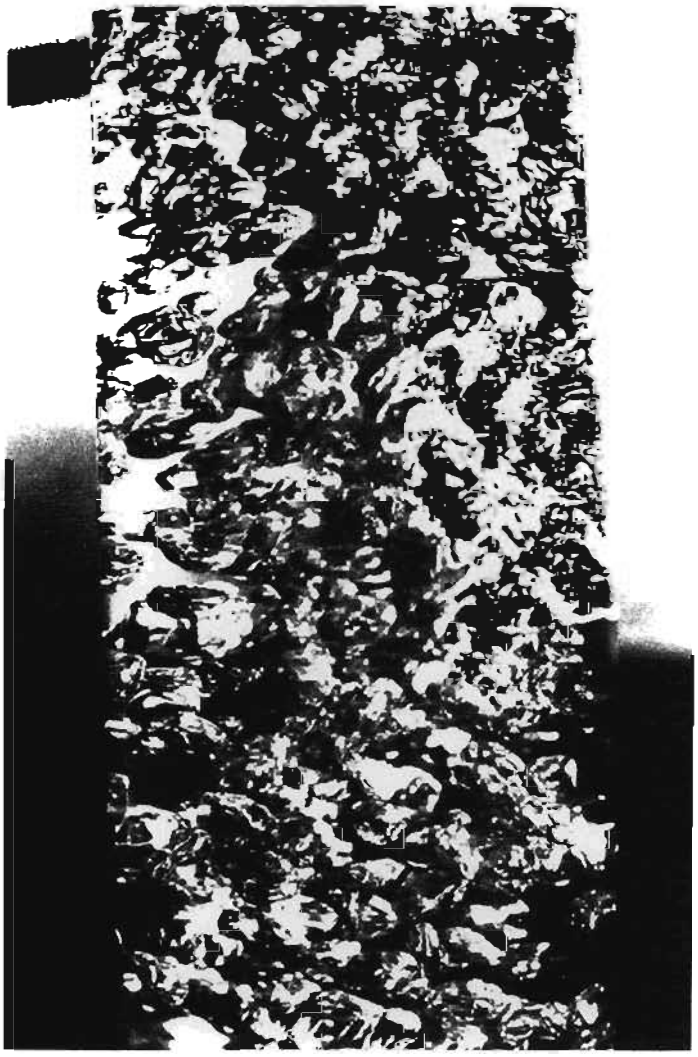

Fig 2·10 • Typical bubble flow produced by sparger C•

These adopted the shape and higher velocity of a cap, and eventually true caps formed by coalescence. At higher gas velocities slugs of increasing length were observed. {The assumption used by Govier and Aziz [85] (see section 2.2.3) that slugs are spaced by seven pipe diameters, was observed to be reasonably well approximated}. At the highest flowrate, slugs lost their distinctive form and frothy slug flow, as described by Oshinowo and Charles [175] was observed.

2.6.3 REGIME MAP IN UPFLOW (50 mm PIPE)

Seven Sparger combinations were tested with various air and water rates as detailed in table 2.3. For each combination the locus of the bubble-slug boundary was determined by visual, and occasionally photographic means. Transition was interpreted as the first appearance of large caps since these spanned nearly the full pipe diameter and formed slugs within a relatively short tube distance. Data were plotted as two phase Froude number vs. the gas to liquid flow ratio.

These boundaries are presented, together with the regime boundaries of Serizawa et al. [194] for purposes of comparison in figure 2.11. The following observations were made.

Spargers A and B appeared very similar in performance.

SPARGER TYPE	WATER SUPERFICIAL VELOCITY (m/sec.)	GAS SUPERFICIAL VELOCITY (m/sec.)
'C'	0.51 - 2.56	0.04 - 1.97
'B'	0.47 - 1.58	0.04 - 1.81
'A'	0.47 - 1.38	0.03 - 1.50
'P' with streamlined insert	0.47 - 1.58	0.03 - 1.05
'A'	0.47 - 1.58	0.03 - 1.05
'A' with mesh	0.47 - 1.58	0.03 - 0.24
'A' with drilled plate	0.47 - 1.18	0.03 - 0.32

TABLE 2.3: TESTS ON SPARGERS IN THE 50 mm DIAMETER APPARATUS (UPFLOW)

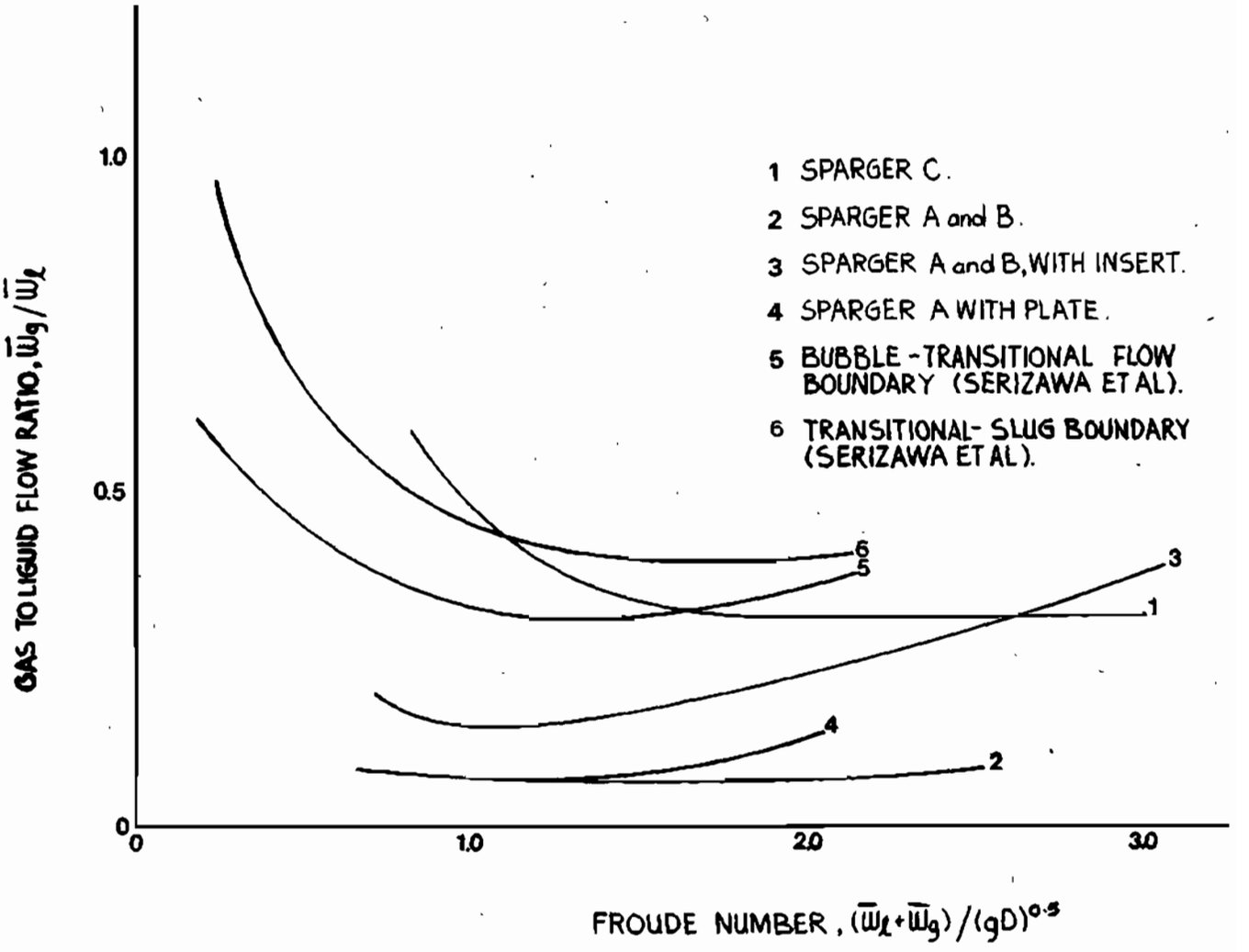

Fig 2·11 • Regime maps in upflow for various spargers (50mm pip

The mesh had no effect in preventing slug formation. The central insert and to a lesser extent the drilled plate suppressed slug formation, especially at higher velocities. It was found that the insert exerted a similar effect whether within or above sparger B, or above sparger A. This suggested that the device was effective due to shearing of bubbles by intense mixing, as in "dispersed bubbly flow" [217], rather than by causing a higher liquid velocity past the sparger orifices, with faster bubble removal. It was concluded that the drilled plate operated on a similar principle, with the flow subject to violent mixing as it passed through the 2 mm holes.

Although, overall, sparger C proved most effective in the range tested, the insert and drilled plate caused smaller bubbles to be formed and trends in the results showed that such devices might become more effective at higher liquid velocities.

2.6.4 REGIME MAPS IN DOWNFLOW (50 mm PIPE)

In downflow, investigation could not be confined to the bubble-slug transition alone as a third regime, the falling film pattern, was observed at even moderate air rates. The position of both the bubble-slug and slug-falling film boundaries were determined.

Spargers A, B and C were tested at liquid flowrates of 0.47, 0.79, 1.18 and 1.97 m/sec. No difference was observed in the performance of the three spargers, all of which provided a satisfactory bubble flow at low air rates. At increased air rates a short length of falling film flow was observed below the sparger. This formed an interface with bubbly flow some distance below the sparger, the bubbles being formed by a process of violent back mixing. Barnea [14] has observed a similar falling film flow close to the sparger in downflow. With increasing gas flow the interface was driven further down the pipe from the sparger and assumed a fairly stable position. Only very occasionally were larger bubbles observed in the flow below the interface, so that no true slug flow was encountered.

It was accordingly impractical to produce a regime map for such an arrangement as flow pattern was clearly dependent on point of observation below the sparger as much as on fluid flowrates. It was of interest to note that whereas Yamazaki and Yamaguchi [241] found difficulty in achieving the bubble flow regime in downflow, in this case slug flow was not achieved. Such a difference must be attributed to the variation in design of apparatus, particularly the sparger. However, Barnea [14] found that the sparger type had little influence on the flow after 10 meters, so that the observed effects may be transitory.

The mechanism of bubble formation in downflow was entirely different from that in upflow, due to the volume of trapped air held below the sparger at higher air rates. This short length of falling film flow was considered to be an afterbody effect induced by the presence of the axial copper tube in sparger A, and the introduction of air over a short distance, so that a standing bubble formed.

To investigate this hypothesis a longer sparger, termed D, was constructed. Two 6 mm copper tubes, each 0,45 m long, were fitted one above the other at the pipe axis, in a similar way to sparger A. Each was randomly drilled with 100 0,5 mm holes. The 6 mm copper tube along the pipe axis was chosen to be thinner than the 10 mm tube used in sparger A. The introduction of air over a greater length of pipe reduced the afterbody effect. Film flow was observed only at very high air rates in the apparatus. A regime of bubbly-slug flow was also observed at air rates below those required for falling film flow. A regime map, figure 2.12, was prepared to describe the performance of this sparger. Since there was still a stable afterbody effect for a small range of gas rates at transition to falling film flow, it is necessary to state that the map was obtained for an observation point 1 m below the sparger.

The presence of a short falling film flow near the sparger

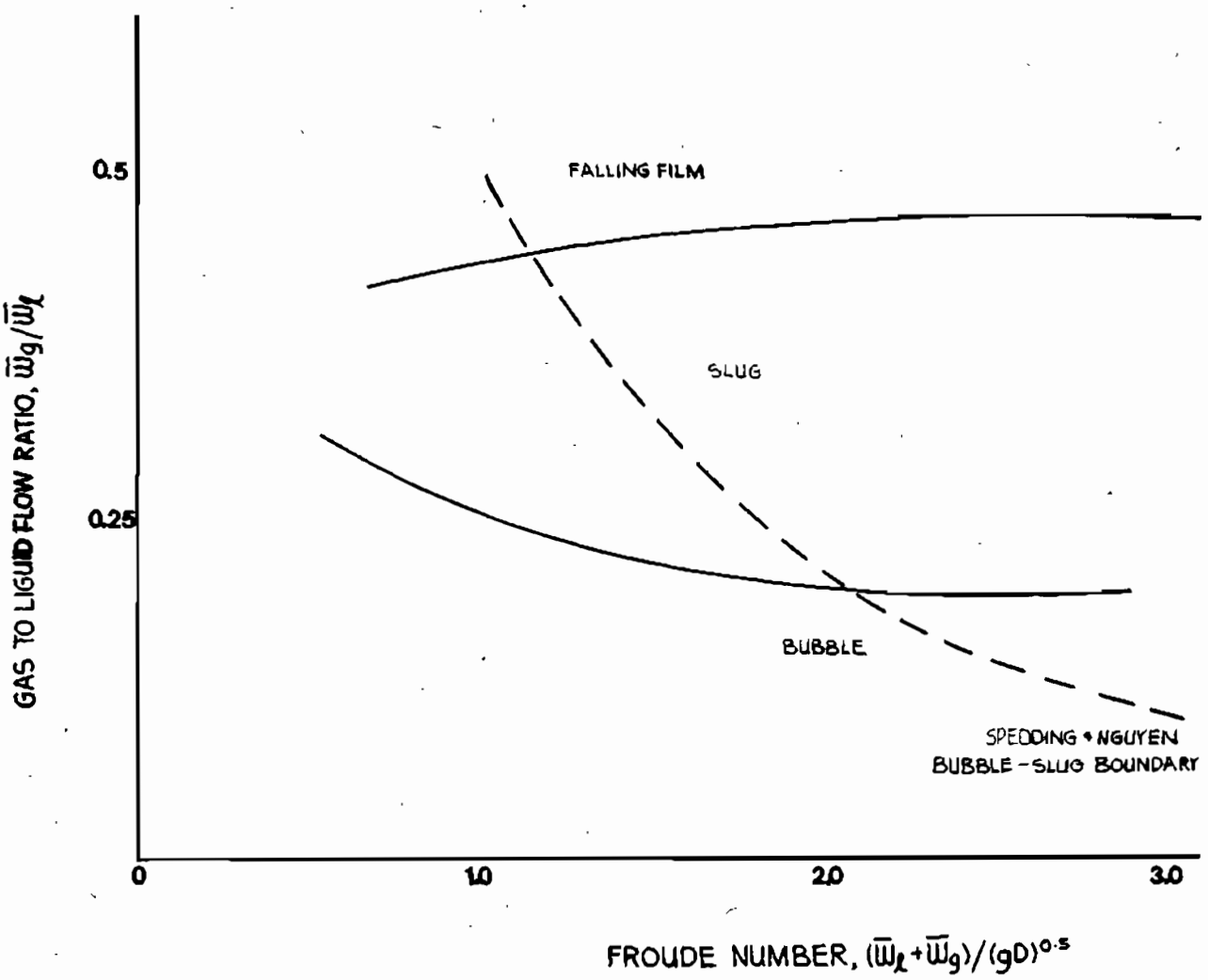

Fig 2·12 • Regime map for downflow (50 mm pipe) •

may also be ascribed to the development of high voidage areas within the sparger section. The liquid velocity near a sparger orifice, whether the orifice is at the wall or situated on a tube in the flow, will be lower than the average liquid velocity in the pipe. The fact that bubble rise velocity is opposed to the direction of flow, and that the flow velocity is low near the orifice, will cause a bubble which has recently detached from an orifice to be carried away from the orifice at a slower velocity in downflow than would be the case in upflow. Thus, if bubble removal from the orifice is retarded in downflow, this may lead to local coalescence near the orifice, and the eventual formation of a standing bubble in the sparger. Certainly local bubble coalescence and fragmentation may occur near an orifice [26]. By introducing the air over a greater pipe length, local coalescence of bubbles might be reduced. However, a detailed study of this phenomenon is not within the scope of this thesis.

2.6.5 RESULTS (100 mm PIPE)

Description of the bubble-slug transition must differ in larger bore pipes as there is a greater difference between the onset of cap bubble formation and the production of slugs which span the whole tube diameter. Serizawa et al. [194] found the need to declare a transition zone in investigating a 60 mm pipe.

In the 100 mm pipe, caps produced at moderate air rates were able to persist over the test length without forming slugs. Only at higher gas rates was sufficient gas present in a local area to form slugs spanning the pipe width. Clearly in the extreme of a very large pipe (or bubble column) true slugs may never form.

The upflow regime map for the 100 mm pipe, figure 2.13, illustrates the transition zone by giving the loci of the first appearance of caps, and the first formation of slugs. It was noted that the sparger encouraged the formation of caps in a similar way to sparger A used in the 50 mm diameter apparatus.

In downflow, the afterbody effect was pronounced. It is proposed that this is due to the large volume of air which must be added through a relatively shorter sparger to achieve significant voidages. In addition, the four copper tubes of the sparger presented a considerable obstruction to the flow. The falling film-bubble flow interface was less stable than in the case of a 50 mm pipe and it was found to be impossible to plot a reproducible regime boundary. Bubble flow was certainly stable in downflow at gas voidages of up to 20%.

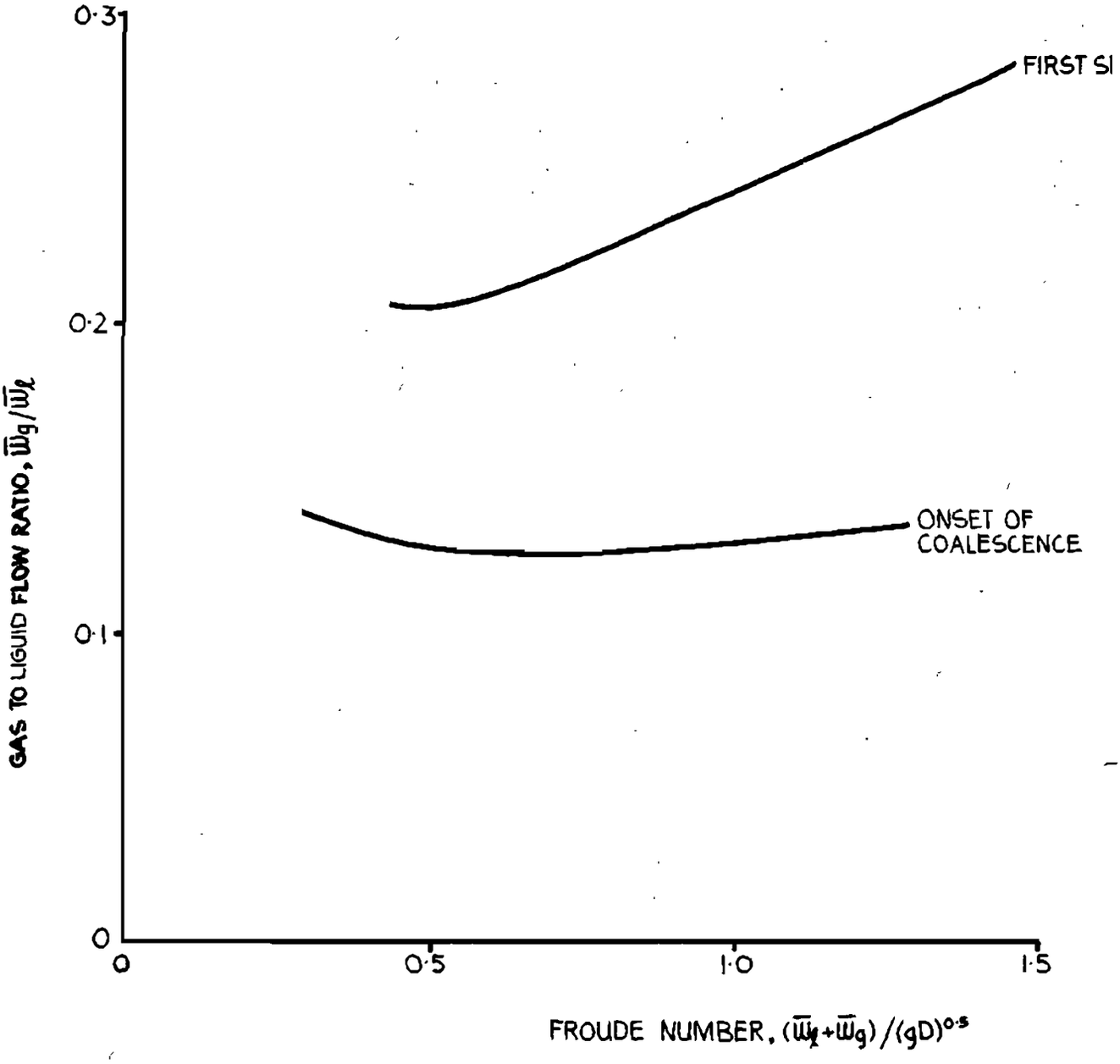

Fig 2·13 · Regime map for upflow (100mm pipe) ·

2.7 CONCLUSION

In vertical flow the bubble-slug transition is far less predictable than in horizontal flow, where most authors agree on positioning of regime boundaries [149]. Whereas in horizontal flow transition is governed to a greater degree by the hydrodynamics of the flow (balance between gravitational and turbulent forces on the bubble), in vertical flow it is strongly influenced by the bubble size distribution. A wide size distribution is likely to contain bubbles of slightly different rise velocities, and this will lead to bubble-bubble collision and coalescence. The bubble size distribution is dependent on the sparger design, and on the fluid behaviour in the region directly downstream. A method of gas introduction which encourages local areas of high voidage may lead to coalescence near the sparger. For upflow this is the failing of spargers introducing air through a set of holes along the line of flow, as with spargers A and B tested above.

It would appear that a sparger may operate satisfactorily in downflow by a completely different mechanism. Bubble downflow, certainly at higher velocities, is formed by transition from a short falling film flow by a mechanism of violent mixing. The cause and hydrodynamics of this interface are not fully understood. This method of bubble formation does, however, imply that bubble size distribution is largely independent of sparger

configuration. Suitable spargers in the downflow case should concentrate on minimising the length of falling film flow, as clearly this pattern is undesirable in the D.S.R. It is plausible that some spargers, with wide orifice spacing and low superficial velocities at each orifice, may operate without the interim falling film flow, but none was encountered in this study. It is unlikely that the problem of falling film flow occurs in pipes of very large diameter, as no such problem has been reported in discussions on large bore D.S.R.'s. In this study falling film flow was found to endure for a shorter distance when air was introduced over a greater pipe length.

No extensive study was carried out on gas introduction in the 1ØØ mm pipe. The spargers used appeared satisfactory for use in holdup work, as for the void fractions used no falling film flow reached the test section.

2.8 LIST OF VARIABLES

D	Pipe diameter (m)
g	Acceleration due to gravity (m sec^{-1})
$\overline{W}_g$	Gas superficial velocity (m sec^{-1})
$\overline{W}_l$	Liquid superficial velocity (m sec^{-1})

CHAPTER 3

3. HOLDUP : THE PREDICTION OF VOID FRACTION

Prediction of gas holdup, the volumetric fraction of gas present in the flowing mixture, is of central interest in DSR design. The gas holdup determines the hydrostatic pressure head in the reactor and influences the frictional pressure losses, the nature of flow interdispersion, and the interfacial surface area available for gas-liquid mass transfer in the reactor. Although many models for the prediction of holdup have been proposed, few prove applicable in the case of two phase bubble downflow, as encountered in the DSR.

3.1 DEFINITIONS

Let the gas and liquid phases have local velocities relative to the pipe given by U_g and U_l respectively, and let the local gas void fraction be E. When the term "local" is taken to the extreme of a single point, clearly either gas or liquid may be present at any one time, t. Several authors [75,121,163] have chosen to evaluate the gas void fraction, E, at a point, as the integral average over some period of time of $\delta(t)$, where

$\delta(t) = 0$ if liquid is present at the point at time t

and $\delta(t) = 1$ if gas is present at the point at time t

This method has not been explicitly employed here, as it is not considered useful in this study of cross sectional average quantities. The application of time-averaged quantities is discussed by Delhaye [71].

Gas and liquid fluxes, or superficial velocities, are given by

$$W_g = EU_g, \text{ and}$$

$$W_l = (1-E)U_l \qquad 3.1$$

and the total flux by

$$W_m = W_g + W_l \qquad 3.2$$

The local relative velocities between the phases, often referred to as local slip velocities, are

$$U_{gl} = U_g - U_l, \text{ and}$$

$$U_{lg} = U_l - U_g \qquad 3.3$$

so that

$$U_{lg} = -U_{gl} \qquad 3.4$$

The difference between phase velocity and total flux is referred to as drift velocity. Drift velocities for the two phases are given by:

$$U_{gm} = U_g - W_m, \text{ and}$$

$$U_{lm} = U_l - W_m \qquad 3.5$$

The instantaneous average over the pipe cross-sectional area, A_p, of some quantity q, is denoted by $\bar{q}$ and defined as

$$\bar{q} = \int_{A_p} q \, dA \qquad 3.6$$

We may define average gas, liquid and total fluxes in this way, and relate them to the gas, liquid and total volumetric flowrates in the pipe, given by Q_g, Q_l and Q_m respectively.

$$\bar{W}_l = Q_l/A_p$$

$$\bar{W}_g = Q_g/A_p$$

$$\bar{W}_m = (Q_l + Q_g)/A_p \qquad 3.7$$

In order to clarify the use of these relationships in two phase flow, it is convenient to consider a conceptual experiment due to Nicklin [165]. Consider figure 3.1. {Some of the relationships presented below require an assumption of constant properties across the vessel cross-section. This is further discussed in the analysis of Zuber and Findlay [243].} Nicklin's case (i) examines a vessel, of cross-sectional area A, containing liquid through which a gas is bubbled at a constant flowrate Q_g. No liquid flow occurs.

$$Q_l = \emptyset$$

The fluxes are - $\overline{W}_g = Q_g/A,$

$$\overline{W}_l = \emptyset,$$

$$\overline{W}_m = Q_g/A$$

The velocities are -

$$\overline{U}_g = \overline{W}_g/\overline{E}$$

$$\overline{U}_l = \emptyset$$

The slip velocity is found to be -

$$\overline{U}_{gl} = \overline{U}_g - \overline{U}_l = \overline{U}_g$$

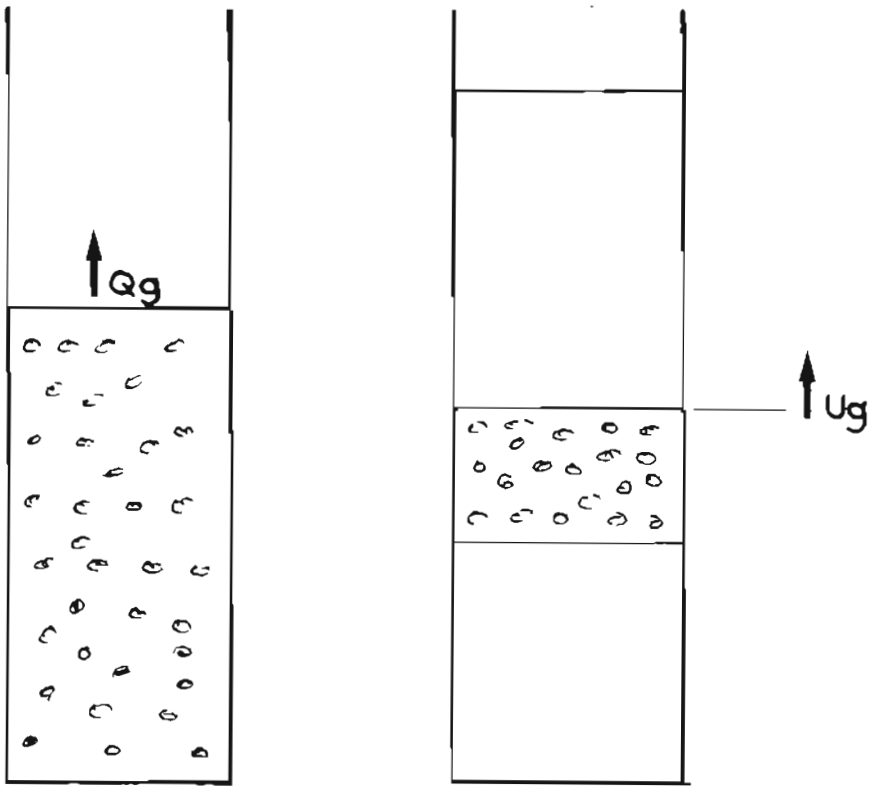

CASE (i) bubble column CASE (ii) rising swarm of bubbles

Fig 3·1 • Nicklin's conceptual experiment •

The drift velocities are

$$\bar{U}_{gm} = \bar{U}_g - \bar{W}_m$$
$$= \bar{U}_g(1 - \bar{E})$$

$$\bar{U}_{lm} = \bar{U}_l - \bar{W}_m$$
$$= -\bar{U}_g\bar{E}$$

In Nicklin's [165] case (ii), a finite group of bubbles rises in a pipe of cross section A. The nett flowrate is zero and water must flow back past the bubbles to permit their rise.

Here $Q_g = -Q_l$

Hence $\bar{W}_g = -\bar{W}_l$, $\bar{W}_m = 0$

The velocities are related by -,

$$\bar{U}_g\bar{E} = -\bar{U}_l(1-\bar{E})$$

and the drift velocities are

$$\bar{U}_{gm} = \bar{U}_g, \text{ and}$$

$$\bar{U}_{lm} = \bar{U}_l$$

The local slip velocity is given by

$$\overline{U}_{gl} = \overline{U}_g - \overline{U}_l$$

$$= \overline{U}_g - (-\overline{U}_g\overline{E})/(1-\overline{E})$$

$$= \overline{U}_g(1-\overline{E})$$

In both cases the gas phase drift velocity, $\overline{U}_{gm}$, and the local slip velocity, $\overline{U}_{gl}$, are related by the equation

$$\overline{U}_{gm} = \overline{U}_{gl}(1-\overline{E}) \qquad 3.8$$

Some further quantities frequently used in two phase flow are defined below.

The flowing gas concentration, B, is given by,

$$B = \overline{W}_g/(\overline{W}_g + \overline{W}_l)$$

$$= Q_g/(Q_g + Q_l)$$

The quality, x, of a flow, refers to the mass fraction flowing in the gas phase.

$$x = M_g/(M_g + M_l)$$

where M_g, the mass flowrate of gas, is given by the product $Q_g \rho_g$, and $M_l = Q_l \rho_l$

Wallis [227] has defined a drift flux, given by

$$W_{gm} = E(U_g - W_m) = E\ U_{gm} \qquad 3.9$$

for the gas phase, and

$$W_{lm} = (1-E)(U_l - W_m) = (1 - E)U_l \qquad 3.10$$

for the liquid phase.

3.2 SURVEY OF MODELS USED TO DESCRIBE HOLDUP

3.2.1 INTRODUCTION

In two phase flow, the average gas void fraction present in the pipe, $\bar{E}$, is not necessarily equal to the flowing gas fraction, B, based on volumetric flowrate. This is due to the effect of gravity which causes local slip between phases and due to the interaction of the velocity and phase distributions. Much attention has been devoted to the prediction of the voidage $\bar{E}$, particularly in vertical upward [31,85,96,227] and horizontal [31,112,118] flows. Vertical downward and inclined configurations have received a good deal less attention [148,164,241]. In general models have been proposed to describe the average

void fraction, $\overline{E}$, as a function of gas and liquid fluxes.

$$\overline{E} = \overline{E}(W_g, W_l)$$

while others have supplied the information equivalently as the holdup ratio, H

$$H = \overline{U}_g/\overline{U}_l \; ; \; H = H(\overline{W}_g, \overline{W}_l)$$

or as the slip velocity,

$$S = \overline{U}_{gl} = \overline{U}_g - \overline{U}_l \; ; \; S = S(\overline{W}_g, \overline{W}_l)$$

Although some predictive methods have been proposed for a specific flow regime, others have claimed to be independent of phase dispersion. Only the cases of vertical up and down bubble flow are of interest in this study.

3.2.2 THE MARTINELLI CORRELATION

The correlation due to Martinelli and co-workers [147,154] has frequently been used to predict the gas phase voidage, and has been a standard comparison for several subsequent models [119,143,205,242].

A parameter X^2 was defined as the ratio of the frictional pressure drop which would occur if the liquid phase were

flowing alone in the pipe to the frictional pressure drop which would occur if the gas phase were flowing alone. The gas and liquid void fractions, $\overline{E}$ and $(1-\overline{E})$, were presented as a graphical correlation in the parameter X.

No effect of flow regime was considered, which renders the correlation insufficiently accurate for precise work on deep shaft reactors, although in its time the correlation was recommended for predictions of voidage in air-lift pumps [147].

3.2.3 FURTHER EARLY WORKERS

Govier et al. [86] published comprehensive data on the holdup ratio for air-water flow in a 25 mm tube, and considered its relationship to pressure drop. The data were relevant to the specific apparatus, and the results are not readily extended to predict holdup in larger pipes. Correlations have been produced by Ros [188] and by Hughmark and Pressburg [116] to cover a wide range of fluid properties, and more models of this type are discussed by Govier and Aziz [85]. In considering the deep shaft reactor, it is advisable to seek a model based solely on air-water flow, rather than broad correlations of this type.

3.2.4 MODELS OF LEVY, ZIVI AND SMITH

Levy [143] used mixing length theory to predict the holdup ratio and density distribution for both horizontal and vertical flow. Solution of the model in the case of vertical flow with gravity effects is somewhat laborious and is not specific to the bubble flow regime. This model is distinct from the momentum exchange model due to Levy [142] which was developed to predict slip for steam-water flow over a wide pressure range.

Zivi [242] proposed a method for predicting void fractions in steam-water flow using a principle of minimum entropy. The derivation was based on annular and annular-droplet flow and is unsuited to bubble flow conditions.

Smith [2Ø5] proposed a model which assumed that the gas and liquid flowed in a homogenous two phase mixture zone surrounded by an annulus of liquid. The velocity head was equated for the two regions and a correlation was produced in the variable, K_s, defined as the ratio of liquid flowing in the mixture zone to that in the liquid zone. Good general correlation was obtained with both air-water and steam-water flow, using K_s=0,4. However, it is noted that as the flowing gas concentration approaches zero, the velocity of the liquid zone approaches that of the mixture zone. This implies that the model does not take local slip into account at the low voidages encountered in the

bubble flow regime, and is therefore unsuited to D.S.R. design.

3.2.5 YAMAZAKI MODEL

Yamazaki and Shiba [238] presented an empirical equation which is not suited to upward flow at low voidages, and took no account of local slip. A simpler formula was subsequently presented by Yamazaki and Yamaguchi [240], viz.

$$\bar{E}/B = (1 - \bar{E})(1 - K_y\bar{E})/(1 - B)$$

Where K_y is a constant, typically 1. As with the formula of Smith [205], the equation predicts no slip for very small voidages. The equation was extended to the case of downward flow [241], where K_y was found to approach 1 only at high gas flowrates ($B > 0.6$), and was strongly dependent on B, the flowing gas fraction, at voidages typical of the bubble flow regime. This may be interpreted as an inability of the model to explain local slip in the downflow case, and some similarity exists in this respect between the Yamazaki model and the model of Bankoff [13], which is discussed below.

3.2.6 MODELS CONSIDERING ONLY LOCAL SLIP

Behringer [23] in 1936 proposed that the velocity of a

bubble in an upward flowing gas liquid mixture was equal to the sum of the mixture velocity and the slip velocity of a bubble in an infinite continuum, U_z.

$$\overline{U}_g = Q_g/A + Q_l/A + U_z$$

Nicklin et al. [167] reached a similar conclusion in extending slug flow theory to the bubble flow regime. Nicklin [165], Brodkey [31] and Wallis [227] have shown that U_z in the formula above should be replaced by the general term $\overline{U}_{gm}$, the gas drift velocity relative to the mixture, which is related to the local slip velocity, $\overline{U}_{gl}$, by the formula

$$\overline{U}_{gl} = \overline{U}_{gm}/(1-\overline{E}) \qquad \text{(see equation 3.8)}$$

This model has found use in the analysis of bubble columns [146] and various formulae are available to predict $\overline{U}_{gm}$ from the bubble rise velocity and voidage, with a knowledge of the nature of bubble interaction [146,227].

The local slip model will frequently provide voidage prediction superior to many more sophisticated models, especially at low flow velocities, but finds limitation at higher flow velocities where the nature of phase interdispersion affects holdup more significantly.

This model should prove readily extendable to the downflow

case, where the sign of the drift velocity term changes relative to the direction of flow.

3.2.7 MODELS CONSIDERING ONLY PROFILE EFFECTS

In two phase bubble flow, the interaction of the void and velocity distributions across the pipe diameter will have a profound effect on the average holdup in the pipe [51]. For example, if the gas phase is concentrated at the pipe center, where the flow velocity is high, the average gas velocity will be higher than if the gas were distributed uniformly across the pipe, or concentrated near the wall, where the flow velocity is lower. In this way the voidage distribution may interact constructively with the velocity distribution across the pipe diameter so that the gas phase has a higher average velocity than the liquid phase, and this in turn alters the holdup ratio of the flow.

Bankoff [13] chose to assume that local slip was negligible in two phase flow, and assumed power law relationships for both voidage and velocity profiles across the pipe.

$$U/U_c = (r/R)^{1/m}$$

$$E/E_c = (r/R)^{1/p}$$

where the subscript, c, refers to the condition at the

pipe centre, r is the radial distance from the pipe centre, and R is the pipe radius. By integrating over the pipe cross-section it was shown that these profiles implied the relationship

$$\overline{E} = K_b B$$

where $K_b = 2(m+p+mp)(m+p+2mp)/(m+1)(2m+1)(p+1)(2p+1)$, and is known as the "Bankoff K factor". This was acknowledged by Bankoff [13] as being equivalent to an empirical constant "C" used by Armand and in the correlations of several Russian authors [29].

Values for K_b have been presented in the literature [29,189], and Bankoff has suggested a relationship with pressure for predicting holdup in steam-water flows. Hughmark [113] has considered a correlation for K_b based on Reynolds and Froude numbers for horizontal and vertical upward flow.

The Bankoff [13] method fails at low velocities where local slip becomes significant. It may, however, be accurately applied at high velocities where such slip is negligible, or in horizontal flows, where the gravitational effect causing slip disappears.

3.2.8 MODELS INCORPORATING SLIP AND PROFILE EFFECTS

Several authors have perceived the benefits of combining the slip and profile effects into a unified model to describe holdup over a wide range of gas and liquid flowrates.

Aoki et al. [9] modified the Bankoff K factor to incorporate slip as a function of radial position. For the assumption of no slip the Aoki model reduces to the Bankoff equation.

A drift-flux model due to Nicklin et al. [167] was developed to describe holdup in slug flow, and has been applied to air-lift pump design [56,57,166]. Nicklin's concept was extended to the general case of two phase flow by Zuber and Findlay [243,244] who proposed a drift-flux equation

$$\overline{W}_g/\overline{E} = C_o(\overline{W}_g+\overline{W}_l) + \overline{E\vec{U}}_{gm}/\overline{E}$$

where C_o is a measure of profile interaction and $\overline{E\vec{U}}_{gm}/\overline{E}$ is a term which accounts for local slip.

The drift-flux model has been used to describe both bubble and slug flow, and has even been extended to predict holdup in pneumatic transport [209]. The model has gained wide acceptance in the literature [47,48,85,162,163,178]

and has been employed in the analysis of high pressure steam-water flow [10,244].

Bhaga and Weber [24,25] have proposed an equation similar to that of Zuber and Findlay [244],

$$\overline{W}_g/\overline{E} = C_o(\overline{W}_g+\overline{W}_l) + \overline{U_{gl}E(1-E)}/\overline{E}$$

where slip is given in terms of the relative phase velocity. This may, however, be reduced readily to the Zuber and Findlay form.

Brown et al. [33] have assumed parabolic rather than power-law profiles to develop the equation

$$\overline{U}_g/\overline{U}_l = U_b/\overline{U}_l + (1 - \overline{E})/(K_p - \overline{E})$$

where K_p is a function of profile interaction, similar to the Bankoff K factor, and U_b is a "bubble rise velocity". This equation may be rewritten

$$\overline{W}_g/\overline{E} = (1/K_p)\overline{W}_m + U_b(K_p - \overline{E})/K_p$$

in which case it exhibits a form similar to the equation of Zuber and Findlay, with $1/K_p$ analogous to C_o. The slip term does, however, differ from that of Zuber and Findlay, and would appear not to be the product of a rigorous analysis.

Of all the models discussed above, the Zuber and Findlay [243] drift-flux model appears to have gained widest acceptance [108]. By incorporating both slip and profile effects in a simple fashion, holdup is readily described by this method. Specific values for C_o and for the drift velocity term are discussed in detail below.

3.3 DISCUSSION OF THE DRIFT-FLUX MODEL

3.3.1 DERIVATION

In dealing with two phase pipe flow one is dealing with a modified case of Nicklin's conception model (described in section 3.1), with liquid flow superimposed. The drift-flux model of Zuber and Findlay [243] may be derived concisely as follows.

By definition, the gas velocity is equal to the sum of the total flux and gas drift velocity,

$$U_g = W_m + U_{gm}$$

multiplying by E and averaging over the cross-section,

$$\overline{U_g E} = \overline{W}_g = \overline{W_m E} + \overline{U_{gm} E} \qquad 3.11$$

dividing by $\overline{W_m E}$ and setting

$$C_o = \overline{W}_m\overline{E}/(\overline{W_m E}) \qquad 3.12$$

one obtains

$$\overline{W}_g/\overline{W}_m\overline{E} = C_o + \overline{EU}_{gm}/\overline{W}_m\overline{E} \qquad 3.13$$

multiplying by $\overline{W}_m$,

$$\overline{W}_g/\overline{E} = C_o\overline{W}_m + \overline{EU}_{gm}/\overline{E} \qquad 3.14$$

which may also be expressed as

$$B/\overline{E} = C_o/\overline{E}\overline{W}_m + \overline{EU}_{gm}$$

The second term on the right hand side of equation 3.14 is termed the "weighted average drift velocity" [243] and, in predicting holdup, takes account of the relative velocity between phases and of the voidage profile. The constant C_o takes account of the interaction between velocity and void profiles (distributions).

Zuber et al. [245] have argued that these distributions are best represented by radial power-law relationships

$$W_m/W_{mc} = (r/R)^{1/a} \qquad 3.15$$

$$(E - E_w)/(E_c - E_w) = (r/R)^{1/b} \qquad 3.16$$

where c and w denote values at the pipe centre and wall respectively and R is the pipe radius.

From equations 3.12, 3.15 and 3.16, C_o is given by

$$C_o = 1 + 2ab(1 + E_w/\bar{E})/(a + b + 2ab) \qquad 3.17$$

Often it is assumed that the gas voidage tends to zero exactly at the pipe wall, so that E_w is taken as zero in equations 3.16 and 3.17.

For negligible drift velocity it may be shown that

$$1/C_o = K_b,$$

the Bankoff K- factor.

3.3.2 VALUES FOR C_o AND FOR THE DRIFT FLUX TERM

Provided that C_o and the drift flux term can be evaluated, holdup may be predicted readily from a knowledge of gas and liquid fluxes. Values for C_o have been presented for a variety of flow types and channel sizes in the literature [10,47,51,81,85,162,227,243-245]. Usually $1 < C_o < 1.5$, although C_o may assume higher values if the void profile is such that the gas voidage tends to zero some distance from the wall. Typically C_o is acknowledged as having values between 1 and 1.3 in most gas-liquid bubble

flows and the opinions of various authors are presented in Table 3.1

The value of the profile constant C_o will depend on flow regime to a significant degree. For purposes of holdup prediction, two distinct types of bubble flow must be identified, and have been separately defined in the literature [10,123,190,227,243]

(i) Ideal bubble flow

Bubbles have uniform size and velocity, and no interaction occurs between bubbles. No coalescence occurs and void profiles tend to be flat, so that C_o assumes a value close to unity. In practice, ideal flow is difficult to achieve, especially at higher voidages, and will be strongly dependent on method of gas introduction [203,245]. This has also been termed regime "B" [161] and "Mode 1" flow [167].

(ii) Churn-turbulent bubble flow

Churn-turbulent flow is characterised by a range of bubble sizes, and by bubble interaction in the form of channeling and waking, where a small bubble will rise fast within the wake of a large bubble or bubble train. This type of flow has been regarded as intermediate between ideal bubble and slug flow (see comments in ref. 243) and has been termed regime "A" [161] and "Mode II" flow [167].

AUTHOR	COMMENT	VALUE OF C_o
Wallis [227]	Recommendation	1.2
Govier and Aziz [85]	"	1.2 - 1.3
Ishii and Grolmes [122]	"	$1.2-0.2(\rho_g/\rho_l)^{0.5}$
Nassos and Bankoff [162]	69 mm pipe	1.1
Best Fit/ Data of Borishanskiy et al. [29]	11 mm pipe	1.187
Hewitt [96]	Recommendation	1.2
Zuber and Findlay [243]	50 mm pipe (includes slug flow)	1.2
Zuber et al. [245]	Recommendation	1.2 - 1.3
Galaup [81]	42 mm pipe	1.13

TABLE 3.1: VALUES DETERMINED FOR C_o IN CHURN-TURBULENT BUBBLE FLOW

A measure of the extent of waking is given by various authors [10,122,123,243] in terms of the exponent n in the equations

$$U_{gl} = U_z(1 - E)^{-(n-1)} \qquad 3.18$$

or, equivalently,

$$W_{gm} = EU_z(1 - E)^{-n} \qquad 3.19$$

where U_z is the slip velocity of a bubble in an infinite medium. Equations 3.8 and 3.9 are similar to the Richardson and Zaki [184] expression for use in fluid-solid systems, with n = 2.39.

The increase of slip velocity with increasing voidage, given by a value of n which is less than unity, indicates significant waking, and a degree of churn-turbulent flow. A decrease of slip velocity with increasing voidage will occur when there is no bubble interaction. This is due to the decreasing average density of the medium through which the bubble is rising. At a value of n = 1 we may view this effect of density reduction as being exactly offset by the effect of increased bubble waking.

Various values of n have been suggested: For the Stokesian regime (very small bubbles) n=3 [243]; for ideal bubble flow, n=2 [227] and n=1.5 [130,243]; for churn turbulent flow n=1/3 [122], n=0 [123,243]. Other relations between bubble rise velocity and voidage have been summarised by Lockett and Kirkpatrick [146].

With practical justification, Zuber and Findlay [243] have used a value n=0 to equate the drift flux term and bubble rise in an infinite medium for churn-turbulent flow.

$$\overline{U_{gm}E}/\bar{E} = \bar{U}_{gm} = U_z \qquad 3.20$$

For ideal bubble flow, using n=1.5,

$$\overline{U_{gm}E}/\bar{E} = U_z(1 - \bar{E})^{1.5} \qquad 3.21$$

Values for U_z may be obtained from the literature [84,90,177,227].

3.3.3 COMPARISON OF THE DRIFT-FLUX MODEL WITH OTHER HOLDUP MODELS

Holdup is dependent on two distinct mechanisms, local slip and the profile effect, and cannot be described adequately with a one-parameter model except in those regions where one effect predominates. The Zuber and Findlay [243] model has been criticised for requiring values which are difficult to specify [241] and not always constant [148], yet it appears to be the most suitable formulation to date.

The models of Behringer [23], Wallis [227], Bankoff [13], Yamazaki [240,241] and Zuber and Findlay [243-245] have

been chosen for comparison and the relationship between gas and liquid velocity is considered below.

Behringer [23]: $\overline{U}_g - \overline{U}_l = U_z/(1-\overline{E})$

{Bhaga and Weber [24] have given the Behringer model as $U_g-U_l=U_z$, but this would not appear to be correct.}

Wallis [227]: $$\overline{U}_g - \overline{U}_l = U_z(1-\overline{E})^{n-1}$$

where n depends on bubble waking. For n=0 (churn-turbulent bubble flow), this reduces to Behringers model.

Bankoff [13]: $$\overline{U}_g/\overline{U}_l = (1-\overline{E})/(K_b-\overline{E})$$

Yamazaki [240,241]: $$\overline{U}_g/\overline{U}_l = (1-K_y\overline{E})^{-1}$$

Zuber and Findlay [243-245]:-

$$\overline{U}_g - \overline{U}_l = \overline{U}_{gm}/(1-C_o\overline{E}) + (Co-1)\overline{U}_l/(1-C_o\overline{E})$$

with $\overline{U}_{gm} = U_z$ for churn-turbulent bubble flow.

For all the above models, U_z was taken as 0,25 m/sec for the rise of air bubbles in water using the formula of Harmathy [90]. The average slip velocity between the phases, as predicted by the above models, is compared at constant voidage, with liquid velocities from 0 to 3 m/sec

in fig. 3.2, and at constant velocity for gas voidages from Ø to 0.3 in fig. 3.3.

It is evident from the figures that no model besides the drift-flux model of Zuber and Findlay [243-245] is able to account for the difference in phase velocities at both low and high flow velocities. The models of Bankoff [13] and of Yamazaki and co-workers [240,241] fail to describe slip at low velocities, while simple slip models [23] fail at high velocities. The Zuber and Findlay model therefore appears most suited to the prediction of holdup in narrow bore D.S.R.'s, which may operate at flow velocities where both local slip and profile interactions affect the holdup significantly.

3.3.4 THE DRIFT-FLUX MODEL IN VERTICAL DOWNFLOW

The Zuber and Findlay drift-flux model has been used widely for vertical upflow, but should be applicable to vertical downflow as well, in which case the local slip term will change in sign. Yamazaki and Yamaguchi [241] and Zuber et al. [245] have claimed that it may be used in downflow, and the latter reference has cited two instances in which both C_o and U_{gm} were identical in up and down flow, viz.

(i) High velocity boiling flow of "Santowax-R" in a circular pipe.

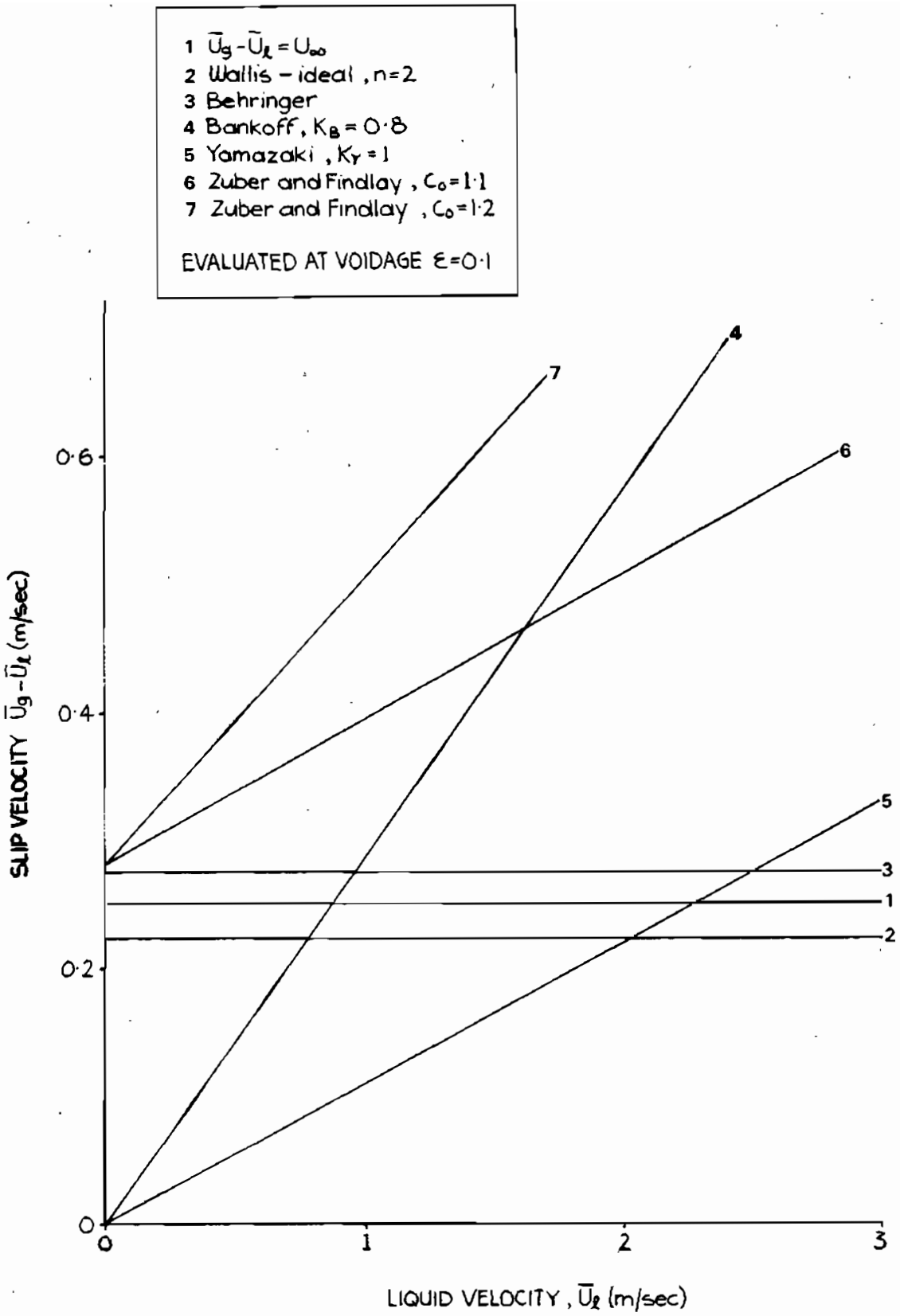

Fig 3·2 • Comparison of holdup models at constant voidage •

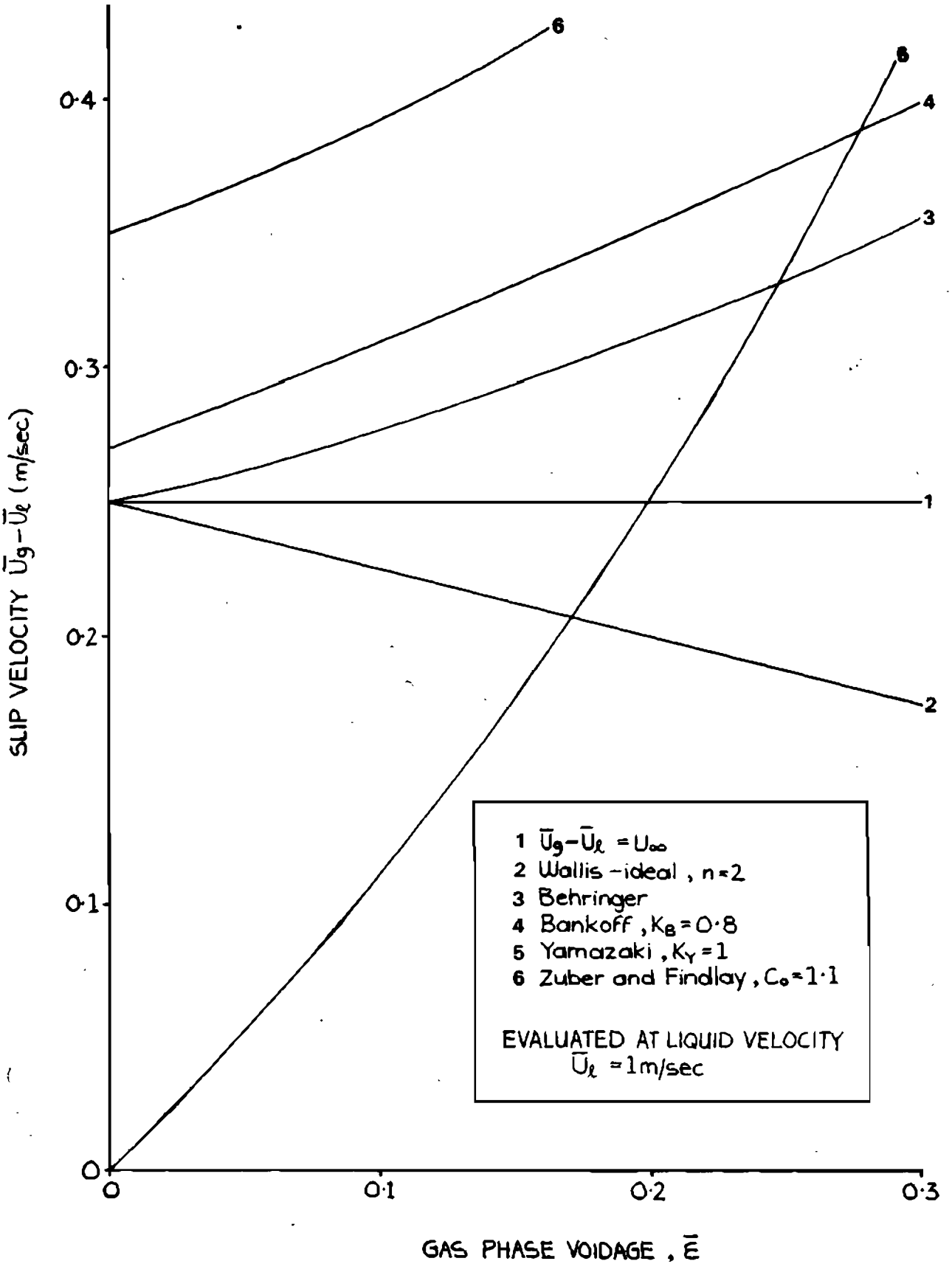

Fig 3·3 • Comparison of holdup models at constant liquid velo

(ii) Steam-water flow in a rectangular conduit.

However, this constancy of C_o in up and downflow has been brought into question (albeit indirectly in some cases) by several authors, enumerated below.

(i) Bhaga and Weber [25] investigated gas-liquid co-current upward and counter-current flow at low liquid velocities. Values of C_o were found to differ between the two cases.

(ii) Brown et al. [33] argued that the profile effect was reversed in downflow, that is, in downflow maximum voidage occurred at the wall, rather than at the centre as in upflow. Brown et al. presented the equation discussed in section 3.2.8 above

$$\overline{W}_g/\overline{E} = (1/K_p)\overline{W}_m + U_b(K_p-\overline{E})/K_p$$

from which it may be seen that the term K_p is similar to the 'Bankoff K factor', and is the inverse of C_o. Brown et al. [33] argue from their profile considerations that K_p is less than unity for upward and K_p is greater than unity for downward flow ie C_o is less than unity for downflow and differs from the upflow case. Few data are presented to confirm this theory, however, and the treatment is open to question. For example, in downflow,

Brown et al. [33] required a bubble rise velocity of 12 cm/sec to verify their data correlation. This value is somewhat low.

(iii) Martin [152] found that C_o differed between up and down flow for slug flow drift-flux plots.

(iv) Oshinowo and Charles [175] have observed (in absolute contradiction to Brown et al. [33]) that in downflow bubbles are located in a central core of flow, which is not the case in upflow. This "bubble coring" implies a difference in voidage profiles, with consequent difference in C_o, between the up and downflow configurations. In a subsequent paper [176] these authors have stated that C_o may not be assumed constant in the two cases. Their observation of bubble-coring flow has led to the presentation of theory explaining profile variation between up and downflow [205].

It has been shown that the constancy of C_o in the two cases has been brought to question. In addition to this, the constancy of C_o within a configuration has even been doubted [148]. An experimental investigation of the values of C_o for both up and downward bubble flow was required to resolve this issue.

3.4 EXPERIMENTAL INVESTIGATION OF HOLDUP

3.4.1 OBJECTIVES

The experimental program was aimed at the verification and extension of the Zuber and Findlay [243] drift-flux model. This involved the investigation of holdup using an air-water mixture for two typical pipe sizes in both up and down flow: 50 mm and 100 mm diameter test rigs were constructed for this purpose and are described in appendices A and B.

3.4.2 MEASUREMENT OF HOLDUP

Various techniques, reported by Hewitt [97], have been used to examine average holdup in two phase flow. Excluding those methods employing probes for local void fraction measurement [71,72,81,82], the two most common methods for measuring average void fraction are by using gamma ray attenuation and by isolating a pipe section with quick-closing valves, thus permitting the measurement of relative phase volumes in the section. The second method was chosen as most suitable. Full bore ball valves were fitted into the 50 mm diameter two phase flow loop so that a 5 m section of pipe could be rapidly isolated. A similar arrangement permitted the isolation of a 4 m vertical pipe length in the 100 mm diameter apparatus. In

each case the lower valve was closed by a quick-response pneumatic ram, and was linked to the upper valve with a tie-rod of adjustable length. The test section was equipped with pressure tappings and a sight glass of 3 mm bore to permit the measurement of the height of the gas-liquid interface after phase separation.

3.4.2 VALVE SYNCHRONISATION

Valve synchronisation was achieved by monitoring pressures in the section before and after closure, using a method developed in detail in appendices C and D, and described briefly below. Let $P(x,t)$ be defined as the pressure at height x above the lower valve in the section and at time t, and $\bar{E}(x,t)$ the average voidage at height x, time t. Before valve closure we may assume that the section, with total volume V_t, will contain a bubble assemblage with voidage well approximated by

$$\bar{E}(x,o^-) = E_oP_o/P(x,o^-) \qquad 3.22$$

with E_oP_o a constant dependent on gas flow rate, and $t=o^-$, the time just prior to closure.

After closure ($t=O^+$), the bubbles will rise and disengage from the fluid, and after some period, a gas phase ullage of volume V_g will form at the top of the section. The final ullage pressure is then $P(x_3,t_1)$, where x_3 is the

height at the top of the isolated section, and t_1 is the time by which all the bubbles have risen to the gas-liquid interface.

Assuming the liquid to be incompressible and mass transfer between phases to be minimal, the use of volume and mass balances yields the relationship, as derived in appendix C,

$$V_t/P(x_3,t_1) = A_p \int_{x=0}^{x=x_3} 1/P(x,o^-)\, dV \qquad 3.23$$

Where V_t is the volume of the whole section. The integral on the right hand side of equation 3.23 can be approximated accurately (see Appendix D) by integrating a quadratic expression for the inverse of pressure in x. Constants for the quadratic are gained by monitoring the pressure prior to closure at three vertical stations in the test section, and solving for the constants in three simultaneous quadratic equations in x and 1/P. An example of this calculation due to Clark and Flemmer [50] is reproduced in Appendix D. All calculation work is done in absolute pressures.

This method has significant advantages over mechanical synchronisation (by exact measurement of the tie rod length), especially in larger bore apparatus, where closing times may be slow. During closure qualities of flow through the two valves will differ. A typical error

of 1% in holdup determination may occur for each millisecond error in synchronisation [50].

In practice the tie-rod linking the valves was adjusted in length until the relationship 3.23 was satisfied, and holdup data then collected. This implied that the holdup in the section was identical before and after closure, and a true representation of the voidage present in the flow.

3.4.3 ASSESSMENT OF BUBBLE RISE VELOCITY

In order to evaluate the drift velocity term in the Zuber and Findlay [243] equation, the bubble rise velocity in the flow must be determined, and some indication gained of the degree of bubble waking in the flow. Two methods were used to evaluate the rise velocity in the case of the 100 mm rig, and one in the case of the 50 mm. These are described below.

(i) By monitoring voidage at zero liquid flow

This method is implicit in the equations of many authors, and relies on the measurement of gas voidage with a knowledge of gas flux [165,203].

The bubble rise velocity relative to the pipe is given by

$$U_g = W_g/E \qquad 3.24$$

where E, the local void fraction, is also the fraction of the local cross-sectional area which is occupied by gas.

For zero liquid flow, $U_{gl}=U_g$, so that

$$U_{gl} = W_g/E \qquad 3.25$$

Equation 3.25 may be extended to an average over the pipe cross-section and written as

$$\bar{U}_{gl} = Q_g/A_p\bar{E} \qquad 3.26$$

{Using the Zuber and Findlay [243] equation in a strict sense shows that equation 3.26 will distort the slip velocity, U_{gl}, by a factor of $(1-\bar{E})/(1-C_o\bar{E})$. However, since this equation considers only low voidages, and is primarily seeking U_z, i.e. the value of $\bar{U}_{gl}$ when $E\approx\emptyset$, profile effects have been neglected here.} The gas flowrate, Q_g, is evaluated at the pressure in the apparatus. In practice Q_g was evaluated using the ideal gas law, at the final ullage pressure $P(x_3,t_1)$, as defined in section 3.2.2,

$$Q_g = Q_{go}P_o/P(x_3,t_1) \qquad 3.27$$

where o denotes atmospheric conditions.

From equation 3.26 the bubble rise in an infinite continuum was given by

$$U_z = \lim[\bar{E} \downarrow 0] Q_g/A_p\bar{E} \qquad 3.27$$

where $\bar{E}$ was determined in the test section by the quick-closing valve method described above.

(ii) By Monitoring Final Ullage Pressure after Valve Closure

After valve closure the phases separate to form a gas ullage. Concurrent with this separation is a rise in pressure of the gas at the top of the section to assume a final value, $P(x_3,t_1)$, given by equation 3.23, after the time taken for all bubbles to rise in the section.

The time taken by the bubbles initially at the base of the section to rise to the final interface may be monitored by noting the rise in pressure at the top of the section with time, and seeking the point in time at which the final pressure is reached. Experimentally, the pressure was monitored using a Foxboro pressure case and high speed flatbed recorder. A typical pressure-time curve is given in fig. 3.4

Where the length of the test section is x_3, the distance travelled by the lowest bubbles to the interface is

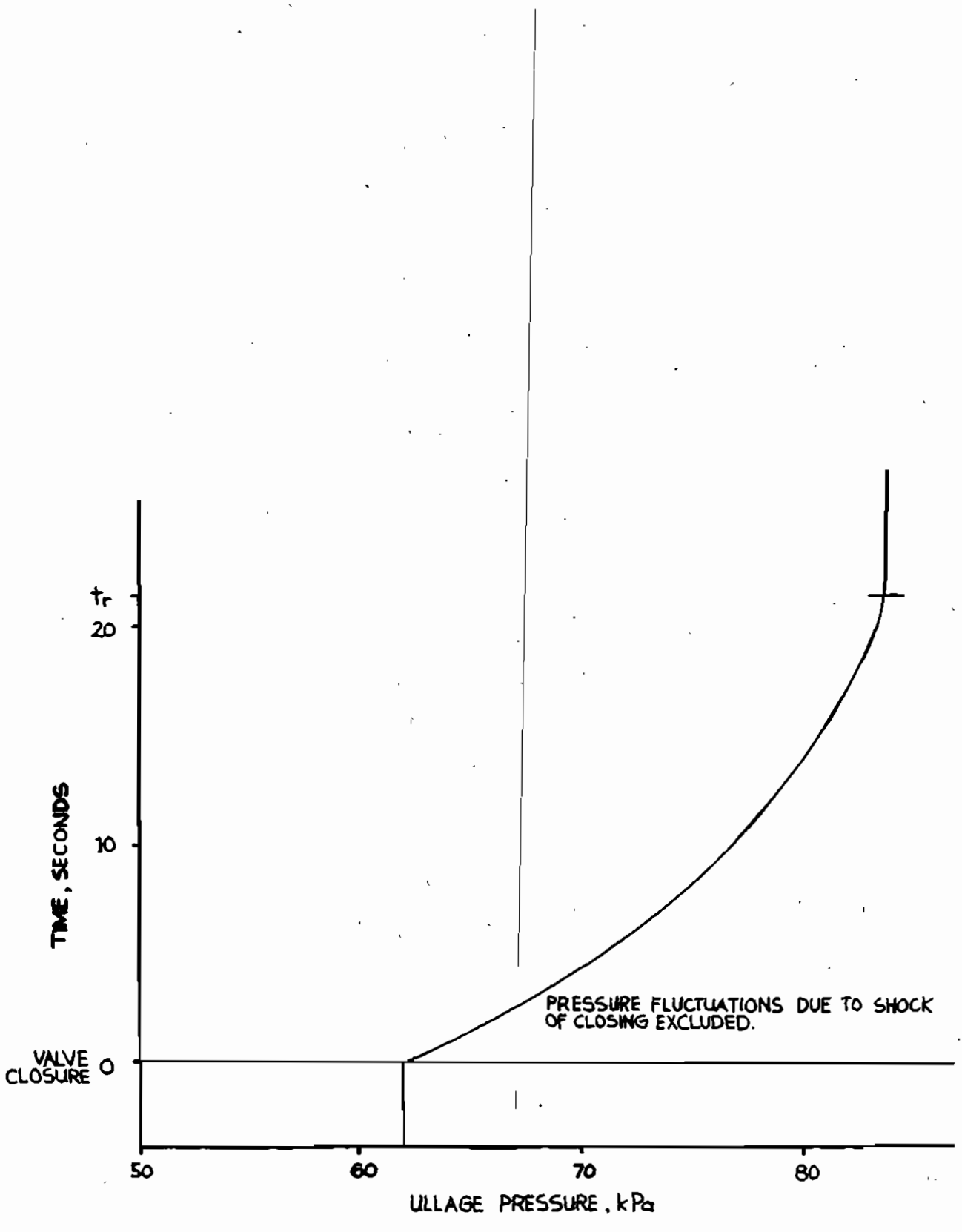

Fig 3·4 · Typical Flatbed plot of ullage pressure after closure. (50mm I $\bar{\varepsilon} = 0{\cdot}09$, $\bar{w}_l = 1{\cdot}06$ m/sec before closure)

$x_3(1-E)$. If the time taken for these bubbles to rise is denoted t_r, then the bubbles have a speed relative to the pipe of

$$\overline{U}_g = x_3(1-\overline{E})/t_r \qquad 3.28$$

The water must, however, flow back around the bubbles to permit their rise (See case (ii) of Nicklin's conceptual model in section 3.1.) so that the slip velocity between the bubbles and liquid ($\overline{U}_{gl}$) and the velocity of the bubbles relative to the pipe ($\overline{U}_g$) are related by

$$\overline{U}_{gl} = \overline{U}_g/(1-\overline{E}) \qquad 3.29$$

From equations 3.28 and 3.29

$$\overline{U}_{gl} = x_3/t_r \qquad 3.30$$

and the bubble rise velocity in the infinite continuum is determined by

$$U_z = \lim[\overline{E} \downarrow 0]\ x_3/t_r \qquad 3.31$$

It should be noted that equation 3.31 is independent of liquid velocity prior to valve closure, and may be employed at any gas or liquid flux in the test section.

Bubble slip velocities in the 50 mm rig using method (ii)

at various water velocities are presented in figure 3.5. Slip velocities are presented for the 100mm rig for both methods (i) and (ii) in figure 3.6.

A linear regression on the data for the 50 mm rig in figure 3.5 yielded a valve of the bubble rise velocity in an infinite continuum of U_z = 0.24 m/sec. Linear regressions and regressions of the form

$$\overline{U}_{gl}=U_z(1-E)^n$$

were performed on the data from the 100mm rig, presented in figure 3.6. For the data of method (i) a linear regression gave a best fit value of U_z = 0.226 m/sec and for method (ii) U_z = 0.248. The alternative regressions on the data from the 100mm rig yielded equations:

$$\overline{U}_{gl} = 0.235(1-E)^{-0.30} \quad m/sec$$

for method (i), and

$$\overline{U}_{gl} = 0.248(1-E)^{0.702} \quad m/sec$$

for method (ii). These values for U_z may be compared with the values recommended by Harmathy [90]

$$U_z = 1.53[g\,\sigma(\rho-\rho_g)\,/\rho^2]^{1/4}$$

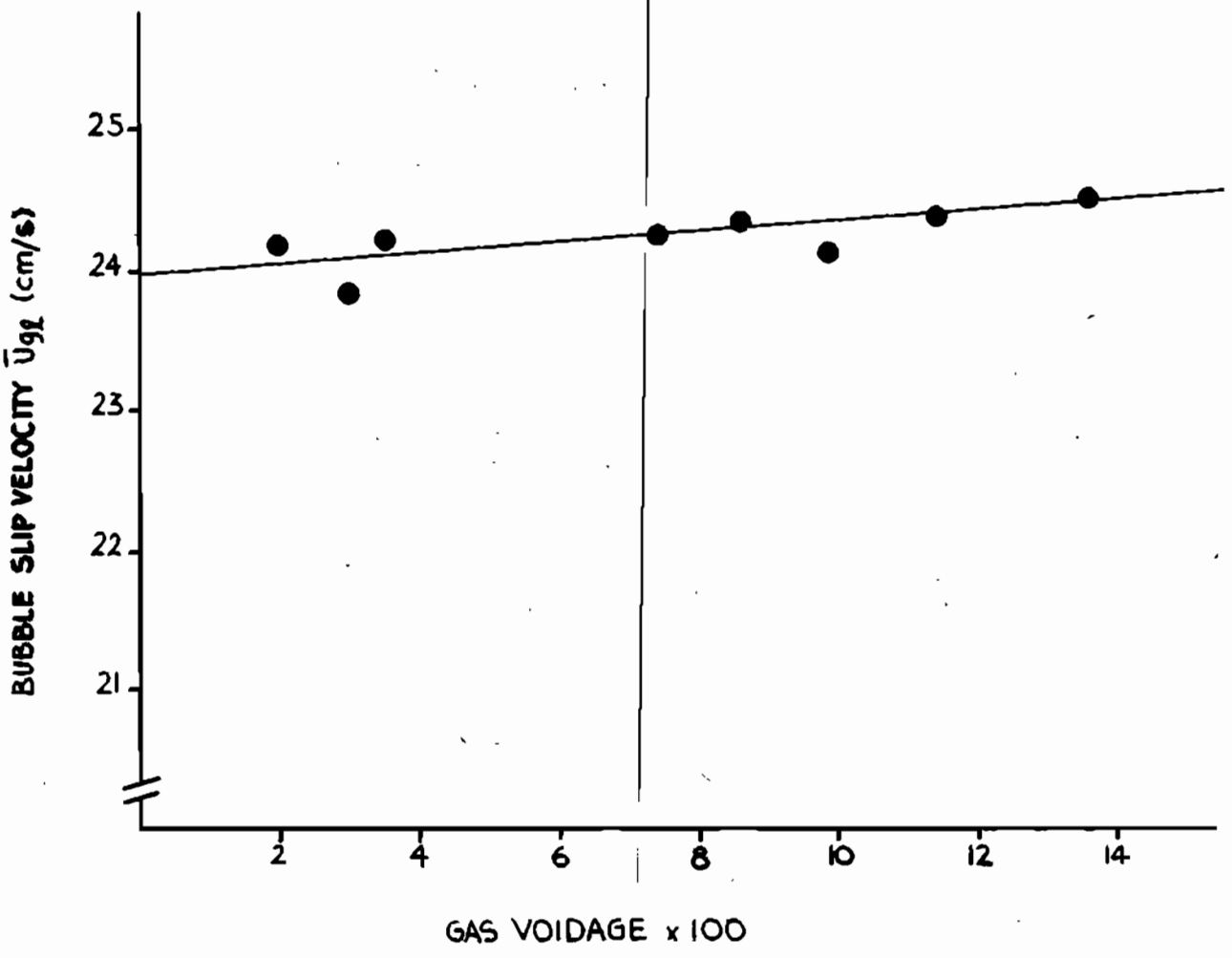

Fig 3·5 · Bubble slip velocity in 50mm rig ·

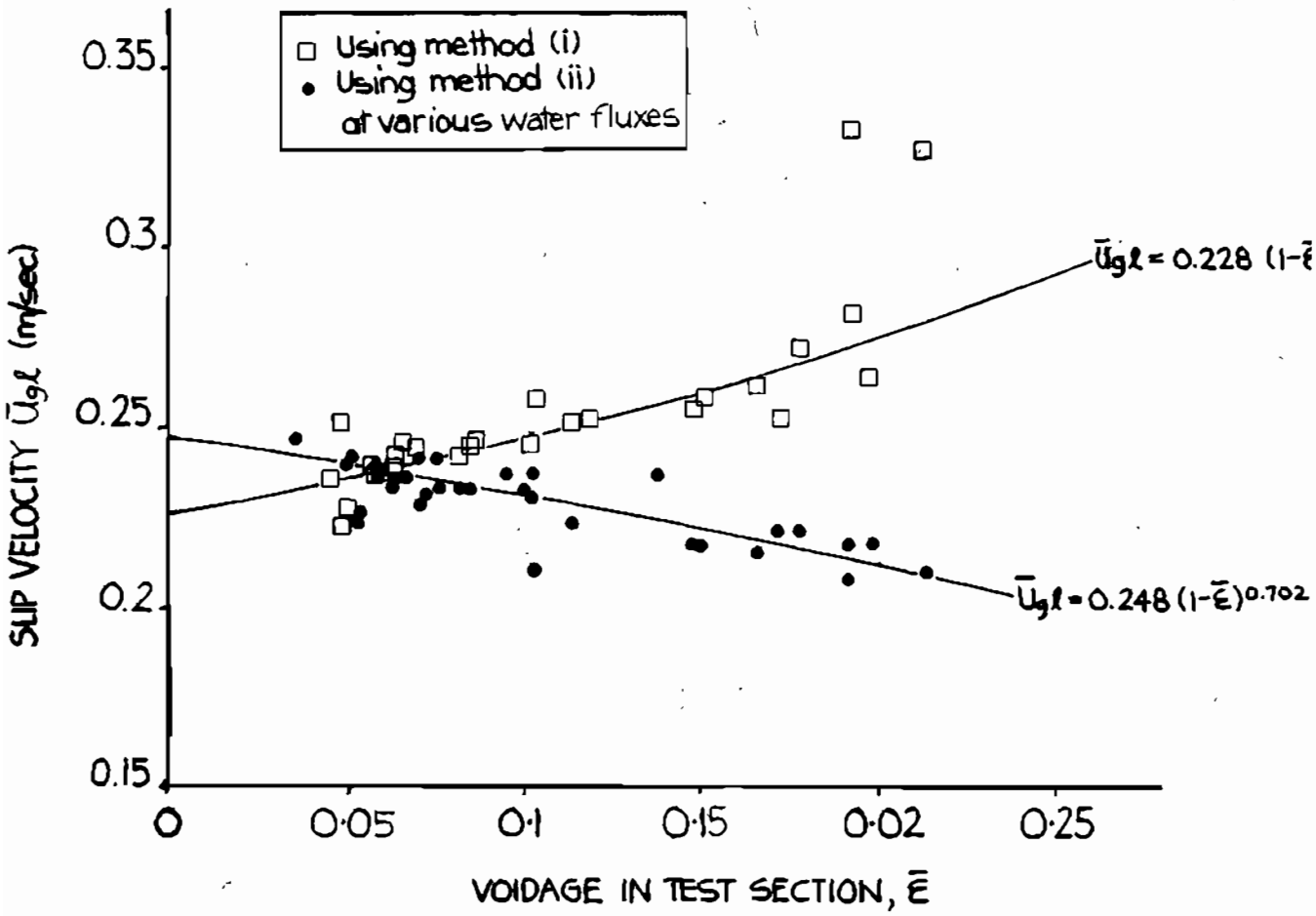

Fig 3·6 · Bubble slip velocities in 100mm rig ·

= 0.25 m/sec for air/water systems

and by Levich [141]

$$U_z = 1.41\{g\sigma(\rho-\rho_g)/\rho^2\}$$

= 0,23 m/sec for air/water systems

Formlae given by Wallis [227] imply that no correction for the wall effect was necessary. Method (ii) relied on somewhat more accurate measuring equipment than method (i), and its results were taken in preference. Accordingly rise velocities of 0.24 and 0.25 m/sec were used in further investigation of the Zuber and Findlay [243] model, for the 50 mm and 100 mm rigs respectively.

From figure 3.6 it may be seen that bubble rise velocity increased with voidage for method (i). Rise velocity increased in a fashion close to that for churn-turbulent flow, given by

$$\overline{U}_{gl}=U_z(1-\overline{E})^{-1}$$

thus implying that significant waking occurred. The two high values in Fig 3.6 ($\overline{U}_{gl}$=0.33 m/sec, $\overline{E}$ = 0.2) were due to the presence of slugs in the flow. Such slugs may be expected to have a rise velocity given by [162]

$$U_{slug} = 0.35(gD_p)^{0.5}$$

$$= 0,35 \text{ m/sec for air-water in a 100 mm pipe.}$$

This data for method (i) has been compared in figure 3.7 with the data of Siemes [203] for a 100 mm square pipe, using a plot of drift flux versus voidage similar to that used by Zuber et al. [245]. Good agreement exists between the data of this study and the data of Siemes [203], for which waking was significant.

Rise velocities behaved differently for method (ii) in the pipes of different diameter, with the 50 mm pipe showing a slight increase in rise velocity with voidage and the 100 mm showing a decrease. The 50 mm case may be attributed to significant waking over the whole pipe diameter whereas the 100 mm pipe is sufficiently wide to permit localised waking to occur at the pipe centre. The effect of waking at only the pipe centre permits the depletion of the bubble assemblage at the base of the test section so that the remaining small bubbles then rise in ideal fashion. This explanation was confirmed by fitting a 700 mm long full bore glass length into the 100 mm test section to permit visual observation. After valve closure, large bubbles rose quickly at the pipe centre, leaving smaller bubbles to reach the gas-liquid interface last. This shows that method (ii) at significant voidages determines the rise velocity of the slowest bubbles which were

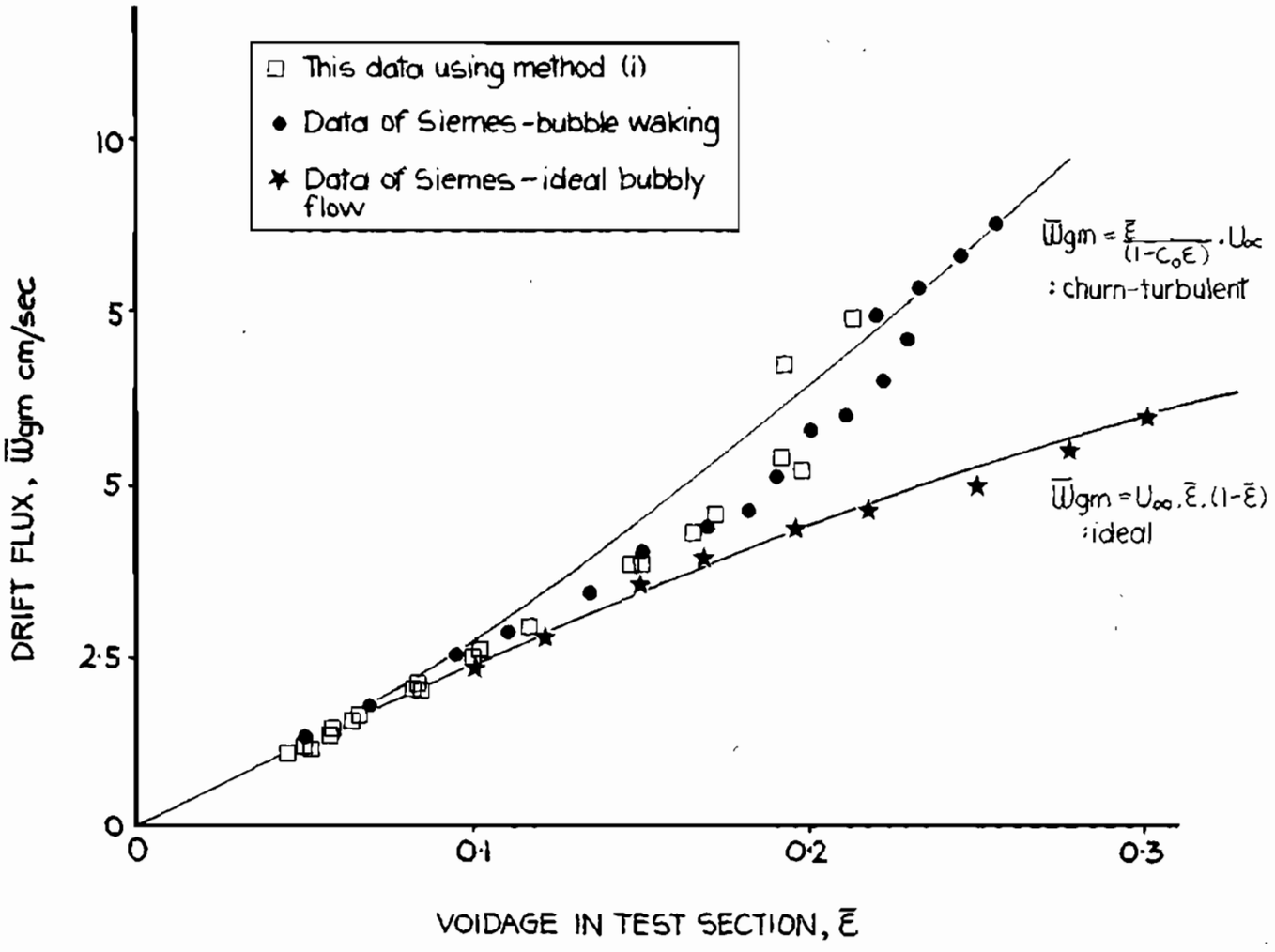

Fig 3·7 · Comparison of data using method (i) with that of Sieme

initially lowest in the test section, and not the average bubble rise. Nevertheless, the rise velocity in an infinite continuum, U_z, may still be accurately determined using equation 3.31.

The behaviour of bubbles in both pipes suggested that the bubble flow was churn-turbulent.

3.4.4 DETERMINATION OF THE PROFILE CONSTANT C_o

The Zuber and Findlay [243] equation may be re-arranged to give the relationship

$$C_o = \frac{(\overline{W}_g/\overline{E}) + \overline{U}_{gm}}{\overline{W_g+W_l}}$$

which implies that C_o may be determined for known local voidage and gas and liquid flowrates at a point in the pipe, provided that $\overline{U}_{gm}$ is suitably evaluated as discussed in 3.2.2

The Zuber and Findlay [243] model is best illustrated as a velocity-flux plot of the average gas velocity, $(\overline{W}_g/\overline{E})$, versus the total superficial velocity, $(\overline{W_g+W_l})$, for churn-turbulent flow. A complete plot of this type similar to that given by Zuber et al. [245] is illustrated in figure 3.8: here the positive direction is upwards. An equivalent diagram to describe up and downflow is given in figure 3.9, and here the positive direction is the flow

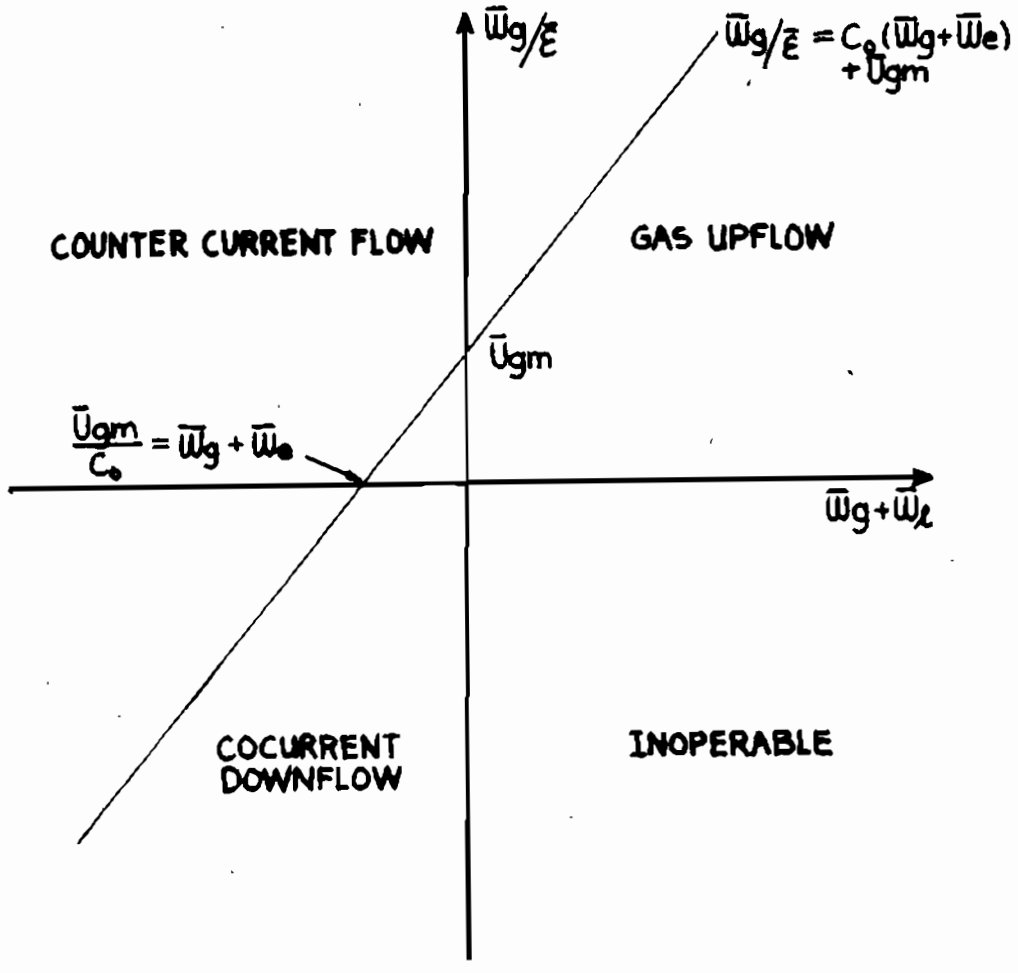

Fig 3·8 • Velocity-flux plot used by Zuber et al •

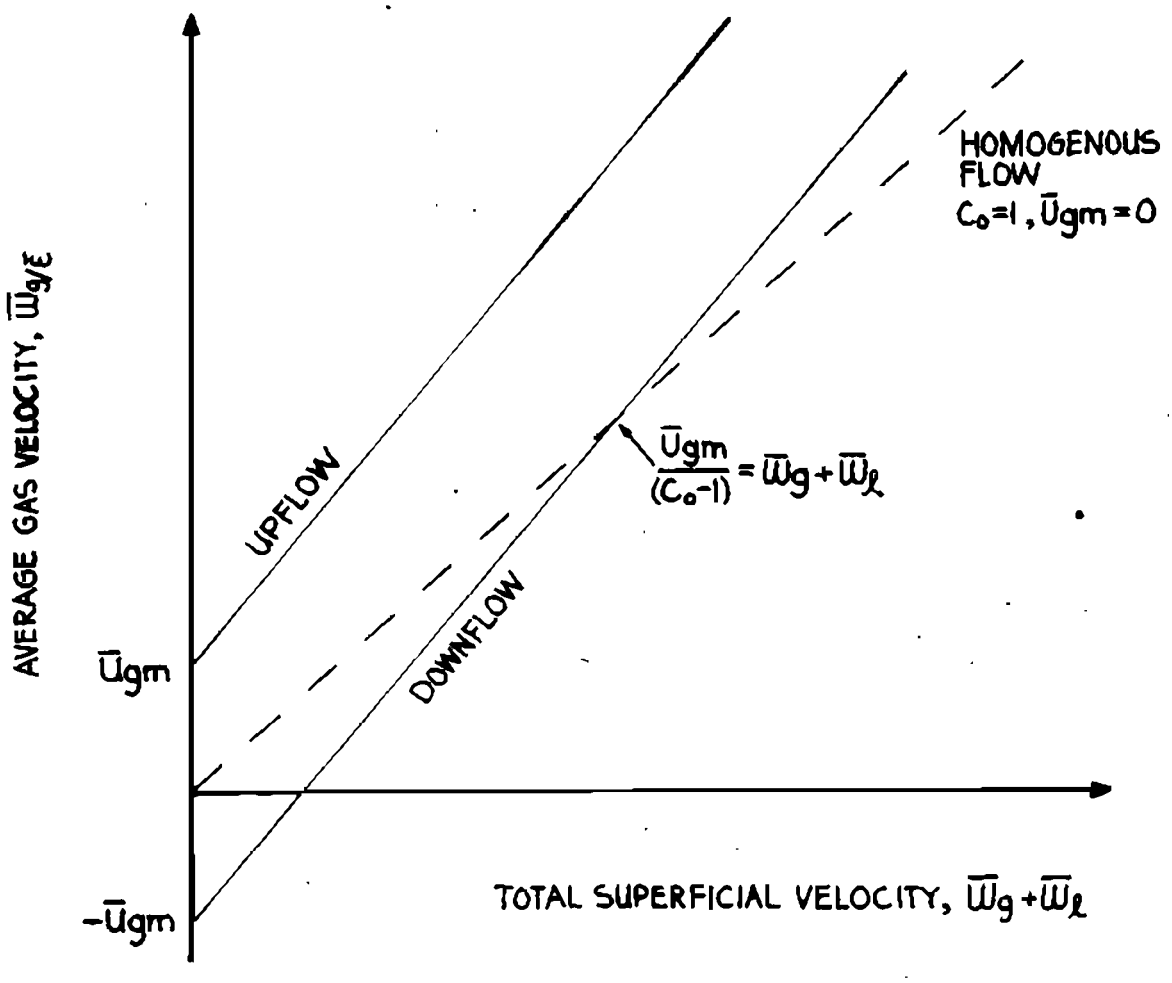

Fig 3.9 · Velocity–Flux plot used here: direction of flow is positive ·

direction. This second type of plot has been used in preference in this thesis because it is more compact.

Ideal bubbly flow may be more easily represented by a plot of $(\overline{W}_g/\overline{E})/(1-\overline{E})^n$ versus $(\overline{W_g+W_l})/(1-\overline{E})^n$ [25]. A family of curves in $\overline{E}$ would be developed if the churn-turbulent plot were used for an ideal flow situation. However, no ideal bubble flow data has been considered here.

Data were gathered from both the 50mm and 100mm rigs. The voidage was determined using quick closing valves on the test sections, and synchronisation was achieved by the pressure balance method previously described. Liquid flowrate was determined by a calibrated rotameter on the 50 mm line and by an orifice fitted to British Standards specification [30] on the 100 mm line. Gas flowrates were measured with rotameters and the flowrate was converted to the value of the flowrate which would occur at the pressure given by the quadratic approximation to

$$\frac{V_t}{A_p \int_{x=0}^{x_3} 1/P(x,o^-)\, dx}$$

where V_t is the total volume of the isolated section, as previously described. Data were obtained for both up and downflow for a range of water flowrates at gas voidages between 0.04 and 0.25.

3.5 RESULTS AND DISCUSSION

3.5.1 DATA FOR 11 mm PIPE

In addition to the data gained from this experimental work, some data were available in the literature for upflow in an 11 mm pipe. The tabulated data of Borishanskiy et al. [29] for upflow at low voidages were processed. These were plotted on a velocity-flux plane in figire 3.10, with $\overline{U}_{gm}$ set to 0.25 m/sec. A regression yielded a value of C_o = 1.187. Inspection of figure 3.10 reveals that there is good agreement between the drift-flux model and these data.

3.5.2 DATA FOR 50 mm PIPE

The data gained from the 50 mm rig are presented in figure 3.11. The data of Nassos and Bankoff [162] for natural and forced two phase upflow in a 69 mm circulation loop are also plotted. A regression was performed on the 50mm data under the constraint $\overline{U}_{gm}$ = 0.24 m/sec. In upflow it was found that Co=1.160 and in downflow Co=1.165. The value for upflow may be compared to values of C_o recommended in the literature for the upflow case, presented in Table 3.1. The value found for downflow may be compared favourably with Oshinowo and Charles' [176] value of Co=1.1 for "bubbly slug downflow".

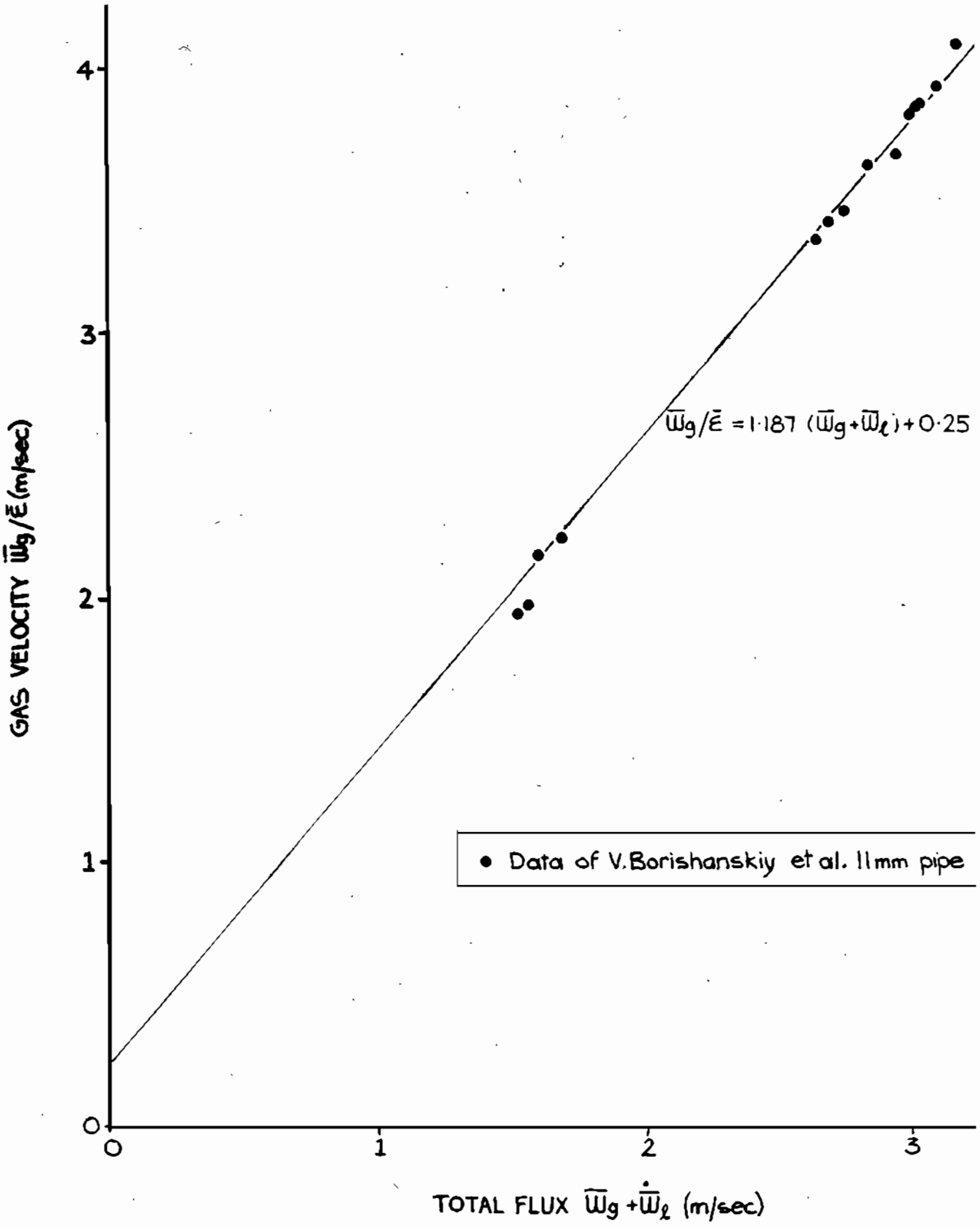

Fig 3·10 • Holdup Data for 11mm pipe in two phase upflow •

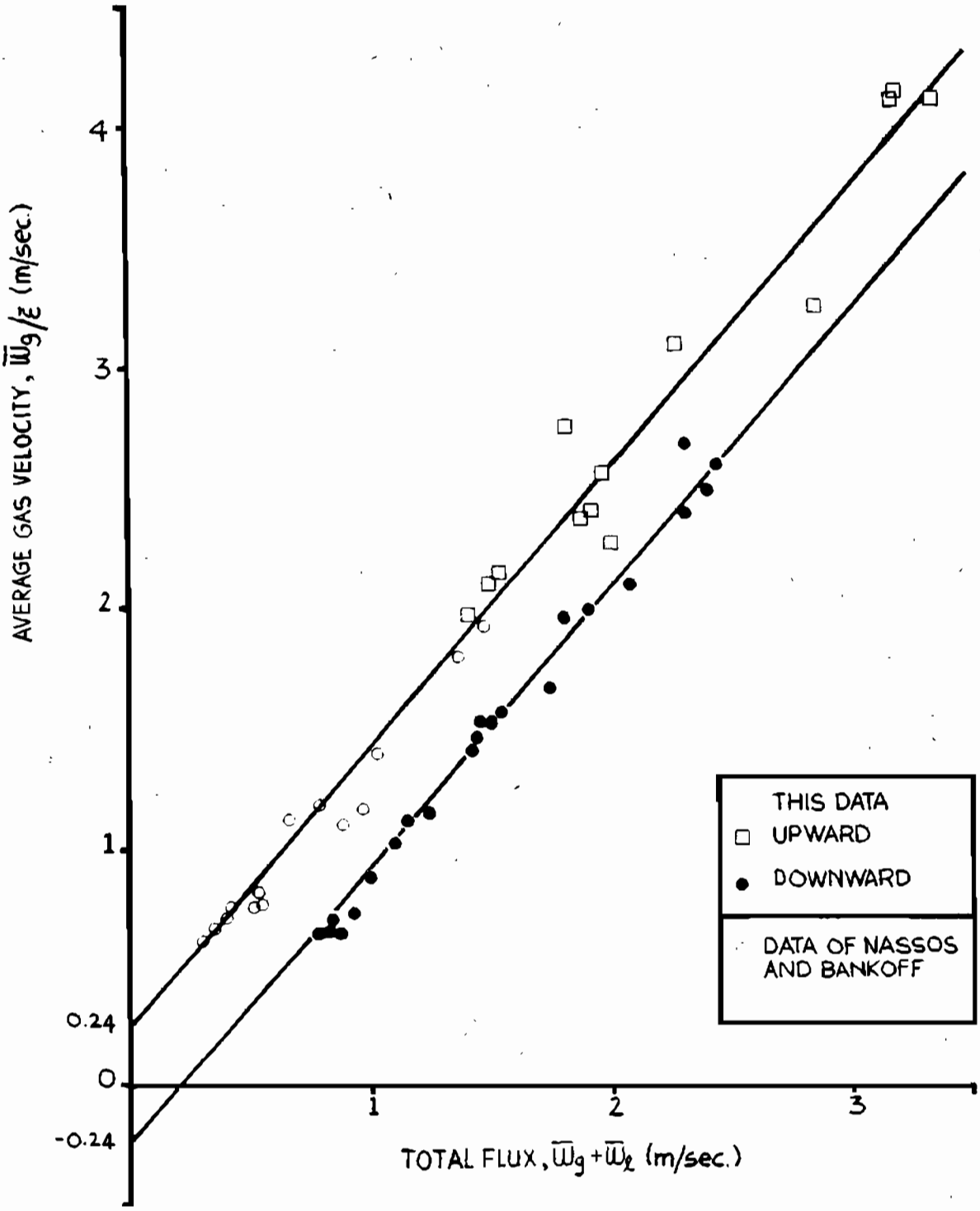

Fig 3·11 • Velocity - flux plot for all 50mm data •

Figure 3.12 compares the observed and predicted values of voidage, from the 50mm data and from the equation

$$\bar{E} = \frac{\bar{W}_g}{Co(\bar{W}_g+\bar{W}_l) + \bar{U}_{gm}}$$

with C_o = 1.16 and $\bar{U}_{gm}$ = 0.24 for upflow, -0.24 for downflow. The predicted and experimental data compare favourably, but there is a slight indication of some void fraction dependence of the Zuber and Findlay [243] equation. This matter is further discussed with reference to the 100 mm diameter pipe data below.

3.5.3 DATA FOR 100mm PIPE

The data for the 50mm pipe were adequately described by the Zuber and Findlay model using constant values of C_o and $\bar{U}_{gm}$ over the voidage and velocity range employed. In contrast, the 100mm data showed a strong variation with voidage. The results are given as velocity - flux plots for downflow in figure 3.13 and upflow in figure 3.16. It was noted that slip velocity increased with increasing voidage in upflow and decreased with increasing voidage in downflow. Although it is acknowledged that bubble rise velocity may have increased with increasing voidage, the variation in slip velocity was too great to be explained by only this factor. In one case, the gas velocity, $\bar{W}_g/\bar{E}$, varied over a range of 0.6 m/sec for a constant total

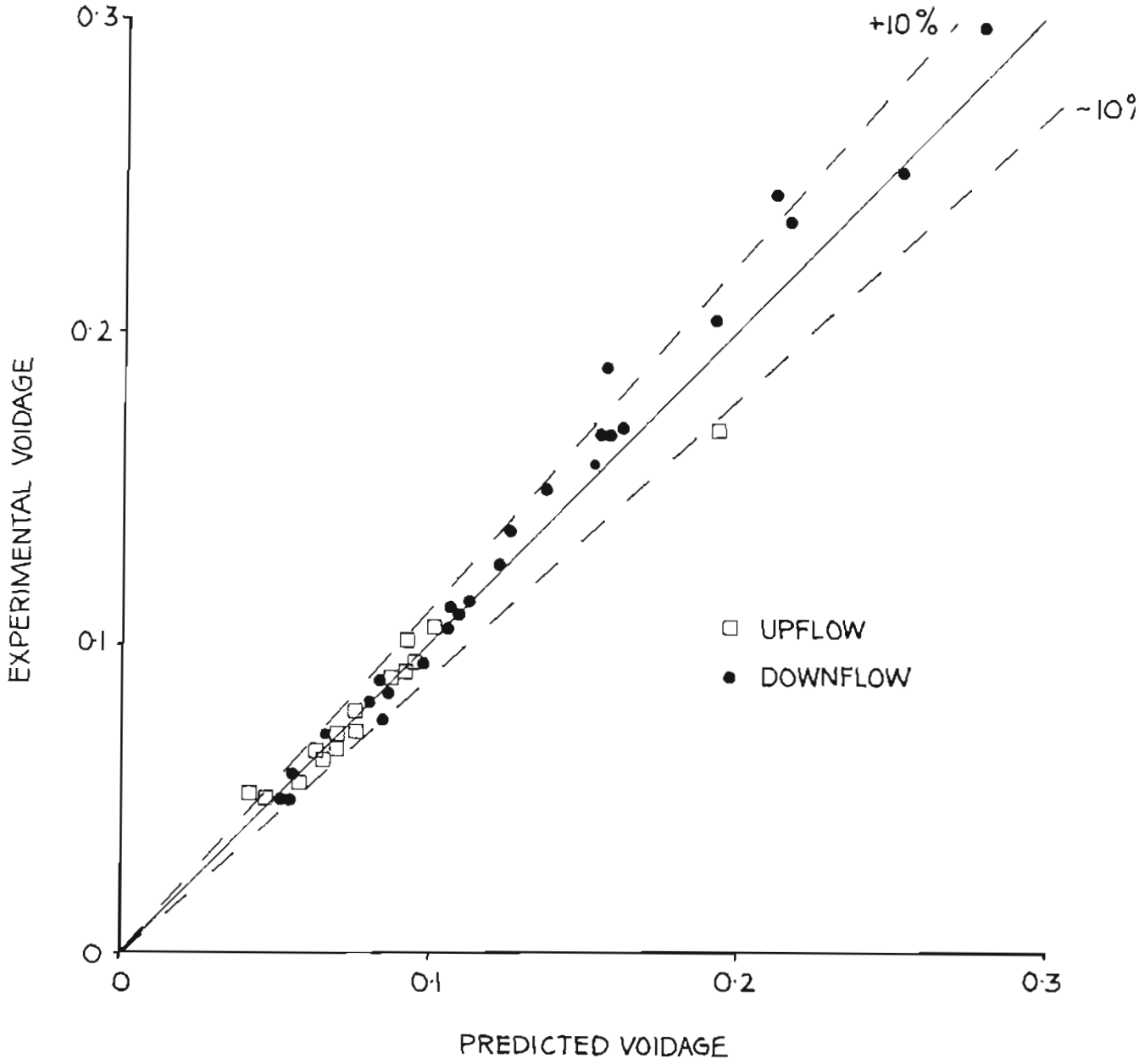

Fig 3·12 · Prediction of voidage by the Zuber and Findlay mod

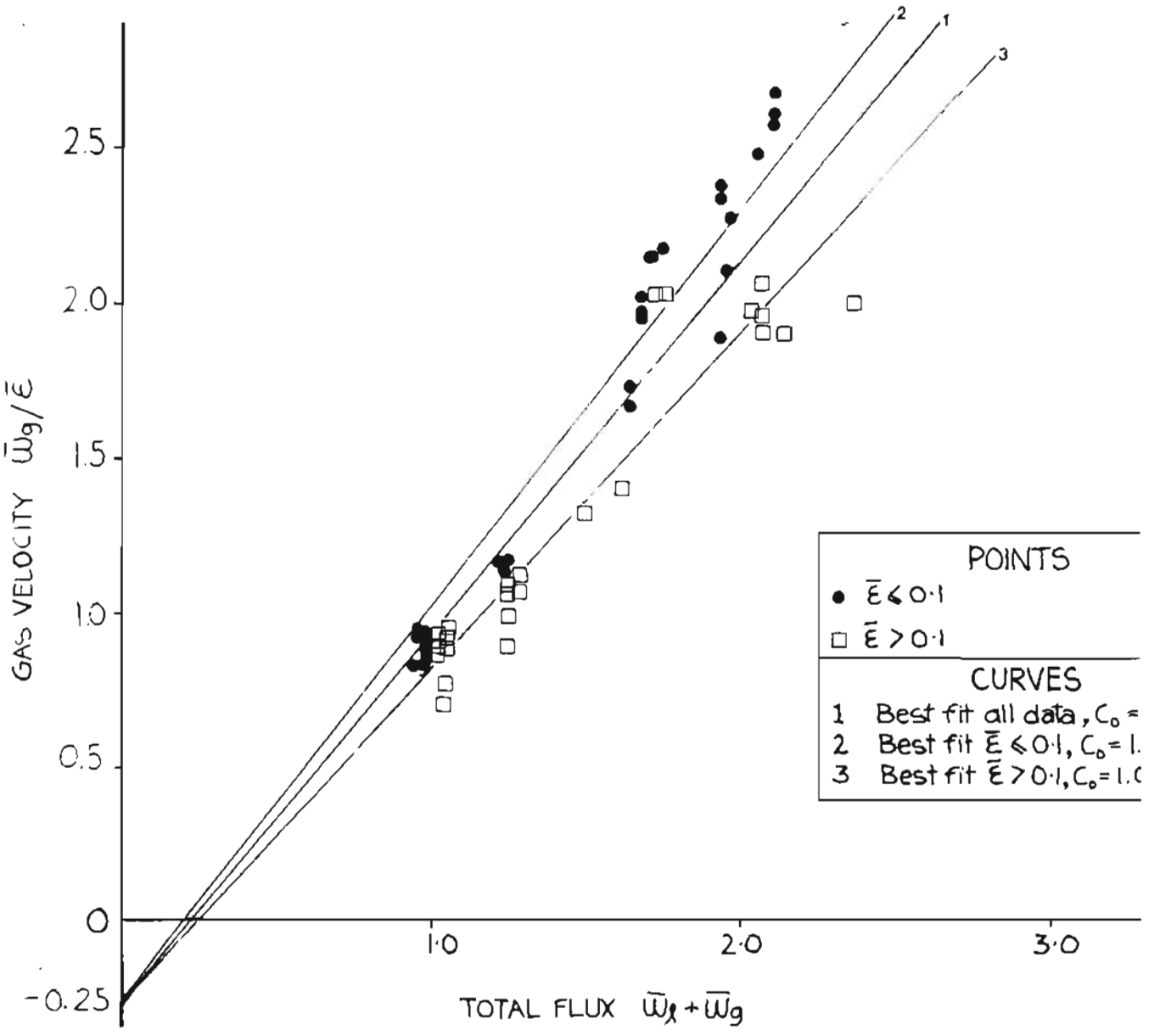

Fig 3·13 · Velocity - Flux plot for downflow in 100mm rig ·

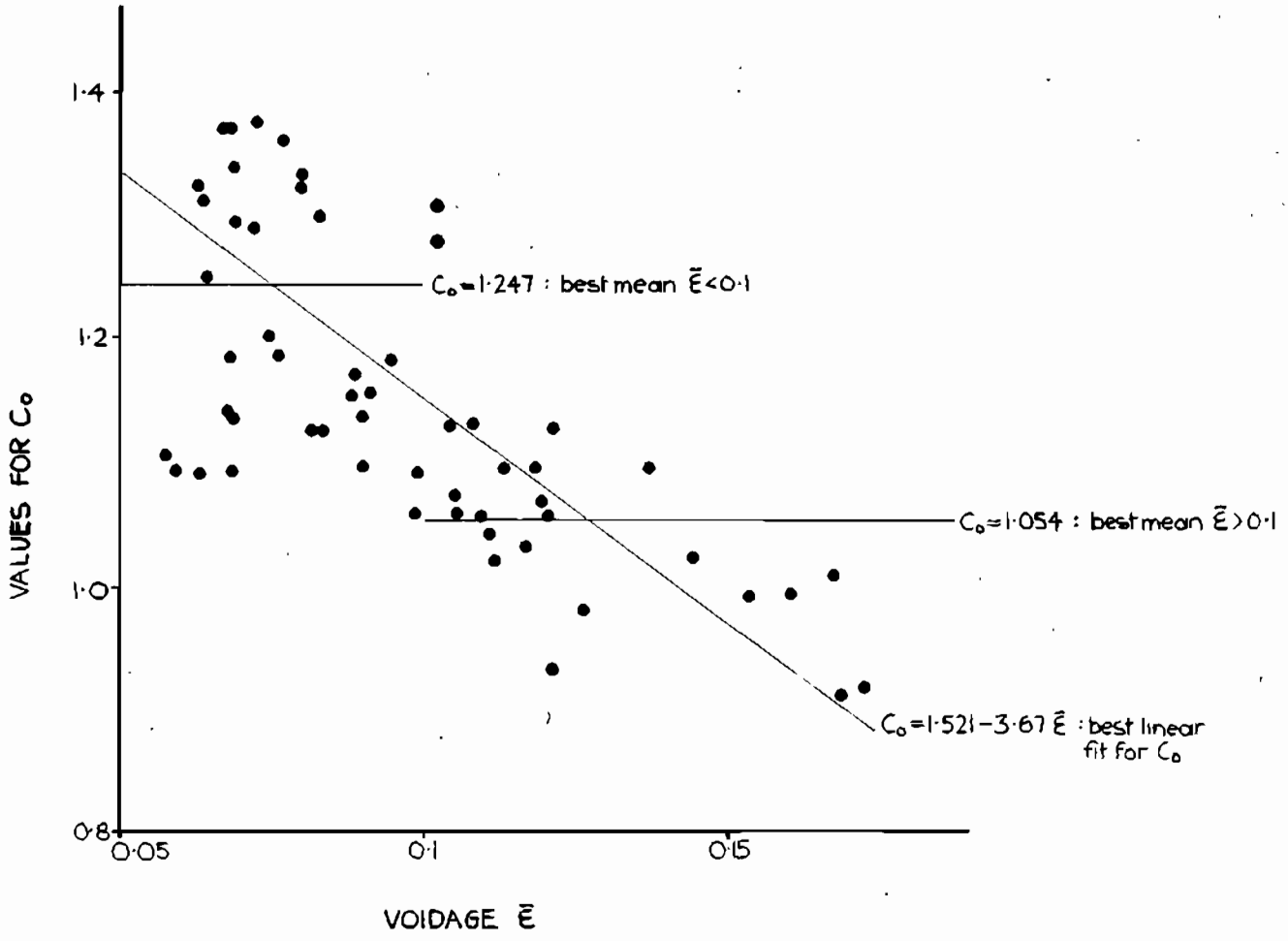

Fig 3·14 • Influence of voidage on values of C_o in downflow. (100 mm pipe) •

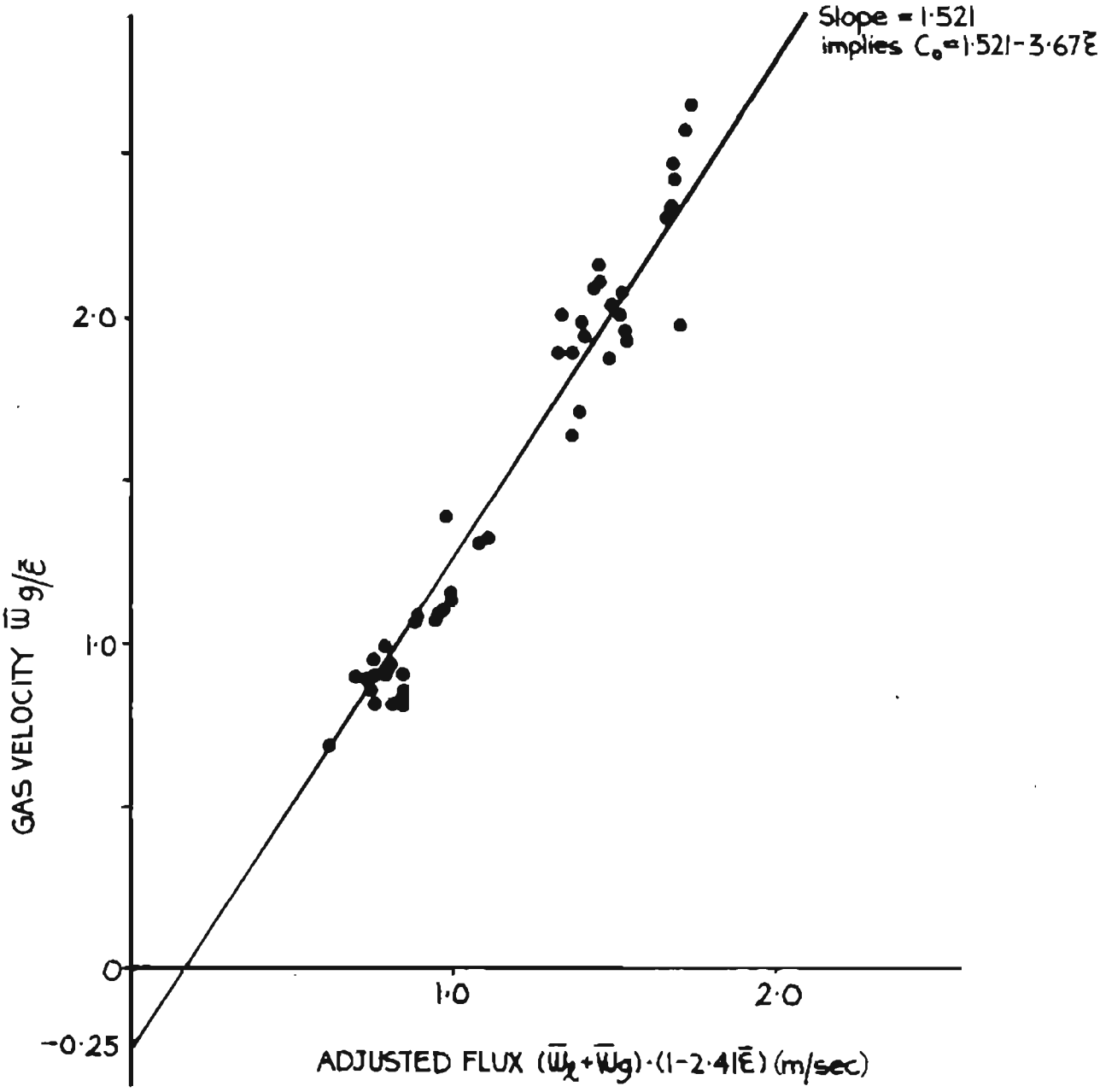

Fig 3·15 • Velocity – modified flux plot for downflow in 100mm rig •

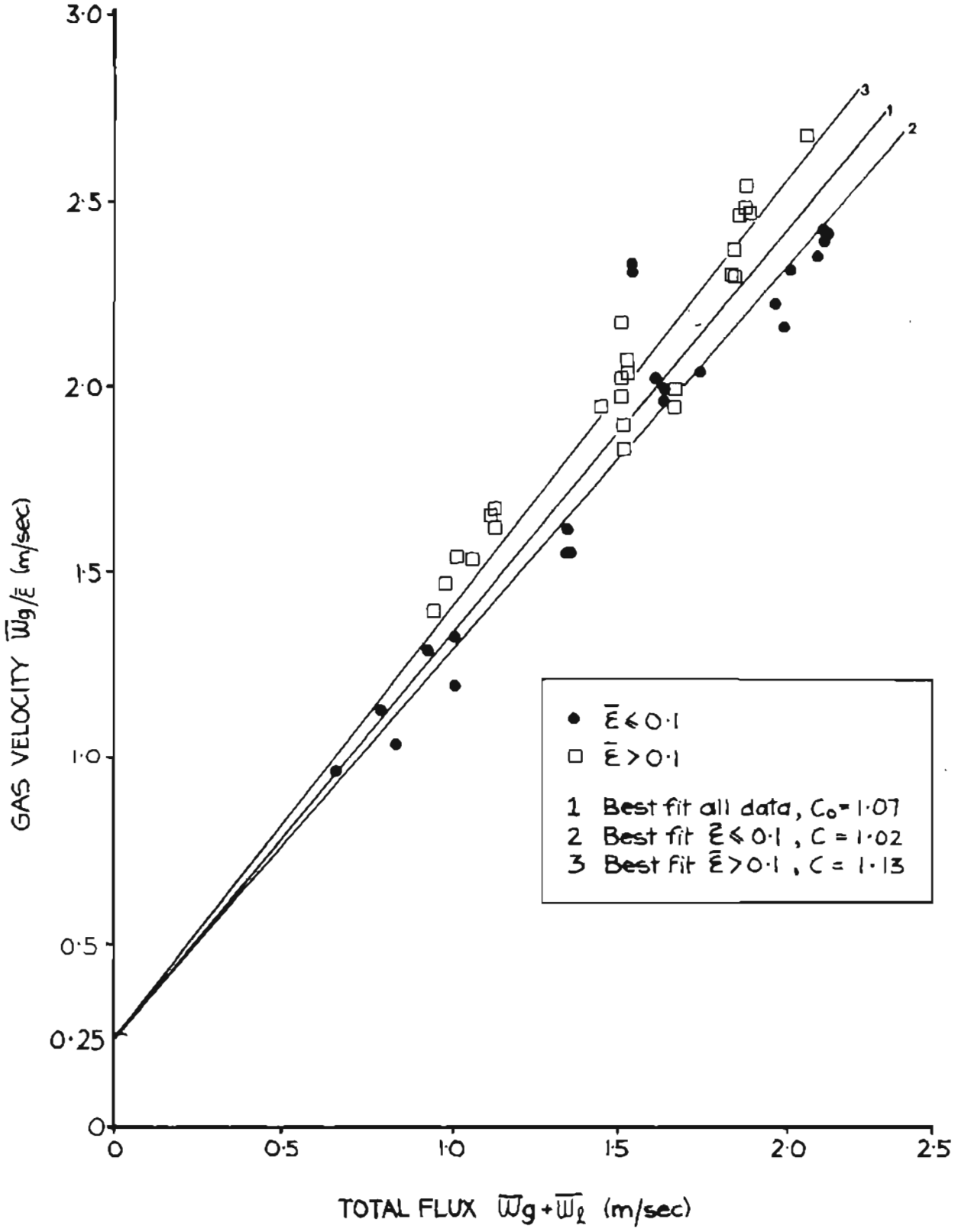

Fig 3·16 • Velocity – Flux plot for upflow in 100mm rig •

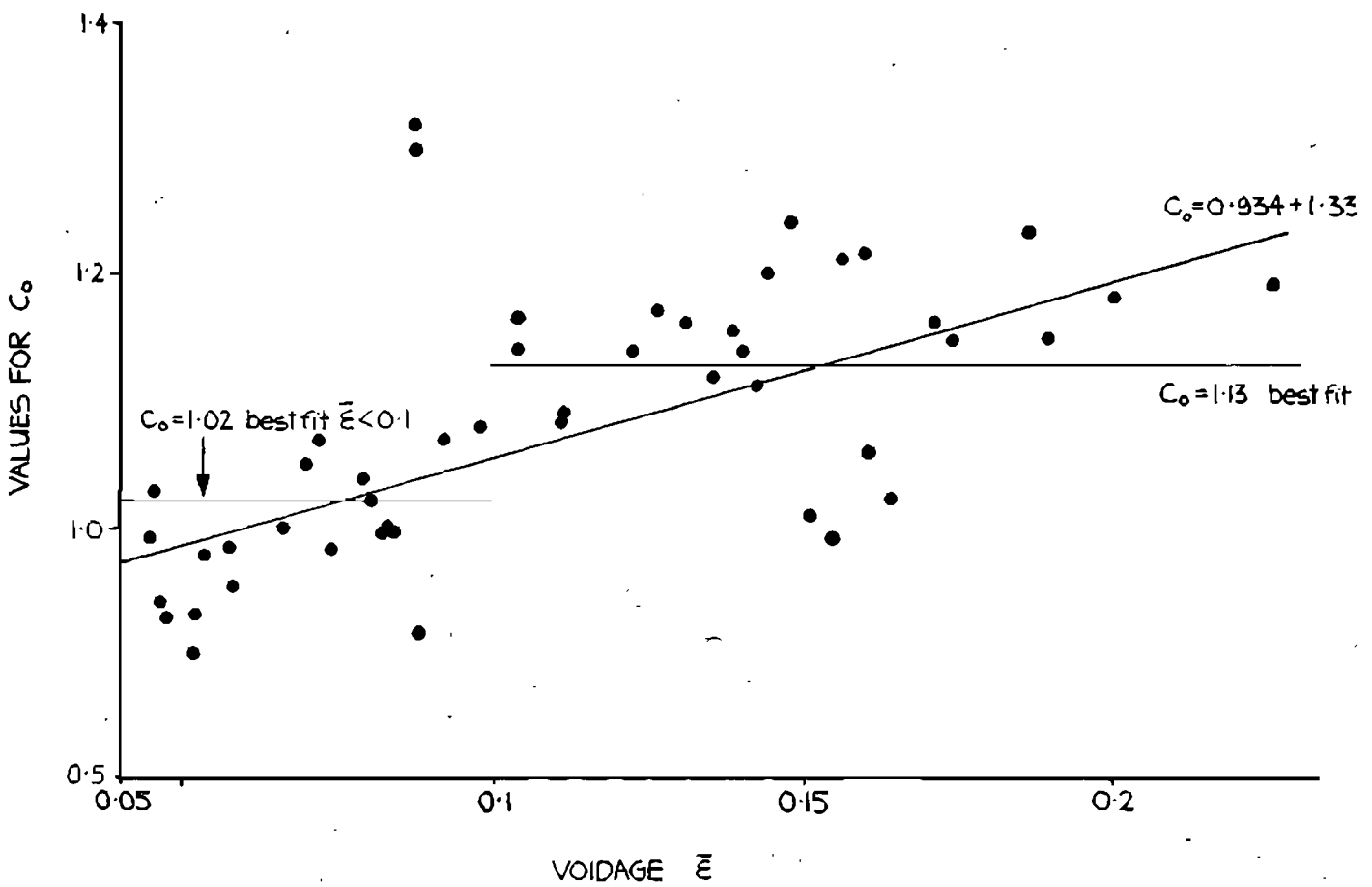

Fig 3·17 · Influence of voidage on values of C_o in upflow. (100mm pipe) ·

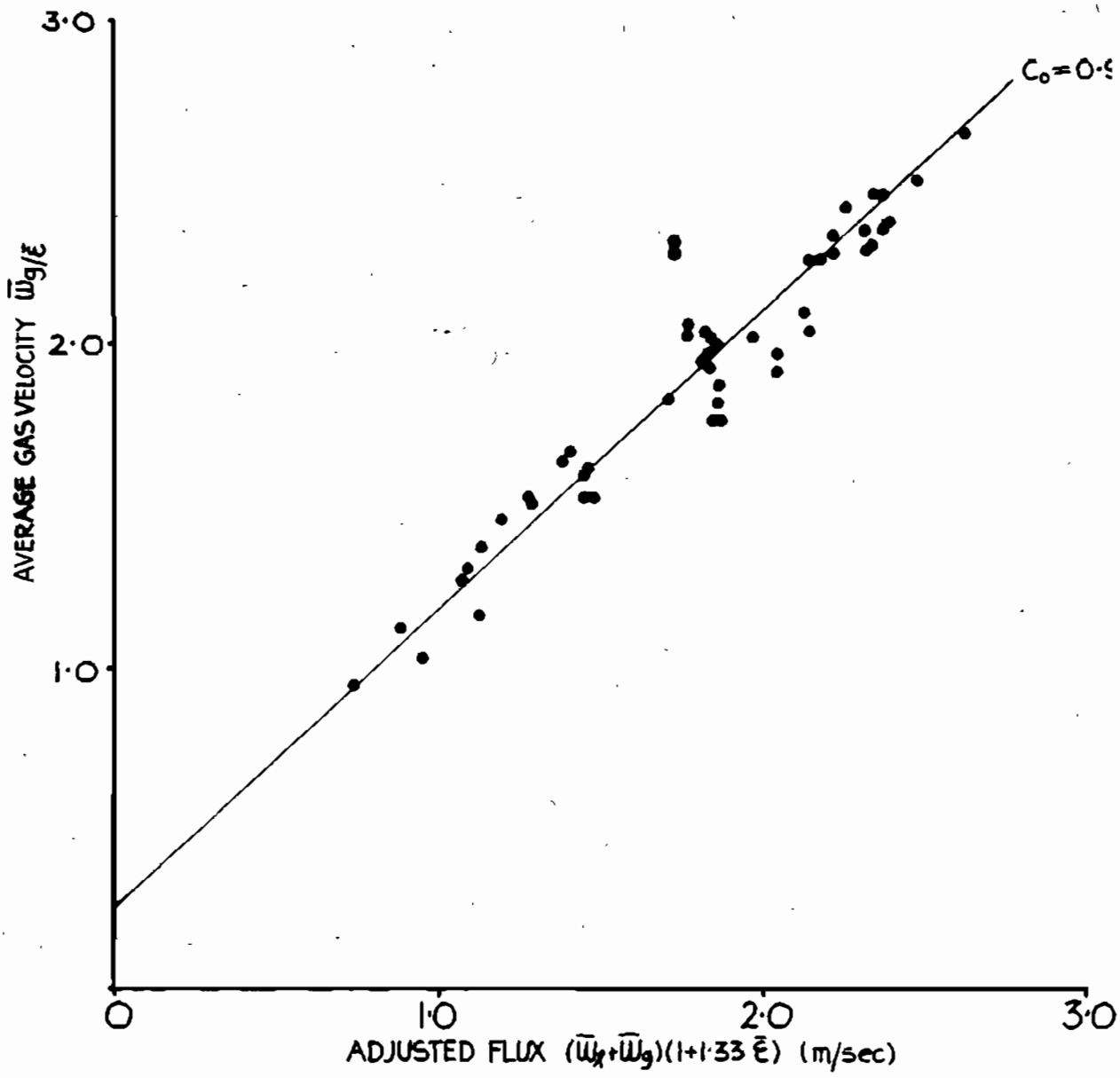

Fig 3·18 · Velocity-modified flux plot for upflow in 100mm rig ·

superficial velocity, $(\overline{W_g+W_l})$. At most, the bubble rise velocity could have varied by Ø.11 m/sec, as is shown by comparing the cases of an ideal, low voidage bubble flow, and a slug flow in the 1ØØ mm pipe.

The drift velocity for an ideal bubbly flow, at $\overline{E}$ = 0,05, is given by

$$\overline{U}_{gm} = 0,25\ (1-\overline{E})^{1.5} = 0,232 \text{ m/sec}$$

and the drift velocity of a fully developed slug flow is given by,

$$\overline{U}_{gm} = 0,35\ (gD)^{1/2} = 0,346 \text{ m/sec}$$

The difference between these two drift velocities (Ø.11 m/sec) is somewhat less than the range of gas velocities, $(\overline{W}_g/\overline{E})$, of up to 0.6 m/sec found experimentally at the same value of $(\overline{W_g+W_l})$.

From this argument it was concluded that the profile constant, C_o, was dependent on voidage. Values for C_o were calculated for each point under the constraint $\overline{U}_{gm}$ = 0.25 m/sec. Figures 3.14 and 3.17 clearly illustrate strong trends in C_o with voidage, although scatter of the data points suggested that another variable was influencing the profile effect. It was noted that there was a tendency for the relationship between C_o and gas

voidage to be emphasised at higher total superficial velocities, but the data were able to provide little more than a qualitative indication of this fact.

Data were divided for voidages above and below 10%, and optimum values of C_o obtained by regression. The best fit lines for $\bar{E} < 0.1$, $\bar{E} > 0.1$ and for all data were plotted for downflow and upflow in figures 3.13 and 3.16 respectively. An approximate relationship between C_o and $\bar{E}$ was obtained by using a linear regression of the form

$$C_o = C_1(1+C_2\bar{E}).$$

Best fits were found in downflow for the values $C_1 = 1.521$ and $C_2 = -2.41$, as plotted in figure 3.14, and for upflow $C_1 = 0.934$, $C_2 = 1.33$ as plotted in figure 3.17. These relationships suggested a modified drift-flux plot, to demonstrate the equation

$$\bar{W}_g/\bar{E} = C_1(1+C_2\bar{E})(\overline{W_g+W_l}) + \bar{U}_{gm}$$

as a graph of $\bar{W}_g/\bar{E}$ versus $(1-C_2\bar{E})(\overline{W_g+W_l})$. Such a line would have a slope of C_1 and intercept $\bar{U}_{gm}$. Plots of this type are given in figures 3.15 and 3.18, and show superior agreement with data.

This great variation in the holdup ratio encountered in

the 1ØØ mm pipe may be explained by the interaction of the voidage and velocity profiles, which govern the value of C_o. At low gas voidages the gas void distribution does not necessarily reach a maximum at the pipe centre [82,194], so that the constructive interaction of voidage and velocity profiles will be reduced. At higher average gas voidages the gas void distributions alter in shape so as to increase the profile effect. Consider voidage profiles determined in a 60 mm pipe by Serizawa et al [194]. In figure 3.19, from Serizawa's paper, it may be seen that at a flow quality of 0,0085% (corresponding approximately to $\overline{E}$ = 0,07) the void profile is saddle shaped, and may be expected to yield a low value of the integral

$$\int_{A_p} \overline{EW_m}\, dA$$

since the velocity profile will still have its maximum at the pipe centre. In consequence C_o will be low in value. A careful numerical integration of void and velocity profiles supplied graphically by Galaup [82] for a liquid superficial velocity of 1.5 m/sec, and a gas voidage of Ø.Ø5, showed that the profile constant would assume a value of below Ø.9 as a result of the saddle-shaped voidage profile. A similar argument may be applied to a case at higher velocity, where both voidage and velocity profiles tend to have maxima at the pipe centre [82,194],

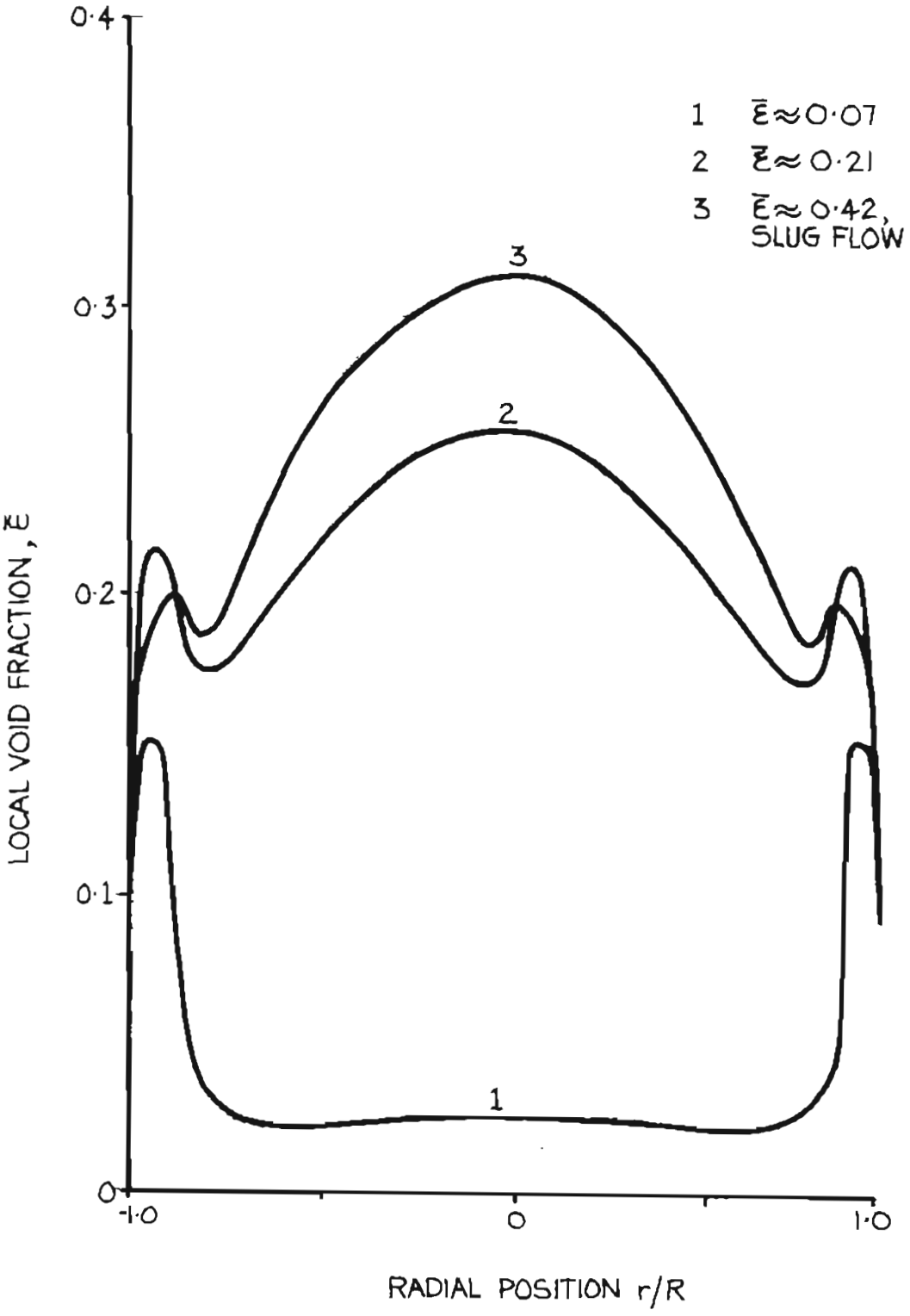

Fig 3·19 • Void fraction profiles for water flux of 1·03 m/sec (Serizawa et al.) •

so that C_o will be large. This would agree with the trend found in upflow.

It has been assumed above that the flow in the 100 mm test section is fully developed, the test section being 20 to 40 diameters from the sparger. Serizawa [194] has assumed the flow to be fully developed for an upstream distance of 30 diameters, although Herringe and Davis [91,92] have demonstrated that void profiles may still change after 36 diameters for certain spargers. Nevertheless, for a flow in a 50 mm pipe with a 10% gas voidage, Herringe and Davis [91] found that the gas void distribution could be saddle-shaped even after 108 pipe diameters, so that the low values of C_o may not just be a transitory effect. There is no reason to assume that bubble flows must eventually assume a parabolic or near-parabolic void distribution. Petrick and Kurdika [178] have commented that developing (upward) flows may often exhibit a gas-to-liquid velocity ratio of less than one at low air to water flow rates. Although the analysis presented here applies to fully developed profiles, this comment might be considered. If flows are still developing, it may be possible that the differing operation of spargers in up and downflow, as described in Chapter 2, may have an effect on the bubble assemblage.

Petrick and Kurdika [178] have found the profiles to change in a manner which disagrees with the data here,

claiming profiles to become flatter and reduce the value of C_o with increasing voidage. Their work is discussed in detail in Appendix E.

The high values for C_o at low voidages in downflow may be described by the 'bubble-coring' flow observed by Oshinowo and Charles [175,176]. In this case bubbles dominate the pipe centre, producing strongly favourable interaction between voidage and velocity profiles. Recent theoretical work by Drew and Lahey [76] supports this hypothesis. Visual observation of the flow in the 100 mm pipe also showed a tendency of bubbles to flow near the pipe axis at low voidages. At higher voidages bubbles occupied the whole pipe cross-section, so that C_o decreased. No other work of this nature for downflow is available for comparison, but Lorenzi and Sotgia [148] have commented on the inconstancy of C_o in both up and downflow at varying voidage.

It is of interest to note that Brown et al. [33] have proposed that gas void profiles become inverted in downflow, with voidage highest at the walls, and low at the pipe centre. Although a consideration of the work of all other relevant authors would dispute this conclusion, there may be some truth in this hypothesis at higher voidages where C_o became less than unity in this work.

3.6 CONCLUSION

The drift-flux model appears the most suitable model for the prediction of holdup in vertical bubble flow. Other models are either developed for different flow patterns, or fail to explain holdup at both high and low mixture velocities. The data of Borishanskiy et al. [29] for an 11 mm pipe, and the data gained in this study from a 50 mm pipe support the use of the drift-flux approach. However, data from the 100 mm apparatus demonstrate that a dependence of gas distribution on the average voidage causes C_o to vary within the bubble flow regime, so that a correlation for C_o in terms of average gas voidage is required.

Nevertheless, use of $C_o = 1.1$ in both up and downflow will not lead to severe errors in voidage prediction. The decrease in constancy of C_o in moving from 50 mm to 100 mm apparatus does, however, suggest that caution should be used in extending this work to pipes of an even larger diameter.

3.7 LIST OF VARIABLES

a	Exponent describing velocity distribution (-)
A_p	Cross sectional area of pipe (m^2)
b	Exponent describing velocity distribution (-)
B	Flowing gas fraction (by volume) (-)
C_o	Profile interaction constant (-)
C_1, C_2	Profile interaction constants (-)
E	Gas void fraction (-)
f	function of (-)
H	Holdup ratio (-)
K_b	Bankoff K - factor (-)
K_p	Holdup constant of Brown et al. (-)
K_s	Holdup constant of Smith (-)
K_y	Holdup constant of Yamazaki and co-workers (-)
m	Exponent for velocity distribution (-)
M	Mass flowrate (kg sec^{-1})
n	Exponent describing degree of waking (-)
p	Exponent for gas void distribution (-)
P	Pressure (Pa)
q	Dummy variable (-)
Q	Volumetric flowrate (m^3 $sec.^{-1}$)
r	Radial distance from pipe centre (m)
R	Pipe radius (m)
S	Slip velocity for describing holdup (m $sec.^{-1}$)
t	Time (sec.)
t_r	Time taken for bubbles to rise in test section

	section (sec.)
U	Velocity (m sec.$^{-1}$)
U_z	Bubble rise velocity in infinite liquid continuum (m sec.$^{-1}$)
V	Volume (m^3)
V_t	Total volume of test section (m^3)
W	Flux, or superficial velocity (m sec.$^{-1}$)
x	i) Quality (-) ii) Height in test section (m)
x_3	Length of isolated section (m)
X	Martinelli parameter (-)
ρ	Density (kg m^{-3})
σ	Surface Tension (N m^{-1})

Subscripts

c	at pipe centre
g	gas
gl	relative difference between gas and liquid property
gm	relative difference between gas and total flow property
l	liquid
lg	relative difference between liquid and gas property
lm	relative difference between liquid and total flow property
m	total flow

o	at atmospheric pressure
w	at pipe wall

CHAPTER 4

4. PRESSURE DROP IN TWO-PHASE FLOW

4.1 INTRODUCTION

The subject of pressure loss in two phase flow has received much attention and has been reviewed in great detail by Butterworth [34] and by Govier and Aziz [85]. However, much of this work is concerned with high velocity, high quality steam-water flow and is inapplicable to stable bubble flow. The flow regime has a profound effect on pressure drop, and broad correlations cannot be expected to yield more than a qualitative estimate of pressure losses.

However, even currently accepted methods for predicting pressure loss in bubble flow underestimate the losses in low velocity bubble flow [161], so that the design of a low velocity D.S.R. might be uncertain. In this thesis, an explanation was sought for the high pressure losses found in low velocity bubble flow, resulting in the development of a mixing length theory, which predicts that the presence of rising bubbles in the flow causes an excess shear at the pipe wall. The mixing length theory finds better agreement with low velocity bubble flow pressure loss data in the literature than the generally

accepted models. Moreover, at higher flow velocities, the mixing length theory agrees with the accepted models.

4.2 CONTRIBUTIONS TO TOTAL PRESSURE CHANGE

The analysis of two-phase flow by means of both energy and momentum balances, given below, has revealed that three separate effects contribute to the overall pressure change along a pipe length, viz:-

(i) Hydrostatic Head (in all but horizontal flow): Gravitational action on the mass in the pipe causes a pressure difference between two stations in the pipe.

(ii) Irreversible Losses: viscous dissipation during flow causes irreversible losses exhibited as a pressure loss along the pipe length.

(iii) Acceleration Effect: as a result of the gas phase compressibility, pressure change along the pipe produces a sympathetic change in gas and liquid void fractions. This change implies a change in velocity, and hence a change in momentum or kinetic energy, of each phase. This change in momentum, or kinetic energy, contributes to the overall axial pressure gradient in the pipe.

4.3 MOMENTUM AND ENERGY BALANCES

4.3.1 THE MECHANICAL ENERGY BALANCE

The mechanical energy balance for two phase flow has been derived by several authors [31,222,225] and a treatment by Brodkey [31] has yielded the equation

$$P_1-P_2 = \Delta P_{fe} + \frac{g(M_g+M_l)(x_2-x_1)}{(M_g/\rho_g + M_l/\rho_l)} + \frac{M_l\{(U_{l2}^3/U_{l2}) - (U_{l1}^3/U_{l1})\}}{2(M_g/\rho_g + M_l/\rho_l)} + \frac{M_g\{(U_{g2}^3/U_{g2}) - (U_{g1}^3/U_{g1})\}}{2(M_l/\rho_l + M_g/\rho_g)} \qquad 4.1$$

where M_g and M_l refer to gas and liquid mass flow rates and subscripts 1 and 2 refer to stations at distances x_1 and x_2 along the pipe. Gas density, ρ_g, is averaged over the section of pipe between the two stations. The term ΔP_{fe} represents the irreversible losses. Equation 4.1 is acceptably accurate for the ratio P_1/P_2 less than 2 [31]. The last two terms in equation 4.1 account for the acceleration effects in the flow. Many authors have chosen to omit these terms [85,111,116,176,188,238] and in bubble flow, where acceleration effects account typically for less than 1% of the axial pressure gradient, they may be neglected.

Equation 4.1 has accordingly been simplified to read

$$P_1 - P_2 = \Delta P_{fe} + \frac{g(M_l+M_g)(x_2-x_1)}{(M_l/\rho_l + M_g/\rho_g)} \qquad 4.2$$

where ρ_g is an average density of the gas phase between stations 1 and 2, and ΔP_{fe} represents the irreversible losses in the section in question.

4.3.1 THE MOMENTUM BALANCE

A rigorous momentum balance for two phase flow [31] has yielded the equation

$$M_l(U_{l1}^2/U_{l1}) + M_g(U_{g1}^2/U_{g1}) - M_l(U_{l2}^2/U_{l2}) - M_g(U_{g2}^2/U_{g2}) + (P_1 - P_2)A - T^*C_w(x_2 - x_1) - g\int_V \{\rho_l(1-E) + \rho_g E\}dx = \emptyset \qquad 4.3$$

where A is the cross-sectional area of the channel, C_w the circumference of the inside of the channel and T_* the average wall shear between the stations x_1 and x_2. Neglecting the first four terms, due to acceleration, and setting the density

$$\rho = \rho_l(1 - E') + \rho_g E' \qquad 4.4$$

Equation 4.3 may be re-written as

$$P_1 - P_2 = \Delta P_{fm} + g\{\rho_l(1-E') + \rho_g E'\}(x_2-x_1) \qquad 4.5$$

where E' is the average gas void fraction between stations 1 and 2, and

$$\Delta P_{fm} = -T^{*}(x_2 - x_1)(C_w/A) \qquad 4.6$$

In dealing with bubbly flow at all but very high pressures, it is convenient to omit the term $\rho_g E'$ from equation 4.5, since $\rho_g << \rho_l$ in low pressure flows.

4.3.2 COMPARISON OF MOMENTUM AND ENERGY BALANCES

The two terms accounting for irreversible losses in the energy and momentum equations, ΔP_{fe} and ΔP_{fm} respectively, are not generally equal in two phase flow. This has caused some confusion in the literature [139,225]. The difference between these terms is explained by the phenomenon of interphase slip, causing a difference between the in situ void fraction, $\bar{E}$ (as used in the momentum equation) and the flowing gas fraction, B (as used in the energy balance).

The energy balance hydrostatic head term

$$\frac{g(M_g+M_l)(x_2-x_1)}{(M_l/\rho_l + M_g/\rho_g)},$$

which is based on flowrates, differs from the momentum balance hydrostatic head term

$$g\{\rho_l(1-E') + \rho_g E'\}\{x_2-x_1\}$$

which is based on the in situ void fraction. Govier and Aziz [85] have observed that ΔP_{fe} is thus not a true reflection of frictional losses, and contains an excess pressure term due to the holdup effect. In fact, the term ΔP_{fe} must include losses due to the movement of bubbles relative to the liquid. The two frictional loss terms, ΔP_{fm} and ΔP_{fe}, will become equal, neglecting acceleration effects, only under the following circumstances:-

(i) where the net holdup ratio is 1, that is when

$$\bar{E}/(1 - \bar{E}) = \bar{W}_g/\bar{W}_l$$

(ii) when the fraction of one phase tends to zero, as in single phase flow.

(iii) when gravitational effects are excluded, such as in horizontal flow, where the static head term disappears.

The use of ΔP_{fe} has an advantage insofar as it may be determined from equation 4.2 with a knowledge of only the total pressure drop and mass flowrates. Several authors, notably Govier and co-workers [85-87], and Hughmark [114,116], have favoured the use of ΔP_{fe}. The term ΔP_{fm} may be obtained from equation 4.5 only with the knowledge

of void fraction in the pipe, but unlike ΔP_{fe}, it is a true representation of wall shear in vertical flow, and may be used to compare results in varying pipe geometries. The use of this term to describe the hydrostatic head has been found preferable by many authors [5,35,69,92,-111,142,154,188,189,238] and has been used exclusively below, so that henceforth $\Delta P_f = \Delta P_{fm}$.

4.4 PREDICTION OF IRREVERSIBLE LOSSES

The static head term may be evaluated with the knowledge of gas-phase voidage as predicted in the previous chapter. The irreversible losses are not readily evaluated and recourse to empirical and semi-empirical means is necessary, as in single phase turbulent flow.

4.4.1 TWO-PHASE MULTIPLIERS

Two phase pressure loss has been conveniently related to single phase losses by means of two phase multipliers. Martinelli and co-workers [147,153] defined multipliers Φ_l^2 and Φ_g^2 as the ratio of the two phase losses to those which would occur if each phase were to flow alone in the same channel.

$$(dP/dx)_{tp} = \Phi_l^2 (dP/dx)_l$$

$$(dP/dx)_{tp} = \Phi_g^2 (dP/dx)_g \qquad 4.7$$

The differential $(dP/dx)_l$ is therefore the pressure loss which would occur if only the liquid present in the two phase flow were flowing in the pipe. Only the multiplier based on liquid flow pressure loss is of interest in bubble flow, where losses are more closely approximated by "liquid-only" than "gas-only" pressure drop.

Another multiplier, Φ_{lo}, used by Baroczy [18] and by Chisolm and Sutherland (cited by Butterworth [34]), is defined as the ratio of two phase pressure loss to the loss which would occur if the whole mass flow were liquid

$$(dP/dx)_{tp} = \Phi_{lo}^2 (dP/dx)_{lo} \qquad 4.8$$

In bubbly flow a negligible proportion of the mass flow is in the gas phase, so that we may assume

$$\Phi_l = \Phi_{lo} \qquad 4.9$$

Butterworth [34] has demonstrated that

$$\Phi_l = \Phi_{lo}(1-x)^{1.8}$$

where x is the quality, or mass fraction of the flow, present in the gas phase. The mass fraction in the gas phase is so small in low pressure bubble flow as to confirm the assumption given in equation 4.9.

In many cases authors have not stated two phase pressure loss models in terms of a multiplier, but rather in terms of the D'Arcy equation, using modified velocity and friction factors predicted from modified Reynolds numbers. In such cases a formula for Φ_1 may be inferred by assuming some relationship between friction factor and Reynolds number, typically

$$f = \text{Const. } Re^{-n} \qquad 4.10$$

with n = 0.2 or 0.25 as in the Blasius equation [212].

4.6.2 CORRELATIONS INVOLVING TWO PHASE MULTIPLIERS

Many authors have provided simple formulae for the estimation of Φ_1^2. These are presented in table 4.1 and those of interest are discussed below.

(i) Formulae such as those of Orkizewski [174] and Govier and Aziz [85] rely on modifying the velocity to include the gas phase in both the D'Arcy equation and the Reynolds number. This Reynolds number is then used to find a single phase friction factor from a conventional friction factor diagram for use in the D'Arcy equation. Liquid densities and viscosities are used. The formulae for Φ_1^2 in table 4.1 are gained by using a Blasius-Type relationship as discussed in the preceding section and in

AUTHOR	MULTIPLIER
Kubota et al. [137]	1 [For large bore D.S.R.]
Orkizewski [174]	$1/(1 - E)^{1.8}$
Griffith and Wallis [89]	$1/(1 - E)^{1.8}$
Govier and Aziz [85]	$\{(W_g + W_l)/W_l\}^{1.8}$
Katsuhara [cited in ref. 238]	$1/(1 - E)^{1.75}$
Aoki [cited in ref. 238]	$1 + 250\{x/(1-x)\}^{0.8}$
Levy [143]	$1/(1 - E)^{2}$
Owen [cited in ref. 111]	$1 + x(\rho_l/\rho_g - 1)$
Turner and Wallis [cited in ref. 34]	$1/(1 - E)^{2.4}$
Beattie (Approximated) [21]:- $\{(W_l+W_g)/W_l\}^{0.8}\{(W_l+2W_g)/W_l\}^{0.2}$	

TABLE 4.1: MODELS FOR THE PREDICTION OF PRESSURE LOSS IN TWO PHASE BUBBLE FLOW
[x is the two phase flow quality]

detail by Butterworth [34].

(ii) Formulae such as those from Owen's Homogenous model [111] and Beattie [22] use a D'Arcy equation in a similar fashion to that described in (i), but choose to adjust the mass flow rather than velocity. Owen proposed the use of an average mixture density and a friction factor equal to that for the liquid alone. Beattie [22] used a modified Reynolds number, and correlated a friction factor with this, so that the multiplier became

$$\Phi_{lo} = \{1 + x(\rho_l/\rho_g - 1)\}^{0.8} \quad X$$

$$\{1 + x(\frac{(3.5\mu_g+2\mu_l)/\rho_l}{(\mu_g + \mu_l)/\rho_g} - 1)\}^{0.2} \qquad 4.11$$

where x is the flow quality. Neglecting gas density and viscosity this becomes the relationship given in table 4.1.

(iii) Turner and Wallis [see ref.34] considered flow in a horizontal tube. They proposed that the two-phase pressure drop was equal to the pressure drop which would occur if each phase were flowing in a channel with the same total cross-sectional area that the phase occupies in the two phase flow. The equation used in table 4.1 was deduced from their hypothesis by Butterworth [34], using a Blasius-type friction factor relationship.

(iv) The equation ascribed to Levy [142] is an approximation to a more rigorous development, recommended by Levy in his article.

Some further models for Φ_l^2 merit attention. The first correlation for Φ_l^2 was given in graphical form by Lockhart and Martinelli [147] and is illustrated in figure 4.1. They considered four cases dependent on whether the gas and liquid phases would be in laminar or turbulent flow, if flowing alone in the pipe. For each of these cases Φ_l^2 was plotted against X^2, the ratio of liquid to gas pressure drop with each phase flowing singly. This correlation has been widely accepted although it is generally acknowledged that it may not be particularly accurate [4,31]. Martinelli and Nelson [154] extended this work to include high pressure steam flow, and this method has been used by other authors [128].

Baroczy [18] proposed a more elaborate correlation for Φ_{lo}^2 in mixture quality and a "property index", Γ.

$$\Gamma = (U_l/U_g)^{0.2}/(P_l/P_g) \qquad 4.12$$

which is given by the ratio

$$\Gamma = (dP/dx)_{lo}/(dP/dx)_{go} \qquad 4.13$$

assuming a Blasius-type relationship with n=0.2. The

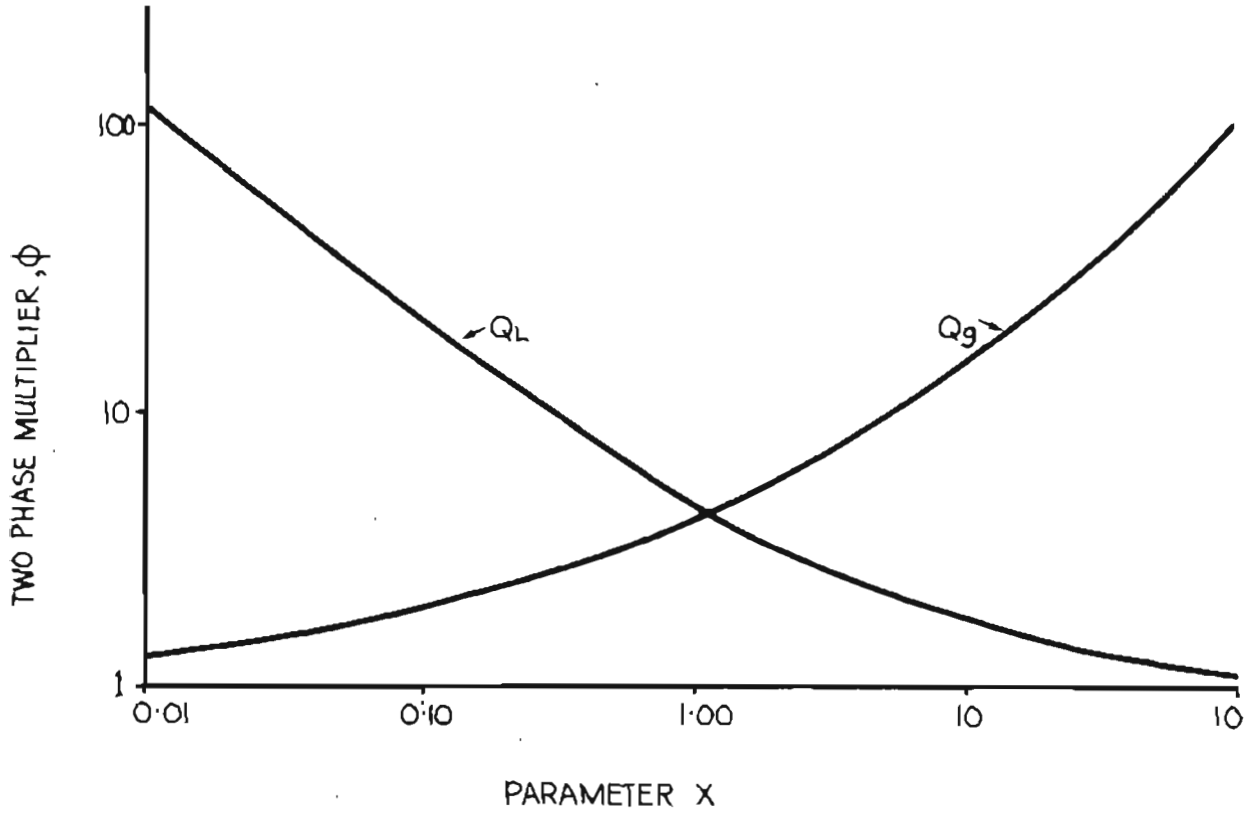

Fig 4·1 • The multipliers ϕ_L and ϕ_g for turbulent flow as given by Lockhart and Martinelli •

effect of mass flowrate was acknowledged, and adjustment was made to Φ_{lo}^2 in terms of a correlation in quality and mass velocity. The Baroczy correlation provided a significant improvement in taking mass flowrate into account, and its accuracy has been acknowledged [34]. It is, however, a very broad correlation concerned with flows of higher quality than the bubbly flow discussed here. Chisolm and co-workers [42, see also ref. 34] have also developed pressure drop correlations, with emphasis on the effect of pipe roughness. Here the multiplier is given as

$$\Phi_l^2 = 1 + C_c/X + 1/X^2 \qquad 4.14$$

where X is the Martinelli parameter, and correlations are developed for C_c in terms of mass velocity and the property index,

$$\Pi \approx (p_l/p_g)^{0.5}/(U_g/U_l)^{0.1} \qquad 4.15$$

which is the inverse square root of the Baroczy index, equation 4.12. This method permitted a far simpler representation of Baroczy's correlation. More recent work by Chisolm [41] has considered another detailed correlation, but this is not suited to bubble flow.

Levy [115] critised the use of the "lumped" models presented above and derived a predictive method for

pressure drop using modified mixing length theory. The solution for Φ_1^2 was presented graphically. Various assumptions in the model reveal it to be more suited to flows of higher quality than bubbly flow.

4.6.3 FURTHER EMPIRICAL CORRELATIONS

An empirical method for predicting pressure loss was developed by Ros [188] which simply presented a friction factor

$$f_R = f_1(f_2/f_3) \qquad 4.16$$

where f_1 was a graphical function of Reynolds Number, f_2 a function of gas-to-liquid superficial velocity ratio and pipe size, and f_3 a viscosity correction factor.

Davis [69] has presented equations of the form

$$f_D^{\emptyset.5} = A_D + B_D \ln(Re\ f_D^{\emptyset.5}) \qquad 4.17$$

where f_D is the predicted friction factor, and A_D and B_D are constants, to describe the friction factor. Kopalinsky and Bryant [136] and Govier et al. [86] have supplied friction factors in graphical form. Govier and Aziz [85] have discussed more broad correlations of this type.

4.4.4 DISCUSSION OF EXISTING MODELS

None of the above correlations is entirely suited to the description of bubbly flow. The correlations are either too broad ("lumped") or too simple. The two phase multiplier, Φ_l^2, may not be determined by one parameter models such as that of Orkizewski [174], since a mass velocity effect certainly exists. This is clearly demonstrated by the data of Nakoryakov et al. [161] for churn-turbulent bubbly flow, and by the recent work of Kytomaa [138], and some unpublished work of Hewitt [99]. Figure 4.2 shows Nakoryakov's data. At low liquid flowrates the pressure loss rose sharply with increasing gas voidage, but at higher flowrates the rise in pressure loss was less dramatic. On this basis we may dismiss all single parameter models for use in the low velocity bubble flow regime.

Models which do not consider flow regime may also be criticised, since even the early work of Govier et al. [86] has shown a relationship between pressure drop and phase interdispersion. This observation is emphasised by the sharp drop in frictional losses in bubble to slug transition found by Niino et al. [168] and Nakoryakov et al. [161] at low flow velocities.

There also appears to be general disagreement over pressure loss trends in low velocity bubble flow. The

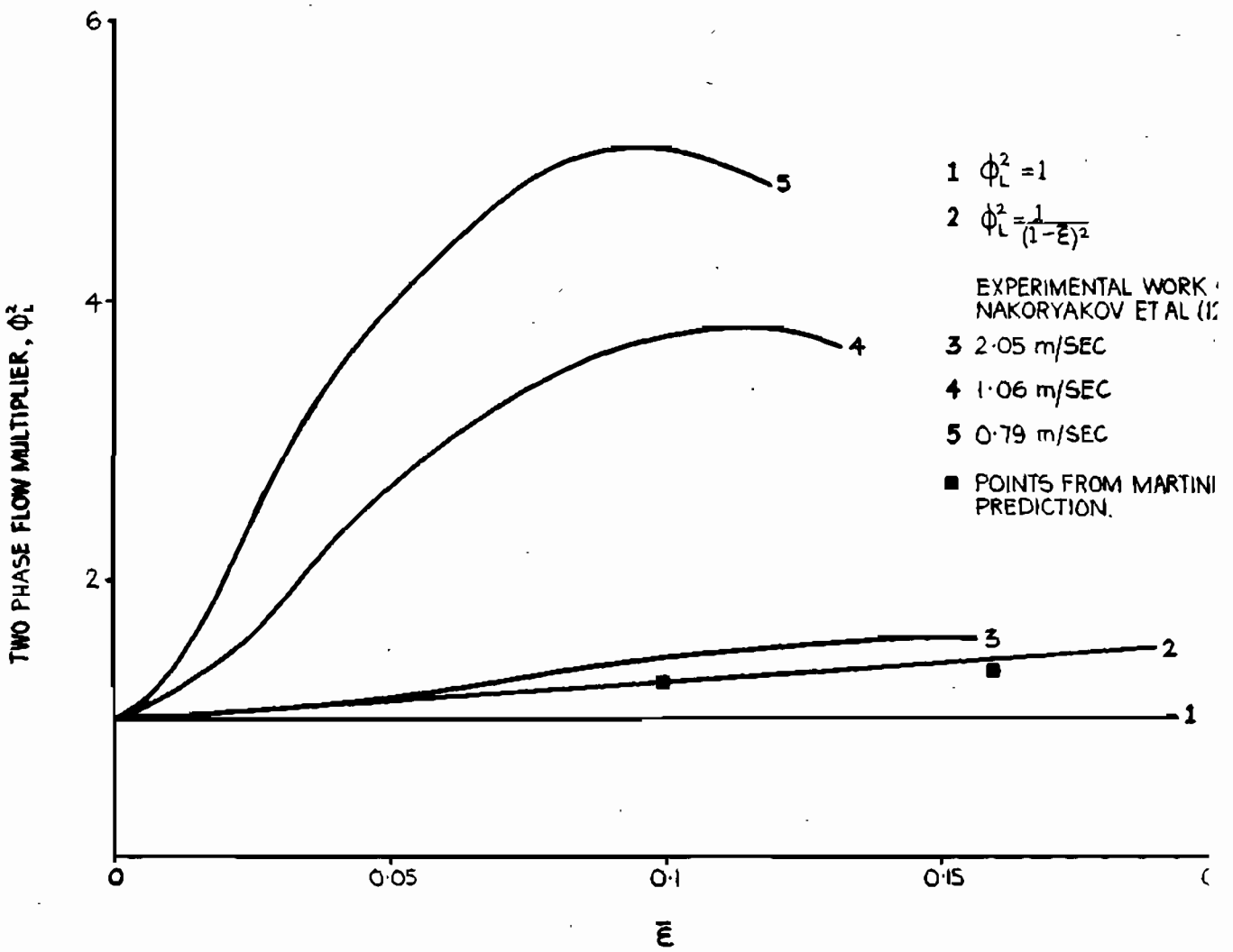

Fig 4·2 • Data of Nakoryakov et al (129) at various velocities •

conclusions of various authors for the cases of upflow and downflow are presented below.

Upflow

(i) Govier et al. [86] investigated pressure losses at a liquid velocity of 0,27 m/sec in a 26 mm pipe. Although few data were obtained at low gas flowrates, trends showed a significant increase in frictional loss with addition of air.

(ii) Oshinowo and Charles [176] conducted a similar study on a 25.4 mm pipe. At a liquid flowrate of 0,22 m/sec frictional loss was observed to decrease and become negative with increasing air rate, remaining negative throughout bubbly flow. Such negative gradients have been reported elsewhere in the literature [114] and are attributed to a downflow of liquid at the wall, with a rapid upflow at the pipe centre. This may be regarded as an extreme case of circulation as found in bubble columns [146]. However, negative gradients in pipe flow are usually associated with slug flow rather than bubble flow, so that the gradient here may be due to the presence of larger bubbles or intense channeling at the pipe centre.

(iii) Niino et al. [168] and Nakoryakov et al. [161] have reported work on an 86,4 mm pipe at a liquid flow of 0,23 m/sec. Wall shear stress was measured by an

electrochemical method and was found to increase sharply with addition of gas to the liquid stream. Shear stress increased almost 10-fold for a 15% gas flowing concentration. Similar results are reported to have been found in a 28 mm pipe [161]. In addition to this trend Nakoryakov et al. [161] noted that different values of shear stress were found when the apparatus was in an ideal or a churn-turbulent flow, the latter giving lower values.

(iv) The recent work of Kytomaa [138] supports the conclusions of Nakoryakov et al. [161]. Hewitt [99] has obtained data which agree, at least qualitatively, with Nakoryakov's findings.

The above examples illustrate that the gas and liquid flowrates alone are insufficient to characterise the flow for pressure drop prediction. It may be concluded that both void and velocity profiles in the pipe may affect losses strongly, as may bubble size distribution. Oshinowo and Charles' [176] "T" junction sparger might be expected to induce a somewhat different flow from that of the porous steel tube used by Nakoryakov et al. [161] and Niino et al. [168].

At higher liquid velocities in upflow Yamazaki and Shiba [238] found that Φ_l^2 increased little with gas addition and that the Lockhart and Martinelli [147] correlation was suitable. Nakoryakov et al. [161], however, found that at

liquid flowrates below 2 m/sec wall shear still increased sharply with increasing gas rate, so that all models shown in table 4.1 would predict too low a pressure drop. However, at liquid superficial velocities over 2m/sec Nakoryakov's results approached the prediction of the models given in table 4.1 more closely. It was noted that the high values of wall shear corresponded to flow with saddle-shaped voidage profiles, with a strong concentration of bubbles near the wall. These gas voidage profiles became parabolic at high velocity, or after the transition to slug flow, where lower values of wall shear stress were observed.

Oshinowo and Charles [176] found values of Φ_l^2 to be a little lower than those predicted by the Lockhart-Martinelli curve, while Serizawa et al. [194] found that the longitudinal turbulent velocity, a measure of turbulence in the system, decreased at first gas addition, especially at higher liquid velocities. With higher gas flow the turbulence increased.

There is some disagreement over values of pressure loss in low velocity bubble flow. However, most authors have argued that pressure loss increases with addition of bubbles to a liquid flow. At least three independent experimental programs have demonstrated that this increase in pressure loss may be very sharp at low flow velocities, a fact not explained by existing models.

Downflow

Little work is available on downflow. Yamazaki and Yamaguchi [241] investigated flow in a 25 mm pipe but observed no bubbly flow. Their predictive model, $\Phi_l^2 = (1-E)^{-1.8}$, may thus not be applicable to this regime. Oshinowo and Charles [176] observed downward bubble flow and found values a little lower than the Lockhart-Martinelli curve at liquid velocities of approximately 2m/sec.

4.4.5 FACTORS INFLUENCING PRESSURE DROP

Disagreements in the literature serve to illustrate the variation in pressure drop findings for bubbly flow. At this point it is judged that the presence of bubbles in a liquid stream may affect pressure drop by the following mechanisms.

(i) The presence of the gas phase serves to increase the total superficial velocity of the flow: this is accounted for in most of the currently accepted models, such as that of Orkizewski [174].

(ii) Bubble voidage profiles may influence liquid velocity to set up velocity distributions that differ from the single phase case [81]. Bubble recirculation may also

affect the velocity distribution across the pipe.

(iii) It would be expected that movement of bubbles through the liquid would increase local turbulence [144].

(iv) Larger bubbles may impede the movement of some turbulent eddies, and may absorb energy from the liquid phase. Serizawa et al. [194] have suggested that circulation and rotation in larger bubbles may serve to dissipate energy, although no precise theory has been developed to explain this hypothesis [195]. The occurrence of corrugated surfaces in some bubbles supports this supposition. Induced circulation in gas bubbles has also received attention from Garner and Hammerton [84].

None of the models reviewed above considers all of the four factors, and it is intended in this thesis to propose a model which will incorporate these effects to provide a more accurate and general mathematical description of frictional losses in two-phase bubbly flow.

4.5 DEVELOPMENT OF MIXING LENGTH THEORY

In the preceding section it was demonstrated that the recent results of Nakoryakov et al. [161] deviated from the pressure loss which currently accepted models would predict. Similar deviations have been noted in recent

work on gas-solid vertical pneumatic transport [120,204], but have been misinterpreted by one author [204] who accounted for the particle weight in the gas-solid flow twice. In gas-liquid flow, the pressure loss deviation at low velocities may be ascribed to an "excess shear" generated by the bubbles rising through the liquid. Such a concept has been proposed by Hughmark and Pressburg [116], and may be considered similar to the turbulence created by particles falling in a fluid, a concept used in mass transfer correlations by Ohashi and co-workers [171].

Mixing length theory is used below to illustrate how this excess shear develops in two phase flow. The detailed mixing length solution is complex and is not intended as a predictive correlation. The model is later simplified for predictive purposes. Although mixing length has been used previously in two phase flow theory [21,143,144] the treatment below is entirely original in its approach and provides the first fundamental explanation for the high values of the two phase multiplier found in low velocity bubble flow.

4.5.1 PRESENTATION OF THEORY: THE SINGLE PHASE CASE

Single phase mixing length theory is developed below briefly for comparative purposes, followed by the extension to the two phase case.

REYNOLDS STRESSES

In dealing with turbulent motion it is convenient to separate velocities into a mean and fluctuating component [192]. In this study we shall assume that there are no rotational velocity components in the pipe, and write

$$U = \underline{U} + U' \qquad 4.18$$

for the x-direction along the pipe axis, and

$$V = \underline{V} + V' \qquad 4.19$$

for the y-direction which is the radial distance in from the wall. The underscore denotes the mean, and the prime the fluctuating component.

Either by analysis of momentum flux, or by a solution of the Navier-Stokes equations [107,192], it may be shown that

$$T_{sp} = -\rho_l U'V' \qquad 4.20$$

where T_{sp} is the shear stress in the x-direction at the surface of an axial cylinder (sp denotes single phase), ρ_l is the fluid density, and U'V' is the time-average of the product of the fluctuating velocity components in the axial and radial directions. Where equation 4.20 is

extended to the case ~~at~~ near the pipe wall, ~~or at least to~~ but not into the laminar sub-layer at the wall,

$$T^*_{sp} = -\rho_1 U'V' \qquad 4.21$$

where T^*_{sp} is the wall shear stress.

PRANDTL MIXING LENGTH THEORY

Prandtl developed the mixing length theory to describe transport in turbulent boundary layers. The mixing length equation is developed below. Refer to figure 4.3.

Consider a "packet" of fluid moving, as a result of a radial velocity fluctuation V', towards the wall. Let it move a radial distance l, from y_1+l to y_1. The velocity in the x-direction of this packet, $U(y_1+l)$, will exceed that of the fluid at y_1 by the amount

$$U_1 = \underline{U}(y_1+l) - \underline{U}(y_1) \approx l(d\underline{U}/dy) \qquad 4.22$$

Similarly a packet moving away from the wall from y_1-l to y_1 will have a velocity in the x-direction lower than the velocity at y_1 by

$$U_2 = \underline{U}(y_1) - \underline{U}(y_1-l) \approx l(d\underline{U}/dy) \qquad 4.23$$

We may consider U_1 and U_2 to be the fluctuating velocity

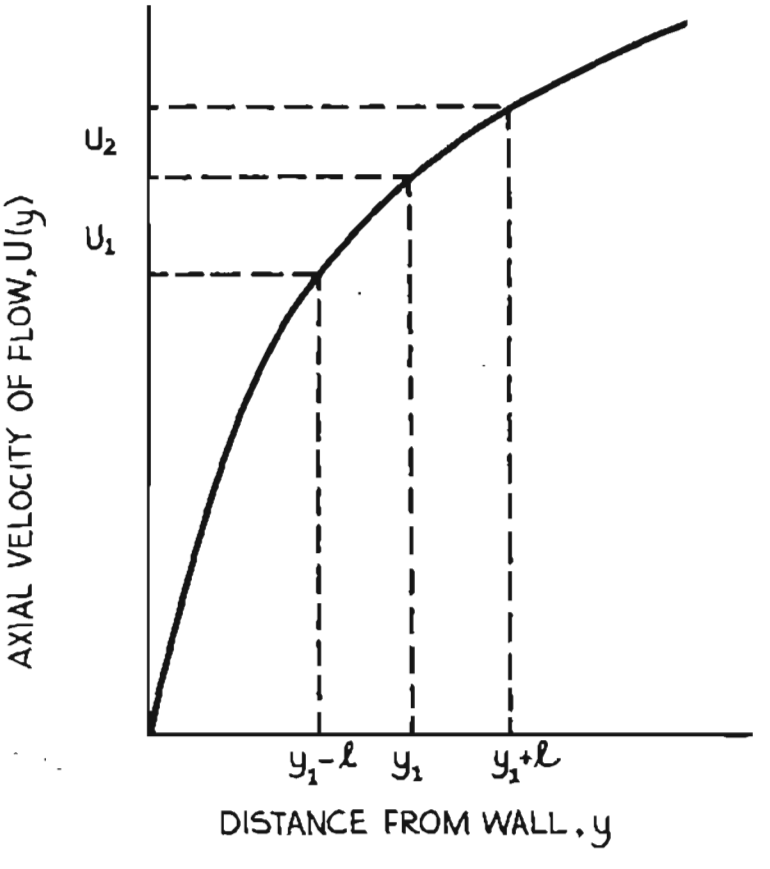

Fig 4·3 • Single phase mixing length theory •

components in the x-direction, so that from equations 4.22 and 4.23

$$U' = \emptyset.5|U_1| + \emptyset.5|U_2| \approx l(d\underline{U}/dy) \qquad 4.24$$

Experimentally V' and U' are found to be anticorrelated, so that

$$V' = -C_1 U' \qquad 4.25$$

for C_1 a positive constant. From equations 4.24 and 4.25

$$|V'| = C_1 l|d\underline{U}/dy| \qquad 4.26$$

The time average value of U'V' is accordingly non-zero, and is given by

$$U'V' = -C_2|U'||V'| \qquad 4.27$$

Modifying the mixing length, l, to incorporate the constants C_1 and C_2, from equations 4.24, 4.26 and 4.27

$$U'V' = -l^2(d\underline{U}/dy)^2 \qquad 4.28$$

From equations 4.2Ø and 4.28

$$T_{sp} = \rho_1 l^2(d\underline{U}/dy)^2 \qquad 4.29$$

For pipe flow where no radial pressure profiles exist, a simple force balance demonstrates that shear stress decreases linearly from the wall,

$$T_{sp} = T^*_{sp}(1 - y/R) \qquad 4.30$$

where R is the pipe radius. From equations 4.29 and 4.30

$$T^*_{sp} = \rho_l l^2 (d\underline{U}/dy)^2/(1 - y/R) \qquad 4.31$$

Rearranging equation 4.31 and integrating yields the equation

$$\underline{U}(y/R) = R \int_{y_b/R}^{y/R} T^*_{sp}(1-y/R)/\ _l l^2 \ d(y/R) \qquad 4.32$$

with boundary condition near the pipe wall $(y_b/R, \underline{U}(y_b/R))$. The boundary condition may be expressed in two ways for a smooth pipe. Either we may take y_b as being equal to the laminar boundary layer thickness,

$$y_b = 5\nu/(T^*_{sp}/\rho_l)^{0.5} \qquad 4.33$$

in which case

$$\underline{U}(y_b/R) = T^*_{sp} y_b/\mu_l \qquad 4.34$$

or we may assign some value to y_b, where y_b is a small distance from the wall, for which $\underline{U}$ may be taken as zero

for purposes of the integration. This is discussed in detail by Schlichting [192], pp578-584 and by Hinze [107], pp635-636. This value of y_b, by analogy to the universal velocity distribution, may be given as

$$y_b = 0.111 \nu / (T^*_{sp}/\rho_l)^{0.5} \; ; \; \underline{U} = 0 \qquad 4.35$$

although values of the "constant" {0.111 in equation 4.35} may be debated [107]. A boundary condition may also be developed for the case of rough pipes [192]. The value of y_b for which $\underline{U}$ may be taken as zero depends on the pipe roughness: y_b may not be taken as zero, since the flow is not turbulent up to the pipe wall, so that the mixing length approaches zero there.

Neglecting the insignificant flow in the boundary layer, the total flowrate through the pipe may be predicted from equation 4.32 by integrating the fluid velocity over the pipe cross-section

$$Q = R \int_{y_b/R}^{1} \underline{U}(y/R)^2 \, (1-y/R) \, d(y/R) \qquad 4.36$$

Using the above equations, given the wall shear stress, and the velocity and mixing length distributions across the pipe, total flowrate in the pipe may be predicted.

4.5.2 THE ANALYSIS EXTENDED TO A BUBBLE FLOW

DENSITY VARIATION

Consider a two phase bubble flow. The mean density ρ in any volume, discounting the mass of the gas phase, may be given by

$$\rho = \rho_l(1-E) \qquad 4.37$$

where E is the average gas volume fraction, or voidage, in that volume. In the subsequent analysis this volume may be reduced to a point, in which case the voidage may be interpreted only as a time-average variable, and the density as a time-average density. The reduction of the voidage in a small volume to the voidage at a point does not affect this analysis, and has been considered in detail elsewhere [71,75,163].

SHEAR STRESS PROFILE

Where local voidage, and hence density, is not uniform across a pipe section, the shear stress profile is not perfectly linear with respect to radius. Levy [143] developed the following force balance for two phase flow:

$$T_{tp} = T^*_{tp}(1 + (\underline{\rho} - \rho_i)/(2T^*_{tp}R))(1 - y/R) \qquad 4.38$$

where the subscript tp denotes the two phase condition, $\underline{\rho}$ is the average density over the whole pipe cross section, and ρ_i is the average density contained within a radius r of the pipe centre, given by the expression

$$\rho_i = \int_{\emptyset}^{r} 2\rho/r \, dr \; ; \; r = R-y \qquad 4.39$$

with ρ the local density at radius r. A rigorous relationship such as equation 4.38 must be used for flows where voidage varies significantly across the pipe cross-section, as in annular flow. However, in bubble flow the average gas voidage is generally small (less than 20%), so that density variation is not large. Typical bubble void profiles are not steep except near the wall [91,243] where values of $\underline{\rho}$ and ρ_i become similar in any case. Analysis shows that for a bubble flow with typical values of T^*_{tp} = 15 N/m^2 and a 15% average bubble voidage distributed as a 1/7th power law across the pipe, the shear stress given by equation 4.30 would deviate from the shear given by equation 4.38 by only 3% at worst. Power law relationships have been used to describe voidage distributions by Bankoff [13] and Zuber and Findlay [243,244]. Equation 4.30 was considered to be sufficiently accurate for the representation of shear stress profile in the analysis below.

REYNOLDS STRESSES IN A COMPRESSIBLE MEDIUM

For a single phase compressible flow the shear stress at the pipe wall is given as [192]

$$T^{*} = -\rho U'V' - \underline{U}\rho'V' - \underline{V}\rho'U' - \rho'U'V' \qquad 4.40$$

where ρ' is the density variation due to local compression. Noting that a density fluctuation may occur only as a result of the transport of material by a velocity fluctuation, we may say that $\rho'/\underline{\rho}$ is no greater than $U'/\underline{U}$. Noting that U' is far smaller than $\underline{U}$, we may neglect the last term with respect to the first two. For pipe flow it is assumed that the transverse velocity, $\underline{V}$, is small with respect to $\underline{U}$, but that U' and V' are of the same order of magnitude, in which case the third term may be neglected. Schlichting [192] has shown that the inclusion of the second term on the right hand side of equation 4.40 is equivalent to the addition of $\rho'V'$ to the term $\rho\underline{V}$ in the continuity equation and has concluded that the incompressible case given in equation 4.20 may be used as a good approximation in the description of compressible pipe flow.

In the case of bubble flow density fluctuation would be caused by voidage change due to bubble compression and rarefaction, and also by bubble movement. The term $\rho'V'$ will attain a significant value only if the transverse

velocity fluctuations are able to compress the bubbles or carry bubbles over a significant distance in the flow. It is judged that the term $\rho'V'$ would be equivalently smaller in a typical bubble flow than in continuous compressible flow, so that we may elect to use equation 4.20 to describe the shear stress for the case of bubble flow, i.e. we shall consider the shear stress arising only from fluctuations in the liquid phase, regarding the shear stress generated directly by the presence of the gas phase as negligible. Any additional Reynolds stresses arising from density fluctuation may nonetheless be incorporated satisfactorily in the term for the "excess shear" generated by the bubble presence, as derived below.

ANALYSIS OF THE CONCEPT OF EXCESS SHEAR

Consider a cross-section of a pipe in two phase bubble upflow. Let a bubble be a little above the cross-section, so that this cross-section cuts the bubble wake. Refer to figure 4.4. Let the bubble rise relative to the liquid with a velocity U_b, and let the velocity of the fluid on the wake centre-line at this cross-section exceed the undisturbed liquid velocity (in an axial direction) by an amount U_w, which would be smaller than U_b. This would cause a distortion of the velocity profile as shown in figure 4.4. Considerations of continuity will indicate that there must be transverse velocity components, V_w and $-V_w$, feeding into the wake to replace fluid below the bubble nadir.

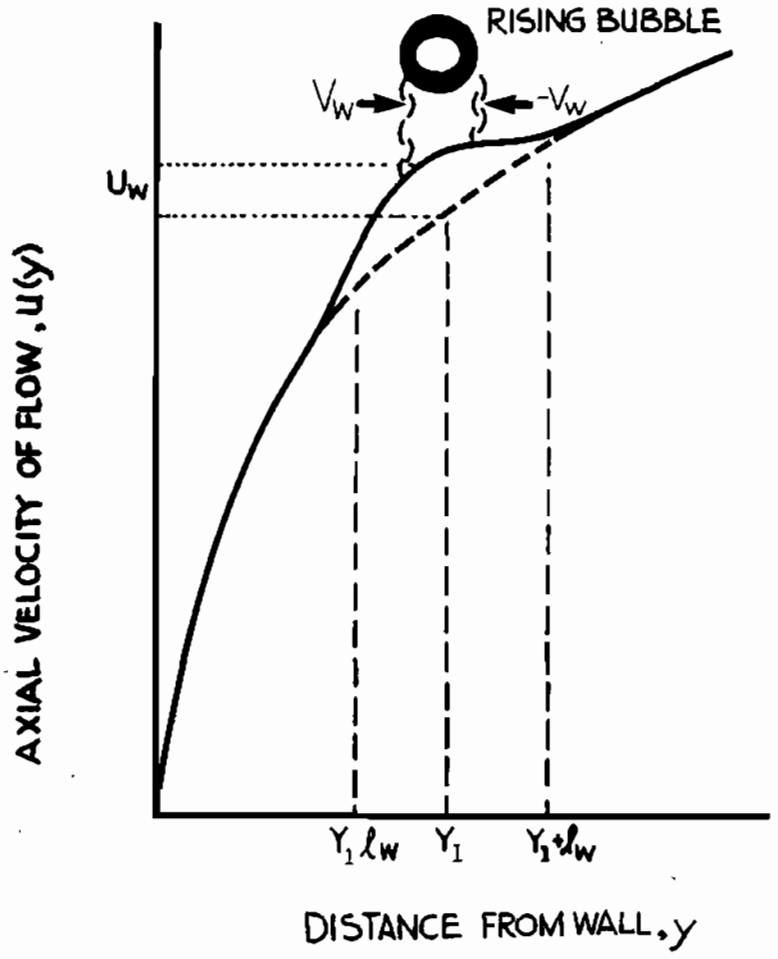

Fig 4·4 • Effect of bubbles on mixing length analysis •

These may be of the same order of magnitude as U_w. The stronger the bubble wake, the greater will be the ratio U_w/U_b, and the smaller and more diffuse the transverse components. The velocities U_w and V_w are strongly dependent on the distance behind the bubble, but the analysis below may proceed by using any local values of U_w and V_w. In the final analysis one must consider some average values for U_w and V_w that are representative of the whole bubble flow.

In the neighbourhood of a bubble wake, there are now additional velocities contributing to the total velocity. The total velocity can be split into the mean velocity (excluding the distortion of the velocity by passing bubbles), the turbulent fluctuating component, and the component arising due to the presence of a bubble in the flow. This last component is termed U_w in the axial direction and V_w in the transverse direction. Thus,

$$U = \underline{U} + U' + U_w \qquad 4.41$$

$$V = \underline{V} + V' + V_w \qquad 4.42$$

If we include these new "bubble-influenced" components, U_w and V_w, in the fluctuating velocity, the Reynolds' stresses in the liquid phase giving rise to wall shear stress are

$$T_{tp} = -\rho_l(U' + U_w)(V' + V_w) \qquad 4.43$$

The significance of the interaction of these new terms must be ascertained. It will be shown below that (i) the presence of axial velocity component, U_w, has no effect on the wall shear, and (ii) the radial component, V_w, serves to increase the wall shear, by producing additional Reynolds' stresses, thus giving rise to "excess shear".

If U' is defined to be the fluctuation arising from liquid bulk turbulence only, and U_w as the "excess" velocity arising from the passage of the bubble, there is no reason to suppose that U' and U_w are correlated. Applying a similar argument to the transverse components, V' and V_w, equation 4.43 becomes

$$T_{tp} = -\rho_l(U'V' + U'V_w + U_wV' + U_wV_w) \qquad 4.44$$

The first term on the right hand side, U'V', does not differ in nature from the single phase case, which is described in equation 4.29. It remains to analyse the effect on the shear stress of the three new terms, $U'V_w$, U_wV', and U_wV_w. To examine the effect of both U_wV' and U_wV_w, consider the interaction of U_w alone with any transverse component V. Refer to figure 4.4. Let V cause the movement of a packet of fluid from y_1-l_o to y_1, a distance l_o. In an analogous way to the single phase case described above, the packet suffers a velocity deficit

relative to the undisturbed liquid at y_1. The deficit is then given by

$$U_1 = l_o(d\underline{U}/dy) + U_w \qquad 4.45$$

where $\underline{U}$ is the steady flow velocity excluding the peturbations arising as a result of the proximity of a bubble, as defined in equation 4.41. This velocity deficit, U_1, is associated with a positive value of V, since it was caused by a movement away from the wall. When a packet moves toward the wall from y_1+l_o to y_1, the velocity deficit, preserving the sign of velocity established in equation 4.45, is

$$U_2 = -l_o(d\underline{U}/dy) + U_w \qquad 4.46$$

This velocity deficit is associated with a negative value of V (i.e. a negative value of V' or V_w). Hence we see that the term U_w is associated with a pair of transverse velocities of different sign, and will give rise on average to a pair of Reynolds stresses of opposite sign. There is no nett stress generated by the presence of the axial component U_w, since the sum of the two products VU_w and $(-V)U_w$ must be zero. The only non-zero stresses which may be derived from equations 4.45 and 4.46 are those from the interaction of U' and V', that is those which would occur in the single phase case, as expressed in equation 4.29. This argument allows us to ignore the last two

terms in equation 4.44, and thus discount the effect of U_w in the remainder of the analysis.

However, the second term on the right hand side of equation 4.44, $U'V_w$, can be shown to assume a significant value in the case of bubble flow. Consider a transverse component, magnitude V_w, feeding into the wake. Let such a component move a packet radially inwards to the wake a distance l_w, from y_1-l_w to y_1. We may proceed with the analysis ignoring the contribution of U_w to the total velocity, since it has been demonstrated that the axial wake velocity, U_w, has no nett effect on the shear stress in the fluid. The packet moved through the distance l_w would have a velocity deficit

$$U_1 = \underline{U}(y+l_w) - \underline{U}(y) = l_w(d\underline{U}/dy) \qquad 4.47$$

similarly a packet moving toward the wall would exceed the local velocity by

$$U_2 = \underline{U}(y) - \underline{U}(y-l_w) = l_w(d\underline{U}/dy) \qquad 4.48$$

There is an anticorrelation between the transverse and longitudinal velocity fluctuations, in a similar way to the single phase case, so that the products for both motions towards and away from the wall are negative. Setting

$$|U'| = 0.5|U_1| + 0.5|U_2| = |l_w(d\underline{U}/dy)|, \qquad 4.49$$

the product of the axial fluctuating velocity and radial wake velocity becomes

$$U'V_w = -C_5|l_w(d\underline{U}/dy)||V_w| \qquad 4.50$$

so that the Reynolds stress arising from this interaction is given by

$$T = \rho_l C_5|l_w(dU/dy)||V_w| \qquad 4.51$$

Equation 4.44 may now be expressed in terms of equations 4.29 and 4.51, where equation 4.29 accounts for the interaction between U' and V', and equation 4.51 accounts for the interaction between U' and V_w. Hence

$$T_{tp} = \rho_l l^2(dU/dy)^2 + \rho_l C_5 l_w|(dU/dy)||V_w| \qquad 4.52$$

The analysis has been presented for a point just below a bubble, in the bubble wake. If the above analysis is repeated with the cross-section taken just above a bubble, where transverse velocity components are outward, away from the bubble path, equation 4.52 is again reached, with no change of sign, although the values of C_5, l_w and V_w would generally differ from those values for the case in the bubble wake. Moreover, the equations are applicable for the case of two phase downflow as well.

Although the analysis presented above is concerned with the influence of the bubble on the liquid flow at a point, in the final analysis one must propose a value for V_w which is an average in some small volume of the flow. Clearly where no bubble is near, the value of V_w at a point must tend to zero, and where a bubble is near, V_w may assume a finite non-zero value. Hence the average value of V_w in a small volume must increase in direct proportion to the number of bubbles in the volume, assuming that the flow structure is unchanged by an increasing number of bubbles in the volume. Where bubble size is invariant, the number of bubbles in a volume of the flow will increase in direct proportion to the gas voidage in that volume. The value of V_w near a bubble will also depend on such factors as bubble size, waking, interaction and bubble rise velocity. It is supposed that V_w will increase with increasing bubble rise velocity, and since no other properties of the two phase flow can be quantized readily, it is proposed that the average value of V_w in the flow is given by the product of gas voidage, bubble rise velocity, and a constant, C_7, which accounts for all other two phase flow properties. This relationship for the average value of V_w may also be deduced on a time-average basis, so that the time-average shear stress at a point may be formulated, but this does not affect the subsequent analysis. The average value may now be substituted into equation 4.52 instead of the local

value, V_w, to form the relationship for the whole two phase flow

$$T_{tp} = \rho_l l^2 (d\underline{U}/dy)^2 + \rho_l C_5 l_w (d\underline{U}/dy) C_7 U_b E \qquad 4.53$$

Equation 4.53 reveals that when no bubbles are present (E = Ø), or where no slip between the phases occurs (U_b = Ø), the two phase model reduces to the single phase case. Collecting constants,

$$T_{tp} = \rho_l l^2 (d\underline{U}/dy)(d\underline{U}/dy + C_9 U_b E/l^2) \qquad 4.54$$

with $C_9 = C_5 C_7 l_w$ and with (dU/dy) taken as positive: C_9 has units of length.

Examination of equation 4.54 reveals that when bubbles are present, shear will increase for two reasons. Firstly, if liquid flowrate is held constant, the velocity, U, must increase. If velocity profiles remain similar in the pipe flow and the velocity increases, this leads to an increase in ($d\underline{U}/dy$) at any fixed point in the flow, and a consequent increase in shear. Such an increase in shear was accounted for by the generally accepted models given in the literature survey. Secondly, there is the "excess shear" generated by the presence of the bubbles, and increasing in proportion to the gas voidage, although the constant C_9 may vary a little with changing bubble flow structure. Nevertheless, shear stress should increase

until a change of flow regime, from bubble to slug flow, takes place. The nature of the bubble to slug transition is discussed in Chapter 1.

Equation 4.54 can not be solved easily to yield the wall shear stress, T^*_{tp}, in terms of flowrate and voidage. The general solution of 4.54 must proceed along the following lines. Equation 4.54 is a quadratic equation in (dU/dy). The solution of the quadratic is found to be

$$dU/dy = -C_9 E U_b/l^2 + \sqrt{C_9^2 E^2 U_b^2/l^4 + T_{tp}/\rho l^2} \qquad 4.55$$

where the positive surd supplies a real solution. Equation 4.55 may now be integrated in the same way as the single phase case. As bubble populations are known to decrease to zero at the wall [91,178,243], it is possible to use the single phase boundary conditions, without incurring any significant error.

$$\underline{U}(y/R) = \int_{y_b/R}^{1} -C_9 E U_b/l^2 + \sqrt{C_9^2 E^2 U_b^2/l^4 + T_{tp}/\rho_l l^2}\ d(y/R) \qquad 4.56$$

where $T_{tp} = T^*_{tp}(1 - y/R)$

Using equations 4.56 and 4.36, it is then possible to predict the flowrate through the pipe, given the wall shear stress. Assumptions must be made concerning the values of the mixing length and voidage distributions

used. Voidage and mixing length may be taken as functions of distance from the wall, y. Boundary conditions must also be specified. Values for the constant C_9 ought to be obtained only from regression performed on known data, as current knowledge of two phase flow is too scant to infer a quantitative value for C_9 directly. Assumption of profiles for mixing length and voidage is dealt with in the section below, but it may be seen that solution of the equation 4.56 is not a convenient predictive tool, since it requires information on local properties of the flow, data which is seldom available to the designer. However, the model provides a fundamental explanation for the generation of excess shear in two phase bubble flows, and is the basis for a simplified model which is developed below.

In cases where large bubbles are present in the flow it may be necessary to modify equation 4.56 to account for the obstruction of turbulent eddies by these bubbles. Serizawa et al. [194] observed that on occasions a drop in turbulent intensity may occur upon introduction of bubbles in two phase flow, and have presented reasons to explain this phenomenon. Nakoryakov et al. [161] found, in agreement with this observation, that pressure drop was higher in a flow containing small uniform bubbles, which they termed "mode A", than in bubble flow where many larger bubbles were present, termed "mode B". These two types of bubble flow would appear to be "ideal" bubble

flow and "churn-turbulent" bubble flow mentioned in much of the two phase flow literature [190,227,243]. "Churn-turbulent" bubble flow contains a wide bubble size distribution, and incorporates strong waking and training or channeling (the following of one bubble by another), so that transverse velocity components may be small, with a consequent reduction in excess shear. Moreover, the bigger bubbles may have some capacity to reduce the turbulence for reasons presented by Serizawa et al. [194]. Where this turbulence reduction is significant, it may be necessary to add a term into equation 4.54 to predict a loss of velocity fluctuation in proportion to the voidage, and hence a reduction of shear stress proportional to the the voidage. In this case equation 4.54 is modified to read

$$T_{tp} = (1-C_{1\emptyset}E)\rho_l l^2 (d\underline{U}/dy)(d\underline{U}/dy + C_9 U_b E/l^2) \qquad 4.57$$

where $C_{1\emptyset}$ is a constant dependent on bubble behaviour, in which case equation 4.56 is modified to read

$$\underline{U}(y/R) = \int_{y_b/R}^{1} -C_9 E U_b/l^2 + \sqrt{C_9{}^2 E^2 U_b{}^2/l^4 + 4T_{tp}/\{\rho_l l^2 (1-C_{1\emptyset}E)\}}\; d(y/R) \qquad 4.58$$

Values of $C_{1\emptyset}$ would become small in the case of small bubbles, so that equation 4.58 would reduce to 4.56.

However, it must be emphasized that the interaction of bubbles and turbulent eddies is not fully understood [195].

4.5.2 COMMENTS ON THE DETAILED MODEL

Although equations 4.56 or 4.58 are cumbersome, and would fail to model two phase flow pressure losses directly, they provide an explanation for the increase in frictional losses with an increase in bubble numbers in the pipe. At high velocities the terms describing the "excess shear" become small with respect to the turbulence generated by the bulk flow, and the equation reduces to a model which agrees with the current correlations reviewed above. At low flowrates, it predicts significant increases in pressure losses over the single phase case, and is able to explain the results of Nakoryakov et al. [161], Kytomaa [138], and Niino et al. [168]. It also provides the theoretical basis for an original, practical, equation for the prediction of dispersed flow losses, as developed in section 4.5.5 below.

4.5.4 USE OF THE DETAILED MODEL

In practice it is possible to use equation 4.56 to relate the shear stress in the pipe to the flowrate and voidage. It is necessary, however, to define the values of all the variables in the integral over the whole pipe radius, or at least from the boundary layer at the wall to the pipe

center. These variables are T_{tp}, U_b, l and gas voidage.

1) T_{tp} was shown to vary almost linearly with the distance from the wall,

$$T_{tp} = T^*_{tp}(1 - y/R) \qquad 4.30$$

2) U_b, the bubble rise velocity, may vary slightly across the pipe diameter [194]. However, variation is slight, so that a constant value may be assumed. For "churn-turbulent" bubble flow the formula of Harmathy [90] may be used,

$$U_b = 1.53\{\sigma g(\rho_l - \rho_g)/\rho_l^2\}^{0.25} \qquad 4.59$$

3) The mixing length, l, was expressed in the original analysis by Prandtl (for boundary layers) as increasing linearly from the wall, where its value was zero.

$$l = Ky \qquad 4.60$$

This relationship is, however, unsuitable for use in pipe flow, being discontinuous at the pipe centre. Some criteria for the relationship between l and y for the case of pipe flow are presented below. Firstly, the mixing length must tend to zero at the wall, secondly the mixing length must not be zero at the pipe centre, as mixing certainly occurs there, and thirdly the derivative of

mixing length with respect to distance from the pipe wall, (dl/dy), should be zero at the pipe centre. The function

$$l/R = K_1(y/R - (y/R)^n/n) \qquad 4.61$$

presents itself as a simple function to meet these criteria; K_1 and n are constants. Equation 4.61 has been compared with the empirical relationship for mixing length given by Nikuradse (see Schlichting [192]),

$$l/R = 0.14 - 0.08(1-(y/R))^2 - 0.06(1-(y/R))^4 \qquad 4.62$$

in figure 4.5, and favourable agreement is found between the two relationships for a value of n=1.3 in equation 4.61.

4) The voidage distribution in the pipe is the most difficult variable to characterize. Petrick and Kurdika [178] and Bankoff [13] have proposed power law relationships for the voidage distribution in a pipe in "churn-turbulent flow".

$$E = E_c(y/R)^{1/m} \qquad 4.63$$

where E_c is the value of the voidage at the pipe centre, related to the average voidage by

$$E_c = E(m+2)(2m+1)/2m^2 \qquad 4.64$$

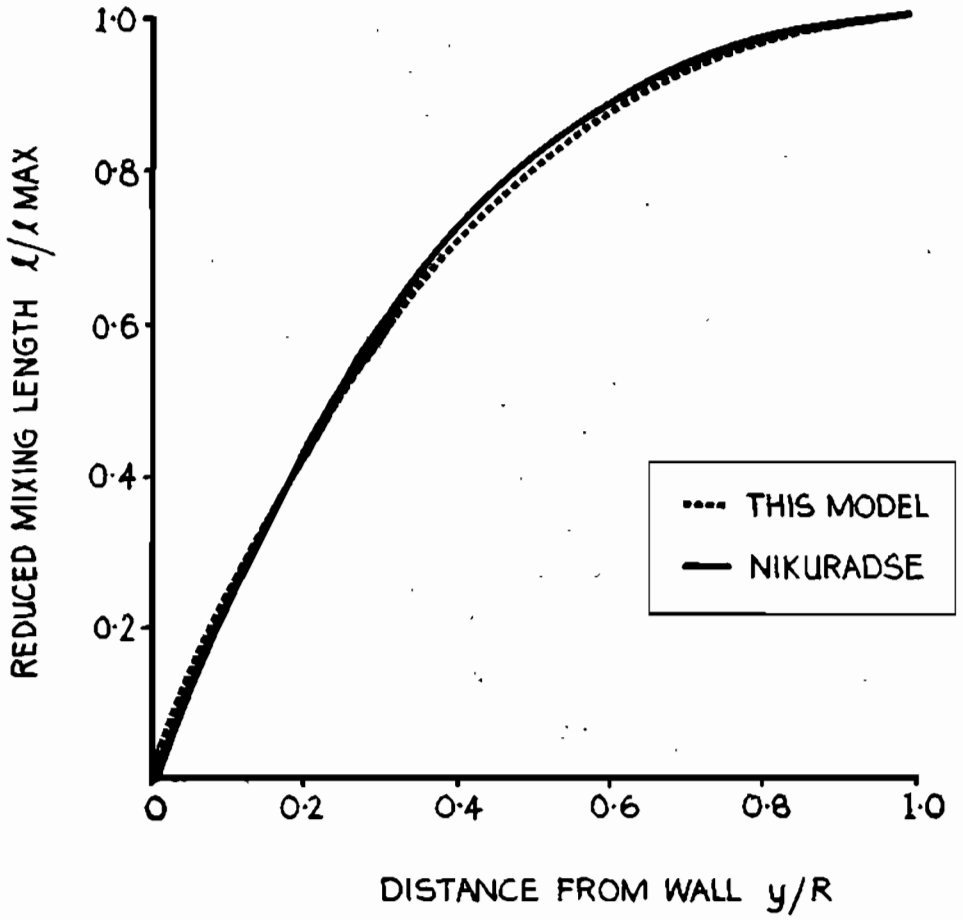

Fig 4·5 • Comparison of this mixing length with that of Nikuradse •

However, the value of m in equation 4.64 may not be estimated easily, and more recent authors [72,81,-82,91,92,161,194] have found that the maximum voidage need not occur at the pipe centre, and that a maximum may occur close to the pipe wall at low gas voidages. This has been the subject of some theoretical analysis by Drew and Lahey [75,76].

Solution of equation 4.56 may therefore be attempted with the use of equations 4.30, 4.60, 4.61 and 4.63, although equation 4.63 would be better adjusted with a more accurate knowledge of the gas voidage distribution.

4.5.5 SIMPLIFICATION OF THE MIXING LENGTH MODEL

The development of two phase mixing length theory has produced a solution to relate the liquid flowrate in the pipe to the wall shear stress and voidage, given knowledge of the voidage and velocity distributions and the nature of bubble waking in the pipe. With some reasonable assumptions, a simplified model based on average quantities in the pipe may be developed. The detailed model has related the shear stress to the velocity gradient, voidage, and degree of bubble waking.

$$T_{tp} = \rho_l^2 (d\underline{U}/dy)(d\underline{U}/dy + C_9 U_b E/l^2) \qquad 4.54$$

Consider some fixed point in the pipe flow. If we assume that the shape of the velocity distribution is invariant with respect to flowrate and voidage in the pipe over some range of voidage and flowrate, then within that region $(d\underline{U}/dy)$ at the point in the bulk flow will vary in direct proportion to the average liquid velocity, $\overline{U}$, in the pipe. The liquid velocity in the pipe is given by the equation

$$\overline{U}_1 = \overline{W}_1/(1-\overline{E}) \qquad 4.65$$

where $\overline{W}_1$ is the liquid superficial velocity. Hence, for some fixed point in the bulk flow,

$$(d\underline{U}/dy) = C_{11}\overline{W}_1/(1-\overline{E}) \qquad 4.66$$

In a similar way, if we assume the shape of the voidage distribution to be invariant with changes in total voidage and flowrate, thenthe voidage at this point in the flow, E, must be related to average voidage, E, in direct proportion, so that

$$E = C_{12}\overline{E} \qquad 4.67$$

at some fixed point in the bulk flow. At the same point, considering equations 4.61 or 4.62, the mixing length must also assume some fixed value, say $l^2 = C_{13}$, and the bubble rise velocity, U_b, may be taken as invariant with respect to flowrate and voidage. From equations 4.54, 4.66 and

4.67

$$T_{tp} = \rho_l C_{13}\{C_{11}\overline{W}_l(1-\overline{E})^{-1}\} \quad X$$
$$\{C_{11}\overline{W}_l(1-E)^{-1} + C_9 U_b \overline{E}/C_{13}\} \qquad 4.68$$

The shear stress at a fixed point in the bulk flow a distance y from the wall can be related to the shear stress at the wall by

$$T_{tp} = T^*_{tp}(1 - y/R) \qquad 4.30$$

Hence, at the fixed point in the flow, the shear stress varies in direct proportion to the wall shear stress. Collecting constants in equations 4.30 and 4.68, we may write

$$T^*_{tp} = B_1\overline{W}_l^2(1 - \overline{E})^{-2} + B_2 U_b \overline{E}\overline{W}_l(1-\overline{E})^{-1} \qquad 4.69$$

where B_1 and B_2 are dimensional, with units of $Nm^{-4}sec^2$, so that wall shear is given in Nm^{-2} and velocity in $msec^{-1}$. Equation 4.69 is the simplified model for pressure loss in vertical dispersed flow. The wall shear stress, T^*_{tp}, is given directly by the equation as a function of liquid flowrate and gas phase voidage, provided that the constants B_1 and B_2U_b are known. Unlike the detailed model, this equation is practical for the prediction of pressure losses in bubble flow. The constancy of B_1 and B_2 in the simplified model relies on

the assumption that the voidage and velocity profiles remain unchanged in shape, which may not be true over a wide range of gas and liquid velocities. Nevertheless, we may assume B_1 and B_2 to be constant over a limited range. Increased availability of data from future studies will demonstrate the dependence of B_1 and B_2 on flow conditions. The constants B_1 and B_2 are analogous to the friction factor, which expresses pressure loss as liquid head, and is dimensionless. The constants B_1 and B_2 could be made dimensionless by dividing them by the product of pipe diameter and acceleration due to gravity (gD_p), and expressing the pressure loss as head of liquid per length of pipe rather than as wall shear.

Equation 4.69 suggests that for zero gas voidage, the case of single phase flow, that shear stress will vary as the square of the liquid velocity in the pipe. However, the Blasius friction factor relationship implies that the shear stress would vary as the 1.8 power of the liquid velocity [212]. Equation 4.69 may be made to agree with the Blasius formula by setting

$$B_1 = \text{const.}\ Re^{-0.2}. \qquad 4.70$$

Where large bubbles may reduce turbulence in the flow, as described above in the development of equation 4.57 in the detailed model, another term, $(1-B_4\bar{E})$, must be employed to account for shear stress reduction by this mechanism.

Hence

$$T^*_{tp} = (1 - B_4\bar{E})\{B_1\bar{W}_l^2(1-\bar{E})^{-2} + B_2U_b\bar{E}\bar{W}_l(1-\bar{E})^{-1}\} \qquad 4.71$$

4.5.7 THE TWO PHASE FLOW MULTIPLIER

The simplified model may also be expressed as a formula for the two phase flow multiplier, which is defined as the ratio of the two phase losses in the pipe to the pressure losses which would occur if only the liquid phase were flowing alone in the pipe. To evaluate this multiplier in terms of the simplified model, we must divide the equation describing the two phase case by the equation for the single phase case. Equation 4.69 describes the two phase case, and the single phase case is found by substituting zero for the voidage in equation 4.69. For liquid flowing alone

$$T^*_{sp} = B_1\bar{W}_l^2. \qquad 4.72$$

The two phase flow multiplier is found by dividing equation 4.72 into equation 4.69 to produce the relationship

$$\Phi_l^2 = (1 - \bar{E})^{-1}\{(1 - \bar{E})^{-1} + B_3U_b\bar{E}/\bar{W}_l\} \qquad 4.73$$

where $B_3 = B_2/B_1$, and is dimensionless.

Equation 4.73 demonstrates that at high velocities, when U_b is smaller than $\overline{W}_l$, the two phase multiplier will become

$$\Phi_l^2 = (1 - \overline{E})^{-2}, \qquad 4.74$$

which is in close agreement with many of the currently accepted models. Equation 4.73 will also reduce to equation 4.74 in horizontal flow, where the bubble rise in the direction of flow, U_b, is zero.

4.5.7 COMPARISON OF THE MODEL WITH EXISTING DATA

Nakoryakov et al.[161] and Niino et al.[168] measured the pressure loss in upward bubble flow, using an 86.4 mm diameter test apparatus. Measurements of wall shear stress were made using electrochemical shear pickups described by Mitchell and Hanratty [159]. Wall shear was measured as a function of the mass transfer to the wall. The pickup electrode was fitted flush into the pipe wall, and a solution of sodium hydroxide and potassium ferri-and ferro-cyanides used with air in the two phase flow. The pickup was calibrated initially using single-phase (liquid) flow, and the shear stress in two phase flow inferred from this calibration. Results demonstrated that there was a sharp increase of wall shear stress with increasing gas voidage, especially at lower mixture flowrates. Results were plotted as the two phase flow

multiplier, Φ_l^2 versus the flowing gas fraction,

$$B = \overline{W}_g/(\overline{W}_l + \overline{W}_g) \qquad 4.75$$

where $\overline{W}_l$ and $\overline{W}_g$ are the liquid and gas superficial velocities. The two phase flow multiplier is the ratio of the pressure loss (shear stress) in the two phase flow to the pressure loss if the liquid phase were flowing alone. To test the mixing length model data were considered for velocities from Ø.22 to 2.Ø5 m/sec and the flowing gas fraction from Ø to 1Ø%. Within this range of flowing gas fraction, the wall shear stress rose sharply with increase in gas flowrate. However, at flowing gas fractions above 1Ø%, the shear stress became relatively constant and independent of further increase in gas flowrate, possibly due to a changing flow structure, and at values of the flowing gas fraction from 2Ø to 4Ø%, transition to slug flow was reported by the investigators. Upon transition to slug flow there was a corresponding drop in wall shear stress.

Although both Nakoryakov et al.[161] and Niino et al.[168] observed two distinct bubble flow regimes, which fit the description of "ideal" and "churn-turbulent" bubble flow, and observed different shear stresses in the two flows, paucity of data has obliged the results for the two distinct flow types to be lumped. Shear stress was slightly higher in "ideal" bubble flow than in

churn-turbulent flow. This would agree with the mixing length model because in churn-turbulent flow bubble waking is strong. When a bubble follows another closely, less liquid will flow into the wake of the upper bubble and away from the zenith of the lower bubble. This reduces the strength of transverse velocity components which give rise to the excess shear.

Thirty nine data points for churn-turbulent and ideal bubble flow were read from the ascending sections of the plots in figures 11 and 12 of Nakoryakov et al.[161]. Data points for upflow were in the form of the two phase multiplier, Φ_l^2 versus the flowing gas fraction, B, and required some manipulation for comparison with the model, which requires data in the form of the multiplier versus the gas void fraction, $\overline{E}$.

The Zuber and Findlay [243] drift-flux model, equation 3.14, was used to find the gas void fraction from the flowing gas fraction and the liquid superficial velocity. Equation 3.14 may be rearranged in the form

$$B/\overline{E} = C_o + \overline{U}_{gm}(1 - B)/\overline{W}_l \qquad 4.76$$

to relate these quantities. For want of better values, $\overline{U}_{gm} = 0.25$ m/sec. and $C_o = 1$ were used: the profile constant, C_o, does assume a value of 1 in ideal bubble flow [243], but will have a higher value in

churn-turbulent flow. Moreover, the drift velocity term may be lower in ideal bubble flow, but gas voidage predicted by these values should be in error by no more than 10% for any vertical bubble flow.

The 39 data points for upflow were found to agree well with the simplified mixing length model, equation 4.73, for a value of B_3U_b = 46.5 $Nm^{-3}sec$. The experimental versus predicted values of the two phase flow multiplier are shown in figure 4.6. Also shown in figure 4.6 is the inability of conventional models, such as those of Orkizewski [174] or Govier and Aziz [85] to predict low velocity pressure loss data. The acceptable agreement of the mixing length model is in strong contrast with the poor agreement found by the conventional models, whose points lie within the narrow band illustrated in figure 4.6. Conventional models cannot predict even trends in the low velocity data. Data scatter about the parity line for the mixing length model in figure 4.6 may be ascribed to several factors:-

i) Nakoryakov et al. [161] showed that error in the RMS value of the shear stress using the electrochemical pickup may be as high as 30% in some cases, although far lower errors would be typical. Hence the data used may have some inherent scatter.

ii) Data for "ideal" and "churn-turbulent" bubble flow

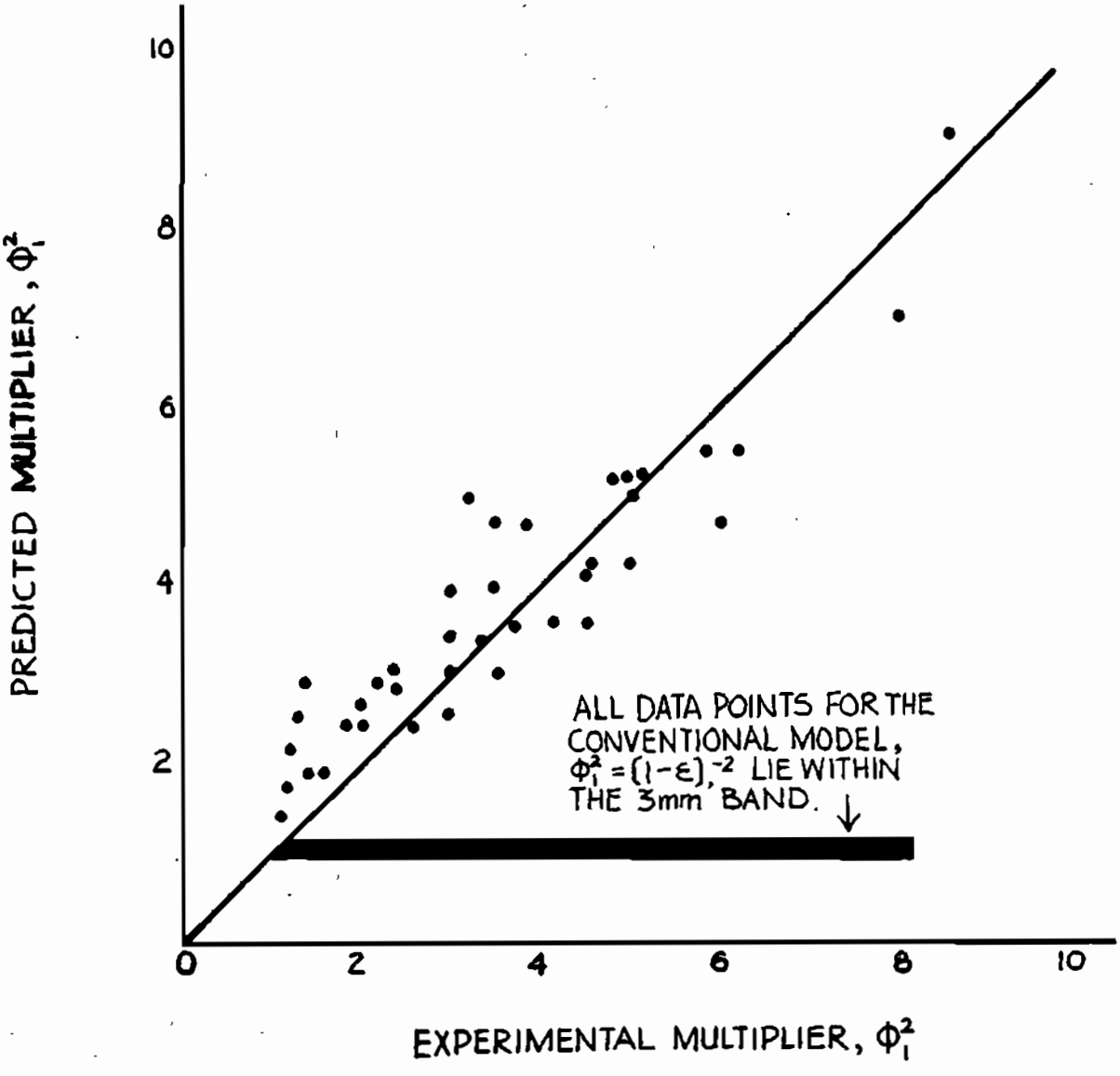

Fig 4·6 • Predicted vs experimental pressure loss for the mixing length model and data of Nakoryakov et al. (1981)

have been lumped: values of the constant B_3 may differ between these two flow types: B_3 would be higher for the ideal flow than the churn-turbulent flow.

iii) Development of the simplified mixing length model model involves assumptions that the void and velocity profiles do not change in shape over some region. However, the voidage and velocity profiles may not necessarily maintain the same shape throughout the experimental envelope. Shape of the velocity distribution will certainly change, even in single phase flow, over a large range of Reynolds' numbers, and void profiles are reported by Serizawa et al. [194] and Galaup and Delhaye [82] to change from a saddle-shape to a parabolic shape with increasing gas voidage. Nevertheless, the disadvantage of the simplifying assumptions is offset by the ability to use average flow quantities in the mixing length model.

iv) The use of C_o=1 in the Zuber and Findlay [243] drift-flux model to evaluate the gas voidage in upflow may be in slight error. A value of C_o=1 is appropriate for ideal bubble flow, but in churn-turbulent flow values above 1 are found [47,85].

Nevertheless, the simplified mixing length model finds far better agreement with the upflow results than any other model tested.

Some further qualitative support for the mixing length model is available in an article by Davis [69]. Two phase pressure loss was measured in both vertical and horizontal bubble flow, and the average pressure loss in bubble flow compared with that for single phase flow. However, data are supplied in a graphical form which does not permit quantitative interpretation. Whereas the two phase flow multiplier was not much affected by flow velocity in horizontal flow, in vertical flow it decreased with increasing flow velocity. This is in agreement with the mixing length model which predicts excess shear only for the case of vertical flow.

In summary, the mixing length model has found far better agreement with the published data of Nakoryakov et al. [161] than have other models, which do not take into account the excess shear generated by the slip of bubbles in vertical flow.

4.6 METHODS OF OBTAINING DATA IN VERTICAL FLOW

In typical bubbly flow at low and moderate velocities the hydrostatic head accounts for the majority of the overall pressure drop and largely masks the effect of frictional losses, which must be obtained by one of the methods given below. It has been shown above that solutions based on the energy equation are unsuitable, although easy to evaluate. Only methods basesd on the momentum equation

are considered here.

4.6.1 USE OF HORIZONTAL APPARATUS

Frictional losses are obtained with little difficulty in horizontal flow, where no hydrostatic head exists in the direction of flow. It is, however, not exact to assume that the cases of horizontal and vertical flow are similar for the following reasons.

(i) Gravitational effects cause velocity and void profiles to differ between the cases of horizontal and vertical flow [92].

(ii) At lower liquid velocities a transition from bubble to stratified flow occurs readily in horizontal flow [149,218]. Such a change in flow regime might be expected to affect frictional losses, so that horizontal bubble flow measurements might be suitable only at sufficiently high velocities [69,112,136].

(iii) Bubbles do not possess a nett local slip due to gravity in fully developed horizontal flow in the same sense as they do in vertical flow. A consideration of the mixing length theory presented above reveals that no additional Reynolds' stresses would be set up in horizontal flow, as they are in vertical flow. This is supported by the data of Davis [69] who found friction

factors, and their dependence on Reynolds Number, to differ between the vertical and horizontal cases.

In view of the considerations presented above, the horizontal method was not employed.

4.6.2 METHOD BY DETERMINATION OF EXACT VOIDAGE

Where acceleration effects are negligible, the frictional losses in vertical flow may be evaluated from the difference between total and static head terms measured between two stations on a vertical pipe. A correct evaluation of the static head requires an exact knowledge of the respective volumes of gas and liquid in the test section. This is found traditionally using quick-closing valves [47,51,147,185,] or X-ray techniques [97,245]. Measurements must be accurate as at low flowrates the frictional term is a small fraction of the total pressure differential. This quick-closing valve method has the disadvantage that the flow must be stopped for each measurement, and the X-ray method may not find the average value of gas voidage between two pressure tappings without a traverse along a length of pipe.

4.6.3 WALL SHEAR MEASUREMENT

Rose and Griffith [189] determined wall shear directly by measuring the force on a pipe suspended between two

flexible sections. They used pipes of 12.5 and 25 mm diameter at velocities over 2 m/sec: the method may be unsuited to larger bore apparatus at low flowrates, where the relative frictional force is lower.

Recently Niino et al [168] and Nakoryarkov et al [161] have used a shear stress pick-up set in the pipe wall to determine friction factors in two phase vertical flow. A platinum plate set in the pipe wall acts as a cathode in the electrolytic reduction

$$Fe(CN)_6^{3-} + e^- \Rightarrow Fe(CN)_6^{4-}.$$

The diffusion of the ferricyanide ions to the electrode is controlled by the thickness of the laminar sub layer at the wall. This thickness is in turn dependent on the wall shear stress, T^*. Accurate calibration during single phase runs permits the electrode's use for the evaluation of two-phase losses. This method has an advantage in being able to determine wall shear at low flowrates.

4.6.4 PROPOSED EXPERIMENTAL METHOD

The quick-closing valve method suffers the disadvantage of requiring frequent stoppage of flow during data acquisition. Where holdup may be predicted accurately in a device, an acceptable value may be estimated for the static head term, and frictional losses may be determined

using only two pressure tappings on a pipe length [49].

Over a very short test length, or at very high pressure, it may be sufficiently accurate to evaluate holdup at the average pressure in the length, but in other circumstances a more rigorous treatment is necessary.

Neglecting acceleration effects and gas phase density one may write the differential equation.

$$-dP = (\rho_l g(1-\bar{E}) + D)dx \qquad 4.77$$

where $\bar{E}$ is a function of pressure, and D the pressure loss per unit length of pipe, taken as constant over the section.

Zuber and Findlay [243] present the equation

$$\bar{W}_g/\bar{E} = C_o(\overline{W_g + W_l}) + \bar{U}_{gm} \qquad 3.14$$

so that

$$\bar{E} = \frac{\bar{W}_g}{C_o(\overline{W_g+W_l})+\bar{U}gm} \qquad 4.78$$

Viewing the gas flow as ideal permits the gas flux to be referenced to atmospheric conditions, viz.

$$\bar{W}_g/P = \bar{W}_{go}P_o \qquad 4.79$$

where the subscript o denotes atmospheric conditions. Where $\overline{W}_g$ is much smaller than $\overline{W}_l$, as in bubbly flow, little error is incurred in assuming $\overline{W}_g$ to be constant in the denominator of 4.78 (see Appendix C). We may write

$$\overline{E} = \frac{\overline{W}_{go} P_o / P}{C_o(\overline{W}_l + \overline{W}_g') + \overline{U}_{gm}} \qquad 4.80$$

Where $\overline{W}_g'$ is the gas flux at the median pressure, $(P_1 + P_2)/2$. The equation has been solved without the simplifying assumption of constant gas flux in the denominator [45,57,58], but for the case of short pipe lengths the slight added accuracy does not offset the more cumbersome solution. Equation 4.80 may be re-written as

$$\overline{E} = E_o P_o / P \qquad 4.81$$

$$\text{where } E_o = \frac{\overline{W}_{go}}{C_o(\overline{W}_l + \overline{W}_g') + \overline{U}_{gm}} \qquad 4.82$$

From equations 4.77 and 4.81, one obtains

$$\frac{-P}{(\rho_l g + D)}\, dP = P - \frac{P_o E_o \rho_l g}{\rho_l g + D}\, dx \qquad 4.83$$

Using the substitution $P' = P - P_o E_o \rho_l g/(\rho_l g + D)$, so that $dP' = dP$, equation 4.83 becomes

$$\frac{P' + P_o E_o \rho_1 g}{\rho_1 g + D}\, dP = -P'(\rho_1 g + D)\, dx \qquad 4.84$$

Rearranging, one obtains

$$(1 + E_o P_o K/P')dP' = (-\rho_1 g/K)dx \qquad 4.85$$

where $K = \rho_1 g/(\rho_1 g+D)$, the ratio of the static to total head. Integrating between points x_1 and x_2, with conditions $P(x_1)=P_1$ and $P(x_2)=P_2$, we have

$$K(P_2-P_1) + E_o P_o K^2 \ln\{(P_2-P_o E_o K)/(P_1-P_o E_o K)\} + \rho_1 g(x_2-x_1) = 0 \qquad 4.86$$

where "ln" denotes the natural logarithmic function. But for the fact that K appears in the logarithmic term, equation 4.86 may be solved as a quadratic equation in K. In practice it is possible to substitute some initial value for K, typically K=1, in the logarithmic term and effect a solution. A single iteration will generally yield an accurate value of K, from which D may be computed by the formula

$$D = \rho_1 g(1-K)/K \qquad 4.87$$

It is noted that for no air flow $E_o P_o=0$, so that equation 4.86 reduces, as expected, to

$$P_1-P_2 = (\rho_1 g+D)(x_2-x_1) \qquad 4.88$$

The above treatment might also be used with holdup models other than that of Zuber and Findlay [243,244], providing E may be given in a similar form to equation 4.78, that is, E is inversely proportional to pressure in the test section.

Equation 4.86 was used to interpret all data described in section 4.7.

4.7 EXPERIMENTAL WORK

4.7.1 VERIFICATION OF THE EXPERIMENTAL TECHNIQUE

The method proposed in section 4.6.4 was compared with the method using quick closing valves described in section 4.6.2. A 5 m long test section illustrated in figure 4.7 was fitted in the 50 mm diameter rig described in appendix A. Valves were synchronized employing the same pressure balance technique that was used in the measurement of holdup (See chapter 3). Bubbly flow was set up in the pipe and the differential pressure across the section and pressure at the top of the length monitored with two Foxboro cells connected to a microcomputer programmed to average 100 readings at each flowrate.

For each gas and liquid flowrate the valves were closed simultaneously and rapidly. The volume fraction of each

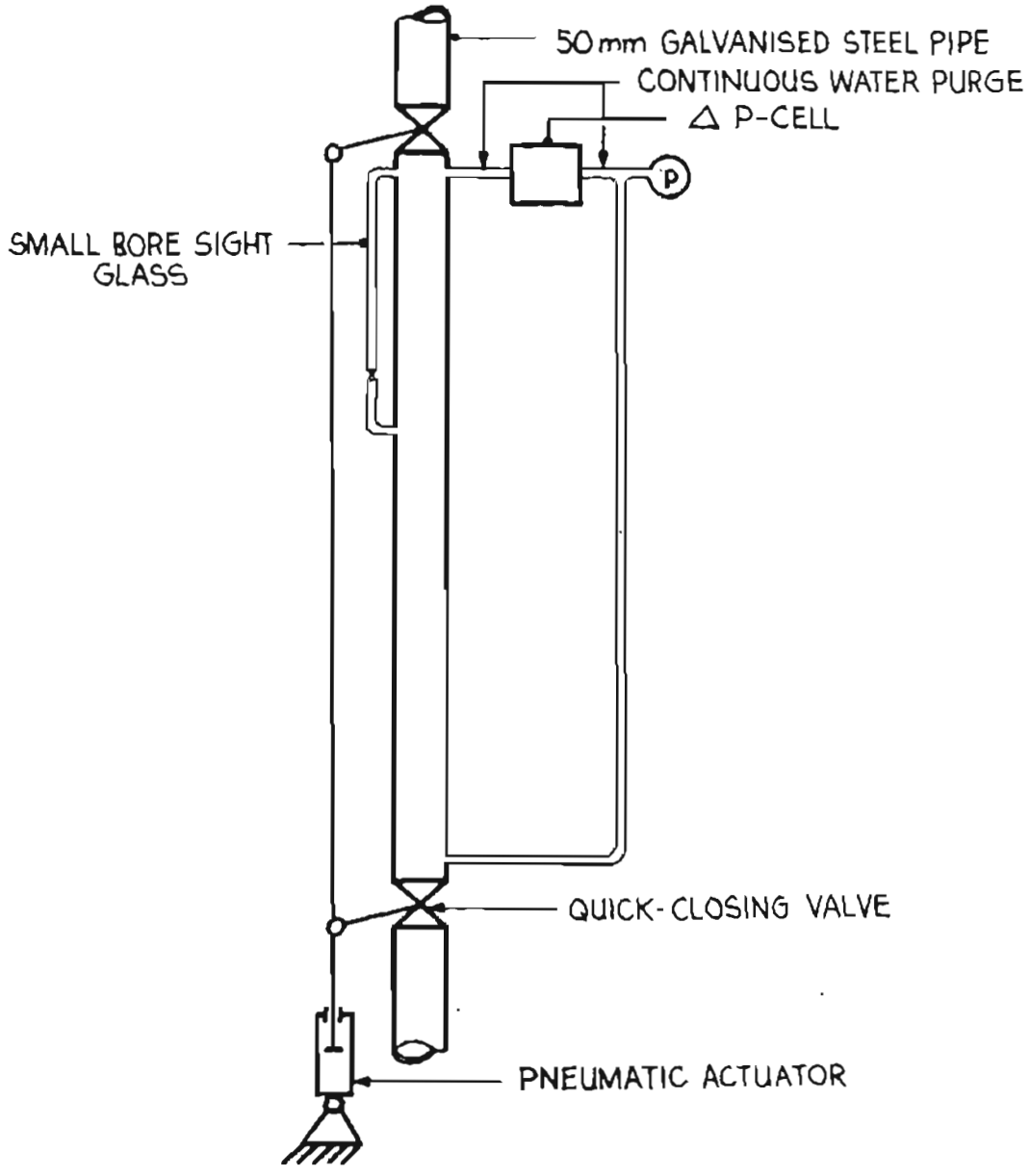

Fig 4·7 • Apparatus for verification of proposed method •

phase was determined from the level in a 3 mm diameter sight glass attached to the isolated section.

From this volume fraction the hydrostatic head in the section was calculated, and the true frictional loss evaluated from the difference between this head and the total differential across the section. Results determined by this conventional method were compared to the frictional losses found using equation 4.86 with P_1 and P_2 the pressures at the top and bottom of the section and with E_o evaluated from the gas and liquid flowrates using equation 4.82. Close agreement was found between the two methods. See figure 4.8

For the evaluation of E_o, values for C_o (C_o=1,16) and $\bar{U}_{gm}$ (0,24 m/sec), known from the holdup work in chapter 3, were employed. For apparatus where these variables are unknown, no severe error would be incurred by using values of C_o recommended in the literature, for example C_o = 1.2 [96,227], and values for the bubble rise in air/water flow as given by Harmathy [90], U_z = 0,25 m/sec or by Levich [141], U_z=0,23 m/sec.

Use of C_o = 1.2 on the data given in fig 4.8 would have caused at worst an error in voidage estimation of 3%, a static head error of 0,6% and an error in frictional loss of 5%. This method was thus considered sufficiently accurate for general use in acquiring data for frictional

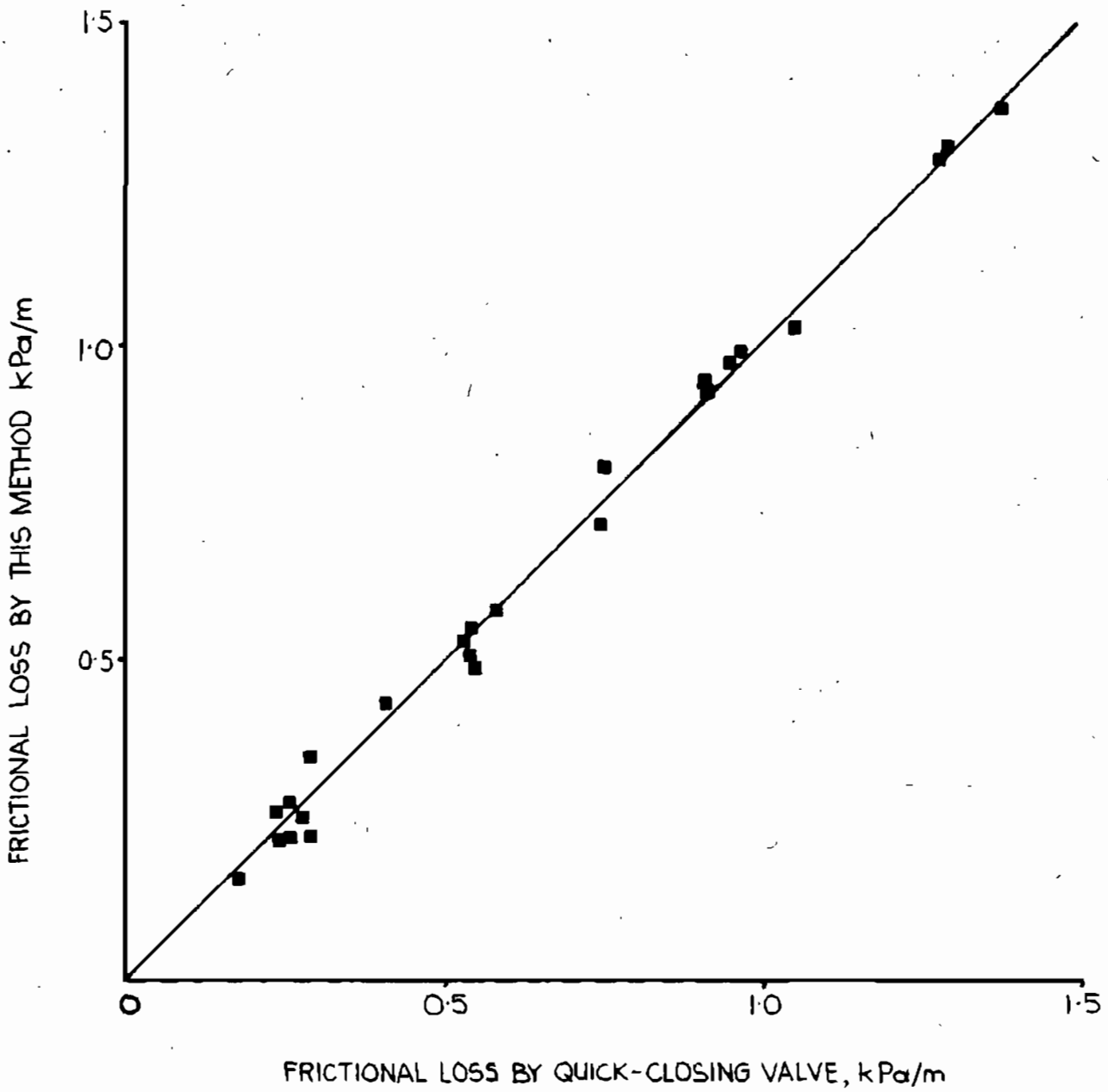

Fig 4·8 • Comparison of prediction with experimental measurements

pressure loss in two phase flow.

4.7.2 DATA FOR TWO PHASE FLOW

The new method was employed to evaluate frictional losses over 2 m and 3 m lengths in downflow, and over a 3 m length in upflow. Pressure was measured at the top of the test section using a Foxboro pressure transducer, and the differential pressure across the section was measured with a Foxboro differential pressure transducer, which was recalibrated regularly using a water manometer. Both of these transducers were connected to a microcomputer which was programmed to average the value of 100 pressure readings taken in quick succession. Gas and liquid flowrates were measured by rotameters, as in the holdup work, and equation 4.86 was used to extract the frictional pressure loss for each data point.

Results are presented in figures 4.9 and 4.10. None of the models in the literature was able to correlate the results satisfactorily. The failure of single parameter models is demonstrated by the comparison of downflow data at 1.38 m/sec with the Orkizewski [174] model in figure 4.11.

As seen in figure 4.9, all upflow results, bar one, lie within 10% of the horizontal line $\Phi_l^2=1$, and showed no trend to increase with increasing voidage: this is in

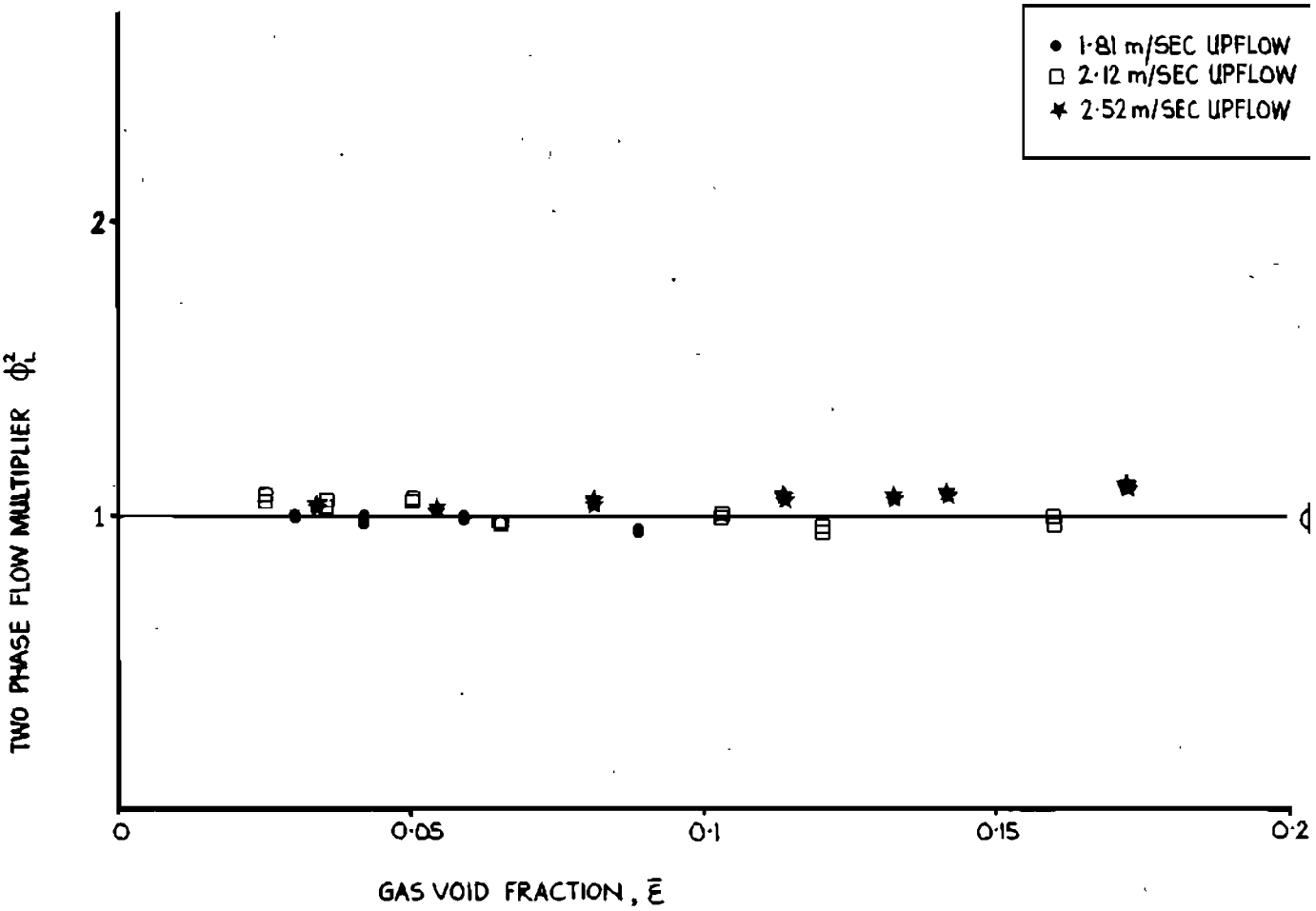

Fig 4·9 • Two phase flow multiplier in upflow •

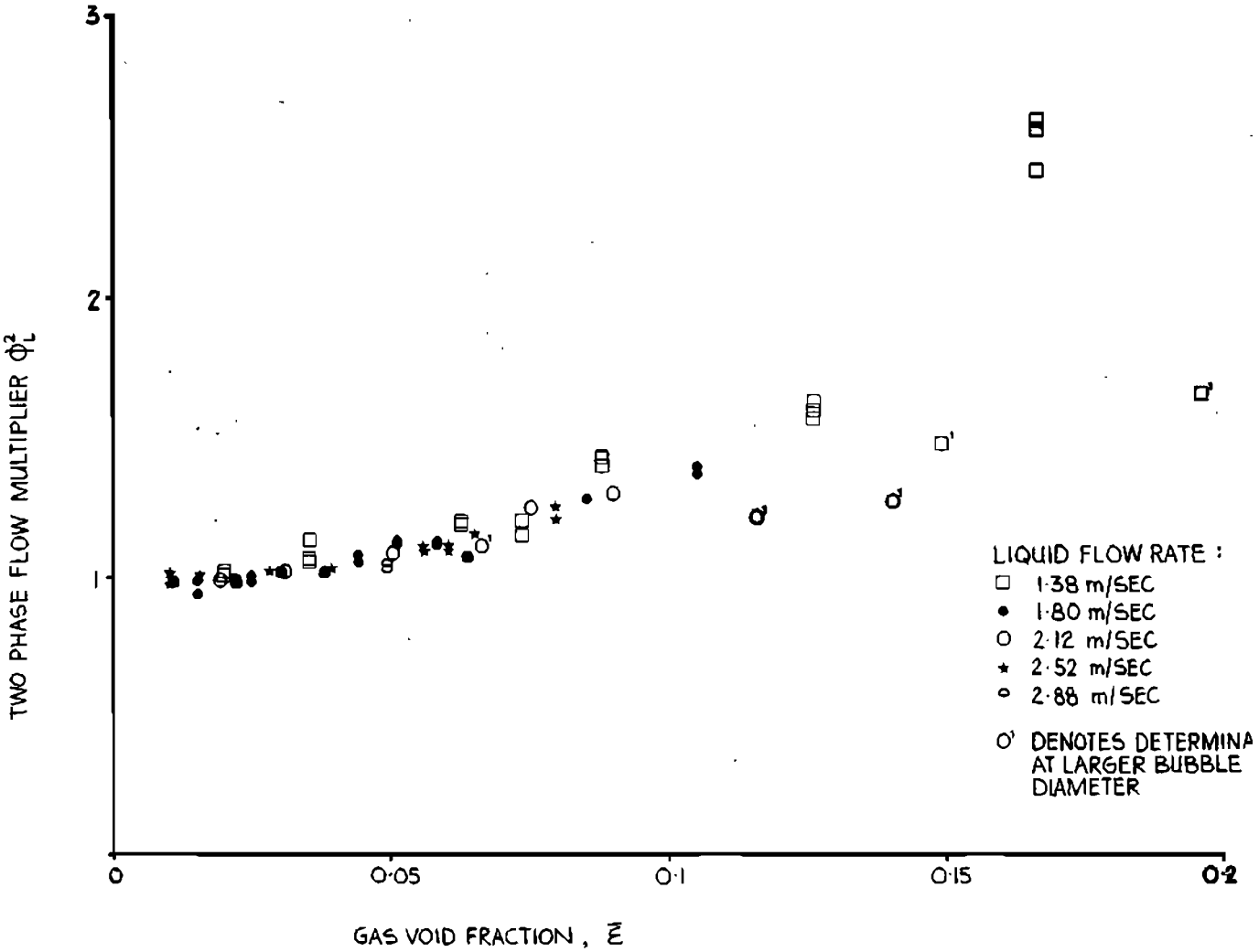

Fig 4·10 • Two phase flow multiplier in downflow •

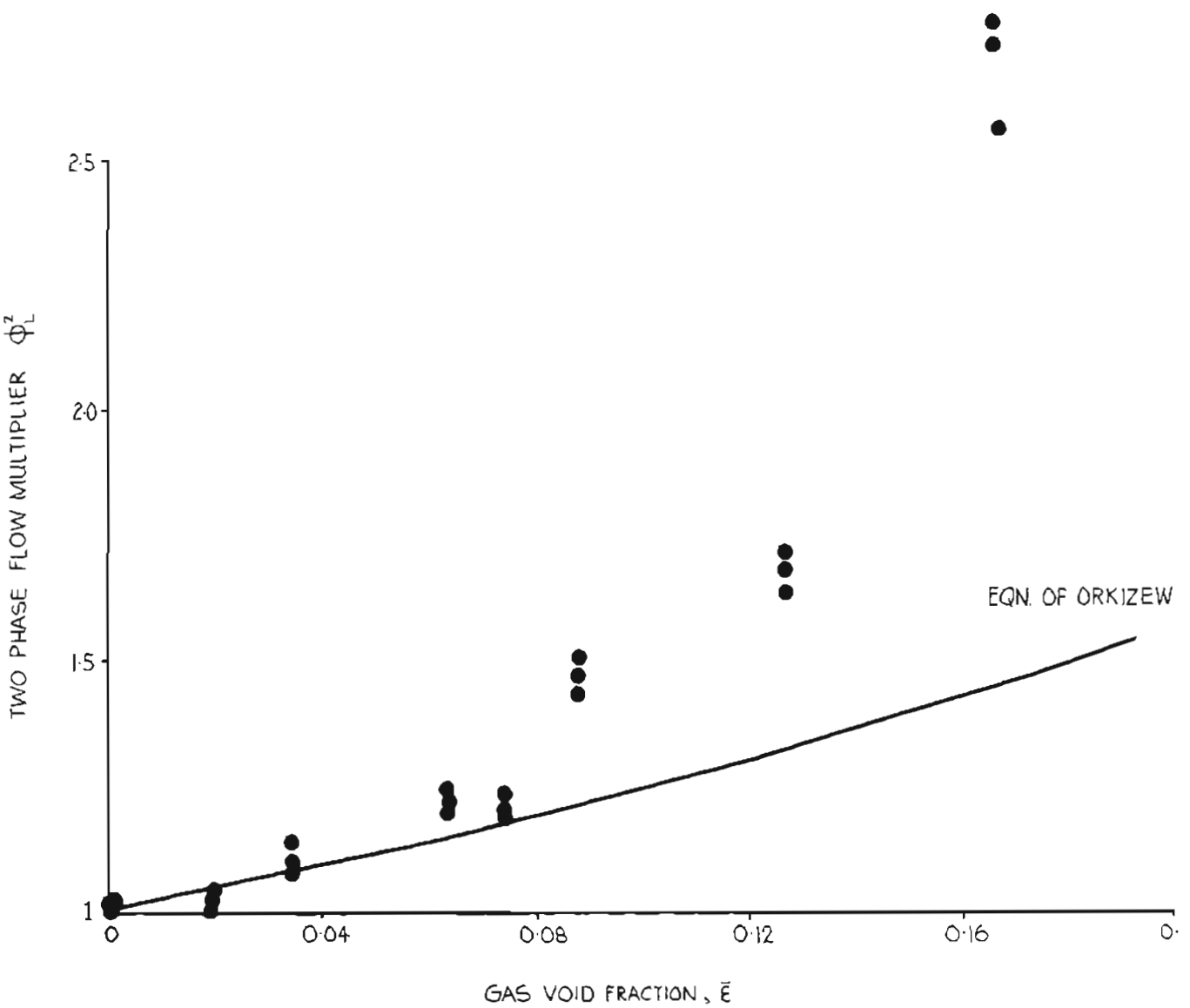

Fig 4·11 • Data for water flowrate of 1·38 m/sec •

strong contrast with the downflow data, and the data of other authors for upflow [138,161,168]. These results and the applicability of the model developed in section 4.5 are discussed below.

The majority of the downflow data (118 points) were determined at considerable depth in the rig, at a pressure of approximately 1.6 kPa gauge. Bubbles produced at the sparger were typically of diameter 2.3 to 2.8 mm, reduced to standard temperature and pressure, as reported in detail in section 5.12 below. This implied that bubbles in the test section were of 1.7 to 2.0 mm diameter. From consideration of the model we might expect that such small bubbles would not reduce turbulence significantly, and that waking would be low, implying a large increase in pressure loss with a gain in voidage. To test this hypotheses used in the model, a few data points (specially denoted in fig. 4.10 by the superscript ^{1}) were obtained in a test section closer to the sparger. Here the pressure was lower and bubble diameter greater (2.1 to 2.5 mm). A drop in values of Φ_1^2 was observed compared with the data taken at higher pressure.

In upflow, data were collected at a lower system pressure, and coalescence in the horizontal section caused some larger bubbles to rise in the upflow. Occasional cap bubbles were present at higher voidages and waking appeared strong. As predicted by the model Φ_1^2 was lower

than in the downflow case, where smaller bubbles were present. It would appear from the constancy of Φ_l^2 around a value of unity that energy absorption by the bubbles compensated for increased turbulence due to the raised superficial velocity of the fluid mixture. Circulation of fluid induced by strong channeling at the pipe centre may also have contributed to the low pressure losses. This may be compared with the results of Oshinowo and Charles [176], who have reported negative pressure losses at low velocity, low voidage upflow, as discussed in section 4.4.4. It is possible that the detailed mixing length model, with correct expressions for the gas void and shear stress distributions in the flow, would be capable of predicting the pressure loss observed in upflow. However, in the fully developed upward flows at higher velocity some increase in pressure loss with rising gas flowrate would be expected, so that the data are not fully understood. Calculation demonstrated that it was not an acceleration effect causing the difference between the up and downflow cases.

Excluding the few points for downflow gained at lesser depth in the rig, regressions using equation 4.71 were performed on 118 data points in downflow and 40 data points in upflow. It was found that single phase pressure drops varied in proportion to velocity to the power 2.Ø5, rather than 1.8 as the Blasius formula would suggest. Considering this trend, the regression on equation 4.73

was performed leaving B_1 as a constant, rather than in the form B_1 = const. $Re^{-0.2}$.

The regression on downflow data initially provided a small negative value for B_4, implying that there was certainly no energy absorbtion by the bubbles. The regression was repeated setting $B_4 = 0$, and values gained for B_1 and B_2 with little increase in error.

It was found for downflow that

$$T_w^* = 2.65W_l^2(1-E)^{-2} + 57.8W_lU_bE(1-E)^{-1} \ Nm^{-2} \qquad 4.89$$

A comparison of predicted (from equation 4.89) and experimental values is given in figure 4.12.

Inspection of figure 4.9 reveals that upflow are best described by assigning the two phase flow multiplier a value of 1, that is, equating frictional losses in single phase and bubbly flow cases. An estimate of the error can be gained from figure 4.9.

4.8 CONCLUSION

Far wider investigation would be necessary to predict suitable values for B_4 and B_2 in bubbly flow. Moreover, the effect of changing void profiles on these parameters has not yet been assessed. It would appear from this

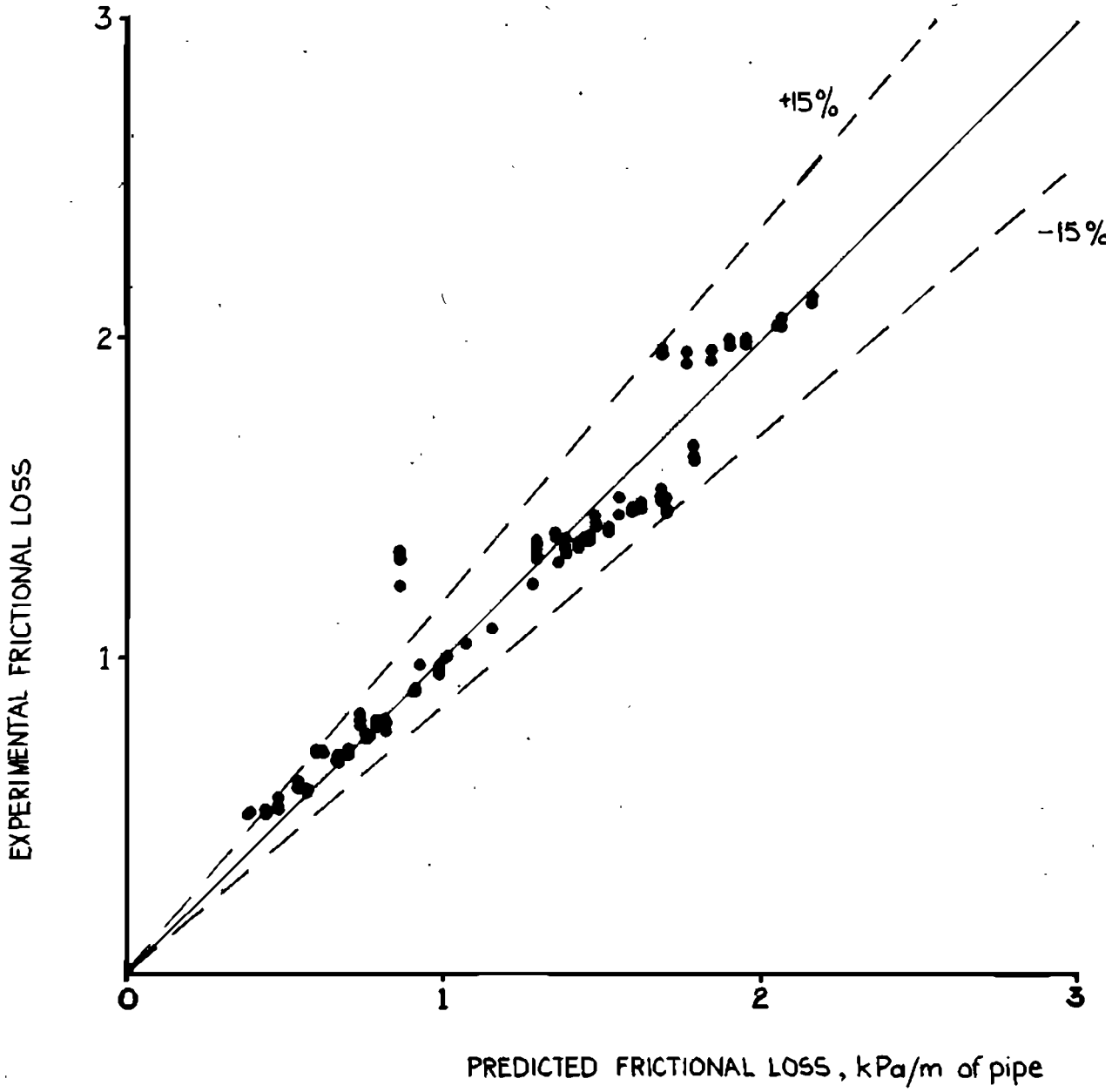

Fig 4·12 • Comparison of predicted and experimental values for downflow pressure drop •

investigation that the designer would be safe in employing a value between Φ_l^2=1 and a conventional model, say

$$\Phi_l^2 = 1/(1-E)^{1.8} \qquad 4.9\emptyset$$

to predict losses in churn-turbulent flow at velocities over 2 m/sec., but should recognise that fairly high values of Φ_l^2 may emerge in low velocity bubble flow, especially when the bubbles are small, as is the case at high pressure. It is fortunate for the designer of a D.S.R. that at high pressure the voidage is also lower, and the effect consequently reduced. However, the simplified mixing length model (equation 4.71) appears to provide an accurate interpretation of losses in bubbly flow, and provides the first fundamental explanation for high values of the two phase flow multiplier observed in low velocity bubble flow.

4.9 LIST OF VARIABLES

A	Cross sectional area of pipe (m^2)
A_D, B_D	Constants used by Davis
B_1, B_2	Dimensional constants in simplified model ($Nm^{-4}s^2$)
B_3	Ratio of B_2 to B_1 (-)
C_c	Constant (-)
C_o	Drift-flux constant (-)
C_w	Circumference of pipe (m)
$C_1..C_{13}$	Constants (-)
D_p	Pipe diameter (m)
E	Gas void fraction (-)
f	Friction factor (-)
g	Acceleration due to gravity (ms^{-2})
K	Mixing length constant
l	Mixing length (m)
l_w	Mixing length due to rising bubble (m)
m	Void distribution exponent (-)
M	Mass flow (kgs^{-1})
n	(i) Exponent-mixing length expression (-)
	(ii) Exponent-pressure loss correlation (-)
P	Pressure (Pa)
Q	Volumetric flowrate (m^3/sec)
r	Radial distance from pipe centre (m)
R	Pipe radius (m)
Re	Reynolds number (-)
T	Shear stress (N/m^2)

U	Velocity of liquid phase in axial direction (m/sec)
U_b	Rise velocity of bubble (m/sec)
V	Velocity of liquid phase in transverse direction (m/sec)
W	Superficial velocity (ms^{-1})
x	(i) Axial distance along pipe (m) (ii) Flow quality (-)
X	Martinelli pressure loss ratio (-)
y	Radial distance inward from wall (m)
y_1	A reference point in the flow (m)
ρ	Density (kg/m^3)
μ	Viscosity ($kgm^{-1}s^{-1}$)
ν	Kinematic viscosity (m^2s^{-1})
σ	Surface tension (Nm^{-1})
ϕ	Two phase multiplier (-)
Γ	Baroczy property index
Π	Chisolm property index

Subscripts

b	At the boundary layer
c	At pipe centre
e	Energy balance
f	Frictional loss
i	Averaged within a central core in the pipe
g	Gas, gas only
l	Liquid, liquid only

lo	Used with Baroczy multiplier
m	Momentum equation
o	Evaluated at atmospheric pressure
sp	Single phase (liquid only)
tp	Two phase
w	Due to presence of bubble wake (or nadir)
1,2	(i) Designating a velocity difference
	(ii) At a station in the pipe

Superscript

*	At pipe wall

CHAPTER 5.

5. INTERPHASE MASS TRANSFER

5.1 INTRODUCTION

As in the preceding chapters, investigation was restricted to the vertical two-phase bubble flow regime. Only interphase mass transfer is considered below because mass transfer to the wall [198,215,223] has little application in deep shaft reactor design.

Existing heat-momentum-mass transfer analogies for pipes are for transfer to the wall [202] and may not be extended directly to interphase transfer. Conversely, interphase heat transfer is of less interest than heat transfer to the wall, so that it is unlikely that a D.S.R. heat-mass transfer analogy will emerge in the literature.

5.2 DEFINITIONS

One may define the liquid side mass transfer coefficient, k_l, by the equation

$$Ra = k_l a(A^*-A^o) \qquad 5.1$$

where R is the mass transfer rate of the species, a is the surface area available for transfer, normally as surface

area per unit volume of mixture, and (A^*-A^o) is a driving force, with A^o the concentration of the species in the bulk of the liquid, and A^* the concentration of the species in the liquid at the gas-liquid interface. This definition, equation 5.1, is true irrespective of the mass transfer model (for example: film model, surface-renewal theory) assumed.

The gas side mass transfer coefficient may be defined in a similar fashion, using partial pressures of the migrating species in the gas bulk, P', and in the gas at the interface, P_i', to define the driving force.

$$Ra = k_g a B (P'-P_i') \qquad 5.2$$

where B has units of moles cm^{-3} Pa^{-1}.

Assuming that there is no resistance at the interface, for small concentrations of a gas in a liquid, one may use the relation

$$A^* = P_i'/He \qquad 5.3$$

where He is the Henry's law constant. Equation 5.3 states that a concentration of the species A^* in the liquid is in thermodynamic equilibrium with a partial pressure of P_i' in the gas. Hence

$$Ra = k_l a \, (P_i'/He - A_o)$$

One may also write an equation using the partial pressure in the gas bulk rather than at the gas-liquid interface

$$Ra = K_l a\ (P'/He - A_o) \qquad 5.4$$

where K_l is termed the overall resistance based on liquid side resistance, and

$$1/K_l = 1/k_l + 1/Hek_g \qquad 5.5$$

It is found in practice that the gas side resistance to transfer is generally far smaller than the liquid side resistance, ie

$$k_l \ll Hek_g \qquad 5.6$$

and the expression 5.6 has been assumed to hold true for oxygen-water and carbon dioxide-water systems in two phase flow [62,93,140,193]. Keitel and Onken [133] have stated that gas resistance may never contribute more than 2% to the overall transfer coefficient, and very high values for k_g have been found in slug and annular interphase mass transfer [131,150]. The assumption in equation 5.6 leads to the relationships

$$k_l \approx K_l \text{ and } P' \approx P_i' \qquad 5.7$$

So that henceforth

$$Ra = K_l a(A^* - A^o) \qquad 5.8$$

and, neglecting resistance in the gas phase, for small gas concentrations in the liquid, A* will be treated as the concentration of the species in equilibrium with the partial pressure in the bulk of the gas,

$$A^* = P'/He \qquad 5.9$$

5.3 SIMPLE MODELS OF MASS TRANSFER

Various models have been proposed to describe mass transfer, the simplest and most noteworthy being the film model. A liquid film, of thickness δ, is presumed to exist in contact with the gas-liquid interface. Beyond the film, the bulk liquid is assumed well mixed, so that there is a constant concentration, A_o, a distance δ from the interface. At the interface the concentration is A*. If the only transport in the film is assumed to be by molecular diffusion, then

$$R = (D_g/\delta)(A^*-A^o)$$

so that

$$K_l = D_g/\delta \qquad 5.10$$

where D_g is the diffusivity of the transferred species in the liquid. Somewhat more sophisticated models are discussed by Danckwerts [67] and by Sherwood et al.[198]. Still surface models view transport as a product of both molecular and eddy transfer, while surface-renewal models consider 'packets' of the bulk liquid to be swept periodically to the interface, to undergo rapid local transfer, and then be returned to the bulk. The simplest form of this model assumes a constant "exposure time", t_e, for these packets, which leads to the equation

$$k_l = (D_g/t_e)^{Ø.5}$$

More advanced models assume a distribution of exposure times, but are not required for the mass transfer analyses presented below.

5.4 INTERPHASE MASS TRANSFER COEFFICIENTS

Little work has appeared on gas-liquid mass transfer in bubble flow at significant liquid velocities. However, several studies have been undertaken on bubble columns and agitated (bubble-dispersion) mixtures in stirred vessels, as well as on pipe flow in other flow regimes. The literature is reviewed below.

5.4.1 BUBBLE COLUMNS

A list of authors concerned with bubble column transfer is given in table 5.1 In addition, work has been completed on transfer from single bubbles in free rise [37,83], which must be considered applicable to columns. Kawagoe [132] has considered gas-liquid mass transfer at high gas superficial velocities in bubble columns.

Mass Tansfer correlations for bubble columns are normally provided for K_l or $K_l a$ either graphically or in terms of dimensionless numbers. Where these numbers require a characteristic velocity or dimension, that of the bubble is normally used, since bubble columns rely almost solely on bubble movement for mixing. Alvarez-Cuenca et al.[2] have noted that in the region of gas introduction (at the base of the bubble column) transfer is higher than in the bulk, since some increased mixing may be induced by the gas entry. Early workers [201] found mass transfer to be improved with increasing liquid flowrate through the column, although such flowrates represent far lower velocities than used in deep shaft reactors, where most of the turbulence is induced by the liquid velocity. For this reason bubble columns, although similar in flow pattern to the D.S.R., have their mass transfer governed by a different turbulent mechanism, and correlations for bubble columns may not be employed directly for D.S.R.'s. Nevertheless, it is useful to compare coefficients for the

AUTHOR	SIZE OF COLUMN	ABSORPTION SYSTEM
Shulman and Molstad [201]	25, 50, 100 mm diam. 1.5 m tall	Absorption and desorption of CO_2, desorption of H_2, from water
Calderbank and Moo-Young [38]	----	Desorption of CO_2 from water/polyacrylate solutions
Hughmark [115]	150 and 400 mm diam.	Oxygen-water, oxygen-glycerol, CO_2-water, absorption
Deckwer et al. [70]	200 mm diam, 7.2 m tall 150 mm diam, 4.4 m tall	Absorption of O_2 into various liquids
Alvarez-Cuenca et al. [2]	660x2.5x2500 mm (flat)	Oxygen-water absorption
Mangartz and Pilhofer [151]	100, 140 mm diam., 2.7 m tall	Air/CO_2-water, N_2/CO_2-propanol
Hikita et al. [102]	100 mm diam, 1.5 m tall 190 mm diam, 2.4 m tall	Various liquids and O_2/ gas mixtures
Andrew [6]	Review Article	Review Article

TABLE 5.1: INVESTIGATIONS OF MASS TRANSFER IN BUBBLE COLUMNS

two devices to evaluate superiority in a specific application. Values of K_l for bubble columns cited in the literature have ranged from 0,01 to 0,05 cm/sec [83,132,151].

5.4.2 AGITATED VESSELS

In industry, gas and liquid are often contacted in stirred tanks, with gas fed to, and dispersed by, a rotating impeller. The efficiency of such a device depends on bubble size and holdup as well as liquid-side turbulence, and all three of these parameters will vary with impeller design [62,235].

Correlations found to characterise these devices normally supply the volumetric absorption coefficient as a function of the power per unit volume consumed in the tank, and of some measure of the dispersed gas holdup [6,62,186].

Agitated vessels may consume up to $3kw/m^3$ of fluid and may in these terms be closer in mass transfer properties to the D.S.R. than the bubble columns.

5.4.3 MASS TRANSFER IN PIPE FLOW

Most studies of mass transfer in pipe flow have been concerned with higher gas to liquid ratios than encountered in bubble flow. The annular flow pattern has

received the greatest attention. Alves [3,4], in discussions on horizontal pipeline reactors, has been primarily concerned with annular flow. Table 5.2 presents the literature on interphase mass transfer in pipe flow. The only studies on bubble flow found in the literature have been for horizontal flow in pipes of rather small bore [140,193,197]. Of these, only Lamont and Scott [140] have presented a correlation for K_l rather than $K_l a$. The product $K_l a$ is not a useful variable for comparing mass transfer devices where pressure may vary significantly, since the interfacial area, a, is dependent on both gas void fraction and bubble size. Mass transfer coefficients in the pipe flow have presented in two different ways. In annular flow, authors have preferred energy correlations, which express the mass transfer rate as a function of the pressure drop per unit length of pipe [126,127,131,-199,219]. Other correlations for the mass transfer rate are in terms of dimensionless numbers or liquid properties.

In cases where dimensionless numbers called for the inclusion of characteristic diameters or velocities, pipe diameters and liquid or mixture velocities have been employed, because in pipe flow the liquid turbulence is generated by the flow of the mixture, rather than by the rise of bubbles, as in bubble columns. Ohashi et al. [171] investigated solid-liquid mass transfer in a vertical pipe, using 300 to 800 micron resin beads in a

AUTHOR	APPARATUS/FLOW REGIME	ABSORPTION SYSTEM
Heuss et al. [93]	25 mm horiz. pipe, 1.2 m long, froth flow	O_2-water
Wales [226]	25 mm horiz. pipe, Annular/mist flow	CO_2-water desorption
Scott and Hayduk [193]	13 to 25 mm horiz. pipe 2.3 m long, single stream of bubbles/slugs	CO_2/He-water/alcohol/ glycol
Lamont and Scott [140]	4 mm horiz. pipe, 4 m long, stream of bubbles	CO_2-water
Jepsen [127]	25 mm pipe, 4.5 m long 100 mm pipe, 5.5 m long (Horiz.), bends, spirals Annular flow	CO_2-water
Kasturi and Stepanek [131]	6 mm vert. pipe, slug, annular, annular-mist flow	CO_2-carbonate buffer
Shah and Sharma [197]	12 mm horiz. pipe, bubble and plug flow	CO_2-carbonate buffer
Tomida et al. [219]	10, 18 mm, 3 m long 18, 25 mm, 4 m long annular flow	Desorption of CO_2 from various liquids
Shilimkan and Stepanek [199]	10, 15, 20 mm vert. pipe	CO_2-carbonate buffer

TABLE 5.2: INVESTIGATIONS OF MASS TRANSFER IN PIPE FLOW

vertical liquid flow, and found that the turbulence due to the settling of the beads had an insignificant effect on the mass transfer coefficient at liquid velocities above Ø.5 m/sec. By analogy, the turbulence due to rising bubbles in pipe flow will not have a significant effect on the mass transfer coefficient except at low flow velocities.

It is expected that the mass transfer coefficient would be strongly dependent on flow pattern. In this case no author listed in table 5.2 presents a correlation suitable for mass transfer prediction in vertical bubble flow. Mass transfer in vertical flow must therefore be examined before a confident D.S.R. design can be proposed.

5.5 METHODS OF EVALUATING MASS TRANSFER PERFORMANCE

To characterise the performance of a device, one must know values for K_l, the mass transfer coefficient, and for a, the area per unit volume available for transfer. Generally the product $K_l a$ is determined, and the individual parameters evaluated from a knowledge of a. Various experimental methods exist to characterise the mass transfer rate in gas-liquid contactors.

5.5.1 DETERMINATION OF $K_l a$

Several methods have been employed to measure $K_l a$;

(i) Dynamic Method

A two-phase flow is set up, and the gas stream feed caused to undergo a step change in concentration. The response of the concentration in the liquid phase is monitored and mathematically manipulated to yield the relevant data. This method is discussed in some detail by Keitel and Onken [133].

(ii) Stationary Method with Physical Absorption

A two phase flow is set up with liquid continuously circulated between the test apparatus and a gas stripper. Liquid leaving the apparatus is richer in the transferred species, and must be stripped of this gas with heat or vacuum stripping before being returned to the apparatus. The mass transfer rate, $K_l a$, is evaluated from a knowledge of the concentrations in the gas and liquid, and from the overall absorption rate, using equation 5.8. The physical absorption method has found favour [2,93,140,151,193], since physical absorption provides a method of examining mass transfer into pure liquids. A disadvantage lies in the fact that the limited solubility of gases in liquids (except where the gas reacts with the liquid) implies that equilibrium is reached rapidly, so that the method may not be used in apparatus with good mass transfer properties and long residence times. The physical absorption method

may distort experimental results in pipe reactors, where flow in a short length of pipe may not be fully developed and therefore may not be representative of the flow in a longer reactor.

A similar approach has also been used for desorption studies, with a gas-rich liquid stream stripped in the apparatus under study [219].

(iii) Stationary Method with Chemical Reaction

It is possible to prevent the transferred gas species from reaching equilibrium in the liquid phase by consuming the dissolved gas in the liquid bulk as fast as it is absorbed. The concentration of the species in the bulk, A^{o}, may be determined from a knowledge of the chemical reaction rate. The product of mass transfer coefficient and specific surface area, $K_l a$, is then evaluated in a similar way to that described for the physical absorption above. With a knowledge of the reaction rate of the chemical reaction it is possible to ensure that absorption is not enhanced by allowing the reaction to occur predominantly in the liquid film near the gas-liquid interface. Fast reaction in the film would cause a steeper concentration profile, and a greater local driving force, and would enhance the mass transfer rate which is determined.

Two chemical systems for determining mass transfer properties have found favour in the literature. The absorption of carbon dioxide into carbonate-bicarbonate buffers [131,132,197,199] is achieved by controlling the reaction rate with pH. The high solubility of carbon dioxide does, however, imply that the reaction rate must be high to consume the gas as fast as it is absorbed, and there is a danger that the gas phase may become totally depleted of carbon dioxide over a long residence time.

The oxygen-sulphite system, employing the reaction

$$O_2 + 2\ SO_3^{=} \Rightarrow 2\ SO_4^{=}$$

has also found favour [62,179] and is described in several reviews [67,145,198]. The lower solubility of oxygen in aqueous solutions makes this system suitable for testing large scale apparatus, but the rate of reaction is difficult to control, being catalysed by metals of variable valency [19,145]. Linek and Vacek [145] have observed that this method is favourable economically, especially for use in large apparatus.

Objections have been raised to the use of chemical absorption to predict transfer in aqueous systems. The presence of ions in solution is known to have an influence on both the mass transfer coefficient and the interfacial area [2,70,134] although Hikita et al. [102] have claimed

that the error involved is not too great. In circumstances where absorption into pure liquids does not provide a practicable method, the investigator may do little but accept the error generated by the use of an ionic solution rather than a pure liquid to measure the mass transfer rate.

5.5.2 SPLITTING THE PRODUCT $K_l a$

Where a value for $K_l a$ has been determined, it is possible to evaluate K_l only by determining the surface area available for transfer in the apparatus. Except in the case of specialised small scale apparatus, which may keep bubble size constant, or may measure variation of bubble size by noting changes in mixture volume, [83,105], the surface area, a, must be evaluated by one of the three following methods.

(i) from the mean bubble diameter

A mean bubble size, which characterises the ratio of bubble surface area to bubble volume, can be determined from photographs of the flow. Such a weighted mean radius will be given by the formula

$$r = \sum_{i=1}^{n} r_i^3 / \sum_{i=1}^{n} r_i^2 \quad \text{for n bubbles} \qquad 5.11$$

where r_i is the radius of a single bubble in the sample. The mean diameter, 2r, has been termed the Sauter mean diameter [36,181]. Noting that the bubble volume per unit volume of two phase mixture is the gas voidage, $\bar{E}$, we may write for spherical bubbles that

$$a = 3\bar{E}/r \qquad 5.12$$

and generally little error is incurred in assuming this to be true for bubbles which are slightly oblate [105]. Where bubbles are more deformed, suitable adjustment to equation 5.11 to account for a differing geometric shape will compensate. Once the specific surface area, a, has been evaluated at one point in a pipeline, an assumption of little bubble coalescence permits the adjustment of surface area with pressure. Since (assuming ideal gas behaviour) the gas void fraction, $\bar{E}$, decreases in inverse proportion to pressure, and the bubble radius varies with pressure to the power 1/3, the surface area will decrease inversely as pressure to the 2/3 power. However, where a significant gas volume is lost by absorption over the reactor length, the surface area, a, must be further adjusted.

(ii) by means of 'totally enhanced' chemical reaction

When chemical reaction rates in the liquid are sufficiently fast, reaction will take place in the liquid film adjacent to the phase interface. Provided that certain conditions are met [11,67,198], the rate of gas absorption becomes independent of the degree of turbulence, and is a function of only the reaction rate, diffusivity and available interfacial area. Thus the interfacial area is determined by monitoring the gas consumption. Two systems can be employed; the absorption of oxygen into highly catalysed sulphite solutions [67,234] and absorption of carbon dioxide into aqueous sodium hydroxide [130,186,197,234]. Problems associated with this method are discussed by Astarita [11]. As in the case of determining $K_l a$ by chemical methods, the surface area may differ from the case that exists in a pure liquid due to the surfactant effect of the electrolyte and consequent suppression of bubble coalescence [134].

(iii) by light scattering techniques

This method has been used by Calderbank [36] and is discussed by Reith [181]. A parallel beam of light travels through the mixture and is partially deflected by bubble presence. A receiver determines the fraction of light transmitted. This method has the disadvantage of

not being able to work at high bubble densities, and may determine only local values. There is also the practical difficulty of the liquid becoming dirty and thus opaque.

5.6 SELECTION OF SYSTEMS FOR EXPERIMENTAL WORK

Of the methods reviewed above, the oxygen-sulphite system was chosen for the evaluation of mass transfer coefficients in vertical pipe flow. Preliminary calculations, using estimates of the mass transfer coefficient in the D.S.R. demonstrated that both physical absorption and the absorption of carbon dioxide with chemical reaction were unsuitable. Physical absorption proved impractical because the mass transfer would have approached equilibrium over a fraction of the length of the reactor. Absorption of carbon dioxide into a buffered solution was also unsuitable, since the 35 m length of the proposed apparatus implied that the gas phase would become totally depleted of carbon dioxide, as a result of the high solubility of carbon dioxide in water. Preliminary calculations showed that if air were used as the gas phase, and sulphite solution as the liquid phase, approximately half of the oxygen in the air bubbles would be consumed over the 35 m length of the reactor. This oxygen-sulphite system was accordingly chosen to determine the mass transfer rate in the apparatus.

Surface areas were determined photographically. For one

experimental run, the "totally enhanced" oxygen-sulphite reaction was used to determine surface area, but there was some loss of accuracy due to high consumption of oxygen. The high oxygen consumption resulted in a very low oxygen partial pressure in the bubbles over a significant fraction of the reactor's length, so that effective surface area could not be inferred accurately from the data.

5.7 APPARATUS AND PROCEDURE

The 50 mm apparatus previously described for use in holdup studies was adapted for mass tranfer investigation. The following changes were made:

(i) The 500 l header tank was fitted with a stirrer to assist initial sulphite solution. The stirrer was not used during data acquisition.

(ii) Pressure gauges were fitted so that pressure profiles through the rig could be obtained.

(iii) Two stainless steel cooling coils were attached to mains water and immersed in the sulphite in the header tank when it was found that the existing refrigeration coils could not keep the temperature sufficiently low.

(iv) Copper is known to interfere with the catalysis of

the oxygen-sulphite reaction, as discussed in appendix F. Therefore the copper sparger and refrigeration coils were replaced with physically identical units made of stainless steel. For a similar reason all brass plugs were replaced with steel plugs and brass gauges were isolated with valves.

(v) To monitor oxygen concentration in the exit gas, approximately 1/3 of the tank was separated with a baffle to below the liquid level and an air-tight lid fitted to this enclosure. A 5 mm line carred samples under slight pressure from the enclosure to an oxygen meter. See figure 5.1. Later, the dead air volume in this section was reduced with empty plastic containers to improve response time between results.

Initially, twenty data points were gained by setting a constant gas and liquid flowrate in the reactor and monitoring the change in aqueous sulphite concentration with time under otherwise constant conditions, a method previously used by Andrieu and Claudel [7]. The change in sulphite was monitored by performing a back-titration of a liquid phase sample with iodine and thiosulphate in an acidified medium, as recommended by Vogel [224]. This method of obtaining results was slow because the aqueous sulphite concentration changed slowly with time, and only one or two data points were obtained from a run. A run lasted typically 2 or 3 hours.

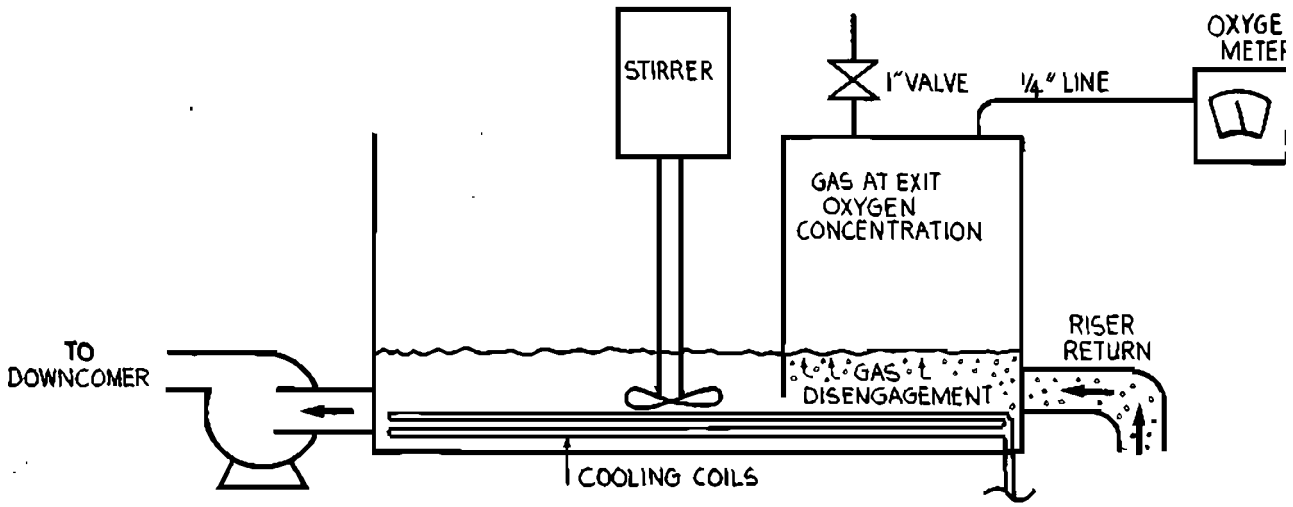

Fig 5·1 • Header tank arrangement for mass transfer •

The majority of the data were gained by the method of monitoring the concentration of oxygen in the exit gas, and calculating overall conversion from this concentration and the gas flow rate. A similar method has previously been used by Danckwerts and Rizvi [68]. This method permitted rapid data acquisition and was considered to be at least as accurate as the titration method: certainly errors in the measurement of gas flowrate became less critical. Calculation revealed that the amount of reaction occuring external to the D.S.R. tube, i.e. in the header tank, was negligible.

Experimental runs were started with a sulphite concentration of approximately 0,8 molar, and stopped when this dropped to 0,4 or 0,5 molar. The oxygen-sulphite reaction rate is found to be invariant with the concentration of sulphite in this range: see appendix F. For every liquid and gas flowrate, pressures in the rig were noted and temperature was kept as constant as possible. pH was controlled using sulphuric acid and sodium hydroxide. Bubble size was determined by fast electronic flash (10^{-4} sec) photographs, and results interpreted using the method outlined in section 5.5.2. A single "totally enhanced" (high reaction rate) oxygen-sulphite run was also conducted for the purpose of determining interfacial area.

5.8 CALCULATIONS FOR SULPHITE-OXYGEN METHOD TO DETERMINE $K_l a$

It is possible with the sulphite system to choose a reaction rate such that the oxygen concentration in the liquid bulk is far lower than that at the gas-liquid interface;

$$A^o \ll A^* \qquad 5.13$$

In this case, assuming $A^o \approx 0$, the rate of absorption may be expressed simply as

$$Ra = K_l a A^* \qquad 5.14$$

For steady state operation, the rate of oxygen absorbed must equal the rate consumed by sulphite in the bulk. The sulphite system is known to be second-order in oxygen, and zero order in sulphite for sulphite concentrations between 0,5 and 0,8 molar [145], so that one may write

$$k_2 (A^o)^2 = K_l a A^* \qquad 5.15$$

From 5.13 and 5.15, then,

$$K_l a \ll k_2 A^* \qquad 5.16$$

which is the criterion for negligible oxygen concentration

in the bulk, and sets a minimum value for k_2 in the experimental work.

However, if k_2 is made too large, the reaction proceeds too fast and a significant fraction of the reaction may take place in the liquid film. This is termed chemical enhancement, and will cause an apparant increase in values of K_1 determined under these conditions. Therefore k_2 must be sufficiently small that negligible reaction occurs in the film.

The rate of reaction occuring in the film, thickness δ, over a unit area must be determined. The average oxygen concentration in the film will be lower than the oxygen concentration at the interface, A^*, and the average sulphite concentration in the film will be lower than the sulphite concentration in the bulk. Hence it is safe to assume that the reaction rate in the film will be lower than that which would occur if oxygen at the interface concentration, A^*, were reacting with the bulk sulphite concentration. The reaction rate in the film per unit area of interface is accordingly less than

$$\delta k_2 . (A^*)^2$$

For negligible reaction in the film, this term must be much smaller than the total oxygen absorbed, so that

$$\delta k_2 (A^*)^2 << K_1(A^* - A^o) \qquad 5.17$$

setting $A^o=0$ and $\delta=D_g/K_1$, according to the film theory presented above, equation 5.17 becomes

$$K_1^2 >> D_g k_2 A^*, \qquad 5.18$$

thus setting an upper limit for k_2.

The value of A* may be estimated from the Henry's law constant for the oxygen-water system, by adjusting for the presence of dissolved species using the method of van Krevelen and Hoftijzer (see appendix G). These values agree acceptably with the recent solubility correlation given by Linek and Vacek [145].

$$A^* = 5.909*10^{-6} \exp\{1602.1/T - 0.9407[SO_4^{=}]/..$$
$$..(1 + \emptyset.1933[SO_4^{=}])\} \qquad 5.19$$

where $[SO_4^{=}]$ is taken as the sum of sulphite and sulphate concentration present.

Suitable values for A* and the diffusivity, D_g, of oxygen in 0,8M sulphite are given by Danckwerts and reproduced in table 5.3. Some preliminary runs on the D.S.R. apparatus revealed approximate values of K_1 so that a suitable rate, k_2, might be evaluated. A value $k_2=10^5$ l/gmol sec. was chosen.

TEMP	SOLUBILITY (A^*/P)	DIFFUSIVITY (D_g)
^oC	gram mole/litre atm.	cm^2/sec
15	$6.8*10^{-4}$	$1.36*10^{-5}$
20	$6.4*10^{-4}$	$1.60*10^{-5}$
30	$5.8*10^{-4}$	$2.10*10^{-5}$
33	$5.7*10^{-4}$	$2.25*10^{-5}$
40	$5.6*10^{-4}$	$2.60*10^{-5}$
50	$5.5*10^{-4}$	$3.26*10^{-5}$
60	$5.5*10^{-4}$	$3.90*10^{-5}$

TABLE 5.3: VALUSE OF OXYGEN SOLUBILITY AND DIFFUSIVITY IN 0.8 MOLAR SULPHITE-SULPHATE SOLUTIONS, AFTER DANCKWERTS

The sulphite reaction is catalysed by cobalt, as discussed in appendix F. The above reaction rate is achieved using approximately 10^{-5} molar cobalt at pH=7.5 and a temperature of 30 to 33°C. Calculations using the value of 10^5 l/gmol sec. for k_2, and preliminary values of K_1, showed that the criterion for no oxygen in the bulk (equation 5.16) would be easily met, although some small enhancement might occur, since at the base of the apparatus for low flowrates, the worst case might be

$$K_1^2 \approx 3D_g k_2 A^* \quad \text{(see equation 5.18)}$$

However, it was not possible to lower k_2 further while retaining confidence in existing rate correlations in the literature. With all cooling coils in operation, the temperature was held steady near 30°C, due to the heat produced by both frictional losses and heat of the sulphite reaction in the apparatus.

From the above considerations, the operating conditions given in table 5.4 were employed on all the experimental runs.

5.9 RESIDENCE TIME DISTRIBUTION IN D.S.R

To interpret the overall absorption data gained, and to extract values for the mass transfer coefficient, it was

PIPE DIAMETER: 2" nominal, 52 mm i.d.

TOTAL LIQUID VOLUME IN APPARATUS: 250 litres

ACTIVE VOLUME OF PIPE: 67.1 litres

LENGTH OF PIPE: 31.6 meters

LIQUID VELOCITY: 0.7-3.0 m/sec.

TEMPERATURE: 29-33^{o}C

pH: 7.46 - 7.60

TOTAL CONCENTRATION: 0.8 - 0.85 molar sulphite + sulphate

SULPHITE CONCENTRATION: 0.8 - 0.85 at start

0.4 - 0.5 molar at end of run

COBALT CONCENTRATION: $1*10^{-5}$ - $3*10^{-5}$ molar, including that present as impurities

TABLE 5.4: OPERATING CONDITIONS FOR MASS TRANSFER STUDY

necessary to measure the residence time distribution (RTD) in the D.S.R. apparatus. Keitel and Onken [133] have demonstrated that great error may arise in calculation of the mass transfer coefficient if the liquid phase is incorrectly assumed to approximate plug flow. It was also demonstrated by Keitel and Onken that the RTD was less critical for the gas phase.

Tests were conducted in the 50 mm rig by injecting a slug of saline solution into the flowing liquid stream some 2 m after the pump. Conductivity was monitored at the discharge into the header tank, and the signal plotted on a chart recorder.

As expected, a single phase water flow in the D.S.R. apparatus at a velocity of 2.4 m/sec exhibited a response characteristic of plug flow. The response changed little at average gas voidages of 5 and 15% in the rig. It was concluded that a plug flow model would be valid for the interpretation of the two phase flow results from this apparatus.

5.10 MODELLING THE REACTOR

It was not possible to generate a closed solution to extract the values of K_1a from data obtained using the 50 mm diameter D.S.R. apparatus. However, an accurate solution was obtained using an incremental numerical

solution, employing a plug flow model. An approximate solution, with a linear assumption explained below, was used for a first estimate of $K_l a$.

The following information was available from each run on the DSR;

(i) Liquid Flow Rate

(ii) Gas Flow Rate

(iii) Pressures around the rig

(iv) Overall absorption, calculated from either exit oxygen concentration, or from liquid phase sulphite analysis.

(v) A bubble radius, or an assumed bubble radius.

The models to treat this information are described below.

5.10.1 PLUG FLOW MODEL

Pressure in the apparatus was described in terms of three quadratic equations: for the downcomer, horizontal and riser sections. The equations yielded pressure in terms of x, the length along the rig past the sparger. Constants were evaluated from pressures measured during the run at known values of x. A constant value of the mass transfer coefficient, K_l, and a typical bubble radius, were assumed at the beginning of the program. The plug flow model was implemented using increments of length 0.1 or 1.0 m around the apparatus. Consider the first

step, just past the sparger. Pressure, P(x) is known from the quadratic in x, so that the superficial gas velocity may be evaluated:

$$\overline{W}_g(x) = W_{go}P_o/P(x) \qquad 5.20$$

where the subscript o denotes reference conditions. Pressures are absolute, and the air is assumed to be an ideal gas. From a knowledge of $\overline{W}_g(x)$ and $\overline{W}_l$, the local voidage may be predicted from the Zuber and Findlay equation,

$$\overline{E}(x) = \overline{W}_g/\{C_o(\overline{W_g+W_l}) + \overline{U}_{gm}\} \qquad 5.21$$

where $\overline{U}_{gm} = U_z$ in the riser, and $\overline{U}_{gm} = -U_z$ in the downcomer. It was assumed that $\overline{U}_{gm} = 0$ in the horizontal section. The value of C_o for the horizontal section was assumed identical with the value for vertical flow. The error involved in these assumptions would be very small, as velocity and void distributions in the horizontal section would not have sufficient length to develop into distributions significantly different from the downflow case.

A mean bubble radius at standard temperature and pressure, r_o, was assumed, and the mean radius at x, assuming no coalescence, was given by

$$r(x) = r_o\{P_o/P(x)\}^{1/3} \qquad 5.22$$

Surface area in the section was thus

$$a(x) = 3\bar{E}(x)/r(x) \qquad 5.23$$

The equilibrium oxygen concentration, $A^*(x)$, was calculated from the local pressure and composition of the air. The total moles of oxygen consumed in the given incremental reactor length, L, was thus given by

$$K_l a(x)A^*(x)L(\text{cross-sect. area of pipe}) \qquad 5.24$$

From this value, both gas flowrate and composition were adjusted for oxygen loss, and the second increment addressed. After proceeding along the whole rig length, the total oxygen comsumption in the rig was given and could be compared with the value found experimentally. The mass transfer coefficient, K_l, was then readjusted until the predicted and experimental values agreed. The program also supplied the average value of the interfacial surface area, a, in the rig.

It should be noted that values of K_l and a obtained in this way are not necessarily true values where an arbitrary bubble radius was assumed. The product $K_l a$ is, however, correct. For example, a doubling of the assumed radius in the program would halve a, but cause the value

of K_l determined to double, keeping the product constant. The program was kept in this configuration to determine true values of K_l where the bubble radius was accurately known.

5.10.2 LINEAR ASSUMPTION MODEL

The method described above in section 5.10.1 is a little slow, requiring trial and error manipulation to determine K_l or $K_l a$. A simpler program was written to provide an initial estimate of K_l.

The procedure was identical to that described above except in the assumption that oxygen was consumed at a constant rate around the rig, so that oxygen concentration decreased linearly with respect to x from its initial (atmospheric) value to its final value, at the top of the riser. A similar method has been used by Deckwer et al. [70] for mass transfer analysis in tall bubble columns. In practice, the oxygen partial pressure profile along the reactor length is complex, being a combination of an exponential decay and the pressure profile.

The mass transfer coefficient, K_l, was obtained by dividing the total oxygen consumption by the integral

$$\int_{x=o}^{x=x_f} 3E(x)P(x)\{C_a - (x/x_f)(C_f-C_a)\}/(r(x)He)\ dx \qquad 5.25$$

where C_a, C_f are the initial and final oxygen fractions in the gas, x_f the total rig length, and He the Henry's Law constant. This method generally underestimated K_l, but was accurate in cases where little oxygen was consumed. It provided a satisfactory initial estimate of K_l for use in the detailed method described in 5.10.1 above.

5.11 MASS TRANSFER RESULTS - $K_l a$

The product of mass transfer coefficient and surface area, $K_l a$, was calculated using the computer programs described above with the data obtained from both liquid analysis and the oxygen meter.

5.11.1 RESULTS USING LIQUID PHASE ANALYSIS

The 19 data points gained using liquid phase analysis showed that high mass transfer coefficients are found in two phase bubble flow. Values of $K_l a$ at S.T.P. are plotted in figure 5.2 against gas flowrate for various liquid flowrates. The mass transfer rate, $K_l a$, was found to be relatively independent of the liquid superficial velocity in the apparatus, because two distinct effects had opposite influence on the rate. Firstly, increased flow velocity caused an increase in turbulence, and therefore increased the mass transfer coefficient, K_l, in

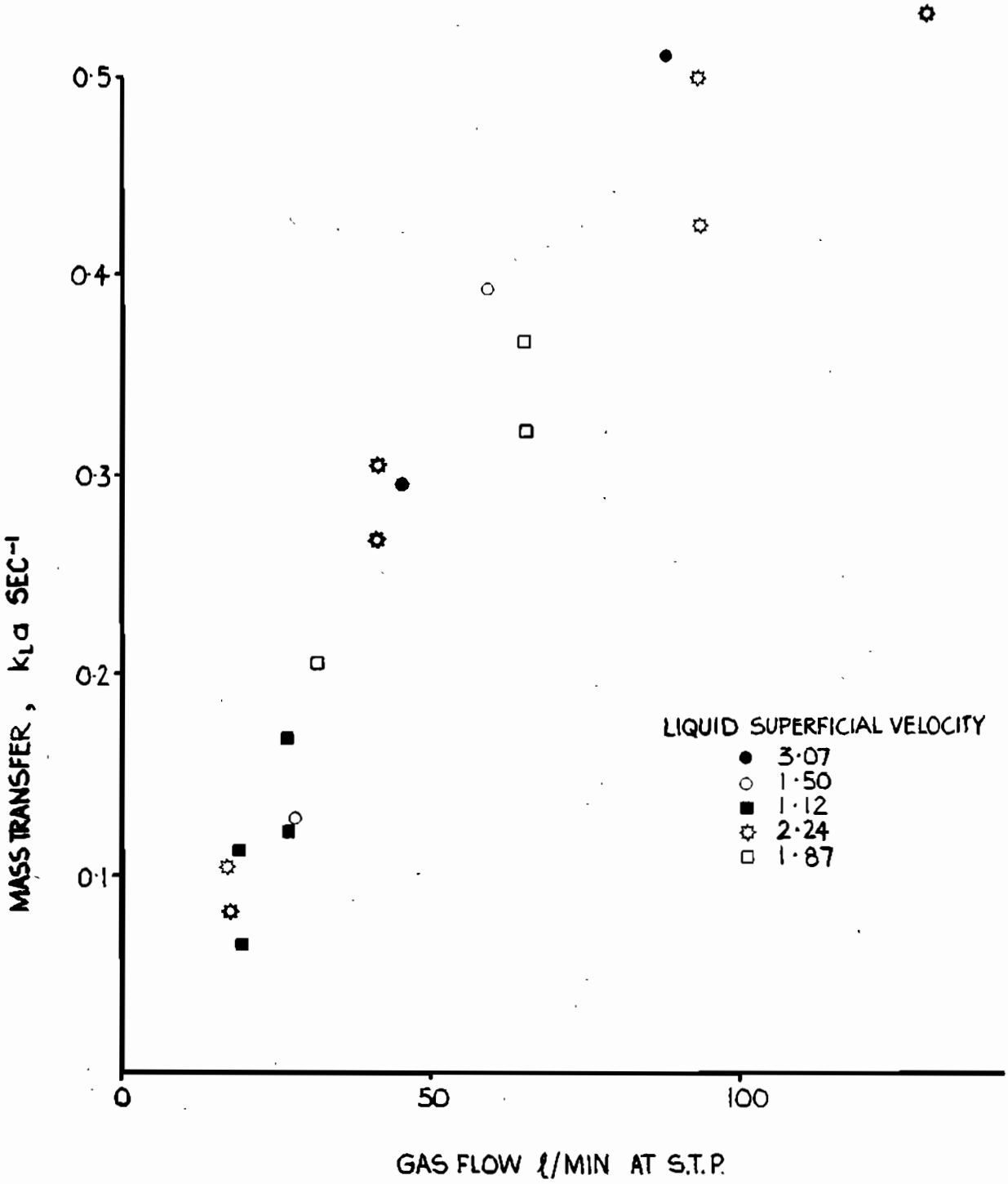

Fig 5·2 • Mass transfer using liquid phase analysis •

the reactor. On the other hand, increasing the liquid flowrate reduced the residence time of the bubbles in the reactor, so that the available surface area was reduced, even though the gas flowrate was held constant. Alternatively, the loss of residence time may be viewed as a loss of gas holdup in the D.S.R; because the gas holdup is given by the quotient of gas superficial velocity, and actual gas velocity relative to the pipe, an increase in gas velocity will reduce the holdup. A reduction in gas holdup in turn causes a loss of interfacial area for mass transfer.

5.11.2 RESULTS USING OXYGEN METER

One hundred and ten data points were obtained by this method, which confirmed the excellent mass transfer properties of the DSR. Figures 5.3 to 5.6 show the variation of $K_l a$ with gas flowrate at four different liquid rates. The large scatter of data is noteworthy and the causes have been discussed in detail in appendix F, and may be attributed to the presence of iron in solution. The increased scatter in this data over that of the previous method is perhaps due to deterioration in the galvanising in the pipes, leading to dissolution of iron from the pipe wall, as the work using the oxygen meter was conducted some time after the liquid phase sulphite analysis work. In addition, between the two sets of runs, the rig was used in a few three phase air-water-sand runs,

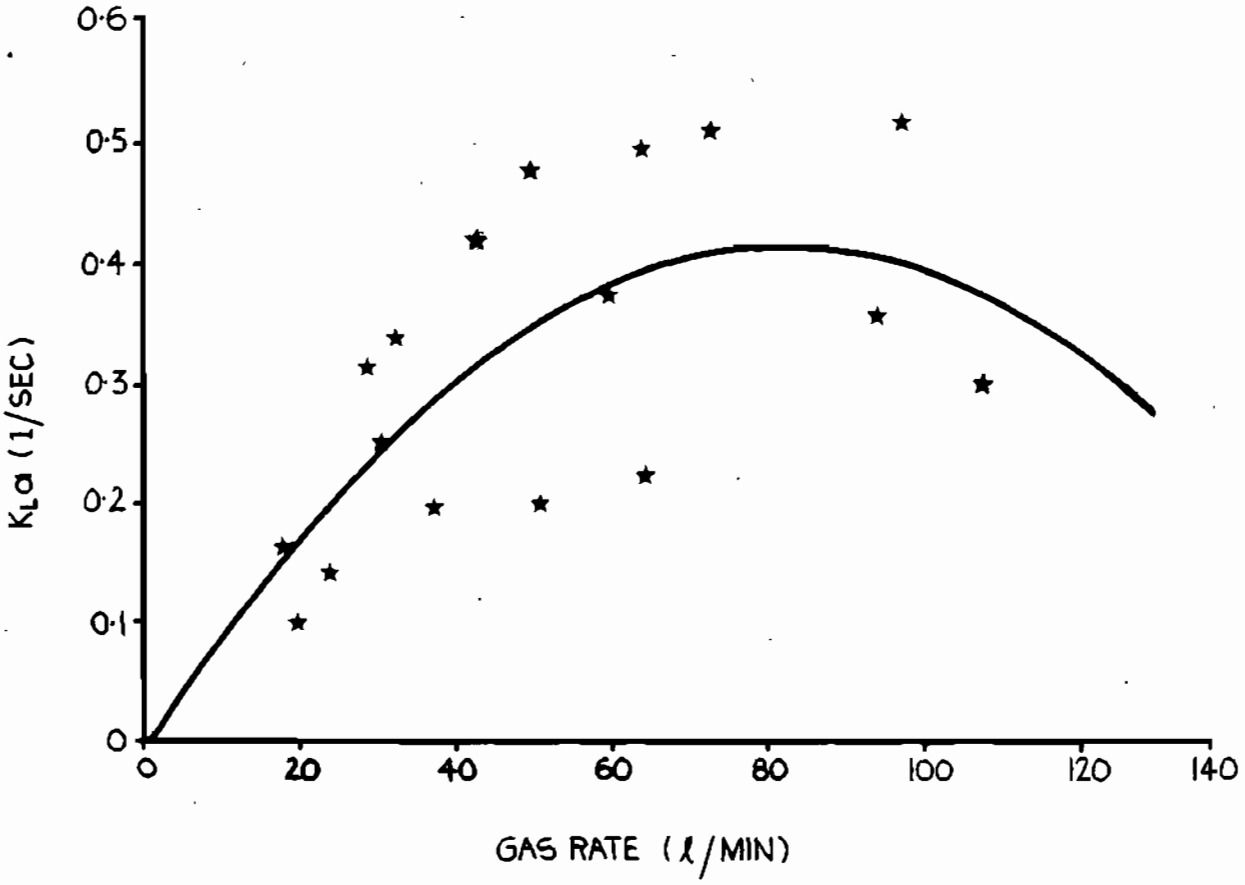

Fig 5·3 • K_La vs. gas flowrate for liquid velocity of 1·5 m/sec

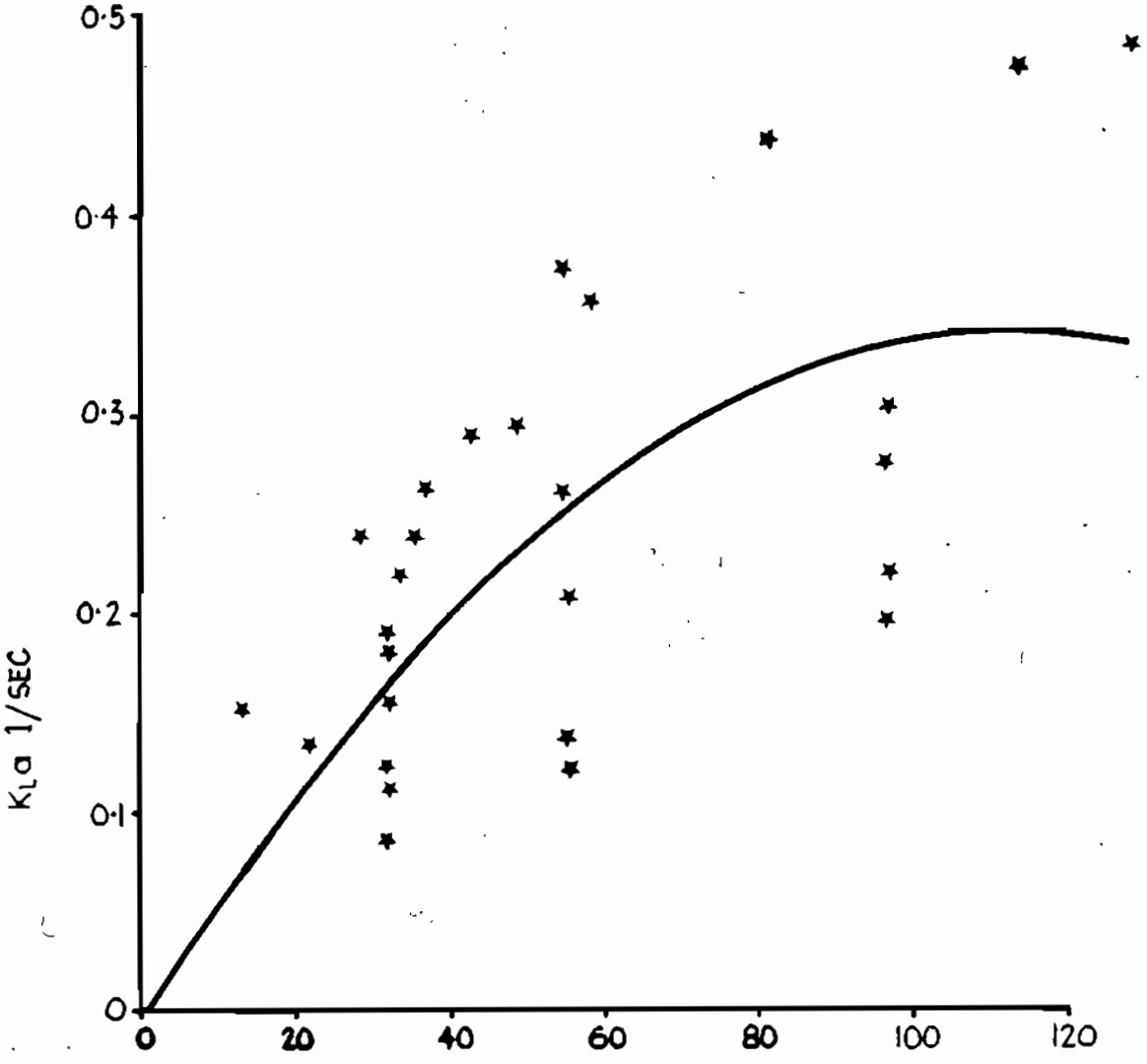

Fig 5·4 • K_La vs. gas flowrate for liquid velocity of 1·9 m/sec •

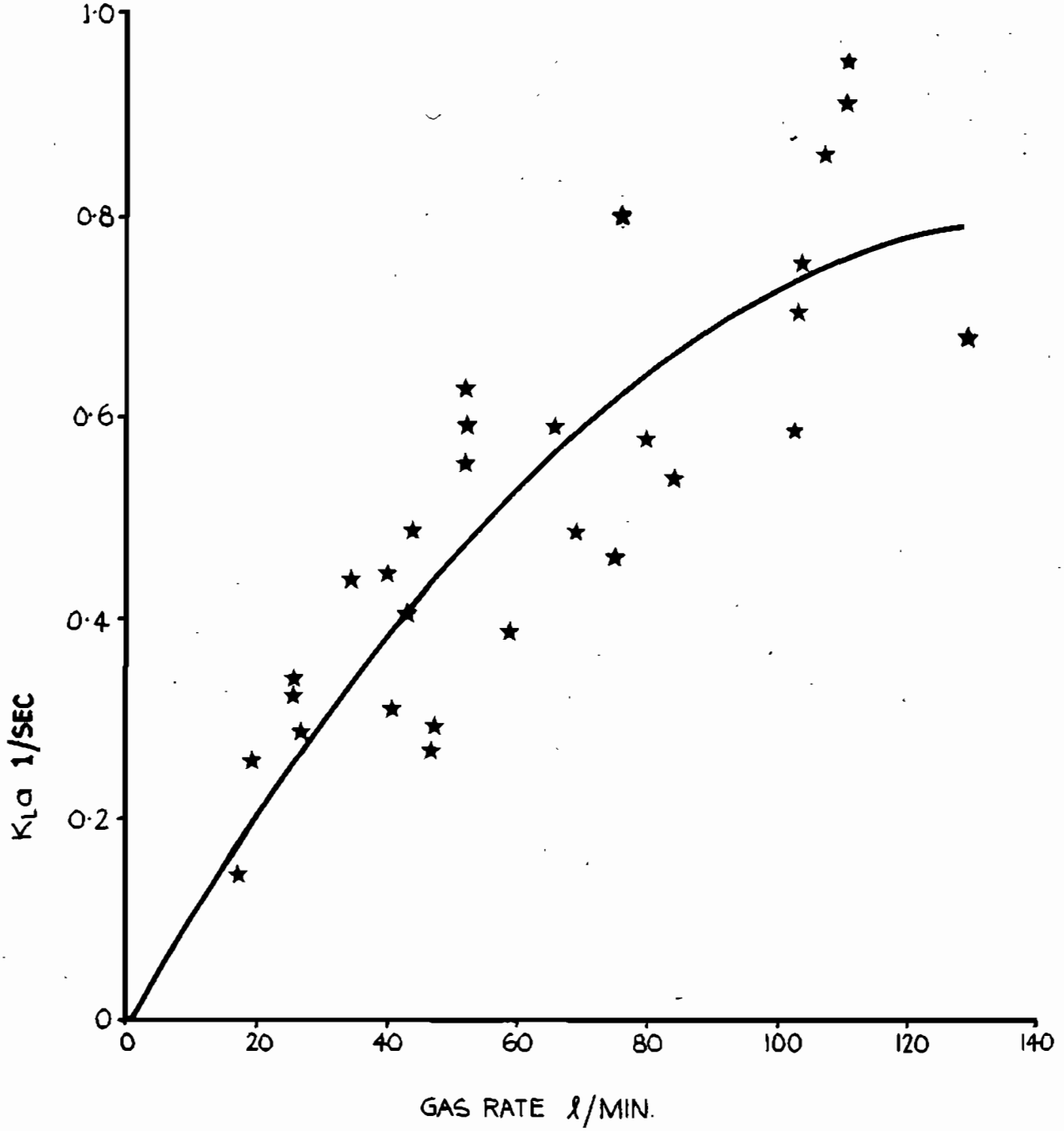

Fig 5·5 • K_La vs. gas Flowrate for liquid velocity of 2·6 m/sec •

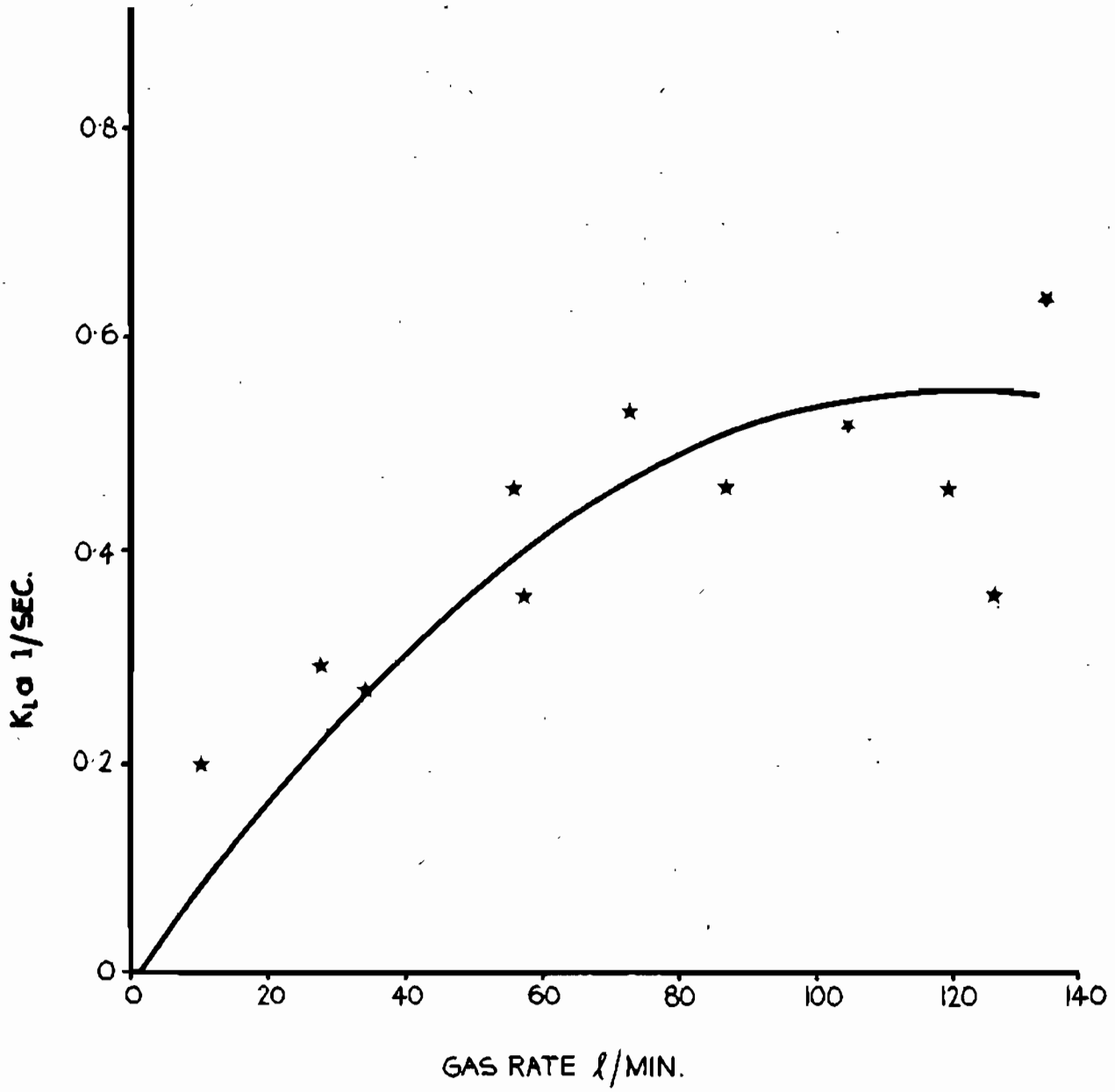

Fig 5·6 · K_La vs. gas flowrate for liquid velocity of 3·1 m/sec ·

which may have further eroded and damaged the pipe surface. Economic considerations prevented experimental work using reagent quality chemicals in a stainless steel and glass rig.

For each liquid flowrate, parabolic curves were found by regression and drawn through the data. The four curves are superimposed in figure 5.7. It can be seen that trends within fixed liquid flowrates appear consistent, although it is suspected that data scatter has caused curves to be displaced relative to one another. The curve for the case of $\overline{W}_l$=1,5 m/sec. certainly appears displaced. The strong falloff in the slope of the curves, $dK_l a/d\overline{W}_g$, at high gas flowrates, is due to slug formation in the riser at the higher gas voidages. The trends in figures 5.3 to 5.6 are similar to those found in mass transfer work on bubble columns [151], and may be attributed to a falloff in the ratio $a/\overline{E}$ due to bubble coalescence in the horizontal section of the rig at higher voidages.

To test the variation in $K_l a$ with varying liquid flow, at a fixed gas flow, the following experiment was conducted in two runs of the rig. Gas flow at STP was set to a constant low value (0.27 m/sec) and liquid flow varied from a minimum (1.5m/sec) to a maximum (3m/sec) and back to a minimum again. At each of five liquid flowrates the mass transfer rate was measured. Hence, for each flowrate two data points were obtained, so that any changes of

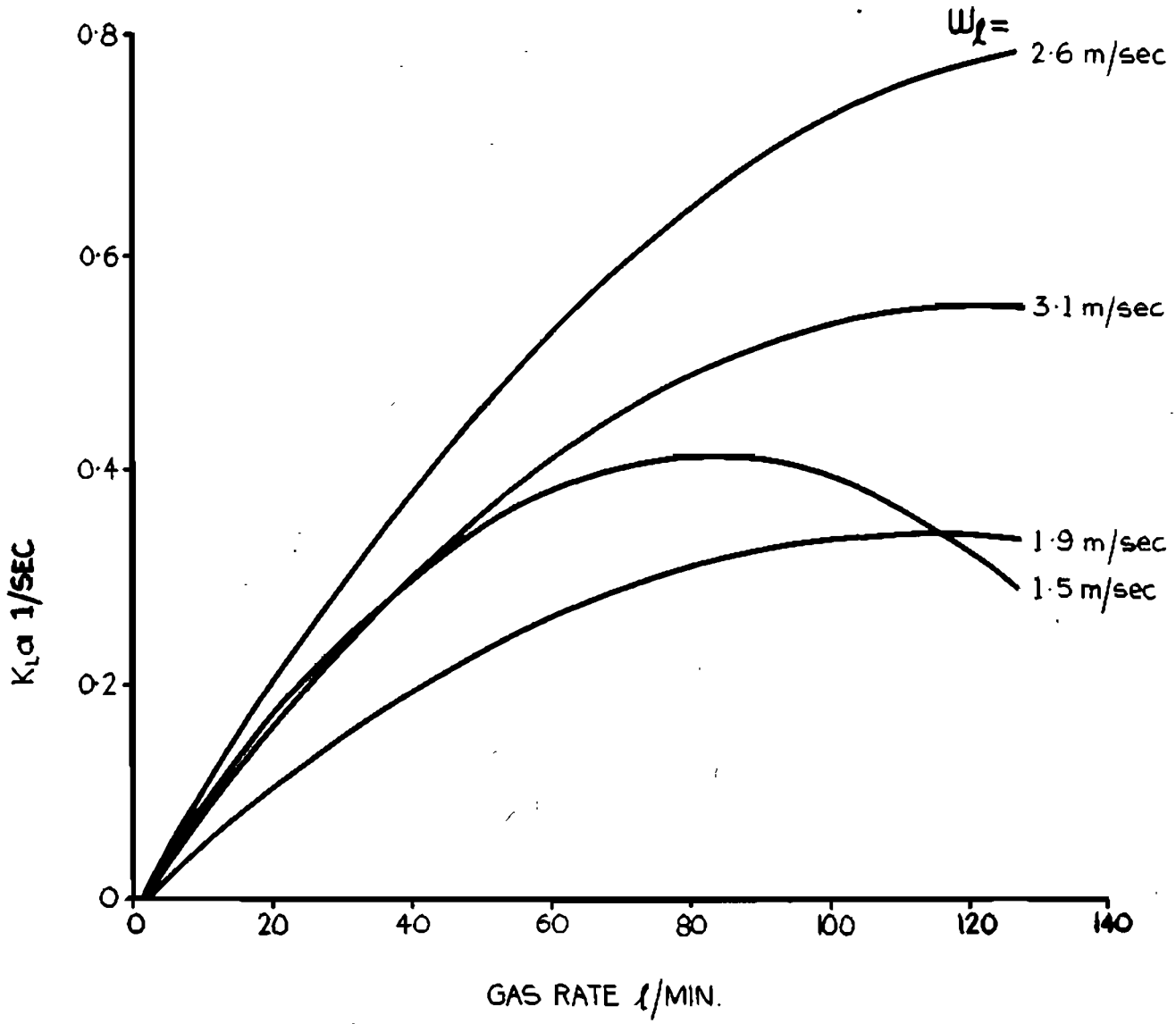

Fig 5·7 • Comparison of transfer at various liquid flowrates •

absorption rate with time might be eliminated by averaging of these points, assuming such change to be linear in time. A further two data points were obtained in the second run. The two runs followed a similar procedure, but the second run was commenced at maximum liquid superficial velocity (3 m/sec.), reduced to minimum (1.5 m/sec.), and raised to maximum again. Thus, four data points were obtained for each of five liquid flowrates in the D.S.R.

The product K_1a varied little with liquid flowrate in these runs, as is shown in figure 5.8. This conclusion agrees with the early data given in figure 5.2, and suggests that figure 5.7 does not typefy the variation of K_1a with liquid flowrate at constant gas flowrate, as mentioned above. It must be concluded that, at a fixed gas flow, K_1a is fairly constant in the 50 mm D.S.R., with the area, a, decreasing and the mass transfer coefficient, K_1, increasing in sympathy with an increase in liquid flowrate

5.12 RESULTS - DETERMINATION OF INTERFACIAL AREA

5.12.1 DETERMINATION OF AREA BY SULPHITE METHOD

One run was conducted using 'totally enhanced' sulphite oxidation, with high cobalt concentration, to determine surface area. The method was not suitable because the gas

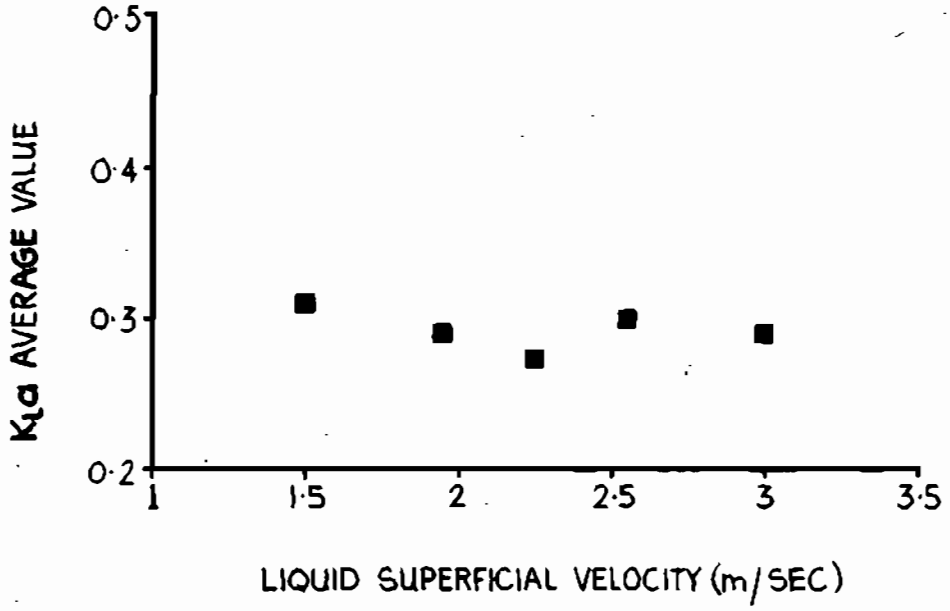

Fig 5·8 • Variation of K_La with liquid flourate •

phase became greatly depleted of oxygen so that results were inaccurate. However, results were processed, and the run indicated a bubble diameter of approximately 2 mm at standard temperature and pressure.

5.12.2 PHOTOGRAPHIC METHOD

Bubble size was measured by photographing the flow at a point approximately 2 m below the gas sparger. The volume-surface average bubble diameter was determined from the measurement of 40 to 50 bubbles in each photograph.

All bubble diameters reported below are converted to S.T.P.

Results showed that:-

(i) Bubble size decreased with increasing liquid flowrate.

(ii) Bubble size changed little with increasing voidage. In most cases a slight decrease in diameter was observed, rather than an increase as might be expected. It was concluded that this was due to an increased total superficial velocity at the sparger at higher gas rates.

Surface-volume mean diameters were difficult to determine because the occasional presence of a large bubble causes significant changes in the mean. Analyses of two photographs of a flow with the same gas and liquid

flowrates may predict diameters differing by up to 40%. Nevertheless, a correlation was proposed to predict bubble radius in terms of total flow.

$$2r = 4.291 - 0.6366\ (\overline{W_g + W_l}) \qquad 5.26$$

where r is the bubble radius in mm, and $\overline{W}_g$ is evaluated at the pressure near the sparger. This correlation may be considered valid over the range investigated ($\overline{W}_l$ = 1.5 to 3.0 m/sec, $\overline{E} < 0.2$ at the sparger). Experimental diameters are compared with the equation in figure 5.9. Since the prime function of determining the surface area was to extract the mass transfer coefficient from the product $K_l a$, it was noted that any error in determining the interfacial area was overshadowed by scatter in the results for $K_l a$, and was thus not of serious consequence.

5.13 RESULTS - VALUES OF K_l

The five average experimental points for $K_l a$ at constant gas rate with varying liquid rate (as in figure 5.8) were treated using the equation for bubble diameter, equation 5.26, and the plug flow program. Values of K_l were obtained for the assumption of no coalescence in the rig. This assumption was reasonable since gas voidage was low, especially in the horizontal section, where coalescence would most likely occur. Results were plotted in figure 5.10 against the two phase Reynolds number,

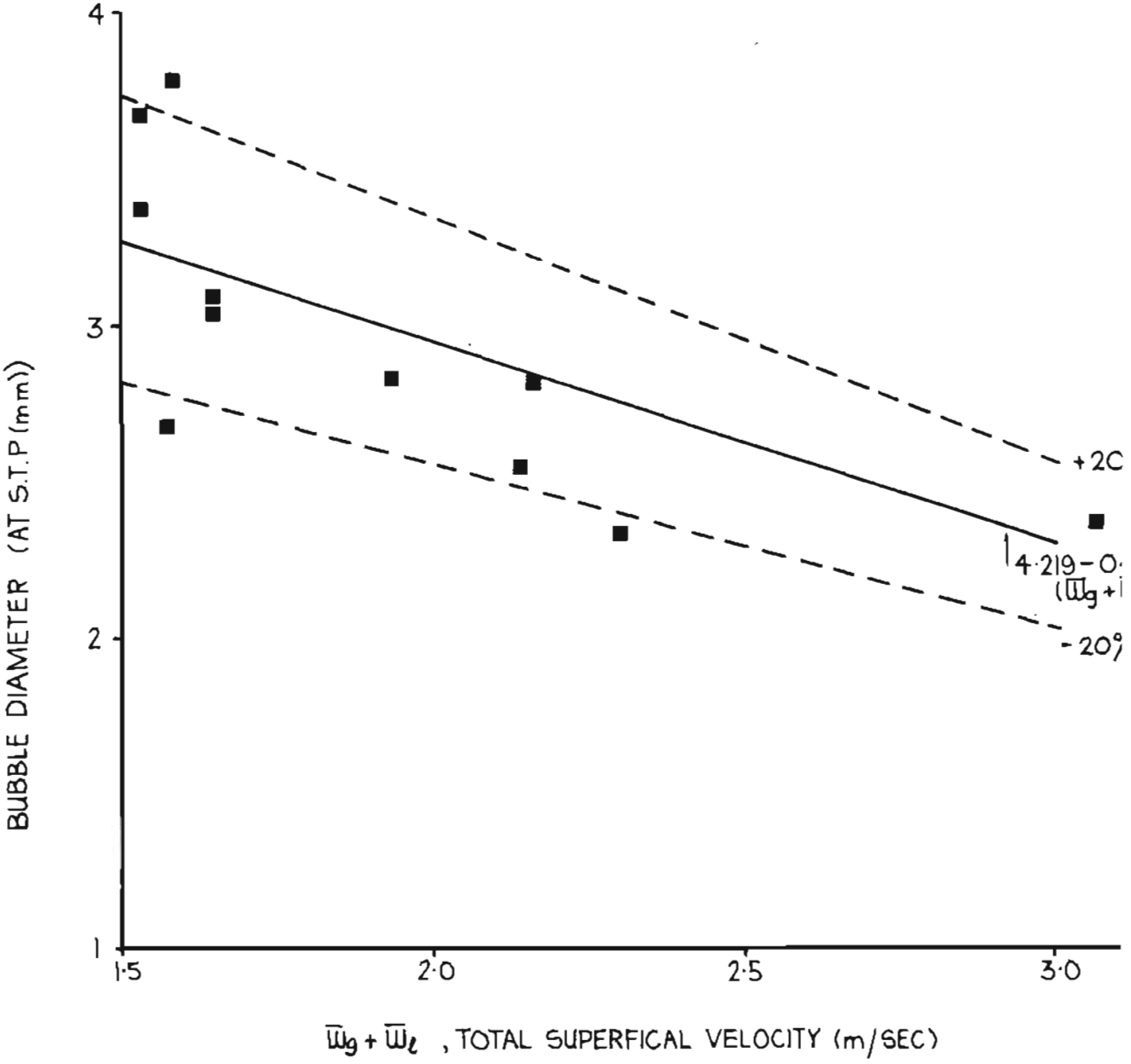

Fig 5·9 • Variation of bubble size with flowrate past sparger •

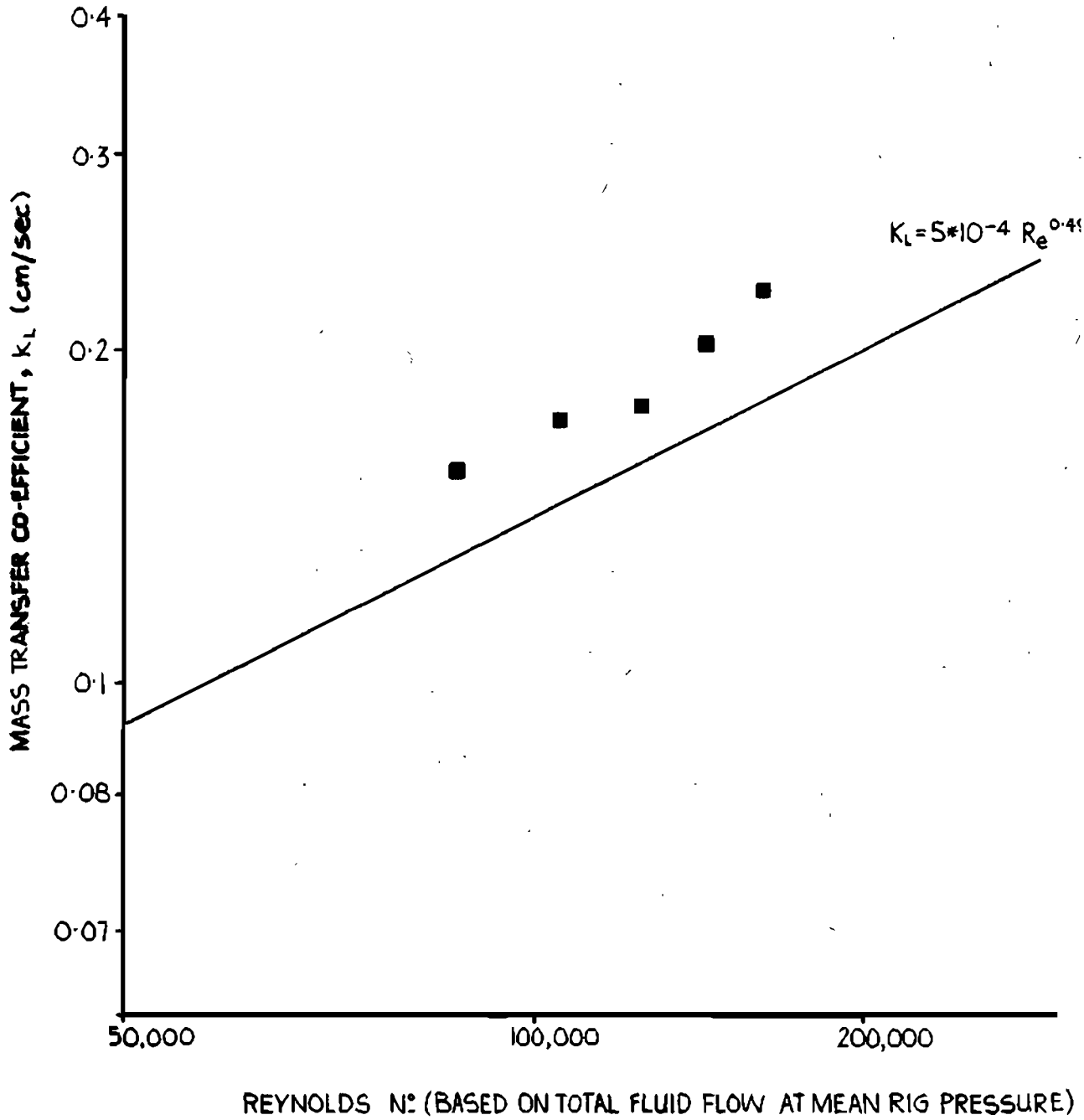

Fig 5·10 • Comparison of values for k_L with Lamont and Scot correlation •

$$Re = \rho_l (W_g + W_l) D_p / \mu_l,$$

taking ρ_l = 1100 kg/m^3, μ_l = 0.0011 Pa sec, and D_p = 0,052m. The viscosity was determined for a solution of sodium sulphate in water at 30°C. The gas superficial velocity, $\bar{W}_g$, was evaluated at the mean rig pressure. Variation in $\bar{W}_g$ about this value would cause little variation in the Reynolds Number. The correlation of Lamont and Scott [140], viz

$$K_l = 5*10^{-4} Re^{0,491}$$

has also been plotted in figure 5.10, and shows similar values and trends to the results of this study. Regression performed on the points produced the relationship

$$K_l = 1,205 * 10^{-4} Re^{0.628}$$

or, under restraint of Lamont and Scott's exponent,

$$K_l = 6.02 * 10^{-4} Re^{0.491},$$

thus yielding a constant some 20% higher than that of Lamont and Scott [140]. Lamont and Scott have justified their exponent in terms of well established theory. It is argued from surface renewal theory that

$$K_l = D_g s$$

with s the inverse of some mean contact time, t_e. Thus,

$$K_l \propto 1/t_e$$

Lamont and Scott [140] assumed that the contact time, t, may be given by the quotient of some eddy length, l, and a root mean square fluctuating velocity representative of the flow u'.

$$t_e = l/u'$$

From mixing length theory,

$$u' \approx l(du/dr)$$

Assuming a constant friction factor and the universal velocity profile, one may state that

$$(du/dr) \propto Re$$

or, assuming a Blasius relationship for the friction factor,

$$(du/dr) \propto Re^{0.9}$$

Combination of the above equations shows that

$$K_l \propto Re^{0.5} \text{ or } K_l \propto Re^{0.45}$$

which is in good agreement with the trend found here.

The value of the exponent of the Reynolds number may also be compared with the results of Ohashi et al. [171]. The mass transfer coefficient between solid resin beads and liquid in a vertical pipe flow was found to increase as the Ø.58 power of the flow velocity. This value is in acceptable agreement with the results of Lamont and Scott [140], and the results of this study for gas-liquid flow.

5.14 CONCLUSION

It may be stated that the mass transfer properties of a narrow bore D.S.R. are excellent. The mass transfer coefficients given in figure 5.10 are approximately an order greater than those given in the literature for bubble columns [83,151]. However, it was not possible using the available data to determine whether K_l varied with gas voidage. Such variation is likely to be small since the the falloff in mass transfer performance with increase in voidage (see figure 5.7) may be attributed to bubble coalescence rather than variation in the mass

transfer coefficient, K_1. Further study is also needed to assess the effect of pipe diameter on mass transfer in DSR's.

5.15 LIST OF VARIABLES

(Units of centimeters are preferred to meters in most mass transfer literature)

a	Surface area per unit volume (m^{-1})
A^o	Concentration in bulk liquid ($mol.cm^{-3}$)
A^*	Concentration at interface ($mol.cm^{-3}$)
C_o	Profile constant in drift flux model (-)
D_g	Diffusivity of gas in liquid (cm^2s^{-1})
E	Void fraction of gas(-)
He	Henry's law constant ($mol.cm^{-3}Pa^{-1}$)
k_g	Gas side mass transfer coefficient (cms^{-1})
k_l	Liquid side mass transfer coefficient (cms^{-1})
k_2	Second order reaction rate constant ($cm^3mol^{-1}s^{-1}$)
K_l	Overall mass transfer coeff., based on liquid side (cms^{-1})
L	Length of incremental pipe section (m)
P	Pressure (Pa)
P'	Partial pressure of species in gas bulk (Pa)
P'_i	Partial pressure of species in gas at interface (Pa)
r	Mean bubble radius (cm)
r_i	Radius of single bubble (cm)
R	Mass transfer rate ($mol.cm^{-2}s^{-1}$)
Re	Reynolds number (-)
s	Inverse of contact time (s^{-1})
t_e	Contact time (s)

u'	Fluctuating velocity (ms^{-1})
U_z	Bubble rise velocity (ms^{-1})
U_{gm}	Drift velocity (ms^{-1})
W	Superficial velocity (ms^{-1})
x	Distance along D.S.R. from sparger (m)
δ	Thickness of film (cm)

Subscripts

a	Initial value (at sparger)
f	Final value (at top of riser)
g	Gas
l	Liquid
o	At reference (atmospheric) condition

CHAPTER 6

6. DISCUSSION OF D.S.R. DESIGN

The preceding chapters have addressed the questions of predicting flow regime, gas holdup, pressure loss and mass transfer capabilities of a narrow bore D.S.R. Together with information available in the literature, sufficient knowledge now exists for the confident design of narrow bore D.S.R.'s from a synthesis of these four research areas. The simplest design philosophy would be to employ a plug flow model computer solution similar to that used in the interpretation of the mass transfer results. However, where gas consumption is small, such as when the reaction in the liquid bulk is relatively slow, a closed solution for D.S.R. hydrodynamics design is proposed. Both the computer model and the closed solution are discussed below.

6.1 COMPUTER MODEL

The design of a D.S.R. relies essentially on trial and error methods. Variables such as pipe diameter, reactor depth, point of gas introduction, and inlet composition of both gas and liquid must be specified. Then an incremental solution on a computer will rapidly predict the reactor performance. The solution is so fast that

design by this method need not be time consuming.

The program must be written along the following lines. The downcomer, horizontal section, and riser are treated separately and sequentially. The pressure at the point of gas introduction in the downcomer is estimated, so that the gas superficial velocity immediately below the sparger may be calculated from a knowledge of the free gas flowrate (at S.T.P.) to the D.S.R. Given the superficial gas and liquid velocities, the program must check that falling film flow or slug flow will not arise, since only the bubble flow regime is suitable for D.S.R. operation. From the gas and liquid superficial velocities, the gas holdup is determined from the Zuber and Findlay [243,244] drift-flux model, which has been verified in both up and downflow.

An incremental length is chosen for the program, and, using the calculated gas holdup, the hydrostatic head over the incremental length is calculated. Frictional pressure loss over the incremental length is estimated from a knowledge of the liquid superficial velocity and gas voidage. For velocities over 2 m/sec in the pipe, the models suggested by Orkizewski [174] or Butterworth [34] will predict the frictional losses, but at lower velocities the presence of "excess shear" due to the rising bubbles will cause the frictional pressure loss to be higher than these models will predict. In this case

the simplified mixing length model developed in chapter 4 should be employed. In an accurate final design run, one may also choose to account for losses resulting from the introduction of the gas at the sparger, and for the acceleration pressure change along the pipe length. Losses at the sparger are given by Hsu and Dudukovic [110] as

$$(\rho_l \bar{W}_l/g)[\{\bar{W}_l/(1-\bar{E})\} - \bar{W}_l] \qquad 6.1$$

and acceleration effects have been treated in detail by Brodkey [31]. However, both of these terms are very much smaller than the overall frictional and hydrodynamic pressure terms in the reactor, and may be neglected with little loss of accuracy.

Mass transfer in the first increment is calculated from the product of mass transfer coefficient, interfacial surface area, and driving force. Although insufficient experimental results exist currently to propose a general correlation for the mass transfer coefficient in two phase bubble flow, the results presented in chapter 5 may be used to estimate the coefficient.

Interfacial surface area is calculated from a knowledge of the gas void fraction and a volume-surface mean bubble diameter. The program must be supplied with a mean bubble diameter at standard conditions in order to predict the

surface area. Noting that the diameter of a (spherical) bubble decreases as the 1/3 power of the pressure applied to the bubble, the interfacial surface area in the first increment is given by the formula

$$(3\bar{E}V/d_o)(P/P_o)^{1/3}$$

where d_o is the diameter of the bubble at atmospheric pressure, P_o; V is the volume of the incremental section, and P the average pressure in the section. The driving force, (A^*-A^o), is calculated from the partial pressure of the reacting gas species in the bubble, and the concentration of the species in the liquid bulk. The partial pressure of the species in the bubble is calculated from the product of the pressure in the incremental section, and the mole fraction of the species present in the input gas. Concentration of the species in the liquid bulk depends on the kinetics of the reaction system in question.

Once the program has been used to predict the pressure change over the length of the increment, and the quantity of mass transferred within the first incremental volume, the second increment may be addressed. Gas superficial velocity is adjusted for both the loss of mass from the gas phase, and the change in pressure, and the hydrodynamic calculations are repeated. The gas composition is adjusted to calculate the partial pressure

of the reacting species in the second increment, and the mean bubble diameter is adjusted to account for the loss of gas volume from each bubble. The change in composition of the liquid phase is calculated from a knowledge of the reaction kinetics, and the overall transfer of mass in the second increment is evaluated.

The program proceeds along the entire reactor length by this process. The drift velocity term in the Zuber and Findlay drift-flux model must be altered to account for the different relative velocities in the downcomer, horizontal section, and riser. In downflow, the drift velocity term is equated to the negative of the bubble rise velocity in an infinite continuum, in horizontal flow the drift velocity term is zero, and in upflow it is given by the bubble rise velocity. Losses in fittings may also be taken into account where they are present [45,110,229].

At the end of the numerical calculation, the pressure and gas and liquid compositions at the top of the riser are reached, and compared with desired values. Initial conditions are then altered, and the incremental process repeated, so that the design proceeds by trial and error methods.

There are, however, two factors for which this method may not account, the coalescence of bubbles and the non-uniform depletion of the reacting species in bubbles

of different size. Bubble coalescence is likely to occur over a great length of pipe where gas void fractions are high, and this will serve to reduce the available surface area. Doubling the bubble diameter will halve the available surface are per unit volume of gas. Coalescence may be minimized by keeping the horizontal section short, so that no stratification of the phases takes place, and by maintaining a sufficiently high mixture velocity in the pipe. Placing distributors in the pipe at intervals will also serve to break up larger bubbles, but will lead to higher pressure losses around the reactor.

Smaller bubbles in the reactor present higher surface area per unit volume of gas than do larger bubbles, and will therefore be depleted of reacting gas species sooner than the larger bubbles. The result will be that mass transfer will proceed at a slower rate than the program predicts some distance along the reactor, where much of the surface area can no longer be exploited for mass transfer due to the preferential depletion of the reacting species in the smaller bubbles. Clearly the extent of this error will depend on both the bubble size distribution and the anticipated consumption of the reacting species over the reactor length.

Nevertheless, sufficient information is available for the confident design of a narrow bore Deep Shaft Reactor for mass transfer applications.

The usefulness of the plug flow model is best demonstrated by using a computer program to predict the variation of pressure, void fraction, bubble diameter, and gas composition, over the length of a D.S.R. A simple D.S.R. system was chosen, and the plug flow computer model used to predict the variation of these variables for the following operating conditions:-

Reactor diameter: 50 mm i.d.

Reactor length: 40 m (riser and downcomer 20 m each, neglecting the turning distance)

Sparger position: At top of downcomer

Gas inlet composition: 20% oxygen

Reaction system: Sulphite oxidation, assume no oxygen dissolved in liquid bulk

Bubble diameter: 2 mm at atmospheric pressure and 20^{o}C, at sparger. Assume no coalescence

Reactor Temperature: 20^{o}C

Liquid Superficial Velocity: 2 m/sec.

Free gas superficial velocity: 0.5 m/sec.

Pressure at sparger: 150 kPa absolute.

The plug flow model solution is shown in figure 6.1. A discontinuity exists in the gas void fraction plot at the base of the reactor (20 m length), because the bubble rise velocity changes direction abruptly at this point, and causes a change in the solution to the Zuber and Findlay

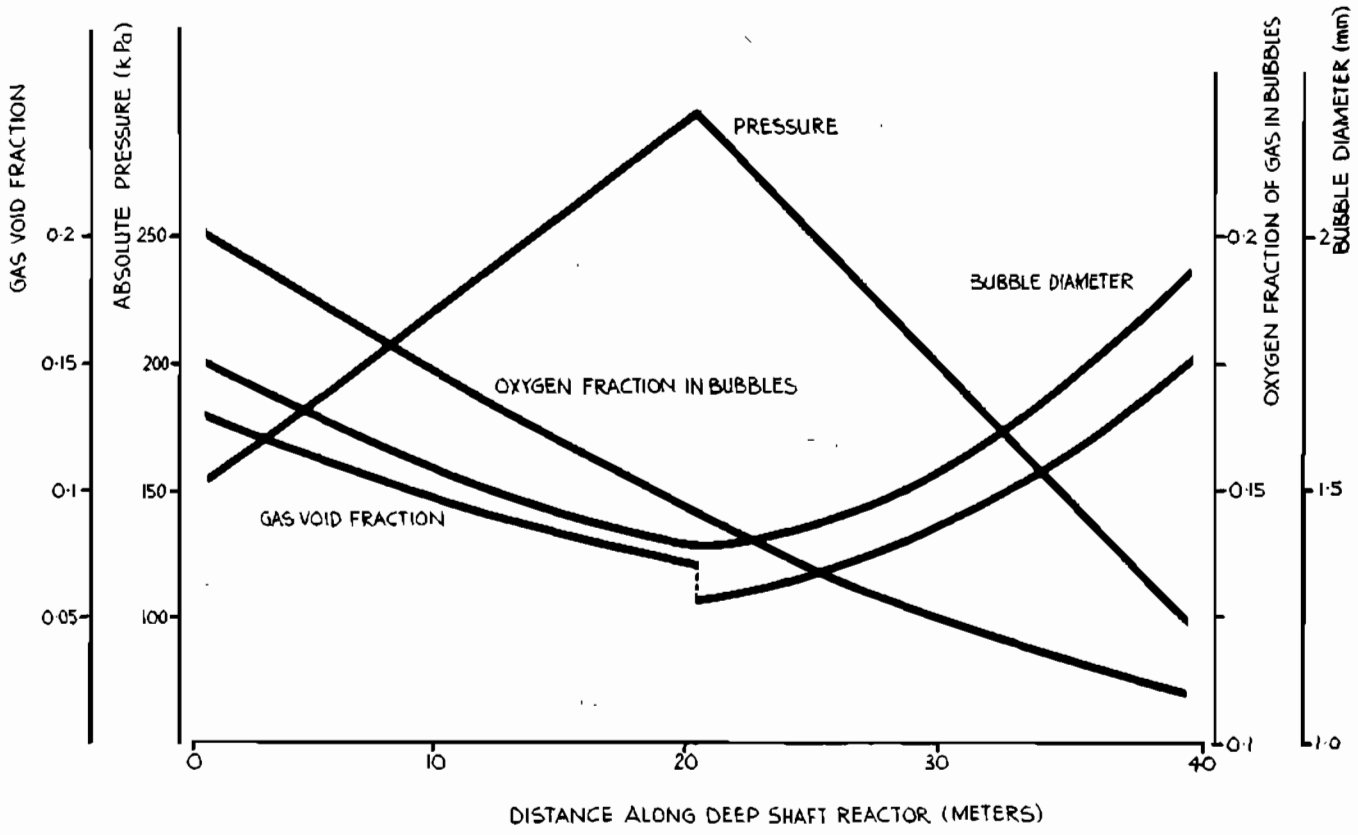

Fig 6·1 • Profiles of variables over the reactor length, predicted using the plug flow model •

[243,244] drift-flux equation. The first derivative of both pressure and bubble diameter is also discontinuous at this point, due to the reversal of the hydrostatic head.

Figure 6.1 serves to illustrate the use of a plug flow numerical solution in D.S.R. design. Solution is rapid and accurate, and can be readily extended to include more complex reaction systems and reactor geometries.

6.2 CLOSED SOLUTION

Besides the computer solution to the D.S.R. design, it is possible to use a closed solution for D.S.R. applications where depletion of the gas phase is small. This solution will also provide approximate initial values for use in the computer solution by solving the basic hydrodynamic design of the reactor, neglecting gas loss due to mass transfer. In addition, the closed solution presented below has been proposed by Clark and Meloy [57] and Clark et al. [56,59] as a method for the design of air-lift pumps and oil well gas-lifts.

The basic problem in the hydrodynamic design of a D.S.R. involves the prediction of change in pressure with height in the riser and downcomer. The closed solution considers the general case of bubble flow in a vertical pipe, and describes the relationship between height and pressure at any station in the pipe, given values for height and

pressure at any other station.

Consider a tube carrying a vertical bubble flow. The overall pressure change along the pipe may be ascribed to hydrodynamic, accelerational, and frictional pressure loss terms. Pressure drop over the height of the tube causes a change in volumetric flowrate of the air phase, and hence a change in the velocity of both the gas and liquid phases in the pipe. This gives rise to a momentum change, which is exhibited as a pressure loss, the acceleration effect. However, acceleration effects in bubble flow are generally small, and are neglected in most analyses. Hence the total differential for the pressure in the pipe may be given by

$$-dP = \{\rho_l g(1 - \bar{E}) + F\}dx \qquad 6.2$$

where E is the cross-sectional average air void fraction, and F is the irreversible loss per unit length, at a height x in the pipe, and where the head due to air density is neglected. By integrating equation 6.2 between some station in the pipe for which the pressure is known, $(x=x_o, P=P_o)$, and another station with unknown pressure, $(x=x_2, P=P_2)$, it is possible to obtain an explicit formula to predict the relationship between x_2 and P_2. However, to integrate, both the average air void fraction and the frictional pressure loss must be predicted as a function of air and liquid flowrates. Stenning and Martin [210],

in their analysis of slug flow air lift pumps, chose to evaluate the void fraction, $\bar{E}$, at the mean pressure in the tube, but this approach may be inaccurate for a long riser or downcomer, where $\bar{E}$ may vary significantly over the tube height.

In vertical two phase bubble flow one may not simply equate the in situ air void fraction, $\bar{E}$, with the volumetric flowing air fraction, $\bar{W}_g/(\overline{W_g+W_l})$, because the velocity of the air and liquid phases differ in the pipe. Firstly, the bubbles of air rise relative to the liquid, and secondly, the bubbles are more concentrated in the central region of the pipe, where the flow is faster than at the pipe walls. Zuber and Findlay [243] perceived that both of these factors must be taken into consideration, and presented the "drift-flux" model to predict air holdup.

$$\bar{W}_g/\bar{E} = C_o\bar{W}_m + \bar{U}_{gm} \qquad 3.14$$

where $\bar{W}_m$ is the total superficial velocitiy in the pipe.

To derive the hydrodynamic design equation for a D.S.R., a functional form for the pressure loss must also be proposed. Lockhart and Martinelli [147] argued that two phase frictional pressure loss per unit length in the pipe, $(dP/dx)_{tp}$, is given by the product of a two phase flow multiplier, Φ_l^2, and the frictional pressure loss,

$(dP/dx)_l$, which would occur in the pipe if the liquid alone were flowing in the pipe.

$$F = D\,\Phi_l^2 \qquad 6.3$$

where $F = (dP/dx)_{tp}$ and $D = (dP/dx)_l$, for simplicity in the derivation of the design equation below.

The pressure loss per unit length which would occur with the liquid flowing alone is given by

$$D = 4\rho_l f W_l^2/2D_p \qquad 6.4$$

where f is the friction factor, found from a conventional friction factor diagram. Orkizewski [174] presented a model for the prediction of the two phase multiplier from the air void fraction in the pipe

$$\Phi_l^2 = 1/(1 - \bar{E})^{1.8} \qquad 6.5$$

and various models similar to equation 6.5 have been presented in the subsequent literature, as described in chapter 4 above. To simplify the derivation, equation 6.5 was expanded as a Maclauren series and truncated after the second term, so that the frictional loss was given by

$$F = D(1 + 1.8\bar{E}) \qquad 6.6$$

The error incurred in truncating the series after the second term is small. In bubble flow the air void fraction at any point would usually be less than 20%, and the average air void fraction in the D.S.R. below 10%. At an air void fraction of 10%, the error in frictional loss prediction is only 4%, and since the frictional loss is typically an order of magnitude smaller than the hydrostatic head in D.S.R.'s, the overall error would amount to less than one half of a percent. However, at low velocities, models such as that of Orkizewski [174] may underpredict the frictional pressure loss, so that equations 6.5 and 6.6 may be inapplicable at low flow velocities. However, at low velocities the frictional loss is small with respect to the hydrostatic head, so that the underprediction of frictional loss will cause only a small error in the overall pressure gradient.

Combining equations 6.2 and 6.6

$$-dP = \{\rho_l g(1 - \bar{E}) + D(1 + 1.8\bar{E})\}dx. \qquad 6.7$$

Equation 3.14 for the prediction of air void fraction is substituted into the total pressure differential, equation 6.7. Clearly the superficial air velocity in equation 3.14, $\bar{W}_g$, will vary with pressure, and account must be taken of this variation in the total differential. Where the mass flowrate of air in the two phase flow is G, the superficial air velocity, $\bar{W}_g$ is given by

$$\bar{W}_g = GP_o/A_p P p_g \qquad 6.8$$

where P_o is atmospheric pressure, A_p is the pipe cross sectional area, and ρ_g is the density of the air at atmospheric pressure and at the temperature of the reactor. Setting $M = GP_o/A\rho_g$, and combining equations 3.14, 6.7 and 6.8,

$$-dP = \rho_l g\left[1 - \frac{M}{C_o(M+\bar{W}_l P)+\bar{U}_{gm}P}\right] + D\left[1 + \frac{1.8M}{C_o(M+\bar{W}_l P)+\bar{U}_{gm}P}\right]dx \qquad 6.9$$

Multiplying through by the term $C_o(M+\bar{W}_l P)+\bar{U}_{gm}P$, and collecting pressure terms on the left hand side of the equation,

$$\left[\frac{C_o M + (C_o\bar{W}_l + \bar{U}_{gm})P}{\rho_l g C_o M - \rho_l g M + DC_o M + 1.8DM + (\rho_l g+D)(C_o\bar{W}_l+\bar{U}_{gm})P}\right]dP + dx = \emptyset \qquad 6.10$$

Integrating between the points $(x=x_o, P=P_o)$ and $(x=x_2, P=P_2)$,

$$\frac{P_2 - P_o}{(\rho_l g+D)} - \left\{\frac{1.8DM - \rho_l gM}{(\rho_l g+D)^2 S}\right\}\log\left\{\frac{R + (\rho_l g+D)SP_2}{R + (\rho_l g+D)SP_o}\right\} + x_2 = x_o \qquad 6.11$$

where $R = \rho_l gM(C_o-1) + DM(C_o+1.8)$ and $S = C_o\bar{W}_l+\bar{U}_{gm}$. Since every variable except x_2 is known in equation 6.11, an explicit equation for the evaluation of x_2 has been developed, thus avoiding the use of incremental methods in the design of a D.S.R. However, since the drift velocity,

$\bar{U}_{gm}$, changes between the riser and downcomer, the D.S.R. must be designed in at least two sections.

The closed solution, equation 6.11, reduces correctly to the single phase pressure differential when the air rate is zero. Equation 6.11 takes into account both the variation of slip velocity and the presence of frictional loss, and may therefore be applied over a wide range of operating conditions for DSR's in bubble flow. Equation 6.11 has been tested against two phase slug flow data in tall air lifts [45], and has found good agreement with experimental results. Although the closed design equation obviates the need for an incremental computer solution for D.S.R. design, it cannot account for mass transfer in the reactor. Moreover, the speed of modern computing equipment does not detract from a numerical solution to the design, so that the incremental method is likely to be preferred.

6.3 LIST OF VARIABLES

A_p	Cross sectional area of pipe (m^2)
C_o	Profile constant in drift-flux model (-)
d_o	Diameter of bubble projected to atmospheric pressure (m)
D	Liquid-only frictional loss per unit length (Pam^{-1})
D_p	Pipe diameter (m)
E	Gas void fraction (-)
f	Friction factor (-)
F	Two phase frictional loss per unit length (Pam^{-1})
g	Acceleration due to gravity (ms^{-2})
G	Mass flowrate of air (kgs^{-1})
M	Product of air superficial velocity and pressure ($Pams^{-1}$)
P	Pressure (Pa)
R	Variable grouping used for convenience
S	Variable grouping used for convenience
U_{gm}	Drift velocity (ms^{-1})
V	Volume of incremental pipe length (m^3)
W	Superficial velocity (ms^{-1})
ρ	Density (kgm^{-3})

Subscripts

g	Gas
l	Liquid

m	Total
o	At atmospheric pressure

CHAPTER 7

7. CONCLUSION

The investigation of D.S.R. design has provided sufficient information for confident design of a narrow bore D.S.R., a device which may find wide application in the field of gas-liquid mass transfer. In addition, much of the work is also applicable to the design of air-lift pump aerators and the prediction of two phase flow behaviour in chemical and nuclear engineering processes. The conclusions of this thesis are reviewed briefly below.

7.1 FLOW REGIME

D.S.R.'s for mass transfer operations should operate in the bubble flow regime, because the bubbles provide a large surface area for contact between the two phases. Moreover, bubble flow is associated with high liquid holdups, so that the hydrostatic head at the base of the reactor will be large, thus encouraging absorption of gas from the bubbles. However, coalescence of bubbles causes a transition from bubble flow to slug flow, a regime where large gas bubbles span the whole pipe diameter. Slug flow is not desirable in D.S.R.'s because it provides a small interfacial area for mass transfer, and may cause cyclic hammer in fittings. It is therefore necessary to predict whether a D.S.R. will operate in bubble or slug flow under

given operating conditions.

Survey of the literature revealed disagreement over the locus of the bubble flow to slug flow transition boundary, a fact attributed to subjectivity in the definition of transition, the type of sparger used, and the extent to which the reported flow was developed in structure. It was shown that sparger design played an important role in setting up a steady bubbly flow in the device, and that the mechanism of bubble production at the sparger differed between the cases of up and downflow.

Although Herringe and Davis [91,92] have reported the development of two phase flow structure downstream of the sparger for a variety of sparger types, further work of this nature should be undertaken to predict the influence of the sparger on the flow regime. The pipe length required for the flow to develop has not yet been modelled satisfactorily.

The operation of spargers in downflow has received little attention. Athough a short falling film flow was observed as a transitory effect below the sparger in both this thesis work, and the work of Barnea [14], no report of this effect has yet been found in the literature. An investigation of the falling film flow as a sparger afterbody effect is essential for the understanding of the mechanism of bubble production at the sparger in downflow.

Nevertheless, sufficient information has been presented in this thesis for the design of a sparger to produce a downward bubble flow, as required in the construction of a D.S.R.

7.2 GAS HOLDUP

Gas void fraction was well predicted using the equation of Zuber and Findlay [243], equation 3.14. The gas holdup is predicted with sufficient accuracy by using a value of 0.25 m/sec for the drift term and 1.1 for the profile constant.

The Zuber and Findlay model was less accurate in predicting holdup in the larger bore apparatus, where the profile constant was dependent on the average gas void fraction in the pipe. This dependence has been explained in terms of the distribution of bubbles across the pipe diameter. In upflow, the distribution is saddle shaped at low average gas voidages, and becomes parabolic at higher voidages. In downflow, it is suggested that this trend is reversed. However, it may be debated whether or not such voidage distribution dependence may be due to the developing structure of the flow; the work of Petrick and Kurdika [178] would suggest so, while the work of Herringe and Davis [91,92] has shown that saddle shaped profiles exist after 108 pipe diameters, where the flow should be

well developed. This dispute may be resolved only by further measurement of the local properties of flows. In particular, the local properties of downward flows have received little attention.

7.3 FRICTIONAL LOSSES

Frictional pressure drop was difficult to predict, being dependent on bubble size and the nature of waking, but was shown to vary significantly from the single phase flow case only at low liquid flowrates and high voidages.

Deviation of pressure loss from the accepted models at low flow velocities has been explained by the generation of additional turbulence in the wakes of the bubbles rising in the flow. Mixing length theory has been used to show that this additional turbulence becomes significant only at low flow velocities. Although the new mixing length theory provides the first accurate model of low velocity bubble flow pressure losses, more data is required for a wider range of pipe sizes and fluid properties before universal constants for the model can be proposed. However, conventional models will provide a pressure loss prediction which is sufficiently accurate at the flow velocities found in D.S.R.'s.

7.4 MASS TRANSFER

Mass transfer rates in the D.S.R. were found to be an order of magnitude higher than those found in bubble columns and industrial scale stirred tanks. Turbulence due to the flow velocity in the pipe serves both to increase the mass transfer coefficient, and inhibit bubble coalescence. Bubble coalescence would reduce the surface area available for mass transfer, and thus reduces mass transfer performance.

The mass transfer coefficient was found to be 20% higher than the correlation of Lamont and Scott [140] would predict, and to vary approximately as the square root of the Reynolds number. However, the effect of pipe diameter has not been fully assessed. Since frictional losses increase as the square of the Reynolds number, the relationship between mass transfer coefficient and Reynolds number implies that the use of very high velocities in D.S.R.'s may not be to economic advantage.

7.5 REACTOR DESIGN

The development of a general closed solution to describe the hydrodynamics as a function of length along the D.S.R. has been presented for the case of constant gas mass flow. However, a plug flow computer solution provides a rapid and accurate means of design, and is able to take account

of mass transfer in the reactor.

Design criteria are not readily presented, because economic optimization will depend on the reaction system involved and the degree to which the gas must be absorbed, as well as attaining a balance between capital cost and operating costs. Whereas a high velocity, narrow bore reactor will be cheaply constructed, pumping costs will be higher than those in a larger bore reactor with a lower flow velocity. The plug flow computer program provides the best means for preparing preliminary designs for economic evaluation.

BIBLIOGRAPHY

1. ADLER, P.M.(1977) Formation of an Air-Water Two Phase Flow, A.I.Ch.E. J. 23, 185-191.

2. ALVARAZ-CUENCA, M., BAKER, C.G., and BERGOUGNOU, M.A. (1980) Oxygen Transfer in Bubble Columns, Chem. Eng. Sci. 35, 1121-1127.

3. ALVES, G.E. (1954) Co-Current Gas-Liquid Flow in a Pipeline Contactor, Chem. Eng. Prog. 50, 449-456.

4. ALVES, G.E. (1970) Co-Current Gas-Liquid Pipeline Contactors, Chem. Eng. Prog. 66, 60-67.

5. ANDERSON, G.H. and MANTZOURANIS, B.G. (1960) Two Phase (Gas Liquid) Flow Phenomena - I. Pressure Drop and Holdup in Vertical Tubes, Chem. Eng. Sci. 12, 109-126.

6. ANDREW, S.P.S. (1982) Gas-Liquid Mass Transfer in Biological Reactors, Trans. I.Ch.E. 60, 3-13.

7. ADRIEU, J. and CLAUDEL, B. (1974) Measurement of a Facial Area with a Packed Column by the Sulfite Oxidation Method. Comparison with Wetted Area, Chem. Eng. Sci. 29, 1263-1271.

8. ANGELIDOU, C., PSIMOPOULOS, M. and JAMESON, G.J. (1979) Size Distribution Function of Dispersions, Chem. Eng. Sci. 34, 671-676.

9. AOKI, S., ICHIKI, T. and TAKAHASHI, T. (1962) Tokyo Inst. Tech. Bull. 49, 127-139

10. ARDRON, K.H. and HALL, P.C. (1980) Prediction of Void Fraction in Low Velocity Vertical Steam-Water, A.S.M.E. J.Heat Trans. 102, 3-8.

11. ASTARITA, G. (1967) Mass Transfer with Chemical Reaction. Elsiever, Amsterdam.

12. BAKER, J.L.L. and CHAO, B.T. (1965) An Experimental Investigation of Air Bubble Motion in a Turbulent Water Stream, A.I.Ch.E.J. 11, 268-273.

13. BANKOFF, S.G. (1960) A Variable Density Single Fluid Model for Two Phase Flow with particular reference to Steam-Water Flow, A.S.M.E. J. Heat Trans. 82, 265-272.

14. BARNEA, D. (1983) Personal Communication on Falling Film Flows. Dr. Dvora Barnea, Dept. of Fluid Mechanics and Heat Transfer, Tel Aviv University, Israel.

15. BARNEA, D., SHOHAM, O. and TAITEL, Y. (1982) Flow Pattern Transition for Vertical Downward Two Phase Flow, Chem. Eng. Sci. 37, 741-744.

16. BARNEA, D., SHOHAM, O. and TAITEL, Y. (1982) Flow Pattern Transition for Downward Inclined Two Phase Flow: Horizontal to Vertical, Chem. Eng. Sci. 37, 735-740

17. BARNEA, D., SHOHAM, O., TAITEL, Y. and DUCKLER, A.E. (1980) Flow Pattern Transition for Gas-Liquid Flow in Horizontal and Inclined Lines, Int. J. Multiphase Flow 6, 217-225

18. BAROCZY, C.J. (1966) A Systematic Correlation for

Two-Phase Pressure Drop, A.I.Ch.E. Symp. Series. 62, 232-249.

19. BARRON, C.H. and O'HERN, H.A. (1966) Reaction Kinetics of Sodium Sulphite Oxidation by the Rapid-mixing Method, Chem. Eng. Sci. 21, 397-404.

20. BATCHELOR, G.K. (1977) An Introduction to Fluid Dynamics. Cambridge U. Press. London.

21. BEATTIE, D.R.H. (1972) Two Phase Flow Structure and Mixing Length Theory, Nucl. Eng. and Des. 21, 46-64.

22. BEATTIE, D.R.H. (1973) A Note on the Calculation of Two Phase Pressure Losses, Nucl. Eng. and Des. 25, 395-402.

23. BEHRINGER, H. (1936) The Flow of Liquid-Gas Mixtures in Vertical Tubes, Zeit. Ges. Kalte. Ind. 43, 55-58 (Translation by Dept. of Commerce, Washington D.C.)

24. BHAGA, D. and WEBER, M.E. (1972) Holdup in Vertical Two and Three Phase Flow - I. Theoretical Analysis, Can. J. Chem. Eng. 50, 323-328.

25. BHAGA, D. and WEBER, M.E. (1972) Holdup in Vertical Two and Three Phase Flow - II. Experimental Investigation, Can. J. Chem. Eng. 50, 329-336.

26. BICKERMAN, J.J. (1973) Foams. Springer-Verlag

27. BIRD, R.B., STEWART, W.E. and LIGHTFOOT, E.N. (1960) Transport Phenomena. John Wiley and Sons, New York

28. BORISHANSKY, I.I. and 8 co-authors (1973) Some Problems of Heat Transfer and Hydraulics in Two Phase

Flows, Int. J. Heat Mass Trans. 16, 1073-1085.

29. BORISHANSKIY, V.M. and 5 co-authors (1977) Void Fraction and Pressure Drop in Two Phase Upflow at Atmospheric Pressure, Fluid Mech. - Soviet Research 6, 51-61.

30. BRITISH STANDARDS INSTITUTION (1968) Measurement of Fluid Flow in Pipes, Part 1: Orifice Plates, Nozzles Venturi tubes /BS 1042.

31. BRODKEY, R.S. (1967) The Phenomena of Fluid Motions. Addison Wesly, Mass.

32. BROWN, F.C. and KRANICH, W.L. A Model for the Prediction of Velocity and Void Fraction Profiles in Two Phase Flow, A.I.Ch.E. J. 14, 750-758.

33. BROWN, R.W., GOMEZPLATA, A. and PRICE, J.D. (1969) A Model to Predict Void Fraction in Two Phase Flow, Chem. Eng. Sci. 24, 1483-1489.

34. BUTTERWORTH, D. (1977) Empirical Methods for Pressure Drop. in Butterworth, D., and Hewitt, G.F. "Two Phase Flow and Heat Transfer" Oxford U. Press.

35. BUTTERWORTH, D. (1977) One Dimensional Flow. IBID.

36. CALDERBANK, P.H. (1958) Physical Rate Processes in Industrial Fermentation. Part 1: Interfacial Areas, Trans. I.Ch.E. 36, 443-459.

37. CALDERBANK, P.H., JOHNSON, D.S.L. and LOUDON, J. (1970) Mechanics and Mass Transfer of Single Bubbles in Free Rise through some Newtonian and non-Newtonian liquids, Chem. Eng. Sci. 25, 235-236.

38. CALDERBANK, P.H. and MOO-YOUNG, M.B. (1961) The Continuous Phase Heat and Mass Transfer Properties of Dispersions, Chem. Eng. Sci. 16, 39-54.

39. CARTER, C.O. and HUNTINGTON, R.L. (1961) Cocurrent Two Phase Flow of Air and Water Through and Open Vertical Tube and Through an Annulus, Can. J. Chem. Eng. 39, 248-251.

40. CHEN, B. (1972) Effect of Liquid Flow on Axial Mixing of Liquid in a Bubble Column, Can. J. Chem. Eng. 50, 436-438.

41. CHISOLM, D. (1978) Influence of Pipe Surface Roughness on Friction Pressure Gradient During Two Phase Flow, J. Mech. Eng. Sci. 20, 353-354.

42. CHISOLM, D. and LAIRD, A.K.D. (1958) Two Phase Flow in Rough Tubes, Trans. A.S.M.E. 276-286.

43. CHOE, W.G., WEINBERG, L. and WEISMAN, J. (1978) Observation and Correlation of Flow Pattern Transitions in Horizontal Co-Current Gas-Liquid Flow, in Veziroglu, T.N. and S. Kakac, eds. "Two Phase Transport and Reactor Safety" Hemisphere, Washington.

44. CHUNG, B.T.F. and PANG, Y. (1980) A Model for Mass Transfer in Turbulent Pipe Flow with a First order Chemical Reaction, Proc. Heat Trans. and Fluid Mech Inst. 64-78.

45. CLARK, N.N. (1984) Air Lift Pumps for the Hydraulic Transport of Solids, Powder Advisory Centre, London.

46. CLARK, N.N. and FLEMMER, R.L.C. The Bubble-Slug

Transition in Gas-Liquid Upflow and Downflow, Under review.

47. CLARK, N.N. and FLEMMER, R.L.C. On Vertical Downward Two Phase Flow, Chem. Eng. Sci., In Press.

48. CLARK, N.N. and FLEMMER, R.L.C. (1983) Narrow Bore Deep Shaft Reactors, CHEMSA 9, 63-64

49. CLARK, N.N. and FLEMMER, R.L.C. A Method for Determining Frictional Pressure Losses in Two Phase Vertical Flow, Int. J. Multiphase Flow. In Press

50. CLARK, N.N. and FLEMMER, R.L.C. A Technique for Synchronising Valves and Determining Bubble Rise Velocities in Two Phase Flow, Under review.

51. CLARK, N.N. and FLEMMER, R.L.C. Predicting Holdup in Two Phase Bubble Upflow and Downflow using the Zuber and Findlay Drift-flux model, A.I.Ch.E. J. In Press.

52. CLARK, N.N. and FLEMMER, R.L.C. Two Phase Pressure Loss in terms of Mixing Length Theory - I: Derivation for the General Case of Dispersed Flow. Under review.

53. CLARK,N.N. and FLEMMER, R.L.C. Two Phase Pressure Loss in terms of Mixing Length Theory - II: Comparison of Model with Up and Downflow Data. Under review.

54. CLARK, N.N. and FLEMMER, R.L.C. Aeration in Two Phase Vertical Bubble Flow. Under review.

55. CLARK, N.N. and FLEMMER, R.L.C. Gas-Liquid Contactng in Vertical Two-Phase Flow. Under review

56. CLARK, N.N., FLEMMER, R.L.C. and MELOY, T.P. (1984) Hydraulic Transport of Abrasive Solids: The Air-Lift Pump, Proc. 9th. Annual Powder and Bulk Solids Conf., Rosemont, Illinois.

57. CLARK, N.N. and MELOY, T.P. Design Equation for Air-Lift Pumps Operating in Slug Flow, Under review

58. CLARK, N.N. and MELOY, T.P. (1984) Design of Oil Well Gas-Lift Pumps, Society of Petroleum Engineers paper no. Ø12820

59. CLARK, N.N., MELOY, T.P., and FLEMMER, R.L.C. Predicting the Lift of Air-Lift Pumps in the Bubble Flow Regime, Under review.

60. COLLIER, J.G. and HEWITT, G.F. (1966) Experimental Techniques in Two Phase Flow, Brit. Chem. Eng. 11, 1526-1531.

61. COLLINS, O.C. and ELDER, M.D. (1980) Experience in Operating the Deep Shaft Activited Sludge Process, Wat. Pollut. Control. 79, 272-281.

62. COOPER, C.M., FERNSTRAM, G.A. and MILLER, S.A. (1944) Performance of Agitated Gas-Liquid Contactors, Ind. and Eng. Chem. 36, 504-509.

63. COULSON, J.M. and RICHARDSON, J.F. (1977) Chemical Engineering (vol. 1), Pergamon, Oxford.

64. COX, G.C. and 7 co-authors (1980) Use of the Deep Shaft Process in Uprating and Extending Existing Sewage Treatment Works, Water Pollut. Control 79, 70-86.

65. DANCKWERTS, P.V. (1965) Absorption of Bubbles from Dilute Gas, Chem. Eng. Sci. 20, 785-787.

66. DANCKWERTS, P.V. (1966) The Influence of Insoluble Gases on the Absorption and Desorption rate of freely rising Bubbles of Soluble Gas in Liquids, Chem. Eng. Sci. 21, 614-618.

67. DANCKWERTS, P.V. (1970) Gas-Liquid Reactions. McGraw-Hill, New York.

68. DANCKWERTS, P.V. and RIZVI, S.F. (1971) The Design of Gas Absorbers Part II: Effective Interfacial Areas for Several Types of Packing, Trans. I.Ch.E. 49, 124-127.

69. DAVIS, M.R. (1974) The Determination of Wall Friction for Vertical and Horizontal Two-Phase Bubbly Flows, A.S.M.E. J. Fluids Eng. 96, 173-179.

70. DECKWER, W.D., BURKHART, R. and ZOLL, G. (1974) Mixing and Mass Transfer in Tall Bubble Columns, Chem. Eng. Sci. 29, 2177-2188.

71. DELHAYE, J.M. (1983) Two Phase Pipe Flow, Int. Chem. Eng. 23, 385-410

72. DELHAYE, J.M. and GALAUP, J.P. (1975) Hot Film Anemometry in Air-Water Flow, pp 83-90 in Zakin and Patterson, eds. "Turbulence in Liquids", Science Press

73. DE WAAL, K.J.A. and OKESON, J.C. (1966) The Oxidation of Aqueous Sodium Sulphite Solutions, Chem. Eng. Sci. 21, 559-572.

74. DOCUMENTA GEIGY : Scientific Tables (1962) 6th Edition, J.R. GEIGY S.A., Basle.

75. DREW, D.A. and LAHEY, R.T. JR. (1981) Phase Distribution Mechanisms in Turbulent Two-Phase in Channels of Arbitrary Cross Section, A.S.M.E. J.Fluids Eng. 103, 583-589.

76. DREW, D.A. and LAHEY, R.T. (1981) Phase Distribution Mechanisms in Turbulen Low Quality Two-Phase in a Circular Pipe, J. Fluid Mech. 117, 91-106.

77. DUCKLER, A.E., WICKS, M. and CLEVELAND, R.G. (1964) Frictional Pressure Drop in Two Phase Flow: A Comparison of Existing Correlations for Pressure Drop and Holdup, A.I.Ch.E. J. 10, 38-43.

78. DUCKLER, A.E., WICKS, M. and CLEVELAND, R.G. (1964) Frictional Pressure Drop in Two Phase Flow, A.I.Ch.E. J. 10, 44-51.

79. FAROOQI, S.I. and RICHARDSON, J.F. (1982) Horizontal Flow of Air and Liquid (Newtonian and Non-Newtonian) in a Smooth Pipe: Part II, Trans. I.Ch.E. 60, 323-333.

80. FRANK-KAMENETSKII, D.A. (1955) Diffusion and Heat Exchange in Chemical Kinetics. Princeton U. Press, New Jersey.

81. GALAUP, J.P. (1975) Contribution to the Study of Methods for Measuring Two Phase Flow, Doctoral thesis, Scientific and Medical University of Grenoble. Translation by Nuclear Regulatory Commission, Washington D.C.

82. GALAUP, J.P. and DELHAYE, J.M. (1976) Utilization de Sondes Optiques Miniatures en Encoulement Diphasique Gaz-liquide, La Houille Blanche 1-1976, 17-29

83. GARBARINI, G.R. and TIEN, C. (1969) Mass Transfer From a Single Gas Bubble - A Comparative Study in Experimental Methods, Can. J. Chem. Eng 47, 35-41.

84. GARNER, F.H. and HAMMERTON, D. (1954) Circulation Inside Gas Bubbles, Chem. Eng. Sci. 3, 1-11.

85. GOVIER, G.W. and AZIZ, K. (1972) The Flow of Complex Mixtures in Pipes. Van Nostrand Reinhold, N.Y.

86. GOVIER, G.W., RADFORD, B.A. and DUNN, J.S.C. (1957) The Upward Vertical Flow of Air-Water Mixtures - I: Effect of Air and Water Rates on Flow Pattern, Holdup and Pressure Drop, Can. J. Chem. Eng. 35, 58-70.

87. GOVIER, G.W. and SHORT, W.L. (1958) The Upward Vertical Flow of Air-Water Mixtures - II: Effect of Tubing Diameter on Flow Pattern, Holdup and Pressure Drop, Can. J. Chem. Eng. 36, 195-202.

88. GOVIER, G.W., SULLIVAN, G.A. and WOOD, R.K. (1961) The Upwards Vertical Flow of Oil-Water Mixtures, Can. J. Chem. Eng. 35, 58-70.

89. GRIFFITH, P. and WALLIS, G.B. (1961) Two Phase Slug Flow, A.S.M.E. J. Trans. 83, 307-320.

90. HARMATHY, T.Z. (1960) Velocity of Large Drops and Bubbles in Media of Infinite or Restricted Extent, A.I.Ch.E. J. 6, 281-288.

91. HERRINGE, R.A. and DAVIS, M.R. (1976) Structural Development of Gas-Liquid Mixture Flows, J. Fluid Mech. 73, 97-123.

92. HERRINGE, R.A. and DAVIS, M.R. (1978) Flow Structure and Distribution Effects in Gas-Liquid Mixture Flows, Int. J. Multiphase Flow 4, 461-468.

93. HEUSS, J.M., KING, C.J. and WILKE, C.R. (1965) Gas-Liquid Mass Transfer in Co-current Froth Flow, A.I.Ch.E. J. 11, 866-872.

94. HEWITT, G.F. (1973) Some Recent Results and Development in Gas-Liquid Flow : A Review, Int. J. Multiphase Flow 1, 139-171.

95. HEWITT, G.F. (1977) Flow Patterns, in Butterworth, D. and Hewitt, D.F. "Two Phase Flow and Heat Transfer", Oxford U Press.

96. HEWITT, G.F. (1977) Vertical Bubble and Slug Flow, IBID.

97. HEWITT, G.F. (1978) Measurement of Two Phase Flow Parameters. Academic Press, London.

98. HEWITT, G.F. (1982) Applications of Two Phase Flow, Chem. Eng. Prog. 79, 38-46.

99. HEWITT, G.F. (1983) Personal Communication on Low Velocity Pressure Losses. Dr. G.F. Hewitt, AERE, Harwell, Didcot, Berks., England

100. HEWITT, G.F. and HALL-TAYLOR, N.S. (1970) Annular Two Phase Flow. Pergamon Press, Oxford.

101. HEWITT, G.F. and WALLIS, G.B. (1963) Flooding and Associated Phenomena in Falling Film Flow in a Vertical Tube, A.S.M.E. Symp. Multiphase Flow, Philadelphia Nov. 1963.

102. HIKITA, H., ASAI, S., TANIGAWA, K., SEGAWA, K. and KITAO, M. (1981) The Volumetric Liquid Mass Transfer Coefficient in Bubble Columns, Chem. Eng. J. (Lausanne) 22, 61-69.

103. HILLS, J.H. (1975) The Rise of a Large Bubble Through a Stream of Smaller Ones, Trans. I.Ch.E. 53, 224-233.

104. HILLS, J.H. (1983) Investigation into the Siutability of a Transverse Pitot Tube for Two Phase Flow Measurements, Trans. I.Ch.E. 61, 371-376

105. HILLS, J.H., ABBOTT, C.J. and WESTAN, L.J. (1982) A Sample Apparatus for the Measurement of Mass Transfer from Gas-Bubbles into Liquids, Trans. I.Ch.E. 60, 369,371.

106. HINES, D.A., BAILEY, M., OUSBY, J.C. and ROESLER, F.C. (1975) The ICI Deep Shaft Aeration Process, I.Ch.E. Conference, New York, April 1975.

107. HINZE, J.O. (1975) Turbulence. McGraw Hill, New York.

108. HODOSSY, L. (1968) Momentum, Heat and Mass Transfer in Two Phase Flow, Int. Chem. Eng. 18, 427-438.

109. HORNER, B., ABBENSETH, R. and DIALER, K. (1982) The Prediction of Mass Transfer Coefficient in Absorption from the Measured Turbulence Properties of the Liquid, Int. Chem. Eng. 22, 226-233.

110. HSU, Y.C. and DUDUKOVIC, M.P. (1980) Liquid Recirculation in Gas Lift Reactors, in Veziroglu, T.N., ed. "Multiphase Transport", Hemisphere, Washington

111. HSU, Y. and GRAHAM, R.W. (1976) Transport Processes in Boiling and Two Phase Systems. McGraw Hill, New York;.

112. HUEY, C.T. and BRYANT, R.A.A. (1967) Isothermal Homogenous Two Phase Flow in Horizontal Pipes, A.I.Ch.E.J. 13, 70-77.

113. HUGHMARK, G.A. (1962) Holdup in Gas-Liquid Flow, Chem. Eng. Prog. 58, 62-65.

114. HUGHMARK, G.A. (1963) Pressure Drop in Horizontal and Vertical Co-current Gas-Liquid Flow, Ind. and Eng. Chem. Fund. 2, 315-321.

115. HUGHMARK, G.A. (1967) Holdup and Mass Transfer in Bubble Columns, Ind. and Eng. Chem. Proc. Des. and Dev. 6, 218-220.

116. HUGHMARK, G.A. and PRESSBURG, B.S. (1961) Holdup and Pressure Drop with Gas-Liquid Flow in a Vertical Pipe, A.I.Ch.E. J. 7, 677-682.

117. IIDA, Y. (1980) Prediction Method of Flow Patterns in Gas-Liquid Two Phase Flow, Bull. Soc. Mech. Eng. of Japan. 3, 247-254.

118. ISBIN, H.S., RODRIGUEZ, H.A., LARSON, H.C. and PATTIE, B.D. (1959) Void Fractions in Two Phase Flow, A.I.Ch.E.J. 5, 427-432.

119. ISBIN, H.S., SHER, N.C. and EDDY, K.C. (1957) Void Fractions in Two Phase Steam-Water Flow, A.I.Ch.E.J. 3, 136-142.

120. IRONS, G.A. and CHANG, J.S. (1983) Dispersed Powder Flow through Vertical Pipes, Powder Tech. 34, 233-242

121. ISHII, M. (1975) Thermo-Fluid Dynamic Theory of Two-Phase Flow. Eyrolles.

122. ISHII, M. and GROLMES, M.A. (1978) Constitutive Equation for One Dimensional Drift Velocity of Dispersed Two Phase Flow, in Veziroglu, T.N. and S. Kakac, eds. "Two Phase Transport and Reactor Safety", Hemisphere, Washington.

123. ISHII, M. and ZUBER, N. (1979) Drag Coefficient and Relative Velocity in Bubbly, Droplet or Particulate Flows, A.I.Ch.E.J. 25, 843-855.

124. IWASYK, J.M. (1983) Personal Communication concerning the activities of The Design Institute for Multiphase Processing of the A.I.Ch.E. Dr. John M. Iwasyk, DuPont Co. Engineering Dept, Wilmington, Delaware, USA.

125. JACKSON, R. (1964) The Formation and Coalescence of Drops and Bubbles in Liquids, The Chem. Engr. CE107-CE118

126. JAGOTA, A.K., RHODES, E. and SCOTT, D.S. (1973) Mass Transfer in Upwards Co-current Gas-Liquid Flow, Chem. Eng. J. (Lausanne) 5, 23-31.

127. JEPSEN, J.C. (1970) Mass Transfer in Two Phase Flow in Horizontal Pipelines, A.I.Ch.E. J. 16, 705-711.

128. JOHNSON, H.A. and ABOU-SABE, A.H. (1952) Heat Transfer and Pressure Drop for Turbulent Flow of Air-Water mixtures in a Horizontal pipe, Trans. A.S.M.E. 64, 977-987.

129. KAMPF, F. and PIETSCH, H.B. (1978) Application of the V.A.W. Tube Digester for Metallurgical Pressure Leaching Process. From Jones, M.J., ed. "Complex Metallurgy", (I.M.M. Int. Symp. Bad Harzburg, Sept. 1978) I.M.M. Offices, London.

130. KASTURI, G. and STEPANEK, J.B. (1974) Two Phase Flow - III: Interfacial Area in Cocurrent Gas-Liquid Flow, Chem. Eng. Sci. 29, 713-719.

131. KASTURI, G. and STEPANEK, J.B. (1974) Two Phase Flow - IV Gas and Liquid Side Mass Transfer Coefficients, Chem. Eng. Sci. 29, 1849-1856.

132. KAWAGOE, M., NAKAO, K. and OTAKE, T. (1975) Liquid Phase Mass Transfer Coefficient and Bubble Size in Gas Sparged Contactors, J. Chem. Eng. Japan 8, 254-256.

133. KEITEL, G. and ONKEN, V. (1981) Errors in the Determination of Mass Transfer in Gas-Liquid Dispersions, Chem. Eng. Sci. 36, 1927-1932.

134. KEITEL, G. and ONKEN, V. (1982) Inhibition of Bubble Coalescence by Solutes in Air-Water Dispersions, Chem. Eng. Sci. 37, 1635-1638.

135. KEMP, H.S. (1983) Formation and Management of A.I.Ch.E. Design Institutes, Chem. Eng. Prog. 79, 9-14

136. KOPALINSKY, E.M. and BRYANT, R.A.A. (1976) Friction Coefficients for Bubbly Two Phase Flow in Horizontal Pipes, A.I.Ch.E. J. 22, 82-86.

137. KUBOTA, H., HOSONO, Y. and FUJIE, K. (1978) Characteristic Evaluations of the ICI Air Lift Type Deep Shaft Aerator, J. Chem. Eng. Japan 11, 319-325.

138. KYTOMAA, H. (1983) Personal Communication on low velocity two phase pressure losses. Mr. Harri Kytomaa, California Institute of Technology, Pasadena, Calif., USA

139. LAMB, D.E. and WHITE, J.L. (1962) Use of Momentum and Energy Equations in Two Phase Flow, A.I.Ch.E.J. 8, 281-283.

140. LAMONT, J.C. and SCOTT, D.S. (1966) Mass Transfer From Bubbles in Cocurrent Flow, Can. J. Chem. Eng. 44, 201-208.

141. LEVICH, V.G. (1962) Physical-Chemical Hydrodynamics. Prentice-Hall, N.Y.

142. LEVY, S. (1960) Theoretical Prediction from Momentum Model, A.S.M.E. J. Ht. Trans. 82, 113-124.

143. LEVY, S. (1963) Prediction of Two Phase Pressure Drop and Density Distribution from Mixing Length Theory, A.S.M.E. J. Ht. Trans. 85, 138-152.

144. LEVY, S. and HEALZER, J.M. (1981) Application of Mixing Length Theory to Wary Turbulent Gas-Liquid Interface, A.S.M.E. J. Heat Trans. 103, 492-500.

145. LINEK, V. and VACEK, V. (1981) Chemical Engineering Use of Catalysed Sulphite Oxidation Kinetics for the Determination of Mass Transfer Characteristics of Gas-Liquid Contractors, Chem. Eng. Sci. 36, 1747-1768.

146. LOCKETT, M.J. and KIRKPATRICK, R.D. (1975) Ideal Bubbly Flow and Actual Flow in Bubble Columns, Trans. I.Ch.E. 53, 267-273.

147. LOCKHART, R.W. and MARTINELLI, R.C. (1949) Proposed Correlation of Data for Isothermal Two Phase Two Component flow in Pipes, Chem. Eng. Prog. 45,39-48

148. LORENZI, A. and SOTGIA, G. (1978) Comparative Investigation of some Characteristic Quantities of Two-Phase Cocurrent Upward and Downward Flow. in Veziroglu, T.N. and Kakac, eds. "Two Phase Transport and Reactor Safety", Hemisphere, Washington.

149. MADHANE, J.M., GREGORY, G.A. and AZIZ, K. (1974) A Flow Pattern Map for Gas-Liquid Flow in Horizontal Pipes, Int. J. Multiphase Flow 1, 537-553.

150. MAH, C.C. and GOLDING, J.A. (1971) Effect of Flow Pattern on Gas Phase Controlled Mass Transfer, Can. J. Chem. Eng. 49, 39-48.

151. MANGARTZ, K.H. and PILHOFER, T.H. (1981) Interpretation of Mass Transfer Measurements in Bubble Columns Considering Dispersion of Both Phases, Chem. Eng. Sci. 36, 1069-1077.

152. MARTIN, C.B. (1976) Vertically Downward Two Phase Slug Flow, A.S.M.E. J. Fluids Eng. 98, 715-722.

153. MARTINELLI, R.C., BOELTER, L.M.K., TAYLOR, T.H.M., THOMSEN, E. and MORRIN, E.H. (1944) Isothermal Pressure Drop for Two Phase Two Component Flow in a Horizontal Pipe, Trans. A.S.M.E. 66, 131-151.

154. MARTINELLI, R.C. and NELSON, D.B. (1948) Prediction of Pressure Drop during Forced Circulation Boiling of Water, Trans. A.S.M.E. 70, 695-702.

155. MASSEY, B.S. (1976) Mechanics of Fluids. Van Nostrand Reinhold, Wokingham, England.

156. MATTHEWS, C.T. and ROBINS, R.G. (1972) Oxidation of Aqueous Ferrous Sulphate Solutions by Molecular Oxygen, Proc. Aust. Inst. Min. Met. 242, 47-57.

157. McMANUS, H.N., Jr. (1963) Experimental Methods in Two Phase Flow, A.S.M.E. Symp. Multiphase Flow, Philadelphia, Nov. 1963.

158. MILLER, N and MITCHIE, R.E. (1970) Measurement of Local Voidage in Liquid/Gas Two Phase Flow Systems using a Universal Probe, J. Brit. Nucl. Energy Soc. 9, 94-100.

159. MITCHELL, J. and HANRATTY, T.J. (1966) A study of Turbulence at a Wall using and Electrochemical Wall Shear Stress Meter, J. Fluid Mech. 26, 199-221

160. MOISSIS, R. and GRIFFITH, P. (1962) Entrance Effects in a Two Phase Slug Flow, A.S.M.E. J. Heat Trans. 84, 29-39.

161. NAKORYAKOV, V.E., KASHINSKY, O.N., BURDUKOV, A.P. and ODNORAL, V.P. (1981) Local Characteristics of Upward

Gas-Liquid Flows, Int. J. Multiphase Flow 7, 63-81.

162. NASSOS, G. and BANKOFF, S.G. (1967) Slip Velocity Ratios in an Air-Water system under Steady State and Transient Conditions, Chem. Eng. Sci. 22, 661-668.

163. NGUYEN, van T and SPEDDING, P.L. (1977) Holdup in Two Phase Gas Liquid Flow - I Theoretical Aspects, Chem. Eng. Sci. 32, 1003-1014.

164. NGUYEN, van T and SPEDDING, P.L. (1977) Holdup in Two Phase Gas Liquid Flow - II Experimental Results, Chem. Eng. Sci. 32, 1015-1021.

165. NICKLIN, D.J. (1962) Two Phase Bubble Flow, Chem. Eng. Sci. 17, 693-702.

166. NICKLIN, D.J. (1963) The Air-Lift Pump: Theory and Optimization, Trans. I.Ch.E. 41,29-39

167. NICKLIN, D.J., WILKES, J.O. and DAVIDSON, J.F. (1962) Two Phase Flow in Vertical Tubes, Trans. I.Ch.E. 40, 61-68.

168. NIINO, M., KASHINSKII (Sic), O.N. and ODNORAL, V.P. (1978) Bubble Mode of Flow of a Gas-Liquid mixture in a Vertical Pipe, J. Eng. Phys. 35, 1446-1450.

169. NORDELL, C.H. (1945) Apparatus for Aerating Sewage. U.S. Patent 2,374,772

170. OGAWA, S., SHIMIZU, Y., TONE, S. and OTAKE, T. (1978) Kinetics of the Oxidation of Aqueous Sodium Sulphite Solutions with Air, J. Chem. Eng. Japan 15, 400-402.

171. OHASHI, H., SUGAWARA, T., and KIKUCHI, K. (1981) Mass

Transfer between Particles and Liquid in Solid-Liquid Two Phase Upflow in the Low Velocity Region through Vertical Tubes, J. Chem. Eng. Japan 14, 489-491

172. OHKI, Y. and INOUE, H. (1970) Longitudinal Mixing of the Liquid Phase in Bubble Columns, Chem. Eng. Sci. 25, 1-16.

173. ONDA, K., SADA, E., KOBAYASHI, T., KITO, S. and ITO, K. (1970) Salting-out Parameters of Gas Solubility in Aqueous Salt Solutions, J. Chem. Eng. Japan. 3, 18-24.

174. ORKISZEWSKI, J. (1967) Predicting Two Phase Pressure Drops in Vertical Pipe, J. Petrol. Tech. 19, 829-838.

175. OSHINOWO, T. and CHARLES, M.E. (1974) Vertical Two Phase Flow - I: Flow Pattern, Can. J. Chem. Eng. 52, 25-35.

176. OSHINOWO, T. and CHARLES, M.E. (1974) Vertical Two Phase Flow - II: Holdup and Pressure Drop, Can. J. Chem. Eng. 52, 438-448.

177. PEEBLES, F.N. and GARBER, H.J. (1953) Studies on the Motion of Gas Bubbles in Liquids, Chem. Eng. Prog. 49, 88-97.

178. PETRICK, M. and KURDIKA, A.A. (1966) On the Relationship Between the Phase Distribution and Relative Velocities in Two-Phase Flow, A.I.Ch.E. Proc. 3rd International Heat Trans. Conf. 4, 184-191.

179. PHILLIPS, D.H. and JOHNSON, M.J. (1959) Oxygen Transfer in Agitated Vessels, Ind. and Eng. Chem. 51,

3-88.

180. RADOVICH, N.A. and MOISSIS, R. (1972) The Transition from Two Phase Bubble Flow to Slug Flow, M.I.T. Report 7-767322.

181. REITH, T. (1970) Interfacial Area and Scaling up of Gas-Liquid Contactors, Brit. Chem. Eng. 15, 1559-1563.

182. REITH, T. and BEEK, W.J. (1973) The Oxidation of Aqueous Sodium Sulphite Solutions, Chem. Eng. Sci. 28, 1331-1339.

183. REYNOLDS, A.J. (1974) Turbulent Flows in Engineering. John Wiley and sons, London.

184. RICHARDSON, J.F. and ZAKI, W.N. (1954) Sedimentation and Fluidisation : Part I, Trans I.Ch.E. 32, 35

185. RIPPEL, G.R., EIDT, C.M., Jr, and JORDAN, H.B. Jr. (1966) Two Phase Flow in a Coiled Tube, Ind. and Eng. Chem. Proc. Des. Dev. 5, 32-39.

186. ROBINSON, C.W. and WILKE, C.R. (1974) Simultaneous Measurement of Interfacial Area and Mass Transfer Coefficients for a Well Mixed Gas Dispersion in Aqueous Electrolyte Solutions, A.I.Ch.E. J. 20, 285-294.

187. ROBINSON, R.E., JAMES, G.S., van ZYL, P.C.N., MARSDEN, D.D. and BOSMAN, D.J. (1958) Preliminary Assessment of the Important Economic Factors in the Pressure Leachiang of Low Grade South African Uranium Ores, Int. Conf. Peaceful Uses of Atomic Energy 1955. Proceedings (Published 1958) 318-325.

188. ROS, N.J.C. (1961) Simultaneous Flow of Gas and Liquid as Encountered in Well Tubing, J. Petrol. Technol. 13, 1037-1049.

189. ROSE, S.C. and GRIFFITH, P. (1965) Flow Properties of Bubbly Mixtures, A.S.M.E. A.I.Ch.E. Ht. Trans. Conf., Los Angeles, Calif. Aug. 1965: paper 65-HT-58.

190. ROUMY, R (1969) Structure of Air-Water Two Phase Flow. Study of the Average Void Fraction and Flow Considerations, CEA-R-3982.

191. SATHYAMURTHY, N., DEGALEESAN, T.E., CHANDRASEKARAN, K. and LADDHA, S. (1979) Absorption of Oxygen by Aqueous Sodium Sulphite Solutions, Can. J. Chem. Eng. 157, 145-149.

192. SCHLICHTING, H. (1968) Boundary Layer Theory. McGraw Hill, New York.

193. SCOTT, D.S. and HAYDUK, W. (1966) Gas Absorption in Horizontal Cocurrent Bubble Flow, Can. J. Chem. Eng. 44, 130-136.

194. SERIZAWA, A., KATAOKA, I. and MICHIYOSHI, I. (1975) Turbulence Structure of Air-Water Bubbly Flow - II: Local Properties, Int. J. Multiphase Flow 2, 235-246.

195. SERIZAWA, A. (1983) Personal Communication on turbulence in two phase flows. Prof. A. Serizawa, Institute of Atomic Energy, Kyoto University, Uji, Kyoto, Japan.

196. SERIZAWA, A., KATAOKA, I. and MICHIYOSHI, I. (1975) Turbulence Structure of Air-Water Bubbly Flow - III:

Transport Properties, Int. J. Multiphase Flow 2, 247-259.

197. SHAH, A.K. and SHARMA, M.M. (1975) Mass Transfer in Gas-Liquid Pipeline Contactors, Can. J. Chem. Eng. 53, 572-574.

198. SHERWOOD, T.K. PIGFORD, R.L.and WILKE, C.R. (1975) Mass Transfer. McGraw-Hill Kogakusha, Tokyo.

199. SHILIMKAN, R.V. and STEPANEK, J.B. (1977) Effect of Tube Size on Liquid Side Mass Transfer Rate in Co-Current Gas-Liquid Upward Flow, Chem. Eng. Sci. 32, 1397-1400.

200. SHINNAR, R. and CHURCH, J.M. (1960) Predicting Particle Size in Agitated Dispersions, Ind. and Eng. Chem. 52, 253-256

201. SHULMAN, H.L. and MOLSTAD, M.C. (1950) Gas Bubble Columns for Gas-Liquid Contacting, Ind. and Eng. Chem. 42, 1058-1070.

202. SKELLAND, A.H.P. (1974) Diffusional Mass Transfer. John Wiley, New York.

203. SIEMES, W. (1954) Gasblasen in Flussigkeiten, Chem. Ing. Tech. 26, 614-630 .

204. SINGH, B. (1982) Analysis of Pressure Drop in Vertical Pneumatic Conveying, Powder Tech. 32, 179-190

205. SMITH, S.L. (1969-70) Void Fractions in Two Phases Flow - A Correlation based upon an Equal Velocity Head Model, Proc. Inst. Mech. Engrs. 184, 647-664.

206. SPECCHIA, V., SICARDI, S. and GIUNETTO, A. (1974) Absorption in Packed Towers with Cocurrent Upward Flow, A.I.Ch.E. J. 20, 646-653.

207. SPEDDING, P.L. and CHEN, J.J.J. (1981) A Simplified Method of Determining Flow Pattern Transition of Two Phase Flow in a Horizontal Pipe, Int. J. Multiphase Flow 7, 729-731

208. SPEDDING, P.L. and NGUYEN, Van T. (1980) Regime Maps For Air-Water Two Phase Flow, Chem. Eng. Sci. 35, 779-793.

209. STAUB, F.W. (1980) Steady-State and Transient Gas-Solids Flow Characteristics in Vertical Transport Lines, Powder Tech. 26, 147-159

210. STENNING, A.H. and MARTIN, C.B. (1968) An Analytical and Experimental Study of Air-Lift Pump Performance, A.S.M.E. J.Eng.Power 90,106-110

211. STEPANOFF, A.J. (1965) Pumps and Blowers - Two Phase Flow. John Wiley and sons, New York

212. STREETER, V.L. and WYLIE, E.B. (1975) Fluid Mechanics. McGraw-Hill, New York

213. STUHMILLER, J.H., FERGUSON, R.E. and AGEE, L.J. (1979) The Statistical Characteristics of the Bubble-Slug Flow Regime Transition, A.S.M.E. Heat Trans. Div. Meeting 1979, 1-6.

214. SUBRAMANIAN, G. and TIEN, C. (1975) Induced Liquid Phase Mixing Due to Bubble Motion at Low Gas Velocity, Can. J. Chem. Eng. 53, 611-620.

215. SURGENOR, B. and BANNERJEE, S. (1981) Wall Shear Stress and Mass Transfer in Vertical Two Phase Flow, Can. J. Chem. Eng. 59, 223-229.

216. TAITEL, Y. (1977) Flow Pattern Transition in Rough Pipes, Int. J. Multiphase Flow. 3, 597-601.

217. TAITEL, Y., BARNEA, D. (Misspelled as Bornea) and DUCKLER, A.E. (1980) Modelling Flow Pattern Transitions for Steady Upward Gas-Liquid Flow in Vertical Tubes, A.I.Ch.E. J. 26, 345-354.

218. TAITEL, Y. and DUCKLER, A.E. (1976) A Model for Predicting Flow Regime Transitions in Horizontal and Near-Horizontal Gas-Liquid Flows, A.I.Ch.E. J. 22, 47-55.

219. TOMIDA, T., YOSHIDA, M. and OKAZAKI, T. (1976) Liquid Side Volumetric Mass Transfer Coefficient in Upward Two Phase Flow of Air-Liquid Mixtures, J. Chem. Eng. Japan 9, 464-468.

220. VALLASCAS, R. (1979) Two Phase Vertical Flow of Air/Water Mixtures: Temperature Influence on Boundary Lines Between Flow Regimes, Proc. Inst. Mech. Engrs. 193, 337-340.

221. VALUKINA, N.V., KOZ'MENKO, B.K. and KASHINSKII, O.N. (1979) Characteristics of Flow of a Monodisperse Gas-Liquid Mixture in a Vertical Tube, J. Eng. Phys. 36, 462-465.

222. VAN DEEMTER, J.J. and VAN DER LAAN, E.T. (1961) Momentum and Energy Balances for Dispersed Two Phase Flow, Appl. Sci. Res. Section A 10, 102-108.

223. VAN SHAW, P., REISS, L.P. and HANRATTY, T.J. (1963) Rates of Turbulent Transfer to a Pipe Wall in the Mass Transfer Entry Region, A.I.Ch.E. J. 9, 362-364.

224. VOGEL, A.I. (1962) A Text Book of Quantitative Inorganic Analysis. John Wiley and sons, New York

225. VOHR, J. (1962) The Energy Equation for Two Phase Flow, A.I.Ch.E. J. 8, 280-281.

226. WALES, C.E. (1966) Physical and Chemical Absorption in Two Phase Annular and Dispersed Horizontal Flow, A.I.Ch.E. J. 12, 1166-1171.

227. WALLIS, G.B. (1969) One Dimensional Two Phase Flow. McGraw-Hill, New York.

228. WALLIS, G.B. (1982) Review - Theoretical Models of Gas-Liquid Flows, A.S.M.E. J. Fluids Eng. 104, 279-283.

229. WANG, T.S. and CHEN, C.K. (198Ø) Study on the Performances of Air-Lift Pump, in T.N. Veziroglu, ed. "Mltiphase Transport", Hemisphere, Washington.

23Ø. WATSON, A.P., CORMACK, D.E. and CHARLES, M.E. (1979) A Preliminary Study of Interfacial Areas in Vertical Co-Current Two Phase Flow, Can. J. Chem. Eng. 57, 16-23.

231. WEISMAN, J and CHOE, W.G. (1978) Methods for Calculation of Pressure Drop in Co-Current Gas-Liquid Flow, in Veziroglu, T.N., and Kakac, eds., "Two Phase Transport and Reactor Safety" Hemisphere, Washington.

232. WEISMAN, J., DUNCAN, D., GIBSON, J. and CRAWFORD, T. (1979) Effects of Fluid Properties and Pipe Diameter on Two-Phase Flow Patterns in Horizontal Lines, Int. J. Multiphase Flow, 5, 437-462.

233. WEISMAN, J. and KANG, S.Y. (1981) Flow Pattern Transitions in Vertical and Upwardly Inclined Lines, Int. J. Multiphase Flow. 7, 271-291.

234. WESTERTERP, K.R., VAN DIERENDONCK, L.L. and DE KRAA, J.A. (1963) Interfacial Areas in Agitated Gas-Liquid Contactors, Chem. Eng. Sci. 18, 157-176.

235. WHITE, D.A. and DE VILLIERS, J.V. (1977) Rates of Induced Aeration in Agitated Vessels, Chem. Eng. J. (Lausanne) 14, 113-118.

236. WHITE, E.T. and BEARDMORE, R.H. (1962) The Velocity of Rise of Single Cylindrical Air Bubbles Through Liquids Contained in Vertical Tubes, Chem. Eng. Sci. 17, 351-361.

237. YAGI, S. and INOUE, H. (1962) The Absorption of Oxygen into Sodium Sulphite Solution, Chem. Eng. Sci. 17, 411-421.

238. YAMAZAKI, Y and SHIBA, M. (1969) Comparative Study on the Pressure Drop of Air-Water and Steam-Water Flows, Int. Symp. Co-Current Gas-Liquid Flow, Waterloo, Ontario, Sept. 1968.

239. YAMAZAKI, Y and SIMIZU, M. (1978) Hydrodynamic and Hydraulic Studies on Void Fractions in Two Phase Flow, J. Nucl. Sci. and Tech. 15, 886-898.

240. YAMAZAKI, Y. and YAMAGUCHI, K. (1976) Void Fraction

Correlation for Boiling and Non-Boiling Vertical Two Phase Flows in Tubes, J. Nucl. Sci. and Tech. 13, 701-707.

241. YAMAZAKI, Y. and YAMAGUCHI, K. (1979) Characteristics of Cocurrent Two Phase Downflow in Tubes, J. Nucl. Sci. and Tech. 16, 245-255.

242. ZIVI, S.M. (1964) Estimation of Steady State Void Fraction by Means of the Principle of Minimum Entropy, A.S.M.E. J. Ht. Trans. 86, 247-252.

243. ZUBER, N. and FINDLAY, J.A. (1964) The Effects of Non-Uniform Flow and Concentration Distributions and the Effect of the Local Relative Velocity on the Average Volumetric Concentration in Two Phase Flow. General Electric Report. GEAP 4592, April 1964.

244. ZUBER, N. and FINDLAY, J.A. (1965) Average Volumetric Concentration in Two Phase Flow Systems, A.S.M.E. J. Ht. Trans. 87, 453-468.

245. ZUBER, N., STAUB, F.W., BIJWAARD, G. and KROEGER, P.G. (1967) Steady State and Transient Void Fraction in Two Phase Flow Systems. General Electric Co. Report GEAP-5417.

APPENDIX A

DESCRIPTION OF 50 mm BORE APPARATUS

Refer to figure A.1

A tank, h, of 500 litre capacity, fed a Warman C32 pump driven by a 10kW motor geared so that the pump delivered a maximum of 450 litres/minute to the flow loop. The flow passed from the pump through a rotameter, a, which had been previously calibrated with a stopwatch and a vessel of known volume. Liquid passed down a 15 m length of 50 mm nominal bore galvanised waterpipe, termed the downcomer. True pipe internal diameter was 52mm. The pipe was flanged at intervals so that a glass observation section, d, could be fitted into the apparatus at various heights. Air was introduced into the liquid phase approximately 1.5 m down the downcomer, through a sparger, c. The sparger used in the holdup and pressure loss work consisted of two identical 0.45 m lengths of 6 mm copper tubing, perforated with 0.5 mm holes, and situated axially, one above the other on the pipe centre-line. This sparger was replaced with a similar sparger of stainless steel construction for the mass transfer work, since copper could affect the liquid side reaction. Various other spargers, described in detail in chapter 2, were employed in the flow regime study.

A 5 m section of the downcomer could be isolated with two

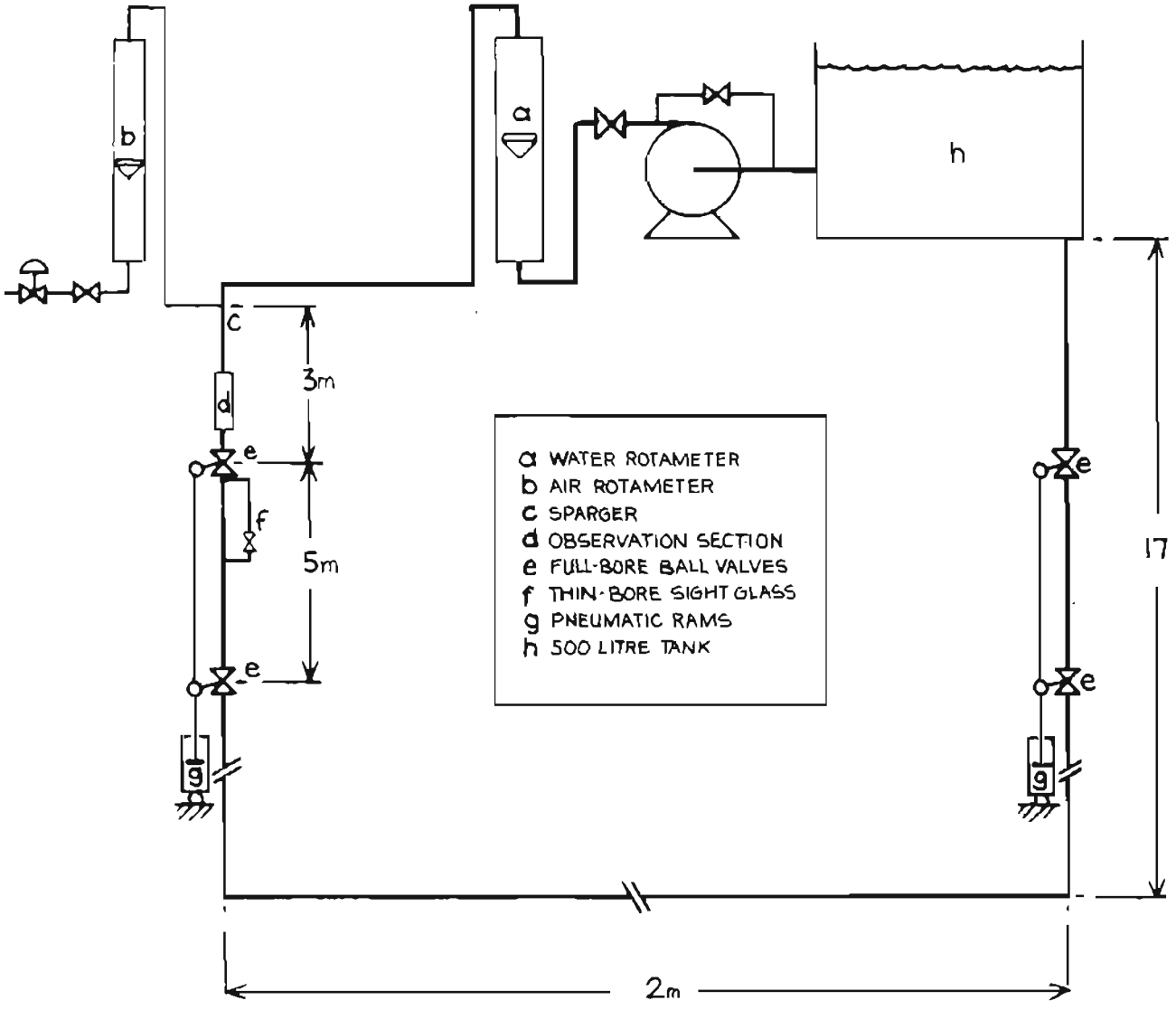

Fig A1 • 50mm apparatus •

full bore ball valves, e, which were linked and synchronised with a tie-rod of adjustable length. The valves were closed rapidly using an air ram, g. A small bore sight glass was attached to the 50 mm pipe between the valves to determine the relative quantities of gas and liquid in the isolated section.

The downcomer fed a 1.5 m horizontal section at the base of the loop. This was in turn connected to the riser, which returned fluid to the header tank. The quick-closing valves and glass section were moved from the downcomer to the riser for upflow studies.

The whole loop was drilled at 1 m intervals to take pressure tappings. These were fitted with either pressure gauges, or to 6 mm water-purged lines, which connected to pressure transducers. The transducer signals were monitored by a computer. Transducers were calibrated with water manometers.

The header tank, h, was fitted initially with copper cooling coils connected to a 3kW refridgeration plant, to sink the heat generated by frictional losses in the loop. Later, for mass transfer work, these coils were re-made with stainless steel tube. Further modifications to the header tank for mass transfer work are described in section 4.7.

APPENDIX B

DESCRIPTION OF 100 mm BORE APPARATUS

Refer to figure B.1

This apparatus was used for holdup studies, and to a lesser degree, for flow regime study.

A tank, capacity 300 litres, fed a Warman C32 pump, b, driven at 2000 r.p.m. by a 15 kW motor, to deliver up to 1000 litres/min. The liquid flow was monitored by a brass sharp-edged orifice, n, fitted to British Standard [30] specification in a 75 mm line attached to the pump discharge. Pressure drop across the orifice was monitored using a glycerine-filled 150 kPa gauge, with a dead volume to limit fluctuations. For some downflow runs, a similar orifice was used in position m.

The flow passed through valvegear, d, which could be set to cause either upflow or downflow in the vertical test section. These valves, together with a pump bypass valve, p, were used to control the flowrate.

The 75 mm line was stepped up to 100 mm line at points f in the horizontal sections. Air was fed through a rotameter, h, to one of the two spargers, q, according to whether the test section was used in upflow or downflow configuration. The spargers consisted each of four 0.5 m

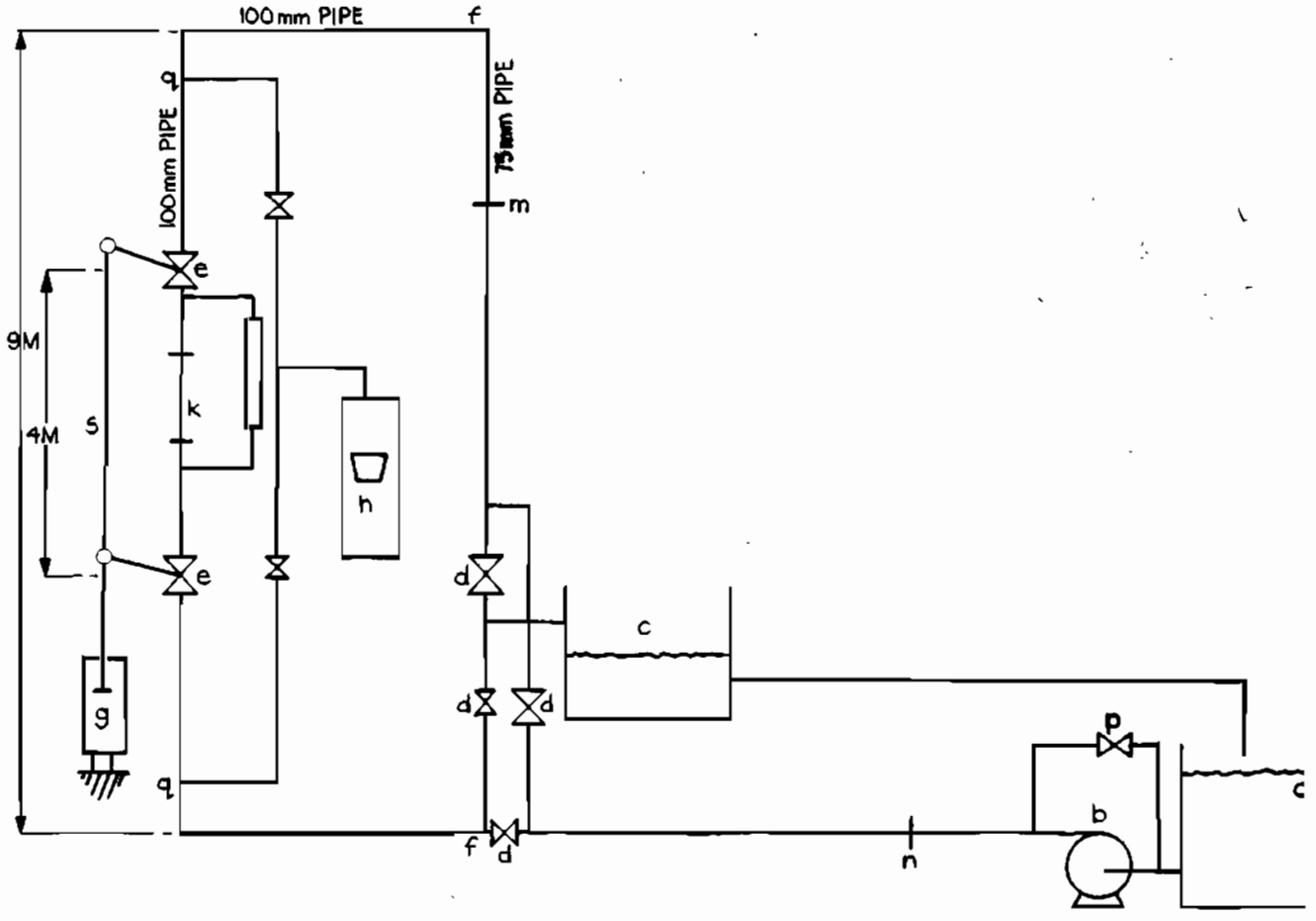

Fig B·1· 100mm apparatus ·

long tubes of 6 mm copper pipe, drilled with 1 mm holes. These were linked to a common air source, and situated in parallel in the pipe, each approximately 2.5 cm from the pipe centre line, and arranged so that they were positioned at the corners of a square in pipe cross-section.

Holdup work was conducted by isolating a 4 m section of the vertical 100 mm pipe with two full bore ball valves, e. These were synchronised with a tie-rod of adjustable length and closed by a high-pressure air ram. A sight glass of small bore, r, permitted observation of the liquid level in the test section after it had been isolated. During runs when visual observation was required, a 0,7 m glass pipe section was fitted into the test length.

The flow returned from the test section, via the valvegear, to an air disengagement tank, c, and was finally returned to tank a.

APPENDIX C

THEORETICAL EXAMINATION OF PRESSURE PROFILES WITH RESPECT TO HEIGHT AND TIME IN HOLDUP APPARATUS

1. INTRODUCTION

The holdup apparatus consists of a length of the deep shaft reactor which may be isolated by means of pneumatically operated ball valves. This action is carried out while an air-water mixture is flowing in the system in order to determine the average void fraction of the two phases in the test section.

It is necessary that the ball valves are closed both rapidly and simultaneously, so that the flow trapped in the isolated section is a true representation of the flow immediately prior to closure. A method for synchronizing the valves using a pressure balance technique, presented in appendix D, requires the analysis of pressure change presented below.

One may examine (as an approximation to this holdup apparatus) the case of an air-water column in an isolated chamber, which is subject to separation of the phases with respect to time. Pressure changes with respect to time are important in the synchronisation of the two ball valves, and critical in the interpretation of the voidage data.

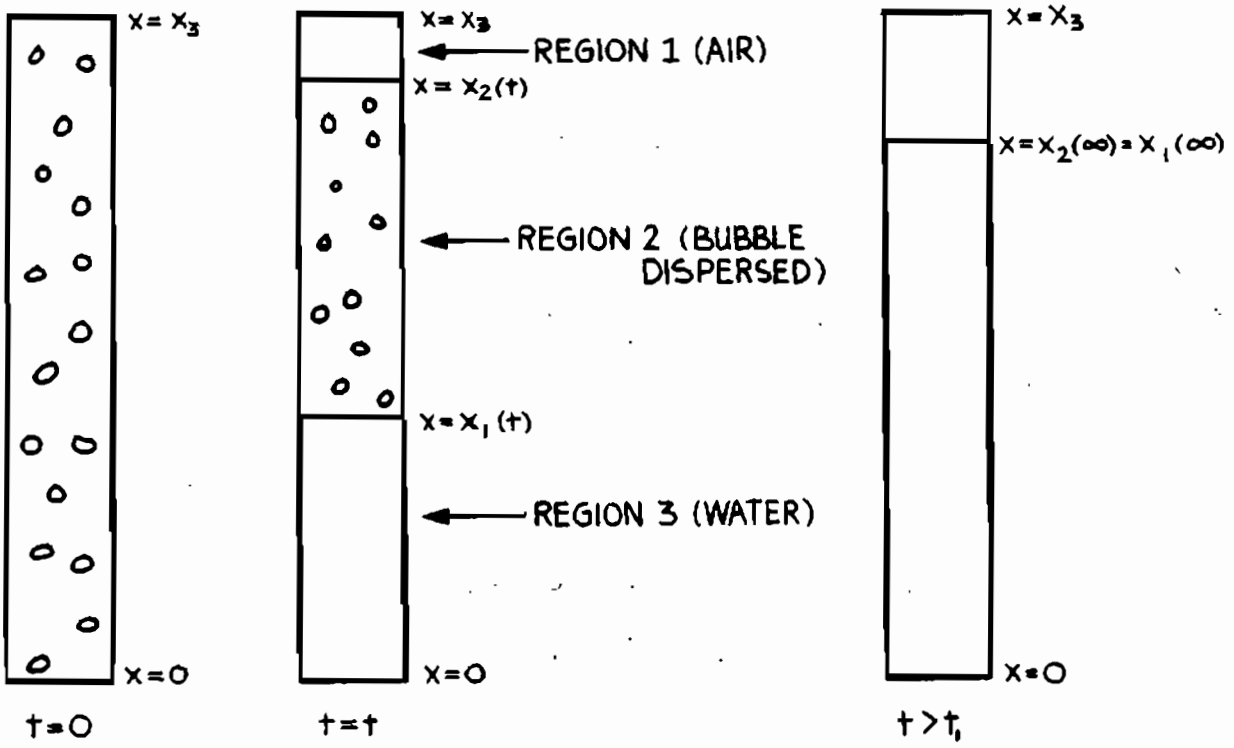

Fig C·1 • Nomenclature for appendices C and D •

Figure C.1 provides the nomenclature for this theoretical study.

2. NECESSARY ASSUMPTIONS

2.1 The friction head loss is constant over a short column length.

Prior to isolation of the holdup section, frictional losses will have some contribution to the axial pressure and voidage gradients over the test section length. The frictional loss is firstly not of great magnitude in comparison with the hydrostatic head, and secondly, at the low gas voidages treated in this study, is influenced little by the changing voidage along the section. One may accordingly assume that the pressure loss per unit length of pipe due to friction is constant over the short length involved.

2.2 The holdup ratio is constant over the column length.

Zuber and Findlay [243] (see chapter 3) show that

$$\overline{W}_g/\overline{E} = C_o(\overline{W_g + W_l}) + \overline{U}_{gm} \qquad C.1$$

where $\overline{U}_{gm}$ is a drift velocity, C_o is the profile constant, and $\overline{W}_g$, $\overline{W}_l$ are the superficial velocities of the gas and water phase respectively.

From equation C.1,

$$\overline{E} = \overline{W}_g/\{C_o(\overline{W_g+W_l})+\overline{U}_{gm}\} \qquad C.2$$

Now, for an ideal gas phase,

$$\overline{W}_g = W_{go}P_o/P \qquad C.3$$

where W_{go} is the "free" volumetric air flux, evaluated at atmospheric pressure, P_o. Hence, from equations C.2 and C.3,

$$\overline{E} = \{W_{go}P_o/P\}/\{C_o(\overline{W}_l + (W_{go}P_o/P)) + \overline{U}_{gm})\} \qquad C.4$$

For the bubble flow regime, $\overline{W}_g$ is generally an order of magnitude maller than $\overline{W}_l$. Noting also that the pressure, P, in the test section will not vary greatly over the short test length, we may assume the gas flux in the denominator to be constant, and set

$$E_o = W_{go}/\{C_o(\overline{W}_l + W_g') + \overline{U}_{gm}\} \qquad C.5$$

where $W_g' = W_{go}P_o/P_m$, and P_m is a mean pressure in the test section.

From equations C.4 and C.5,

$$\overline{E} = E_oP_o/P \qquad C.6$$

so that $\bar{E}$ is the voidage in the test section where the pressure in the test section is P. Equation C.6 implies a constant holdup ratio over the length of the test section.

3.3 Surface tension effects are negligible.

The excess pressure in a bubble due to surface tension is given by

P_e = 2(Surface Tension)/bubble radius

which implies, for an air-water system, with the surface tension of $7.3*10^{-2}$ Pam,

P_e = 146.0/bubble radius (mm) Pa C.7

which is a negligible pressure, since the average bubble diameter in the apparatus approached 3 mm.

4. PRESSURE GRADIENTS

The irreversible (frictional) axial pressure gradient is given by

$-dP = Ddx$ C.8

where D is the pressure loss per unit pipe length.

The hydrostatic head is given by

$$-dP = \rho_l g(1-\bar{E})dx \qquad C.9$$

where p is the liquid density, and the contribution by the air is neglected. Excluding acceleration effects, which are small, the total gradient is

$$-dP = (\rho_l g(1-\bar{E}) + D)dx = (\rho_l g(1-E_o P_o/P)+D)dx \qquad C.10$$

A solution for the above equation is found in terms of a Taylor expansion. The first three derivatives of P with respect to x are given by

$$dP/dx = A + B/P$$

$$d^2P/dx^2 = -BA/P^2 - B/P^3$$

$$d^3P/dx^3 = 2BA^2/P^3 + 5AB^2/P^4 + 3B^3/P^5$$

for $A = -(\rho_l g+D)$, and $B = \rho_l g E_o P_o$

The Taylor series is observed to be alternating with terms in 1/P as high as $1/P^{(2n+1)}$ for the nth. derivative.

An approximation may be made by truncating at the third term. Expanding about the point x_o,

$$P(x) = P(x_o) + \{A + B/P(x_o)\}(x-x_o)$$

$$- \{BA/P^2(x_o) + B^2/P^3(x_o)\}(x-x_o)^2/2 \qquad C.12$$

Applying this to the column at time t=Ø, and expanding about the point x=Ø, at the base of the column,

$$P(x,Ø) = P(Ø,Ø) + \{A + B/P(Ø,Ø)\}x$$
$$- \{BA/P^2(Ø,Ø) + B^2/P^3(Ø,Ø)\}(x^2/2) \qquad C.13$$

When the flow is stopped, frictional losses no longer play a part in the profile, and equations C.12 and C.13 hold with $A = -\rho_l g$, $B = \rho_l g P_o E_o$.

5. VOID FRACTION GRADIENTS

From equation C.6

$$dP = -\{E_o P_o/\bar{E}^2\}d\bar{E}$$

Thus equation C.1Ø may be written

$$dE = \{(\rho_l g+D)\bar{E}^2/E_o P_o - p_l g\bar{E}^3/E_o P_o\}dx \qquad C.14$$

$$\text{setting } dE = (C\bar{E}^2 + F\bar{E}^3)dx \qquad C.15$$

an analogous expansion to that of P in x is found.

Truncating after three terms, this expansion is written,

$$\bar{E}(x,\emptyset) = \bar{E}(\emptyset,\emptyset) + [C\bar{E}^2(\emptyset,\emptyset) + F\bar{E}^3(\emptyset,\emptyset)]x$$

$$+ \{2C^2\bar{E}^2(\emptyset,\emptyset) + 5CF\bar{E}^4(\emptyset,\emptyset) + 3F^2\bar{E}^5(\emptyset,\emptyset)\}(x^2/2) \qquad C.16$$

For the case where flow is stopped, equation C.16 holds, with $C = \rho_l g/E_o P_o$, $D = -\rho_l g/E_o P_o$.

The analysis given above demonstrates that both pressure and voidage profiles may be represented as polynomials in axial pipe length, x. The error incurred in truncating after the third term may be examined. An alternating, converging, series should have a truncation error smaller than the next term. Consider the fourth term in the pressure expansion.

$$(x^3/6)[2BA^2/P^3(\emptyset,\emptyset) + 5AB^2/P^4(\emptyset,\emptyset) + 3B^3/P^5(\emptyset,\emptyset)]$$

The "worst case" for bubble flow might be,
$P(\emptyset,\emptyset) = 100kPa$; $E_o = \emptyset.2$; $D = 2kPa/m$.

in which case the fourth term has a magnitude of $6.8x^3$ Pa. This implies that the error increases approximately as the cube of the distance from the point about which the expansion is developed. Thus the error incurred over 4 meters would be less than 1% of the total pressure gradient in the pipe. Considering the nature of the

alternating series, the actual error will be less than this predicted quantity.

Calculation has shown that the error in the case of the voidage expansion is of similar proportion.

5. ANALYSIS OF THE SYSTEM AFTER PHASE SEPARATION

The object is to predict the value of the final pressure, $P(x_3,t_1)$ in the ullage formed at the top of the column by the disengaged gas. The height of the gas-liquid interface, $x_1(t_1)$, is also of interest.

Let A be the cross-sectional area of the column. The volume of liquid present in the closed column must remain constant, taking the liquid as incompressible. Thus the gas volume may also not vary. Let the gas volume be V_g. Equating gas volumes before phase separation ($t=\emptyset^-$) and after complete separation ($t=t_1$), yields the relationship

$$V_g = Ax_1(t_1) = \int_{x=\emptyset}^{x=x_3} E(x,\emptyset^-)\, dx \qquad C.17$$

from which $x_1(t_1)$ may be found.

The mass of air in the column is also constant, so that the pressure-volume product for the gas phase must be constant over the disengagement, assuming an ideal gas, and assuming that no mass transfer takes place between the

phases.

$$V_g P(x_3,t_1) = A\int_{x=\emptyset}^{x=x_3} P(x,\emptyset^-)E(x,\emptyset^-)\,dx \qquad C.18$$

$$= A\int_{x=\emptyset}^{x=x_3}\{P(x,\emptyset^-)E_oP_o/P(x,\emptyset^-)\}dx$$

$$= AP_oE_o(x_3-x_o)$$

Therefore

$$P(x_3,t_1) = P_oE_o(V_t/V_g) \qquad C.19$$

where V_t is the total volume of the column. Substituting into equation C.17,

$$P(x_3,t_1) = \frac{P_oE_oV_t}{A\int_{x=\emptyset}^{x_3} E(x,\emptyset^-)dx}$$

so that

$$x_3/P(x_3,t_1) = \int_{x=\emptyset}^{x_3}\{1/P(x,\emptyset^-)\}dx \qquad C.20$$

So that the final ullage pressure is determined by an harmonic integral mean of the pressure prior to valve closure.

The final pressure at the base of the column is given

simply by the sum of the final ullage pressure, and the hydrostatic head of the liquid in the column.

$$P(\emptyset,t_1) = P(x_3,t_1) + \rho_l g(V_t-V_g)/A \qquad C.21$$

No analytic solution for the description of the ullage pressure from time $t=\emptyset$ to time $t=t_1$ has been found, although two simultaneous equations, one an integral equation, are available for numerical solution. The rise in ullage pressure after valve closure has been determined experimentally in this thesis (see section 3.2.3 and figure 3.4).

The relation between final ullage pressure, and ullage pressure prior to valve closure, is necessary for the development of a valve synchronization technique presented in appendix D.

APPENDIX D

PREDICTION OF FINAL ULLAGE PRESSURE FROM PRESSURES DURING FLOW

Pressure, voidage, and height nomenclature developed in appendix C is retained.

To obtain representative holdup data by isolating a two phase flow between quick-closing valves, the valves must be accurately synchronised. A method is presented below for synchronosing the valves by equating the final ullage pressure in the isolated section, to a function of the pressure monitored at three tappings in the test section prior to valve closure.

It was demonstrated in appendix C that a a sufficiently accurate solution to the pressure gradient, equation C.1Ø, was obtained by using a Taylor expansion truncated after the third term, as given by equation C.13. A similar solution exists to describe the inverse of the pressure gradient, as a solution to equation C.1Ø. The Taylor series is expanded about the point $x = Ø$ at the base of the test section.

$$1/P(x,\emptyset^-) = 1/P(\emptyset,\emptyset^-)$$

$$+ [\{(\rho_1 g+D)/P^2(\emptyset,\emptyset^-)\} - \{\rho_1 g E_o P_o/P^3(\emptyset,\emptyset^-)\}]x$$

$$+ \frac{2(\rho_1 g+D)^2}{P^3(\emptyset,\emptyset^-)} - \frac{5\rho_1 g E_o P_o(\rho_1 g+D)}{P^4(\emptyset,\emptyset^-)} + \frac{3\rho_1^2 g^2 P_o E_o}{P^5(\emptyset,\emptyset^-)} \quad x^2/2$$

D.1

The fourth term typically has a value less than Ø.Ø1% of the value of $1/P(x,\emptyset^-)$, so that the truncation is well justified.

Equation D.1 may be re-written as

$$1/P(x,\emptyset^-) = B + Cx + Fx^2 \qquad \text{D.2}$$

with B,C and F constants for a particular flow. The arguments leading up to equation 3.23 in the text, and equation C.2Ø in appendix C, have demonstrated that the final ullage pressure after phase separation in the isolated section is given by a harmonic integral average of the pressure in the test section prior to valve closure

$$x_3/P(x_3,t_1) = \int_{x=\emptyset}^{x_3} \{1/P(x,\emptyset)\}dx \qquad \text{C.2Ø}$$

with x_3 the length of the test section.

An approximate solution to C.2Ø exists by substituting the polynomial relationship, equation D.2, into the integral

on the right hand side of equation C.2Ø. In practice, it is possible to find suitable values for the constants B,C, and F by monitoring the pressure at three pressure tappings in the test section. Designating these tappings with heights x_a, x_b and x_c above the base of the test section, one may obtain the corresponding values of $1/P(x_a,Ø^-)$, $1/P(x_b,Ø^-)$ and $1/P(x_c,Ø^-)$ at the three tappings. Substitution of these three data points into equation D.2 permits simultaneous solution for values of B, C and F. From equations C.2Ø, D.2, and the matrix solution for B, C, and F, the following relationship arises.

$$1/P(x_3,t_1) = G/P(x_a,Ø^-) + H/P(x_b,Ø^-) + I/P(x_c,Ø^-) \qquad D.3$$

where G, H and I are constants depending only on the values of x_3, x_a, x_b and x_c. From a single calculation, the constants G, H and I are evaluated, so that the final ullage pressure, $P(x^3,t_1)$, may be predicted by monitoring only three pressures during flow, and employing equation D.3. Equation D.3 is naturally true only when the valves are correctly synchronised, so that a test for synchronisation involves predicting the final ullage pressure using equation D.3, and comparing this value to the measured value of the final ullage pressure after the phases have completely separated in the isolated section. The tie-rod, which links the two valves, is adjusted in length until the predicted and measured values agree, at

which time the valves are synchronised.

This method of synchronisation is best illustrated by a numerical example due to Clark and Flemmer [50].

Consider the three pressure tappings to be situated in a test section, length x_3, and let $x_a=0$, $x_b = x_3/2$, and $x_c = x_3$. $P(x_a,0^-)$ is the pressure at the height x_a, prior to valve closure ($t=0^-$), and the pressures at the other two tappings are similarly defined.

The simultaneous equations arising from equation D.2 are

$$1/P(x_a,0^-) = B + C \times 0.0 + F \times (0.0)^2$$

$$1/P(x_b,0^-) = B + Cx_3/2 + F(x_3)^2/4$$

$$1/P(x_c,0^-) = B + Cx_3 + Fx_3^2$$

These may be solved to yield

$$B = 1/P(x_a,0^-)$$

$$Cx_3 = -1/P(x_c,0^-) -3/P(x_a,0^-) +4/P(x_b,0^-)$$

$$Fx_3^2/2 = 1/P(x_c,0^-) + 1/P(x_a,0^-) -2/P(x_b,0^-)$$

Substituting into equation D.3 gives the relationship

$$1/P(x_3,t_1) = (1/6)[1/P(x_a,\bar{\emptyset})] + (4/6)[P(x_b,\bar{\emptyset})]$$

$$+ (1/6)[1/P(x_c,\bar{\emptyset})]$$

The symmetry of the solution is due to the symmetry of the pressure tappings on the test length. The solution demonstrates that, within the accuracy of the polynomial approximation, $P(x_3,t_1)$ depends only on the pressures at the three stations, so that only one calculation of the type given above is required for an apparatus with fixed configuration.

APPENDIX E

DISCUSSION OF THE PROFILE CONSTANT WITH SPECIFIC REFERENCE TO THE WORK OF PETRICK AND KURDIKA

Zuber and Findlay [243,244] in their analysis of holdup have chosen to use void and velocity distributions of the form

$$E/E_c = 1 - (r/R)^{1/n} \qquad E.1$$

and

$$W_m/W_{mc} = 1 - (r/R)^{1/m} \qquad E.2$$

With R the pipe radius, r the radial distance from the pipe centre, and the subscript c denoting the condition at the pipe centre. These equations imply that the profile constant,

$$C_o = (EW_m)/(E)(W_m) \qquad E.3$$

is given by

$$C_o = 1 + 2mn/(m+n+2mn) \qquad E.4$$

In equations E.1 and E.2, high values of m and n imply a high value of C_o, whereas low values of m and n represent

flat void and velocity profiles, where the value of C_o is low.

Bankoff [13] used different power law relationships to describe the void fraction and velocity distributions:

$$E = E_c(y/R)^{1/p} \qquad E.5$$

and

$$W_m = W_{mc}(y/R)^{1/q} \qquad E.6$$

with $y = R-r$.

Using profiles given in E.5 and E.6, C_o would be given by

$$C_o = (p+1)(p+2)(q+1)(q+2)/2(p+q+1)(p+q+2) \qquad E.7$$

In Bankoff's analysis, high values of p and q imply flat distributions, so that C_o is close to one in value, whereas low values of p and q correspond to distributions with maxima at the pipe centre, so that the value of c_o will be high.

Thus the power law relationships of Bankof [13] and Zuber and Findlay [243] are quite distinct, and values for the power law exponents may not simply be exchanged between the two systems.

Petrick and Kurdika [178] performed measurements of void profiles, and concluded that, for fully developed flow, the exponent p in equation E.5 varied with voidage and superficial velocity according to the relationship

$$1/p = \emptyset.\emptyset 1\emptyset 9(\overline{W}_1)^{\emptyset.67}\overline{E}^{-1} \qquad \text{E.8}$$

This implies that p increases with increasing voidage, so that the void fraction distribution will become flatter with increasing voidage, and the value of C_o will drop with increasing voidage. This conclusion is in contrast to the upward flow results of this thesis, and the trends which may be inferred from the work of Serizawa [194], Galaup [81], Galaup and Delhaye [82], and Drew and Lahey [76]. However, Petrick and Kurdika [178] have used the variable "n" interchangably in their paper to represent the variables p and n, as well as the inverse of p, as used in this thesis. Such loose definition of terms may have caused confusion in the interpretation of equation E.8.

Petrick and Kurdika [178] have also presented void profile plots for developing flows, which demonstrate the characteristic high bubble concentration at the pipe wall for flows with a low average void fraction. If this is so, equation E.8 suggests that this trend is reversed once the flows are fully developed, since equation E.8 states

that fully developed flows with a low void fraction will have the gas concentrated more at the pipe centre than will flows of higher quality. Further investigation of local two phase flow properties will be required to resolve this issue.

APPENDIX F

KINETICS OF THE OXIDATION OF AQUEOUS SODIUM SULPHITE AND PROBLEMS ENCOUNTERED IN USE OF THE REACTION

1. SUMMARY OF LITERATURE

Use of the oxygen-sulphite method for measuring mass transfer performance has been the subject of two detailed reviews [67,145], and the kinetics of the reaction have been the subject of several papers [73,170,182,191,237]. A synthesis of this work, insofar as it is applicable to determining mass transfer coefficients in the D.S.R., is given below.

The reaction is usually studied using the sodium salt, in which case the balanced reaction equation is

$$2\ Na_2SO_3 + O_2 \Rightarrow 2\ Na_2SO_4$$

A pure sulphite solution will oxidise slowly if exposed to the atmosphere, but the reaction is catalysed by some metal ions of variable valency, notably copper and cobalt. Iron and manganese may also form complexes which enhance the reaction rate. However, some oxidation states of these metals can also retard the reaction, for example the Cuprous ion (Cu^{+}), Stannous ion (Sn^{++}), and Ferrous ion (Fe^{++}). For this reason, copper and iron are considered to be unsuitable as catalysts, and copper catalysis is not

generally reproducible. By far the most attention has been given to cobalt as a catalyst.

The reaction rate is zero order in sulphate from Ø.5 to Ø.8 molar [73], although this range has been extended to lower concentrations [67,145]. Through this range of sulphite concentration, for oxygen concentrations of less than $3.6*10^{-4}$ molar, the reaction is second order in oxygen. Experiments conducted in this range have shown that the second order reaction rate constant, k_2, is proportional to the concentration of cobalt ions in the solution, and is also dependent on temperature and pH. Data are available for cobalt concentrations between 10^{-5} and 10^{-3} molar. Data are not available for higher concentrations of cobalt, because cobalt salts are precipitated in the solution above 10^{-3} molar. The useful pH range is considered to be between 7.5 and 8.5. Most existing data are due to Reith and Beek [182], whose results are reproduced in figure F.1, together with the recent results of Ogawa et al. [170], over a temperature range of 15 to 60°C. In addition, these results have been tabulated by Danckwerts [67]. Linek and Vacek [145] have observed that the results of Reith and Beek [182] yield too high a value of k_2, since too low an oxygen solubility was used in calculation, and this would affect k_2 by the third power of the error. However, in the reaction region chosen for study of the D.S.R., the discrepancy was small, as explained in appendix G. In figure F.1, Reith and

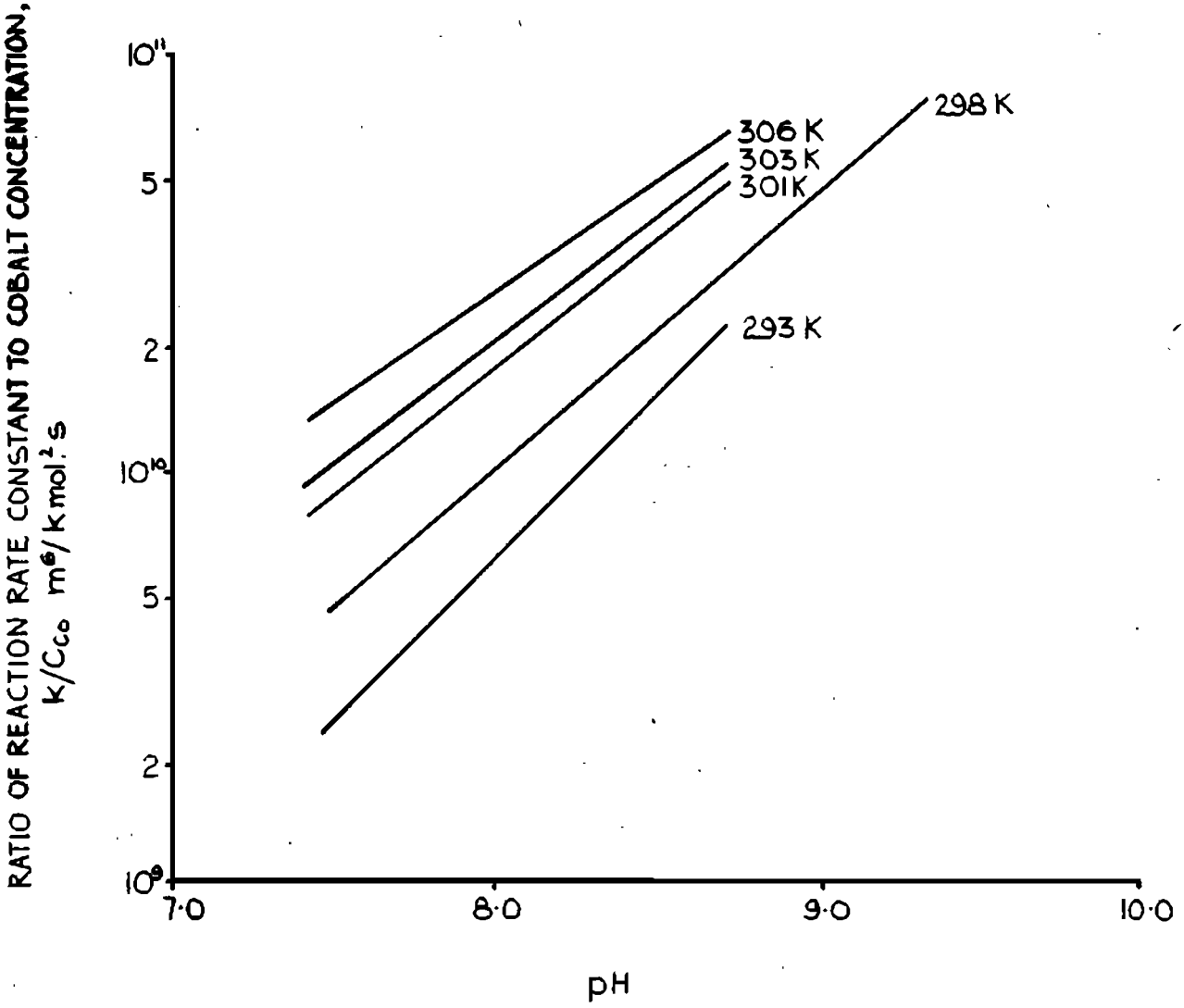

Fig F·1 • Effect of pH of solutions on second-order rate constant •

Beek's results have been adjusted to account for the correct solubility.

2. PROBLEMS ENCOUNTERED IN USING THE REACTION

Mass transfer results using the oxidation of aqueous sulphite in the 50 mm D.S.R. apparatus were scattered, and data was not accurately reproducible. The variation in data was too large to be explained by variation in gas and liquid flowrates, or by a change in gas-liquid interfacial area due to varying surfactant effects. It was concluded that variation in the reaction rate had caused data scatter. Because no previous mass transfer coefficient data exist for the case of vertical bubble flow, it was not possible to determine whether the reaction rate was being retarded, so that the concentration of oxygen in the liquid bulk was not very small, or whether the reaction rate was being enhanced, so that reaction was occurring in the film near the interface. Figure F.2 illustrates four regimes of the sulphite oxidation reaction, as given by Linek and Vacek [145] and Sherwood et al. [198]. In region I, the reaction is so slow that the oxygen concentration in the bulk liquid is significant. In region II, in which the D.S.R. was projected to be operating, bulk oxygen concentration is negligible, yet the reaction is not so fast that it causes significant reaction in the liquid film. In region II, the absorption of oxygen from the gas is controlled entirely by physical

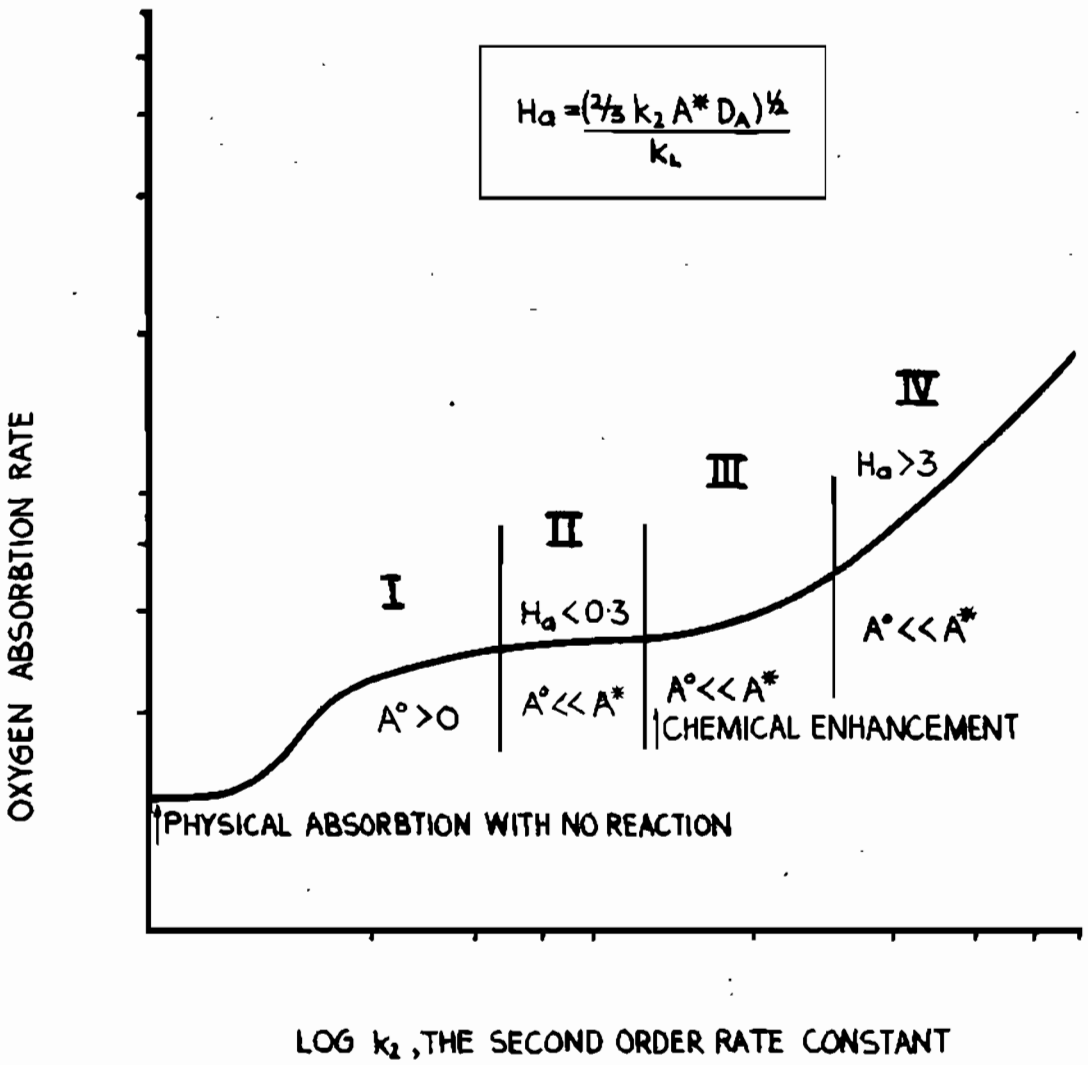

Fig F·2 • The regions of absorption with accompanying second-order chemical reaction •

transfer in the apparatus. In region III, enhancement of absorption due to the reaction is significant, and in region IV, allthe reaction occurs in the film, so that the rate of absorption is independent of local hydrodynamic conditions.

Although the reaction rate was supposed to be in region II in the apparatus, it was possible that the rate had fallen into either region I or region III. The first experimental runs had been conducted with copper and brass fittings still present in the D.S.R., and it was suspected that dissolution of copper was affecting the reaction, which had been catalysed with cobalt salts. Atomic absorption analysis indicated a significant amount of copper (up to three times the cobalt concentration) present in the solution after an experimental run. However, it was still not known whether copper catalysis was driving the reaction from region II to region III, or whether the copper was retarding the cobalt catalysis, so that the apparatus was operating in region I. Determination of the effective oxidation state of copper is difficult, as Linek and Vacek [145] point out that interface conditions may differ significantly from those in the bulk.

To reduce the copper contamination in the apparatus, all copper and brass fittings were removed from the apparatus, and stainless steel parts were substituted. However, the

results were still scattered, so that a more thorough investigation of the reaction rate was undertaken. This is described in detail below.

2.1 VARIATION IN THE ABSORPTION RATE WITH COBALT CONCENTRATION

An experimental run was conducted using the usual quanties of sulphite, under the usual operating conditions, but no cobalt was added. Over the duration of the run, cobalt was added to increase the concentration in a stepwise fashion, up to a maximum of $1.2*10^{-3}$ molar cobalt. Hydrodynamic conditions remained unaltered throughout the run. For each cobalt concentration, the outgoing oxygen concentration was noted, and the rate of oxygen consumed was plotted against cobalt concentration, figure F.3. This curve assumed the correct shape to infer that at low cobalt concentrations the mass transfer was operating, as desired, in region II, and served to show that the reaction rate was not far from the desired value.

2.2 THE EFFECT OF COPPER AND IRON IN SOLUTION

Tests similar to that outlined in section 2.1 above were performed using copper and iron salts, to determine their effect on cobalt catalysis. Sudden additions of both cupric and ferrous ions catalysed the reaction, but in both cases the effect was lost over a short period of

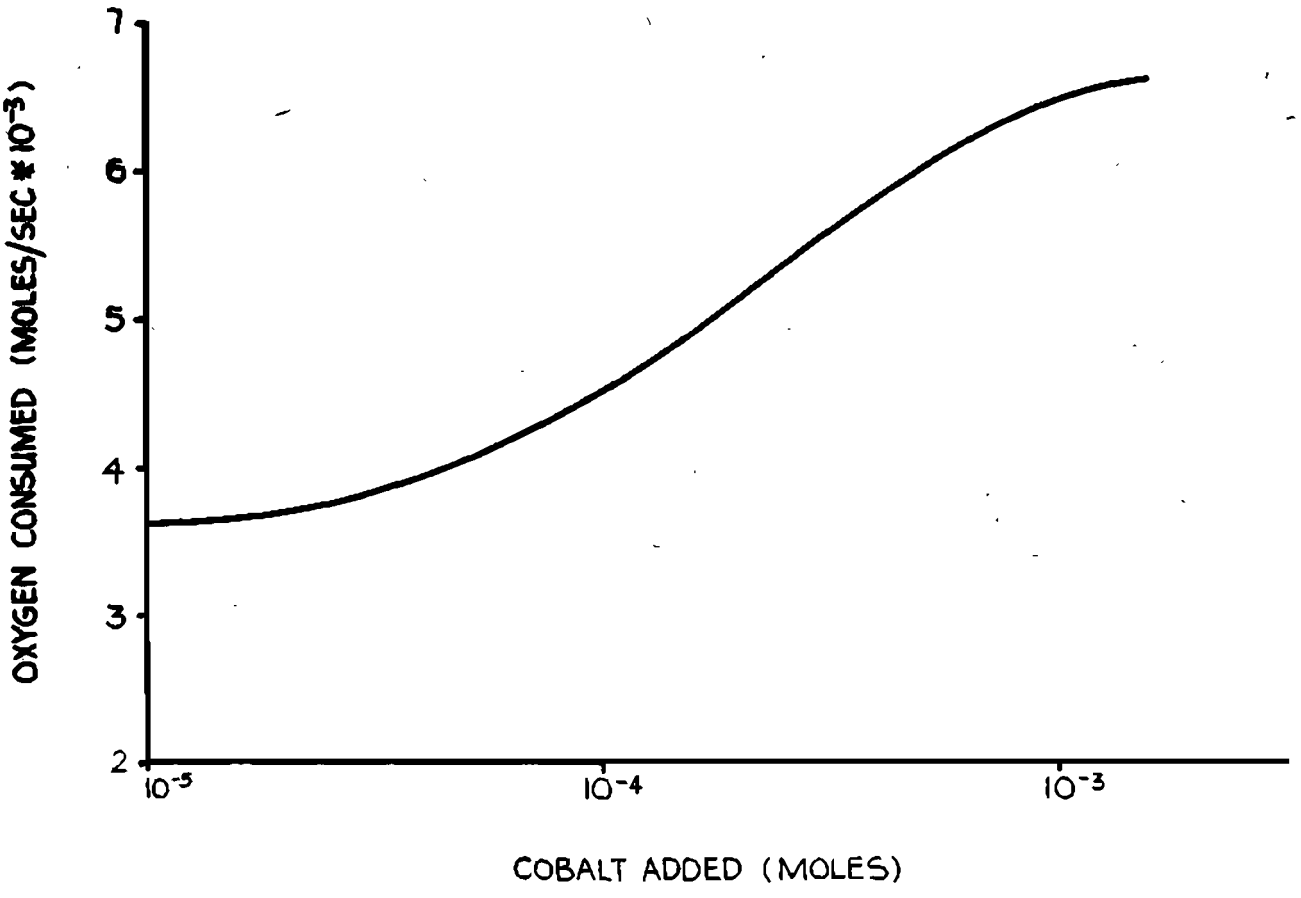

Fig F·3 • Increase of oxygen consumption with addition of coba

time. The copper served eventually to retard the reaction, while in the case of iron, the reaction rate returned to its original value before the iron addition. When a large concentration of copper was present in solution ($4*10^{-4}$ molar), even the addition of additional cobalt did not enhance the reaction, so that the copper appeared to poison the cobalt catalysis. It was concluded that both copper and iron might affect the reaction, the former to a greater degree.

2.3 EFFECT OF TEMPERATURE AND pH

Tests varying the temperature and pH by small amounts from the usual operating point had little effect on the absorption rate of the oxygen in the apparatus. It was concluded that these variables were not the primary cause of data scatter.

2.4 CONCLUSIONS ON DATA SCATTER

Although some metal ions present might be affecting the reaction, lack of reproducibility might be explained only by variations in the chemical content of the solution between different experiments, or by the presence of a highly sensitive equilibrium in the system. Commercial grade sulphite might vary in its content of impurities from bag to bag. To obviate differences in chemical composition, 150 kg of dry sulphite powder was well mixed

to produce a stock of set composition, and stored in a nitrogen atmosphere, so that the top of the stock was not oxidised more than the remainder. In addition, commercial grade sulphuric acid, used to hold the pH at 7.5, was used from a single batch for further mass transfer runs.

Atomic absorption analysis was used to determine the origin of impurities in the solution in the D.S.R. Both local tap water, and a Ø.8 molar solution of the sulphite stock, in distilled water, were both tested. Results are given in table F.1. It was noted that cobalt present in the sulphite was already sufficient to bring the reaction into region II, using the work of Reith and Beek [182] to predict the reaction rate from the cobalt concentration. To avoid enhancing the mass transfer by moving the reaction rate into region III, no cobalt catalyst was added to runs after this analysis. The presence of both copper and iron in the solution was disturbing, but economic factors and the size of the apparatus prevented the use of reagent grade chemicals and distilled water in the D.S.R. Besides the iron present in the initial solution, iron would be leached from the pipes into solution during a run.

Despite the mixing of the sulphite, and more stringent control of temperature and pH, data scatter was still evident in the mass transfer results. A test indicated, moreover, that the reaction rate during one run was time

SPECIES	CONCENTRATION, mg/l		
	TAP WATER	0.8 M SULPHITE	TOTAL
Chrome	0.0	2.0	2.0
Iron	0.1	3.2	3.3
Copper	0.2	0.2	0.4
Manganese	0.0	Trace (0.07)	Trace
Cobalt	0.0	1.0	1.0

TABLE E.1: ATOMIC ABSORPTION ANALYSIS OF TAPWATER, AND OF A 0.8 MOLAR SOLUTION OF SULPHITE IN DEIONISED WATER, TO DETERMINE SOURCE OF METAL SPECIES IN APPARATUS

dependent, as shown in figure F.4. The data scatter could be reduced no further, and the scatter was attributed to the following causes

(i) Iron might be causing erratic behavior in the apparatus. Examination of a Pourbet diagram for pH=7.5 and the electrochemical potential of sulphite indicated close proximity to the ferrous-ferric hydroxide boundary. The effect of the two iron valency states is different, so that this might be the cause of different reaction behaviour between two runs.

(ii) The copper present in the commercial grade sulphite might also affect the reaction.

(iii) The reaction rate constant, k_2, was probably different from that found using pure salt, in the literature. Linek and Vacek [145] have noted that commercial grades may differ in performance from pure solutions by up to 30%.

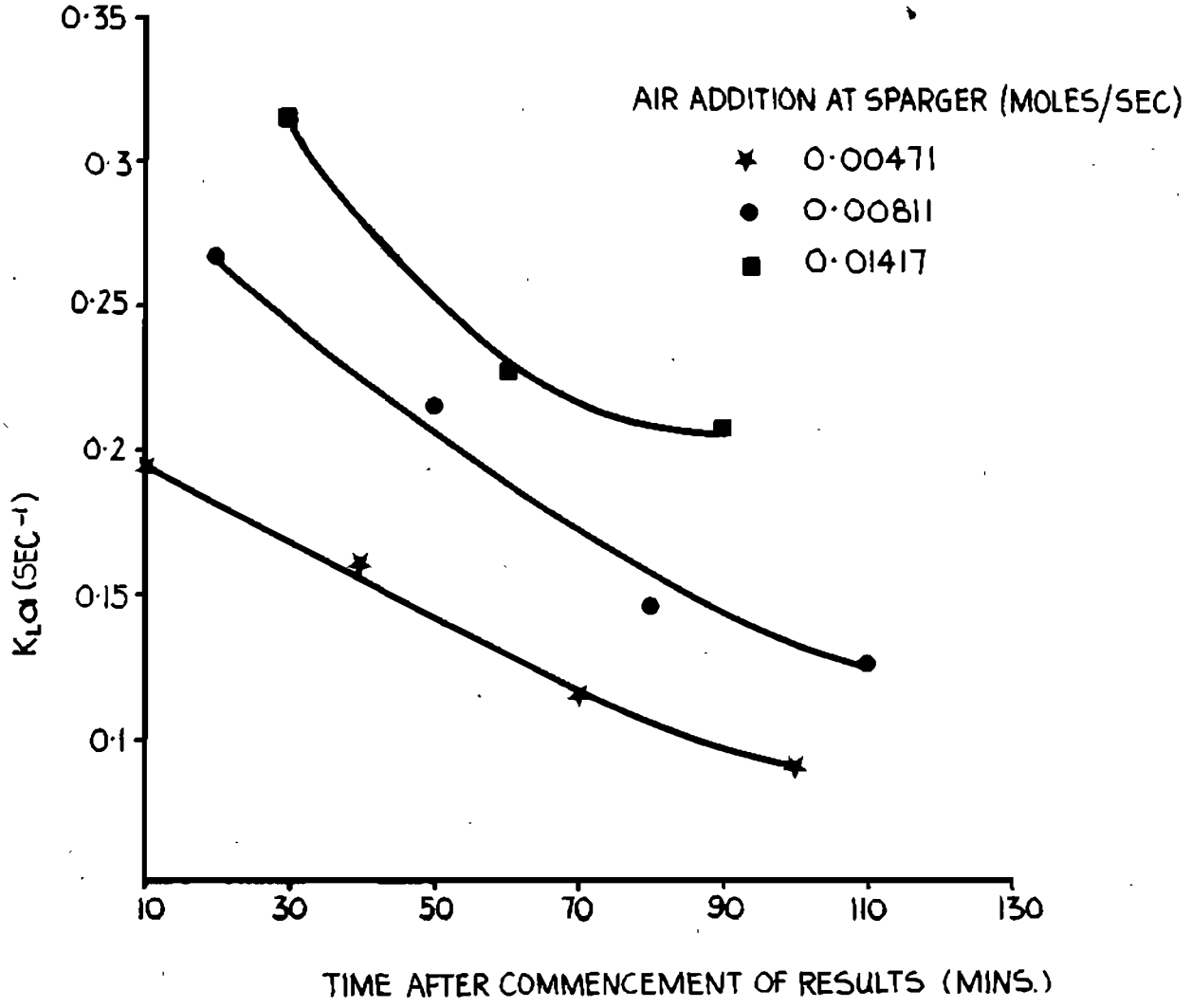

Fig F·4 · Variation in absorption with time •

APPENDIX G

CALCULATING THE SOLUBILITY OF OXYGEN IN SULPHITE SOLUTION

The method of Van Krevelen and Hoftijzer, as presented by Danckwerts [67], is used to determine the solubility of a gas in an ionic aqueous solution. The Henry's law constant, He, for the solution of a gas in an aqueous solution is related to the constant for solution of the gas in pure water, He°, by the equation

$$\log_{10}(He/He^{\circ}) = hI,$$

where h is determined from the sum of contributions of positive, negative, and gaseous species in solution, and where I is given by

$$I = 0.5 \sum c_i z_i^2.$$

where c_i is the concentration of ions of valency z_i.

For the case of a 0.8 molar sulphite solution, values reported by Danckwerts [67] are

Sodium, Na^+: $h_+ = 0.091$

Sulphite, $SO_3^=$, is taken to be the same as sulphate: $h_- = 0.022$

Oxygen, O_2: $h_g = 0.016$

Thus h = Ø.Ø91 + Ø.Ø22 + Ø.Ø16 = Ø.129

for z_i = 1 (sodium), c_i = 1.6 molar
for z_i = 2 (sulphite), c_i = Ø.8 molar

Therefore

$\log_{1Ø}(He/He^{O})$ = Ø.3Ø96,
and He/He^{O} = 2.Ø39

Taking the solubility of oxygen in water at one atmosphere and 35° C as $1Ø.94*1Ø^{-4}$ moles per liter, the ratio of He/He^{O} implies a solubility of oxygen of $5.39*1Ø^{-4}$ moles/liter under the same conditions in a Ø.8 molar sulphite solution.

This value of solubility compares favourably with actual values reported in the literature

Linek and Vacek [145], experimental.....$5.69*1Ø^{-4}$ moles/liter
Danckwerts [67], interpolated from table....$5.67*1Ø^{-4}$ moles/liter
Linek and Vacek [145], solubility equation..$5.59*1Ø^{-4}$ moles/liter

The method of van Krevelen and Hoftijzer is accptably accurate for the operating conditions in the D.S.R.